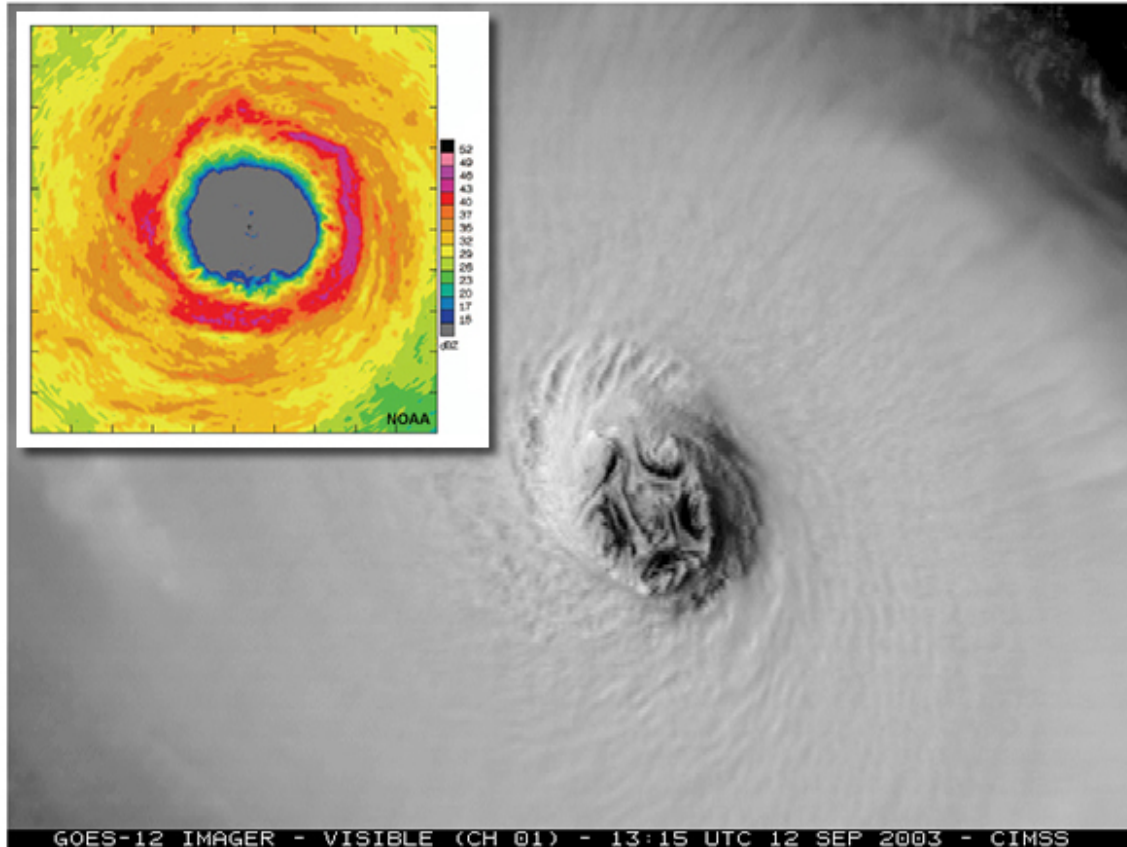


## CHAPTER 10

# TROPICAL CYCLONES



Hurricane Isabel, Sep 2003

NOAA / CIMSS

This chapter focuses on tropical cyclones, one of the most destructive natural phenomena on Earth. We will explore where these systems form around the globe and what the regions with tropical cyclones have in common. We will also become familiar with the various names and intensity scales used to discriminate among these storms around the globe. Sources of variations in tropical cyclone activity on many timescales will be discussed and the current modes of seasonal tropical cyclone forecasts will be briefly reviewed. The three-dimensional structure of a tropical cyclone will be documented and the variety of paths to tropical cyclone formation (*cyclogenesis*) will be elucidated. The various physical processes helping or hindering the intensification of these storms will be presented. Mechanisms influencing tropical cyclone motion will be discussed. The important changes in tropical cyclone characteristics after landfall and the resulting societal impacts will be reviewed.

**Contents**

	Chapter 10, Page Number
Learning Objectives	4
Global Distribution and Monitoring of Tropical Cyclones (TC)	5
Naming conventions and tropical cyclone intensity classifications	9
Who is responsible for monitoring and warning on tropical cyclones?	16
Three-Dimensional Structure and Flow Balances	
Key structural features of a mature tropical cyclone	19
Mass balance solutions and scaling considerations	24
Geostrophic, gradient, and cyclostrophic balances in the TC	24
Inertial stability	28
Thermal wind	30
Details of the core	31
Post-landfall structure	32
The Cyclone Phase Space (CPS) as a measure of storm structure	34
Tropical Cyclogenesis	
Necessary conditions for the formation of a tropical cyclone	37
Dynamic controls on genesis in the monsoon trough environment	41
Tropical cyclogenesis associated with the TUTT	43
Alternative monsoon trough modes	44
Equatorial waves	46
African Easterly Waves (AEW)	49
Mesoscale influences on tropical cyclogenesis	54
Development from a subtropical storm	54
Development from an MCS	57
Vortex Survival and Evolution	58
Using Eddy Angular Momentum Flux to describe TC development	64
Saharan Air Layer (SAL)	67
Summary of possible tropical cyclogenesis mechanisms	70
Intensity	
Key stages of a typical tropical cyclone lifecycle	72
Potential intensity	81
Why isn't every storm a Cat 5? Environmental factors governing intensity	92
Links between inner core dynamics and cyclone structure and intensity	95
Estimation of TC intensity by Remote Sensing	97
Climatology of Tropical Cyclones	
Seasonality of tropical cyclone formation	114
Intraseasonal variability	121
Modulation by the Madden-Julian Oscillation	121
Modulation by the Saharan Air Layer	123
Interannual variability	124
Modulation due to ENSO	126
Modulation due to the QBO	127
Decadal cycles and influences	128
Seasonal forecasting of tropical cyclone activity	130
Motion	

The “ $\beta$ -Effect”	141
Environmental “ $\beta$ ” effects	146
Interaction of vortices: the Fujiwhara effect	149
Structure and intensity impacts on motion	151
Extratropical transition	
Climatology of ET around the world	154
Definitions of ET onset and completion	159
Mechanisms that lead to extratropical transition	160
Societal and Environmental Impacts	
Storm surge and wind-driven waves	164
Flooding and landslides	169
Strong winds and tornadoes	172
Lightning	173
Impacts of Extratropical Transition	173
Hazard mitigation	175
Operational Focus	178
Summary	180
Keywords	181
Appendix A: Acronyms	182
Appendix B: List of Principal Symbols	183
Questions for Review	185
References	186
Brief biographies	202
Glossary	203
Box 10-1 Tropical Cyclone Ingrid, 3-16 March 2005	7
Box 10-2 Historical Etymology of the Term “Typhoon”	10
Box 10-3 Classification of Tropical Cyclone Intensity	13
Box 10-4 They Lived to Tell the Tale!	53
Box 10-5 Record tropical cyclones in the eastern and western hemispheres	78
Box 10-6 Sloping angular momentum surfaces and their link to the eyewall	91
Box 10-7 South Atlantic Tropical Cyclone Catarina (2004)	117
Box 10-8 Tropical Cyclone Gonu (2007)	120
Box 10-9 Unusual Tropical Cyclone Seasons around the Globe	134
Box 10-10 Absolute Vorticity Conservation and the $\beta$ -Effect	143
Box 10-11 The Deadliest Storms on Record	166
Box 10-12 Hurricane Mitch (1988): A Devastating Storm in Central America	171

## Learning Objectives

At the end of this chapter, you should understand and be able to:

- Describe tropical cyclone global climatology (where and when they form, where most form, least, or none form)
- Identify distinguishing features of tropical cyclones (eye, eyewall, spiral bands, surface inflow, upper outflow)
- Identify inner core features such as eye-wall vortices
- Describe ingredients needed for formation or genesis (including subtropical genesis)
- Define the stages of a tropical cyclone lifecycle (wave, depression, tropical storm, tropical cyclone, severe tropical cyclone, decay)
- Using satellite remote sensing, describe how you could detect changes in intensity of tropical cyclones
- Describe the links found between inner core dynamics and changes in cyclone structure and intensity
- Describe the mechanisms that influence tropical cyclone motion from its precursor tropical wave to its landfall in a midlatitude continent
- Describe various mechanisms that lead to extratropical transition
- Describe the hazards of tropical cyclones particularly those at landfall (storm surge, heavy rain and floods, strong winds, tornadoes, ocean waves) and understand the basic mechanisms for each type of hazard

## 10.1 Global Distribution and Monitoring of Tropical Cyclones

Tropical cyclones have impacted the course of history, confounding the attempts of the Kublai Khan to invade Japan in 1266<sup>1,2</sup> and changing the course of early European settlement<sup>3</sup> in North America. We have also witnessed 20<sup>th</sup> century tropical cyclones bringing devastation to all of the continents with footholds in the tropics: names such as Tracy (Australia), Bhola (Bangladesh), Mitch and Katrina (the Caribbean, Mexico, Central America and the United States) bring to mind tragedy to millions around the world.

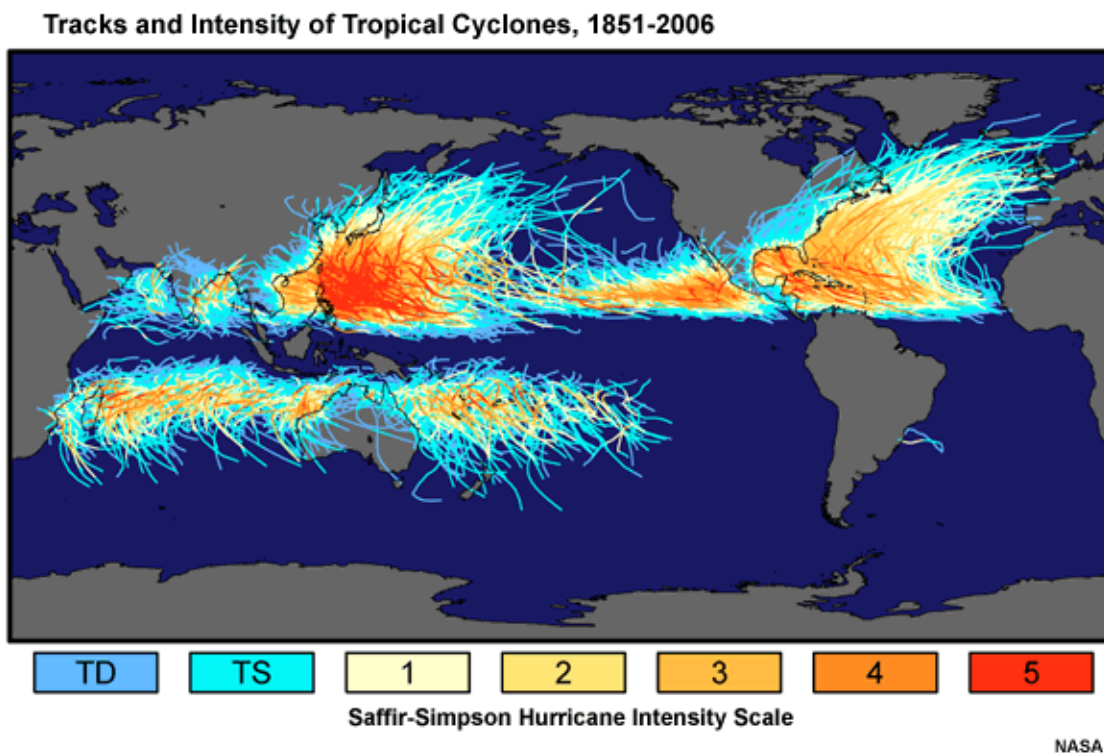


Fig. 10.1. Global distribution of observed tropical cyclone tracks from 1851-2006 (where available).

Fig. 10.1 illustrates some key things about the global distribution of tropical cyclones:

- Tropical cyclones do not form very close to the equator and do not ever cross the equator;
- The western North Pacific is the most active tropical cyclone region. It is also the region with the largest number of intense tropical cyclones (orange through red tracks);
- Tropical cyclones in the western North Pacific and the North Atlantic can have tracks that extend to very high latitudes. Storms following these long tracks generally undergo extratropical transition;
- The North Indian Ocean (Bay of Bengal and Arabian Sea) is bounded by land to the north and the eastern North Pacific is bounded by cold water to the north. These environmental features limit the lifetimes of storms in these regions.

- The Bay of Bengal has about five times as many tropical cyclones as the Arabian Sea. The high mountain ranges and low-lying coastal plains and river deltas of the Bay of Bengal combine to make this region extremely vulnerable to tropical cyclones. Indeed, the two most devastating tropical cyclones on record occurred in this region (Box 10-11).
- Southern Hemisphere (SH) tropical cyclones are generally weaker than storms in the North Pacific and Atlantic basins;
- The extension of the subtropical jet into tropical latitudes in the SH acts to constrain the tracks of tropical cyclones. Even so, a few SH tropical cyclones undergo extratropical transition;
- Although rare, systems resembling tropical cyclones can occur in the South Atlantic Ocean and off the subtropical east coasts of Australia and southern Africa.

Tropical cyclone monitoring occurs in almost every country impacted by these systems. Since tropical cyclones do not observe political boundaries, the WMO has designated official forecasting centers with regional forecasting responsibilities. Although the WMO applies a standard definition of tropical cyclone intensity (10-minute mean of the 10-meter wind), many countries have developed their own measures of intensity. Further, regional terms and intensity designations for tropical cyclones have historical roots in each region. These regional variations can confuse our discussions of tropical cyclones around the world. Thus, we will begin our study of tropical cyclones with a typical tropical cyclone case study followed by a review of these rather prosaic regional aspects of tropical cyclone monitoring, including the inadvertent aircraft monitoring described in Box 10-4. This material will provide us with the reference frame for a comprehensive study of tropical cyclones around the globe.

### Box 10-1 Tropical Cyclone Ingrid, 3-16 March 2005

During its 10 days as a tropical cyclone, tropical cyclone Ingrid (2005) remained in close proximity to the northern Australian coast (Fig.10B1.1) impacting many population centers in the Northern Territory and the states of Queensland and Western Australia as a Cat 4 or 5 tropical cyclone (Australian intensity categories; Box 10-3).

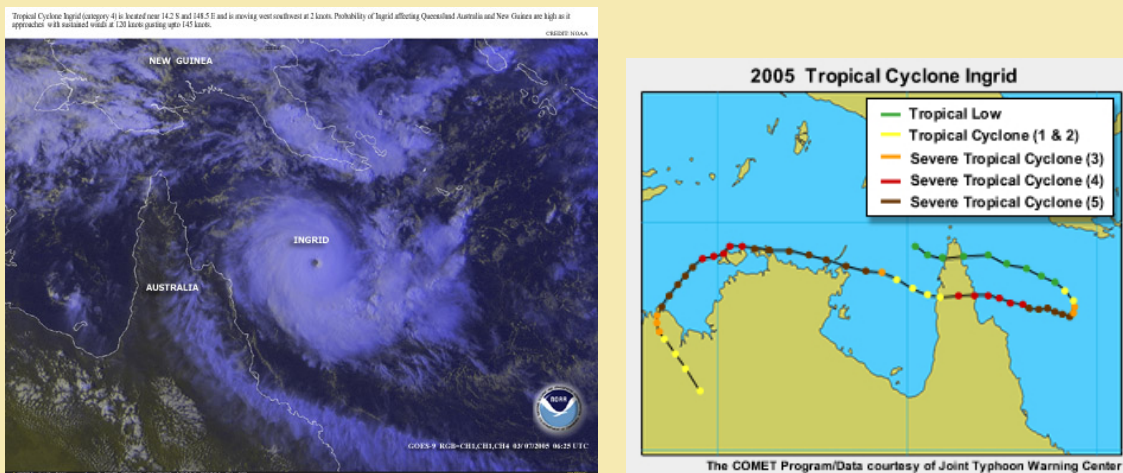


Fig. 10B1.1. (Left) Satellite image of Tropical Cyclone Ingrid as it approached Cape York peninsula. At this time, Ingrid was estimated to have gusts up to  $75 \text{ m s}^{-1}$  (145 knots). (Right) The track with intensity stages indicated by color.

A tropical low developed in the eastern Arafura Sea in an environment with both low vertical shear and anomalously warm SST on 3 March 2005. The northwesterly monsoon flow steered this developing low pressure system east-southeast into the Coral Sea where pre-Ingrid reached cyclone intensity on 6 March. Tropical Cyclone Ingrid developed to a Category (Cat) 5 system by 8 March. Ingrid subsequently moved westward under the influence of a mid-tropospheric ridge to its south; around 0600 CST on 10 March Ingrid made landfall on Cape York as a Cat 4 tropical cyclone. Ingrid weakened during its passage over the peninsula, emerging into the Gulf of Carpentaria late on 10 March as a Cat 1 tropical cyclone.

Ingrid rapidly reintensified again to a Cat 5 in an environment of weak easterly vertical shear over the anomalously warm Gulf of Carpentaria. Gove radar imagery (in the northwestern Gulf of Carpentaria) provides a “land’s eye” view of Ingrid (Fig. 10B1.2). Gove set a new record daily rainfall for March of 192 mm to 9 AM on 12 March.

## Box 10-1 continues

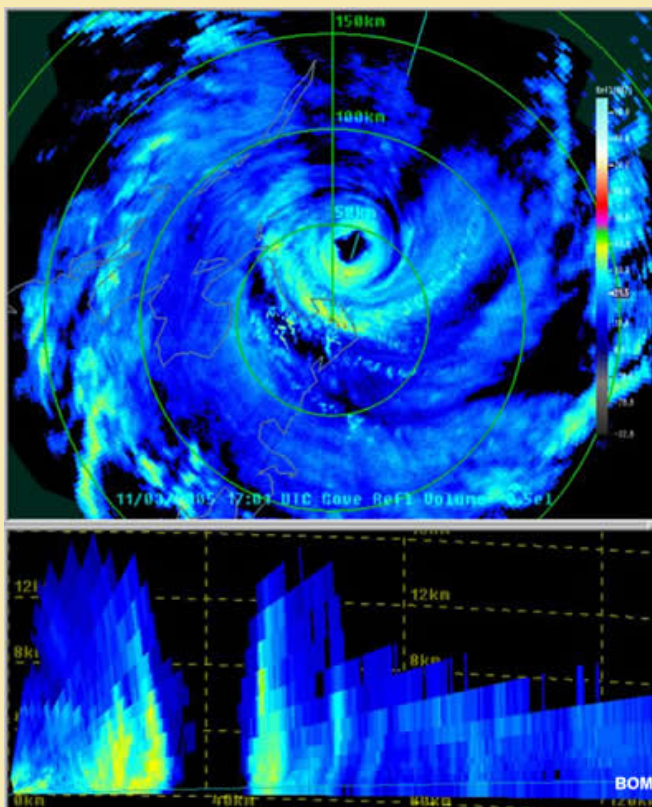


Fig. 10B1.2. Gove radar base scan and cross-section from 11 March 2005 at 1700 UTC. Radar courtesy of the Australian Bureau of Meteorology.

Ingrid skirted the “Top End” of the Northern Territory on 12 and 13 March impacting many coastal communities. While land interactions continued to weaken Ingrid, tree damage at Cape Don (on the Cobourg Peninsula northeast of Darwin) is evidence that Ingrid was a Cat 4 at that time.

Once west of the Tiwi Islands, Ingrid slowed and turned southwestward across the Timor Sea, regaining Cat 5 intensity at 2330 UTC on 14 March. Ingrid weakened rapidly after making landfall near Kalumburu on the rugged terrain of the north Kimberley coast of Western Australia. On the morning of 17 March, Ingrid weakened below cyclone strength near Wyndham, where a 272 mm of rainfall was recorded in 48 hours.



“Land’s eye-views” of Tropical Cyclone Ingrid (2005)



[A video of Ingrid’s passage over Cape Don on the Cobourg Peninsula](#)

[A 5-minute animation from Gove radar 11 March 2005 commencing at 1701UTC](#)



### 10.1.1 Naming Conventions and Tropical Cyclone Intensity Classifications

Accurate observational records are not always available after the passage of a tropical cyclone. The instruments may have been blown or washed away – or the instruments may not be located in the path of the storm. Thus, in the late 1960s Herb Saffir and Robert Simpson<sup>4,5</sup> devised a classification convention to relate the observed damage due to a North Atlantic tropical cyclone with the peak surface winds or minimum surface pressure (two measures of the “*intensity*” of a tropical cyclone) and storm surge in vulnerable coastal locations. The resulting classification system has become known as the “Saffir-Simpson Scale” and has become shorthand for describing the destructive power expected from tropical cyclones around the world. The Saffir-Simpson scale for storm surge has since been shown to be not valid, as the surge is strongly affected by other parameters such as storm size and local bathymetry.

The generic name “tropical cyclones” may be used anywhere in the world for tropical storms with peak wind speeds (1-minute mean, 10-minute mean or gust wind speed are used in different regions) exceeding  $17 \text{ m s}^{-1}$ . In 1848<sup>6</sup> the word “cyclone” was first used to refer to rotating storms. This term was inspired by the Greek word  $\text{Κυκλωζ}$  which means “coiled like a snake.”

While the variety of appellations for tropical cyclones is a little cumbersome, it reflects the local culture and history relating to these important weather systems. However, there is one more wrinkle in the classification of these storms: the averaging time used to measure the peak winds differs around the globe! The *World Meteorological Organization (WMO)* convention for recording peak wind speeds is to record the 10-minute average surface wind speed; however, the United States only applies a 1-minute average to the instruments’ surface wind speed measurements. Thus, it is typical for a western North Pacific storm to be assigned two very different intensities depending on whether recorded by one of the national meteorological agencies of the region (Fig. 10.3) or the US Joint Typhoon Warning Center (JTWC) in Pearl Harbor.

Tropical cyclones have impacted the consciousness of the local populations in regions affected such that local designations for these storms pre-date the current naming conventions. A tropical cyclone with rotating winds between  $17 \text{ m s}^{-1}$  and  $32 \text{ m s}^{-1}$  (gale force) is referred to as a *tropical storm in the North Atlantic and North Pacific*. In the Caribbean – and, more recently, in the eastern Pacific – the strongest of these storms are also referred to as “*hurricanes*” (peak wind speeds exceeding  $33 \text{ m s}^{-1}$ ) after the god of evil, *Hurican*. In the western North Pacific storms of the same intensity are called “*typhoons*.”<sup>6</sup> The derivation of the term typhoon is still debated and may derive from Greek, Chinese, or Arabic provenance (Box 10-2).<sup>6</sup>



#### **Global Naming Conventions**

WMO, <http://www.wmo.ch/pages/prog/www/tcp/documents/FactShtTCNames1July05.pdf>  
NOAA NHC, <http://www.nhc.noaa.gov/aboutnames.shtml>

### Box 10-2 Historical Etymology of the Term “Typhoon”

Tropical cyclones in the western North Pacific are generally known as *typhoons* (English), *Tai-feng* (Chinese) and *Taifu* (Japanese). These three words sound very similar. Are their origins related? According to the American Heritage College Dictionary the word *typhoon* has roots in Chinese, Arabic, East Indian, and Greek background. But the word typhoon is not used now in the Indian Ocean. Does this put the connection to an East Indian source into question? What about the other possibilities? We will explore this here.

#### The Origin of Tai-Feng in the Chinese Language



In Chinese, the word corresponding to typhoon is written using the two characters *Tai* and *Feng*. *Feng* is an old character, used to describe any kind of wind. Thus, the key to the origin of *Tai-Feng* in Chinese is to understand the origins of the word *Tai*.

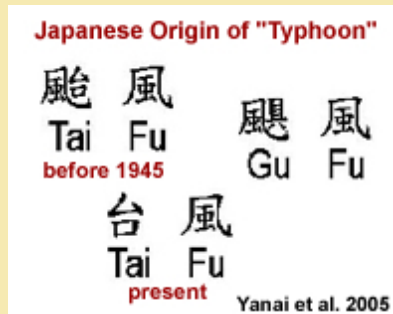
Some scholars have linked the Chinese characters *Tai* and *Chu* in Chinese. The term *jufeng* or *chufeng* was first mentioned in the 5<sup>th</sup> century.<sup>7</sup> Hung et al.<sup>8</sup> explored many possible origins for *Tai*, noting that the character *Tai* was being used as early as the 17<sup>th</sup> century. For example, in 1694 the text *An introduction to Taiwan Province (Tai-Wan-Fu-Chih)* was published. This book links the *Tai* and *Chu* in a description of the winds in intense rotating storms: *Tai* storms linger for days and are stronger than the more quickly moving *Chu* storms. This text attributes *Tai* as deriving from *Tsai* – a Taiwanese term describing the wind of *Chu* that was “dancing in the sky in all directions.”

#### The Origin of “Taifu” in Japanese

The characters *Tai Fu* did not appear in the documents describing the tropical storms that destroyed Kublai Khan’s fleets in 1274 and 1281,<sup>1</sup> so we know that this term is more modern than the 13<sup>th</sup> century.

A book written in 1708, *Chi-Nan-Kuang-Yi* by Chen Shuen-Jer, explained the use of *Tai* and *Gu* (or *Chu*) in China (see Hung et al.<sup>8</sup> for a complete description) and *Tai* also appeared in Togai Ito’s 1724 text *Six chapters for famous things*.<sup>9</sup> Still, Mr. Okada (Director General

of the Japanese Central Meteorological Observatory, CMO) was still using the term *Gu Fu* in his 1937 textbook. So the term *Tai Fu* appears very new to Japan.



#### Europe and the Middle East

One of the Homeric Hymns (a collection of thirty three poems addressed to various gods and goddesses, usually attributed to Homer) addressed to Apollo can be translated as: “*Then Apollo fights and kills the female snake, which had been living in a nearby spring. This was the snake that had guarded the monster Typhon.*” In this hymn Typhon’s mother was Hera and he had no father. However, according to the poet Hesiod, Typhon was the son of Earth and Tartarus.

### Box 10-2 continues

Some scholars question whether the ancient Greek word Typhon is connected to the Arabic word *tufan*. Around 820 BC, the Greek and Assyrian Empires were in direct contact. By around 670 BC, the Assyrian Empire had conquered vast areas including modern-day Syria, Iraq, Israel and Egypt. Thus, it is possible that the Greeks, through the Assyrian language influenced the Middle East and that the words *Typhon* and *tufan* may share some common history.

#### East meets West

By 14 AD, Alexandria (Egypt), China, India and Indonesia were already engaged in trade of silks and spices. The Arabs explored the ancient Greek civilization, producing a series of important Arab versions of major Greek writings on science and philosophy. So the Arab word *tufan* may have evolved from the Greek word *Typhon* here. The Mongol emperors of China counted Muslims among their employees – could the word have spread to China in this way? The Chinese dominated shipping in the Indian Ocean from the 12<sup>th</sup> to 17<sup>th</sup> centuries and we know that China and Japan were in communication prior to the 13<sup>th</sup> century. By the 16<sup>th</sup> century, European ships reached the Arabian Sea – so in the 16<sup>th</sup> and 17<sup>th</sup> centuries, shipping and trade in Southeast Asia involved Arabs, Chinese, Japanese and Europeans! It is sure that their ships met and that their sailors experienced typhoons. It is easy to imagine a natural mixing of words of similar pronunciation: so *Tai Fu*, *Typhon* and *tufan* may have merged around this time.

#### What can we conclude about the origins of the term, “Typhoon”?

- The Greek Typhon is the oldest of these words, dating back further than 900 BC.
- Records of the 13<sup>th</sup> century Mongol invasions of Japan – in which the Mongol fleets were twice sunk by typhoons – do not use either *Tai* or *Gu*.
- The first recorded usage of the English *typhoon* is AD 1588, when Europeans, Asians and Arabs were all sailing the Pacific and Indian Oceans.
- The oldest known use of *Tai* in Chinese was in 1685; *Chu* was used prior to 470 AD.
- This means that *typhoon* appeared in English before *Tai Fu* in Chinese!

So the debate continues to choose between the two most likely evolutions of *typhoon*:

Greek → Arabic → European (Spanish or Portuguese) → Chinese  
 Unknown → Chinese (Cantonese, Taiwan, Ryukyu) → Arabs/Europeans

Which is right? We still do not know...but history and meteorology meet here.



<http://hsu.as.ntu.edu.tw/images/CNJPTyphoon.jpg>

This box summarizes work of Professors Chih-wen Hung, Robert Fovell and Michio Yanai who have completed a comprehensive analysis of this topic.

In the North Indian Ocean, tropical cyclones with peak surface winds exceeding  $33 \text{ m s}^{-1}$  are known as *severe cyclonic storms*, while in the Australian region they are referred to as *severe tropical cyclones*. Typhoons in the western North Pacific with peak 1-minute average surface wind speeds in excess of  $65 \text{ m s}^{-1}$  are given the designation *super typhoon* by the US Joint Typhoon Warning Center. In the Atlantic and eastern Pacific, Category 3-5 hurricanes on the Saffir-Simpson scale (peak winds  $\geq 50 \text{ m s}^{-1}$ ) are labeled *major* (or *intense*) *hurricane*.<sup>10</sup> Although there are relatively few major hurricanes, their destructive potential is so great that they are responsible for almost 85% of all hurricane-related damage even though they only comprise one fifth of the US landfalls.<sup>10</sup> A more complete summary of the intensity range naming conventions for each basin is given in Box 10-3.



Fig. 10.2. Track of Hurricane Joan (#11) which weakened as it crossed Central America. On emerging into the eastern North Pacific and re-intensifying, it was renamed Miriam.

The concept of assigning individual names to tropical cyclones was initiated in the late 19<sup>th</sup> century by an Australian meteorologist, Clement Wragge.<sup>10,11</sup> Wragge used the Greek alphabet and names of politicians whom he did not like. Later, the names came from the military alphabet. In the 1960s the WMO stepped in and developed a consistent, regionally-applicable naming convention for tropical cyclones in each of the affected ocean basins. While the early lists consisted only of women's names, by the 1970s the lists were broadened to include both male and female names and to encompass the languages of all of the affected countries. The names of people are no longer used for storms in the western North Pacific: storm names for this region are drawn from a list of generic words.

If a tropical cyclone moves from one region to another, it is typically renamed to the next name on the list in the new region. This means that in rare cases, the same storm is assigned two names depending on its track (Fig. 10.2).

### Box 10-3 Classification of Tropical Cyclone Intensity around the World

Tropical cyclone classification schemes for the different regions are summarized here. Where associated damage is provided it refers to the expected damage in the maximum wind zone. Damage will vary across locations depending upon: (1) distance from the zone of maximum winds; (2) exposure of the location (i.e., sheltered or not); (3) building standards; (4) vegetation type; and (5) resultant flooding and wave action. The effects of storm surge, tide, or wave action are not explicitly included in any of the following tables.

#### North Atlantic and Eastern North Pacific: Saffir-Simpson Scale

The Saffir-Simpson scale was initially intended to provide a link between the observed damage and the effects of wind, pressure and storm surge that could lead to such damage. In the first table, the hurricane categories are related to maximum sustained winds (1-minute average and 10 meters above ground) and minimum central pressure. Maximum wind speed is used to determine the category of a hurricane, so where a conflict arises between the choice of category for an observed storm, wind speed should be used (ranges for minimum central pressure are for reference to past classifications<sup>a</sup>).

Table 10-3.1 The Saffir-Simpson Scale

Saffir-Simpson Category	Maximum Sustained Wind Speed ( $V_{MAX}$ ; 1-minute average) <sup>b</sup>			Minimum Central Pressure ( $p_{MIN}$ )
	$m s^{-1}$	$km h^{-1}$	mph	
1	33-42	119-153	74-95	> 980
2	43-49	154-177	96-110	979-965
3	50-58	178-209	111-130	964-945
4	59-69	210-249	131-155	944-920
5	70+	250+	156+	< 920

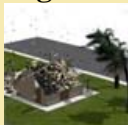
<sup>a</sup> In earlier times minimum surface pressure was used, likely because it could be deduced from flights over the ocean.

<sup>b</sup> Use the following conversions for units of wind speed:  $1 m s^{-1} = 3.6 km h^{-1}$ , 1.94 knots, and 2.237 mph.

## Box 10-3 continues

Table 10-3.2 Expected Damage for Saffir-Simpson Hurricane Categories

Category	Expected Damage	Description of Typical Damage Expected
1	Minimal	Damage primarily to vegetation and unanchored homes. No real damage to other structures.
2	Moderate	Major damage to exposed mobile homes. No major damage to buildings, but some damage to roofing materials, windows and doors possible. Considerable damage to vegetation; some trees blown down.
3	Extensive	Most mobile homes destroyed. Some structural damage to small buildings. Some damage to roofing materials, windows and doors. Large trees blown down and other vegetation damaged. May need to evacuate low-lying homes near the shoreline.
4	Extreme	Complete destruction of mobile homes. Extensive damage to roofing materials, windows and doors, with complete failures of roofs on many small residences. Vegetation extensively damaged. Major erosion of beaches. Evacuation of all residences within 500 yards of shore, and of single-story residences within 2 miles of shore may be required.
5	Catastrophic	Some complete building failures. Small buildings blown away. Complete destruction of mobile homes. Considerable damage to roofs of buildings, with many complete roofing failures. Very severe, extensive damage to windows and doors. Extensive shattering of glass in windows and doors. Vegetation decimated. Evacuation of low-lying homes within 5-10 miles of shore likely.


**Animated damage to a typical house and vicinity with increasing intensity:**


Wind



Storm surge and wind


**Labeling storms based upon intensity at operational centers**

 Joint Typhoon Warning Center (US), <https://metocph.nmci.navy.mil/jtwc/menu/JTFAQ.html#labels>

 National Hurricane Center (US), <http://www.nhc.noaa.gov/aboutssh.shtml>

 Australian Bureau of Meteorology, <http://www.bom.gov.au>
**Background on Saffir-Simpson hurricane scale**

 History of Saffir-Simpson Scale, <http://www.aoml.noaa.gov/hrd/tcfaq/J6.html>

Summary of the Saffir-Simpson scale,

[http://www.nhc.noaa.gov/HAW2/english/basics/saffir\\_simpson.shtml](http://www.nhc.noaa.gov/HAW2/english/basics/saffir_simpson.shtml)

## Box 10-3 continues

Australian Region: Gust Wind Speed Ranges for Tropical Cyclones

A tropical cyclone scale linking maximum *gust* (3-5 second, 10 meter) wind speeds to expected damage in the maximum wind zone has been instituted in the Australian Region. As with the Saffir-Simpson scale, the weakest tropical cyclones are designated as Category 1, with the strongest possible tropical cyclones being assigned Category 5.

Table 10-3.3 Australian region gust wind speed categories

Categories	Range of strongest gusts (km h <sup>-1</sup> )	(m s <sup>-1</sup> )	Summary Description of Typical Damage Expected
1	< 125	< 34	Negligible house damage. Damage to some crops, trees and caravans.
2	125 - 170	34 - 47	Minor house damage. Significant damage to trees and caravans. Heavy damage to some crops. Risk of power failure.
3	170 - 225	47 - 63	Some roof and structural damage. Some caravans destroyed. Power failure likely.
4	225 - 280	63 - 78	Significant roofing loss and structural damage. Many caravans destroyed and blown away. Dangerous airborne debris. Widespread power failure.
5	> 280	> 78	Extremely dangerous with widespread destruction.

Western North Pacific and Indian Ocean Tropical Cyclone Intensity

The tropical cyclone intensity scale in these basins is based upon the maximum *sustained* (10-minute average) surface (10 meter) wind speeds. While the wind speed ranges in these basins are consistent, their naming conventions vary.

Table 10-3.4 Western North Pacific and Indian Ocean categories

Range of 10-min mean wind (km h <sup>-1</sup> )	Range of 10-min mean wind (m s <sup>-1</sup> )	Categories by Region		
		Western North Pacific	North Indian	South Indian
60 - 119	17 - 33	Tropical Storm	Tropical Storm	Tropical Storm
120 - 227	34 - 63	Typhoon	Severe Cyclonic Storm	Tropical Cyclone
>227	> 63	Super Typhoon		Severe Tropical Cyclone

### 10.1.2 Who is Responsible for Monitoring and Warning on Tropical Cyclones?

There are six tropical cyclone Regional Specialized Meteorological Centres (RSMCs) together with five Tropical Cyclone Warning Centres (TCWCs) around the world. These centers have been designated as regional warning centers for tropical cyclones (including tropical depressions). Together, these centers cover all regions of the global tropics affected by tropical cyclones. A list of the RSMCs and TCWCs as well as webpage links to these centers is given in Table 10.1. Note that, while the US Navy/Air Force Joint Typhoon Warning Center (JTWC) is not a designated warning center, its forecasts and archive information are also made widely available. Other centers that are not designated centers, but make more localized forecasts include the Hong Kong Observatory, The Shanghai Weather Bureau, and the Korean Meteorological Agency.

The RSMCs and TCWCs have responsibility to provide advisories and bulletins with up-to-date first level basic meteorological information on all tropical cyclones to their regions. First level basic meteorological information includes track and intensity observations and forecasts, but may also include a detailed discussion of the underlying reasoning leading to the forecasts and other information that is available to that center (e.g., satellites, computer forecast model outputs). These and the above-mentioned national centers also prepare comprehensive best track archives of tropical cyclones in their warning area.

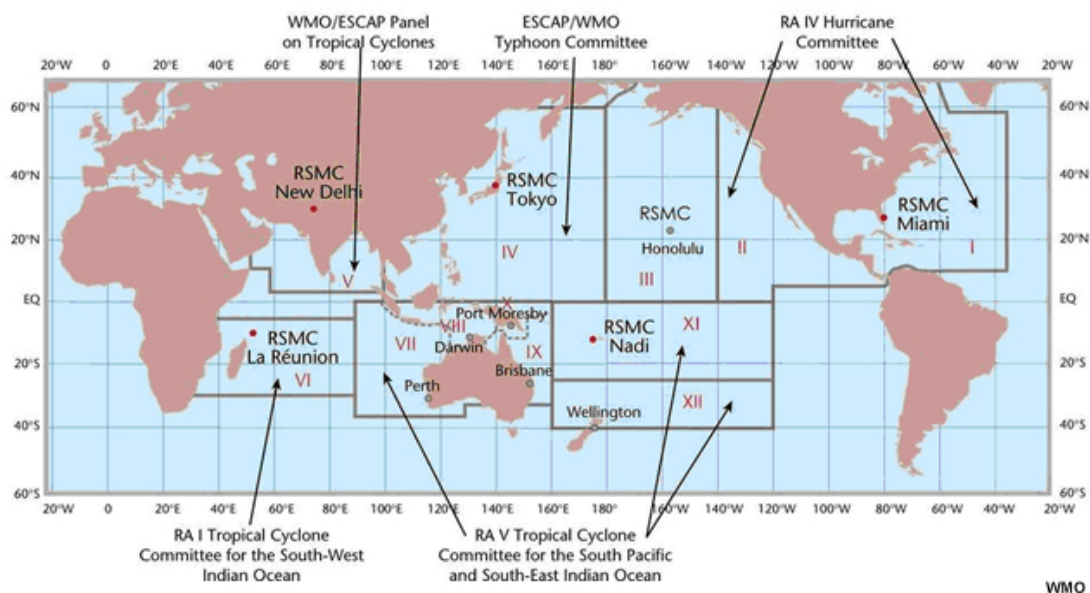


Fig. 10.3. WMO Regions and Institutions with Tropical Cyclone forecasting responsibility. Image obtained from <http://www.wmo.ch/pages/prog/www/tcp/Advisories-RSMCs.html>.

WMO links to the latest RSMC and TCWC advisories,  
[http://www.wmo.int/pages/prog/www/tcp/index\\_en.html](http://www.wmo.int/pages/prog/www/tcp/index_en.html)

US Naval Research Lab (NRL), [http://www.nrlmry.navy.mil/tc\\_pages/tc\\_home.html](http://www.nrlmry.navy.mil/tc_pages/tc_home.html)  
 University of Wisconsin, Cooperative Institute for Meteorological Satellite Studies (CIMSS),  
<http://cimss.ssec.wisc.edu/tropic2/>



Table 10.1 Global list of the WMO Regional Specialized Meteorological Centres (RSMCs) together with six Tropical Cyclone Warning Centres (TCWCs). Note that the Indonesian TCWC (Jakarta) was activated in January 2008.

<b>Tropical Cyclone Regional Specialized Meteorological Centres (RSMCs)</b>	
<b>RSMC Miami-Hurricane Center</b> NOAA/NWS National Hurricane Center (NHC), USA. <a href="http://www.nhc.noaa.gov/products.html">http://www.nhc.noaa.gov/products.html</a>	Caribbean Sea, Gulf of Mexico, North Atlantic and eastern North Pacific Oceans
<b>RSMC Tokyo-Typhoon Center</b> Japan Meteorological Agency <a href="http://www.jma.go.jp/en/typh/">http://www.jma.go.jp/en/typh/</a>	Western North Pacific Ocean and South China Sea
<b>RSMC-tropical cyclones New Delhi</b> India Meteorological Department <a href="http://www.imd.gov.in">http://www.imd.gov.in</a>	Bay of Bengal and the Arabian Sea
<b>RSMC La Réunion-Tropical Cyclone Centre</b> Météo-France <a href="http://www.meteo.fr/temps/domtom/La_Reunion/TGPR/saison/saison_trajGP.html">http://www.meteo.fr/temps/domtom/La_Reunion/TGPR/saison/saison_trajGP.html</a>	South-West Indian Ocean
<b>RSMC Nadi-Tropical Cyclone Centre</b> Fiji Meteorological Service <a href="http://www.met.gov.fj/">http://www.met.gov.fj/</a>	South-West Pacific Ocean
<b>RSMC Honolulu-Hurricane Center</b> NOAA/NWS, USA <a href="http://www.prh.noaa.gov/hnl/cphc/">http://www.prh.noaa.gov/hnl/cphc/</a>	Central North Pacific Ocean

<b>Tropical Cyclone Warning Centres (TCWCs) with Regional Responsibility</b>	
<b>TCWC-Perth</b> Bureau of Meteorology, Australia <a href="http://www.bom.gov.au/weather/wa/cyclone/">http://www.bom.gov.au/weather/wa/cyclone/</a>	South-East Indian Ocean
<b>TCWC-Darwin</b> Bureau of Meteorology, Australia <a href="http://www.bom.gov.au/weather/cyclone/">http://www.bom.gov.au/weather/cyclone/</a>	Arafura Sea and the Gulf of Carpentaria
<b>TCWC-Brisbane</b> Bureau of Meteorology, Australia <a href="http://www.bom.gov.au/weather/cyclone/">http://www.bom.gov.au/weather/cyclone/</a>	Coral Sea
<b>TCWC-Port Moresby</b> National Weather Service, Papua New Guinea <i>Website under construction</i>	Solomon Sea and Gulf of Papua
<b>TCWC-Wellington</b> Meteorological Service of New Zealand, Ltd. <a href="http://www.metservice.co.nz/forecasts/severe_weather.asp">http://www.metservice.co.nz/forecasts/severe_weather.asp</a>	Tasman Sea
<b>TCWC-Jakarta</b> Badan Meteorologi and Geofisika <a href="http://maritim.bmg.go.id/cyclones/">http://maritim.bmg.go.id/cyclones/</a> See the announcement of this new TCWC at <a href="http://www.wmo.ch/pages/mediacentre/press_releases/pr_787_e.html">http://www.wmo.ch/pages/mediacentre/press_releases/pr_787_e.html</a>	Maritime Continent

## 10.2 Three-Dimensional Structure and Flow Balances

A tropical cyclone is a warm-core, non-frontal, low pressure system that develops over the ocean and has a definite organized surface circulation.<sup>12</sup> Before proceeding further with our discussion of tropical cyclones, we pause and examine the details of their structure. First, we examine the fundamental features of the system, and then focus more on the details of the eye of the storm. Next, we consider balanced flow solutions and how they can help us to delineate different regions of the storm. Changes in storm structure associated with landfall are briefly reviewed. Finally, the *Cyclone Phase Space (CPS)*,<sup>13</sup> a framework for tracking storm structure evolution, is introduced.

### 10.2.1 Key Structural Features of a Mature Tropical Cyclone

A few structural elements are common to all tropical cyclones. The (i) boundary layer inflow, (ii) eyewall, (iii) cirrus shield, (iv) rainbands, and (v) upper tropospheric outflow (Fig. 10.4) are found in all tropical depressions and tropical storms. As these storms become more intense, a (vi) clear central eye becomes visible from satellite (Fig. 10.5).

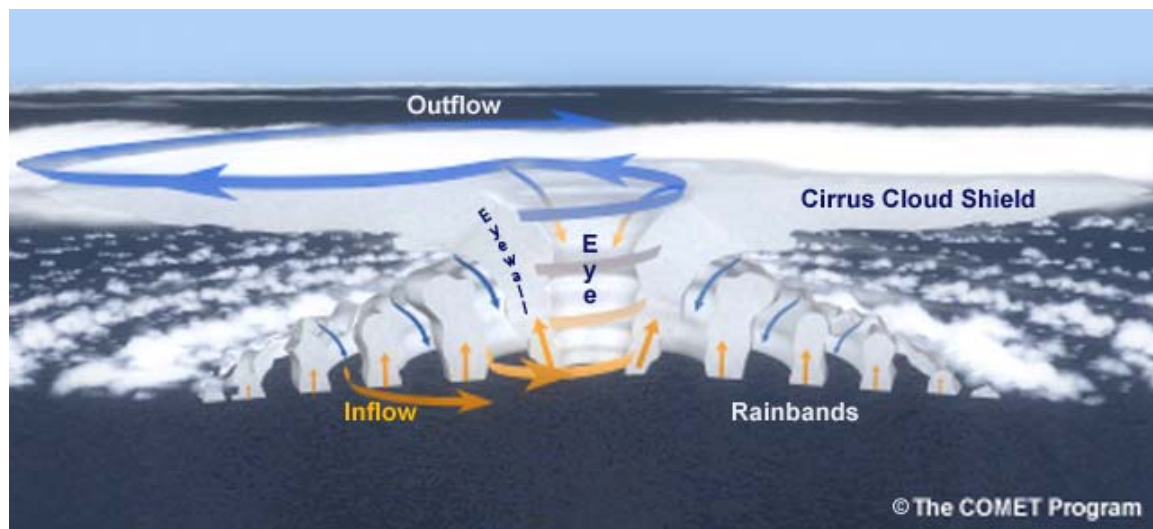


Fig. 10.4. Main structural elements of tropical cyclones. Notice the (i) boundary layer inflow, (ii) clear central eye, (iii) eyewall, (iv) cirrus shield, (v) rainbands, and (vi) upper tropospheric outflow.

Documentation and analysis of the outflow have received relatively little attention compared to the cyclonic region of the storm, however, a study in 1996<sup>14</sup> examined the three-dimensional structure of the outflow of Typhoon Flo (1990). The equatorward outflow jet was found to be confined to higher elevations and to span a smaller potential temperature range than the poleward outflow channel of the storm. In this analysis, potential temperature was used as a proxy vertical coordinate.

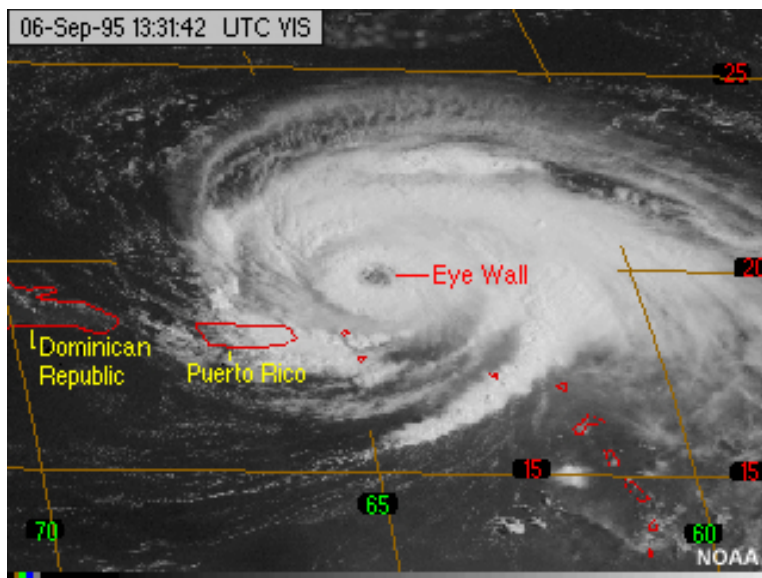


Fig. 10.5. Visible satellite image of Hurricane Luis (1995). At this time, Luis had a minimum central pressure of 943 hPa and peak surface winds of  $60 \text{ m s}^{-1}$  making it a marginal Category 4 hurricane on the Saffir-Simpson scale.

Due to the differing sense of cyclonic flow across the equator, tropical cyclone wind and cloud patterns are reflected for storms north and south of the equator: tropical cyclones spin counter-clockwise in the Northern Hemisphere (NH) and clockwise in the Southern Hemisphere, with corresponding variations in their spiral rainband structure. In a tropical cyclone, the wind flows inward cyclonically at lower levels, spiraling upward in the zones of deep convection (the central eyewall or the spiral rainbands), ultimately spiraling outward aloft, just below the tropopause (Fig. 10.6).

The convergent boundary layer flow spirals into the eyewall forcing dynamically-driven convection. Under the eyewall, this convergence is enhanced due to the “frontal” nature of the boundary layer structure there. Thermal (convective) instability may enhance the eyewall convection, contributing to overshooting convection into the stratosphere. Lower to mid-tropospheric convergence of drier air above the boundary layer<sup>12</sup> can be entrained into the rainbands, contributing to the weaker convection in these bands compared to the eyewall. The image of the rainbands spiraling out from the eyewall is one of the most recognized satellite signatures today (Fig. 10.5).

This animation in Fig.10.6 illustrates many fundamental aspects of tropical cyclone systems.

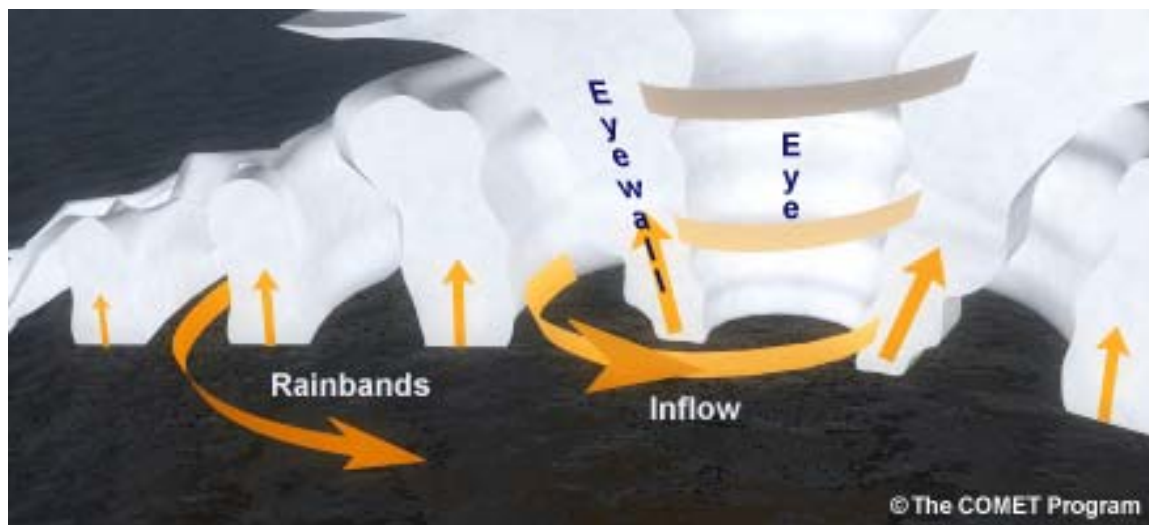


Fig. 10.6. Conceptual model of the boundary layer flow in a tropical cyclone, illustrating the (i) boundary layer inflow, (ii) flow into the eyewall, and (iii) rainbands.

 [Animated conceptual model of the boundary layer flow in a tropical cyclone](#)

Traditional observational studies<sup>12</sup> concluded that the hurricane boundary layer was isothermal, in spite of the drop in surface pressure between the outer reaches of the storm and its center. However, detailed observations of the hurricane boundary layer have recently shown<sup>15</sup> that the tropical cyclone boundary layer is only approximately isothermal inside the strong pressure gradient and high wind region of the tropical cyclone (about  $1.25^\circ$  radius from the storm center). Outside this region, the near-surface air in the hurricane boundary layer cools more than would be expected from adiabatic expansion – and so the hurricane boundary layer is neither isothermal nor isentropic between about  $1.25^\circ$  and  $3.0^\circ$  radius (Fig. 10.7). This additional cooling is not due to expected increases in near-surface relative humidity. In fact, inflowing boundary layer air outside the high wind regime is cooling and drying. Inside the high wind region, the air becomes isothermal, with both the dry entropy and the relative humidity increasing rapidly, much more in line with the traditional view of the tropical cyclone boundary layer.<sup>15</sup> Other studies<sup>16</sup> have confirmed this new view of the tropical cyclone boundary layer.

This new model of the hurricane boundary layer has consequences for understanding the complete hurricane system. For example, the Carnot engine model of a tropical cyclone assumes an isothermal boundary layer for air flowing in from a great distance away from the storm (from the ambient tropical environment). In this model of the tropical cyclone, the boundary layer relative humidity (and hence,  $\theta_e$ ) is continually increasing as air flows in towards the center of the storm. The recent observations we have just discussed challenge these assumptions about the boundary layer temperature and humidity structure in a tropical cyclone. The importance of this new information lies in its use to determine the maximum intensity that a tropical cyclone could reach: the Carnot theory relies on the difference in the mean thermodynamic profiles of the environment and the core to

determine the amount of thermodynamic energy available to be converted into mechanical energy (and hence, to surface winds and pressure deficit).<sup>17,18</sup> This model does not consider the variations of temperature or the decrease then increase in relative humidity along the inflowing air trajectory in the boundary layer. The impact of these more realistic variations on the maximum intensity derived from the Carnot theory has not yet been determined.

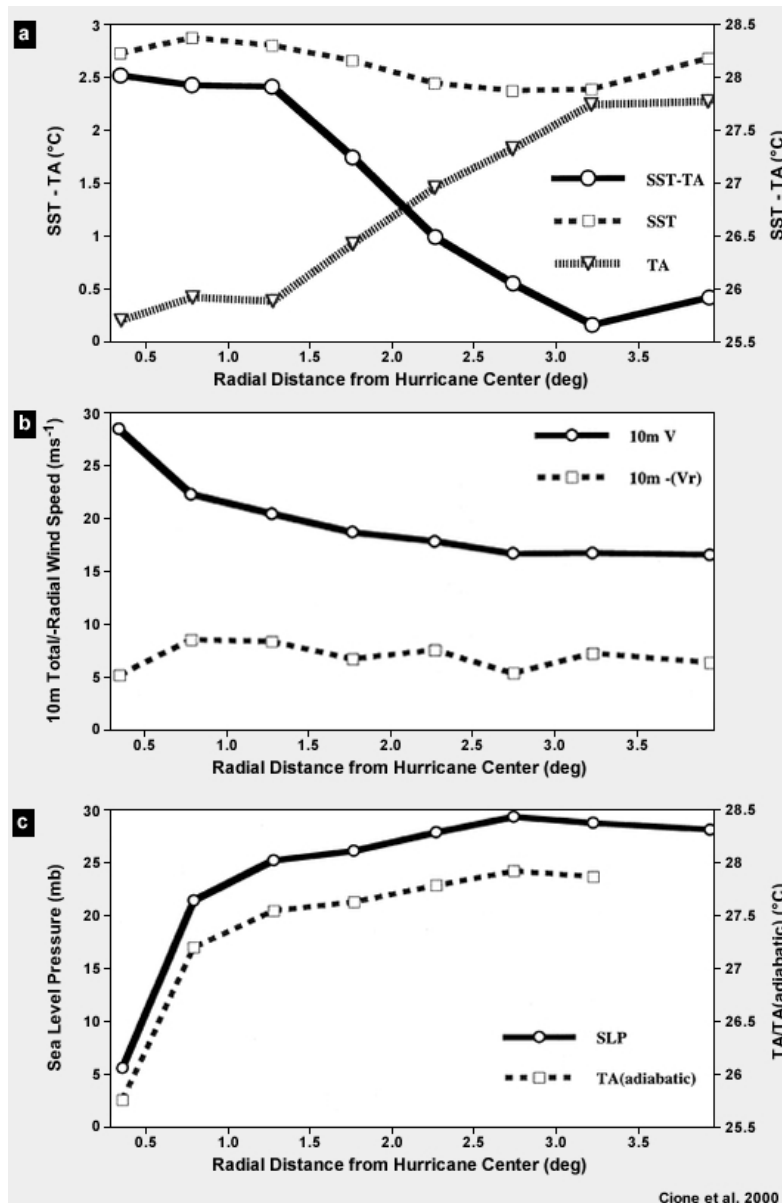


Fig. 10.7. Radially-averaged values of (a) surface air temperature  $T_A$  (dark gray), SST (dotted) and  $(SST - T_A)$  (black); (b) surface (10-m 1-minute) wind speed (black) and radial inflow (dotted); and (c) sea level pressure (black) and  $T_A$  due to adiabatic expansion (dotted).

Observations of the tropical cyclone boundary layer using GPS dropsondes have identified well defined jet structures in the storm boundary layer.<sup>19</sup> These jets were initially proposed to result from downward mixing of higher momentum air from above via convective downdrafts. Detailed analyses of dropsonde information from two storms led to a hypothesis that radial import of higher angular momentum air<sup>20,21</sup> was responsible for the formation of these jets. Numerical simulations of a dry (no convection) tropical cyclone have demonstrated the existence of boundary layer jets, suggesting that these jets can form without convection. These studies also compared the radial structure of the surface winds with the winds expected if gradient wind balance applied. Gradient wind balance operates<sup>20,22</sup> inside the radius of maximum winds; winds near the eyewall are about 90% of the gradient wind expected there; and winds outside the eyewall are only 70% of the local gradient wind.



Animation of TC inflow and outflow, <http://www.comet.ucar.edu/nsflab/web/hurricane/324.htm>



#### **GPS dropsondes**

Brief description, <http://www.aoml.noaa.gov/hrd/nhurr97/GPSNDW.HTM>

Detailed technical information, <http://www.eol.ucar.edu/rtf/facilities/dropsonde/gpsDropsonde.html>

## 10.2.2 Mass Balance Solutions and Scaling Considerations

The key stages in the lifecycle of a typical tropical cyclone are incipient disturbance, tropical storm, tropical cyclone (hurricane, typhoon), and possibly severe tropical cyclone (major hurricane, supertyphoon). Having reached its peak intensity at one of these stages (see Box 10.3 for storm intensity classifications), the storm will either decay or undergo extratropical transition. These stages are associated with changes in the storm intensity and structure. In this section, we review the physical stages of the storm lifecycle as illustrated by the stages of Hurricane Rita (Figs. 10.36–10.40).

Many investigators have considered the tropical cyclone in terms of a symmetric balanced vortex,<sup>23,24,25,26</sup> yet inspection of this vortex reveals differing balance conditions in different regions of the vortex.<sup>22</sup> In this section we explore the tropical cyclone vortex, identifying regions in which the balance constraint is cyclostrophic, gradient or even close to geostrophic, and then we introduce inertial stability and evaluate its spatial variation and evolution in the TC. Finally, we consider the three-dimensional, symmetric thermal wind balance.

### 10.2.2.1 Geostrophic, Gradient and Cyclostrophic Wind Balances in the TC

An example of the close agreement between observations of rotational winds in Hurricane Diana (1984) and the corresponding gradient winds (calculated from the observed height field) is given in Fig. 10.8.<sup>22</sup>

The Rossby number is a nondimensional parameter that identifies the relative importance of the inertial and Coriolis terms in the Navier Stokes equations. It is defined by doing a scale analysis of these two terms and taking their ratio. The equation for the Rossby number is

$$Ro = \frac{V}{fL} \quad (1)$$

where  $V$  is the scale speed,  $L$  is the scale distance and  $f$  is the Coriolis parameter.

Another interpretation of the Rossby number is that it gives the ratio of the vorticity of the flow to the Earth's vorticity,  $f$ . The magnitude of the Rossby number gives insight into the type of force balance dominating:

$$Ro \begin{cases} < 1 & \text{geostrophic} \\ \sim 1 & \text{gradient} \\ >> 1 & \text{cyclostrophic} \end{cases} \quad (2)$$

*Thus, calculation of the Rossby number for various regions of a typical tropical cyclone will tell us about the important force balances in this region. We now consider three distinct regions of the storm: the eye, the area inside the gale force wind radius, and the “outer” storm (Fig. 10.9).*



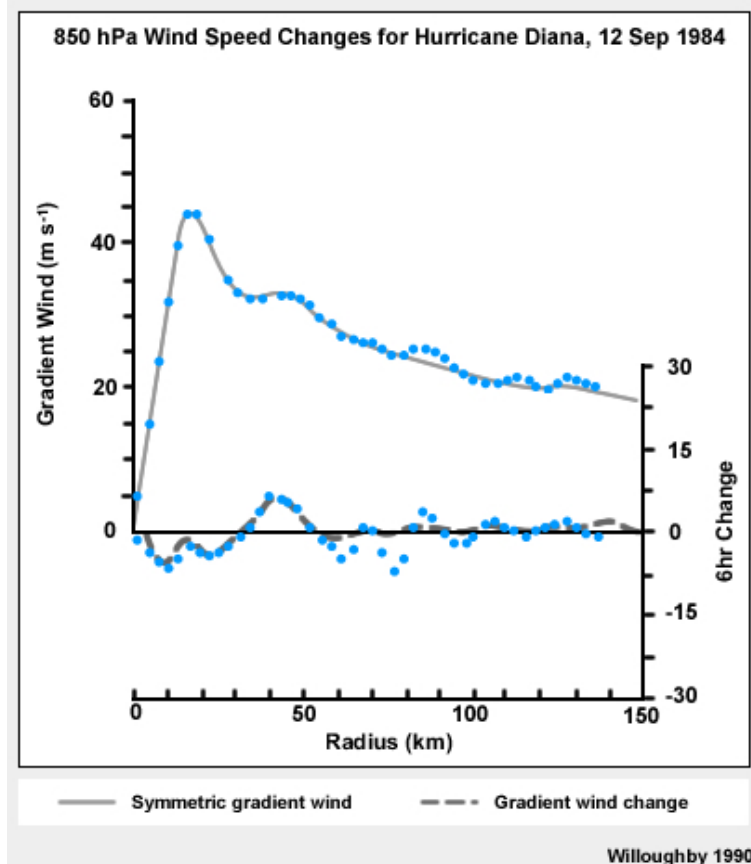


Fig. 10.8. 850 hPa wind observations (dots) for Hurricane Diana on 12 Sep 1984, symmetric gradient wind (solid) and gradient wind change (dash) deduced from the observed height field. Adapted from Willoughby (1990).<sup>22</sup>

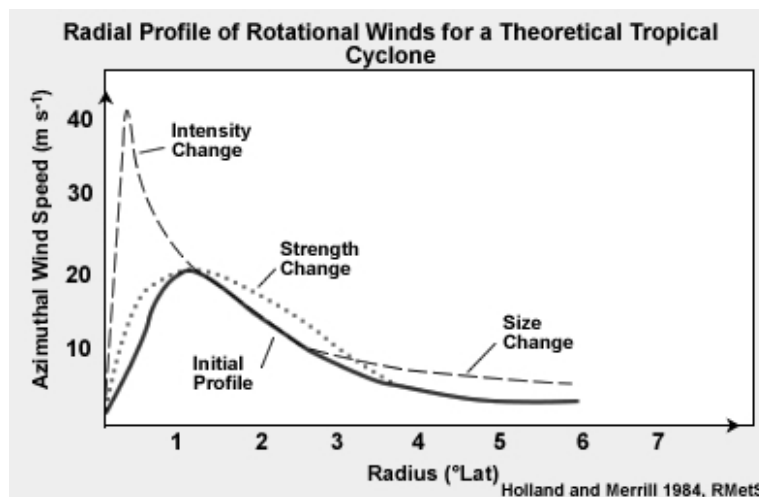


Fig. 10.9. Radial profile of rotational winds for a theoretical tropical cyclone: i) the eye (inside the radius of maximum winds), ii) the region of winds storm strength ( $17 \text{ m s}^{-1}$ ) or higher; iii) the outer storm. Also pictured here are the variations in this radial profile due to intensity, strength, and size changes. Adapted from Holland and Merrill (1984).<sup>27</sup>

Based on Figures 10.8 and 10.9, typical power of 10 values for wind speed and spatial scale for the three regions of this tropical cyclone are:

Eye	$V \sim 10 \text{ m s}^{-1}$	$L \sim 10^4 \text{ m,}$
Storm strength	$V \sim 10 \text{ m s}^{-1}$	$L \sim 10^5 \text{ m,}$
Outer	$V \sim 1 \text{ m s}^{-1}$	$L \sim 10^6 \text{ m.}$

These numbers correspond to winds of  $10 \leq V < 100 \text{ m s}^{-1}$  over a spatial scale of  $\sim 10 \text{ km}$  for the eye,  $V > 10 \text{ m s}^{-1}$  over a spatial scale  $\sim 1000 \text{ km}$  for the storm-force wind area, and  $V < 10 \text{ m s}^{-1}$  over a spatial scale  $> 1000 \text{ km}$  for the outer region of the storm. Recalling that a degree of latitude is roughly  $100 \text{ km}$ , these numbers are consistent with Fig. 10.9.

To calculate the Rossby number, we still need a value for the Coriolis parameter,  $f$ . Assuming a reasonable latitude of  $15^\circ$  gives  $f = 4 \times 10^{-5}$ . Again, for an order of magnitude analysis, we round this value of  $f$  to the nearest power of 10. Thus, we will use  $f \sim 10^{-5} \text{ s}^{-1}$ .

Now let us calculate the Rossby number for each region:

Eye	$Ro \sim \frac{10}{10^4 \times 10^{-5}} \sim 100$	$\Rightarrow$	<b>cyclostrophic,</b>
Storm strength	$Ro \sim \frac{10}{10^5 \times 10^{-5}} \sim 10$	$\Rightarrow$	<b>gradient,</b>
Outer	$Ro \sim \frac{1}{10^6 \times 10^{-5}} \sim 10^{-1}$	$\Rightarrow$	<b>geostrophic.</b>

So we see that different balances can apply to the different regions of a tropical cyclone.<sup>22,23</sup>



Use Fig. 10.9 to select typical numbers (not orders of magnitude) for wind speed and spatial scale for each of the three regions (eye, storm-force, outer) for both an intense ( $40 \text{ m s}^{-1}$ ; long dash) and a weak ( $20 \text{ m s}^{-1}$ ; solid line) tropical cyclone. Use  $f \sim 10^{-5} \text{ s}^{-1}$  as before. In both storm analyses take (a)  $15 \text{ m s}^{-1}$  for the “strength” wind value and (b)  $500 \text{ km}$  for the outer wind radius.

Compare the resulting values for Rossby number for each storm in each region. Now compare these values with the order of magnitude analysis given above and decide whether the fundamental balances in each region would change with changing intensity.



Using Fig. 10.9 as a guide, typical values for wind speed and spatial scale in the three regions for each tropical cyclone are:

40 m s<sup>-1</sup> tropical cyclone

Eye	$V \sim 40 \text{ m s}^{-1}$	$L \sim 50 \text{ km} = 5 \times 10^3 \text{ m}$ ,
Storm strength	$V \sim 15 \text{ m s}^{-1}$	$L \sim 150 \text{ km} = 1.5 \times 10^5 \text{ m}$ ,
Outer	$V \sim 10 \text{ m s}^{-1}$	$L \sim 500 \text{ km} = 5 \times 10^5 \text{ m}$ .

The Rossby numbers for each region of the 40 m s<sup>-1</sup> tropical cyclone are

Eye	$Ro \sim \frac{40}{5 \times 10^3 \times 10^{-5}} \sim 800$	$\Rightarrow$	<b>cyclostrophic,</b>
Storm strength	$Ro \sim \frac{15}{1.5 \times 10^5 \times 10^{-5}} \sim 10$	$\Rightarrow$	<b>gradient,</b>
Outer	$Ro \sim \frac{10}{5 \times 10^5 \times 10^{-5}} \sim 2$	$\Rightarrow$	<b>gradient.</b>

20 m s<sup>-1</sup> tropical cyclone

Eye	$V \sim 20 \text{ m s}^{-1}$	$L \sim 120 \text{ km} = 1.2 \times 10^4 \text{ m}$ ,
Storm strength (as above)	$V \sim 15 \text{ m s}^{-1}$	$L \sim 150 \text{ km} = 1.5 \times 10^5 \text{ m}$ ,
Outer	$V \sim 4 \text{ m s}^{-1}$	$L \sim 500 \text{ km} = 5 \times 10^5 \text{ m}$ .

The Rossby numbers for each region of the 20 m s<sup>-1</sup> tropical cyclone are

Eye	$Ro \sim \frac{20}{1.2 \times 10^4 \times 10^{-5}} \sim 167$	$\Rightarrow$	<b>cyclostrophic,</b>
Storm strength	$Ro \sim \frac{15}{1.5 \times 10^5 \times 10^{-5}} \sim 10$	$\Rightarrow$	<b>gradient,</b>
Outer	$Ro \sim \frac{4}{5 \times 10^5 \times 10^{-5}} \sim 0.8$	$\Rightarrow$	<b>geostrophic.</b>

We can glean a number of interesting results from these analyses:

- The balance structures of different storms vary with radius.
- The 20 m s<sup>-1</sup> storm agrees with our order of magnitude scale analysis in all regions.
- The gradient wind region extends further for the 40 m s<sup>-1</sup> storm than the 20 m s<sup>-1</sup> storm. This means that we can expect different balances to occur at different radii for tropical cyclones with different radial structure (i.e. cyclones whose rotating winds change differently as you move out from their center).

The horizontal wind balances just discussed are not the only balance constraints operating in a symmetric, steady state tropical cyclone. The inertial stability and the thermal wind of the vortex provide information about the vertical wind shear of the balanced flow associated with the storm and its resistance to outside influences.

### 10.2.2.2 Inertial Stability Variations in a TC

Inertial stability, symbolized as  $I$ , is a measure of the resistance of a vortex to forcings such as convective heating or other weather systems acting to change its structure.

For a vortex in which the horizontal winds dominate the flow, the inertial stability is defined using symmetric measures of the storm: the vertical component of the absolute vorticity and absolute angular momentum for a rotational flow with wind speed  $v$  at radius  $r$  from the center of the vortex via

$$I^2 = (\zeta + f_o) \left( f_o + \frac{v}{r} \right) \quad (3)$$

Clearly, the inertial stability will increase proportionally with the relative vorticity,  $\zeta$ , the local Coriolis parameter,<sup>c</sup>  $f_o$ , or the relative angular momentum,  $v/r$ . Thus, a storm that is contracting and increasing in intensity will rapidly increase its static stability. The cyclonic component of this storm is increasing its resistance to horizontal forcing by external weather systems<sup>27,28</sup>. However, the anticyclonic outflow aloft has very weak absolute vorticity ( $\zeta$  has the opposite sign to  $f$  and the rotational winds are weak; the signs of both  $\zeta$  and  $v$  act to reduce the effect of the Coriolis parameter on  $I$ ). Thus, while the storm is now more protected from influences that might weaken it, the strong inertial stability does not extend to the tropopause. This means that upper tropospheric weather systems may still act to weaken the storm. Further, inertial stability cannot protect the storm from surface influences.



The concept of inertial stability can be illustrated by a thought experiment in a swimming pool. Perhaps some of you have done this. If you walk around and around a circular swimming pool you can force the water into rotation in the same direction. Once the water is in motion, will it be easy or difficult to (a) walk into the center of the pool; and (b) to turn around and walk the other way around the edge of the pool (against the current)?

Based on the mathematical definition, we see that inertial stability at a given location in the storm depends directly on the Coriolis parameter,  $f$ , and the local rotational wind speed,  $v$ , and varies inversely with radius  $r$ . Thus, for a given radius and latitude, as wind speed increases the inertial stability at that location increases. *This means that we expect the inertial stability to vary with location in the tropical cyclone*—and indeed it does (Fig. 10.10).

This understanding of inertial stability helps explain why tropical cyclones of increasing intensity are more likely to survive adverse environmental influences. One example of inertial stability evolution with storm structure changes is a contracting eyewall.

---

<sup>c</sup>  $f_o$  is the value of the Coriolis parameter at the center of rotation.  $f_o$  is a constant.

**Think** Inertial stability evolution due to a contracting eyewall: What happens to the inertial stability (a) of the eye; and (b) to the flow at the “old” eye radius? Use the above equation to guide your thinking.

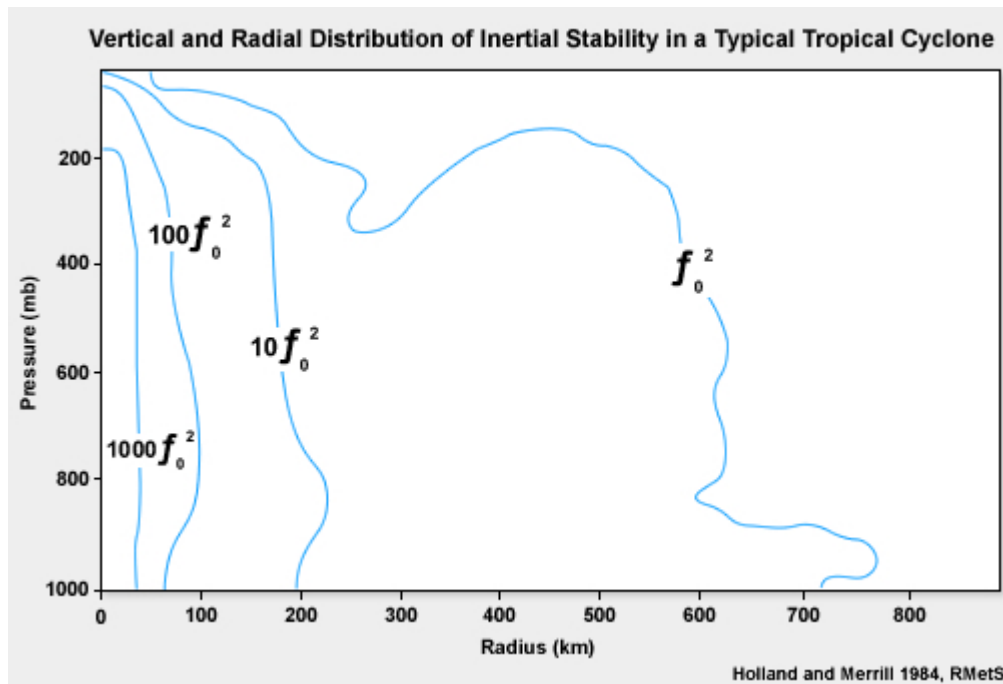


Fig. 10.10. Vertical and radial distribution of inertial stability in a typical tropical cyclone. Following Holland and Merrill (1984).<sup>27</sup>

**💡** Inertial stability illustrated in a swimming pool: It will be difficult both to walk into the center of the pool *and* to turn around and walk against the current. The inertial stability of the rotating water resists motions across the flow and against the flow.

If you have not done this before, give it a try – how often do you get to play and call it meteorology research?

**💡** Inertial stability evolution due to a contracting eyewall: (a) As the eyewall contracts the wind speed stays the same, but the radius decreases (we do not know what is happening to  $f$ , so we assume that it remains constant). As a result of the radius decreasing, we see that inertial stability of the contracting eye increases. (b) At the “old” eye radius, the radius is unchanged while the wind speed has decreased. Thus, the inertial stability at this radius decreases.

### 10.2.2.3 The Thermal Wind

The horizontal temperature gradient at the level of the warm core, along with the surface wind structure, can be used to infer the three-dimensional symmetric wind field of the system. This takes advantage of another balance condition, the thermal wind balance, where the thermal wind is defined as the difference between the geostrophic wind at two vertical levels

$$\overline{V}_T = V_g(p_A) - V_g(p_B), \quad (4)$$

where  $p_A$  and  $p_B$  are the pressures “above” and “below” so that  $p_A < p_B$ . Thus, the thermal wind represents the vertical wind shear of the geostrophic wind.

For geostrophic flow, the thermal wind balance is written as

$$\begin{aligned} \overline{V}_T &= \frac{g}{f} \vec{k} \times (z_A - z_B) \\ &= \frac{R}{f} \vec{k} \times \nabla \bar{T} \ln \left( \frac{p_B}{p_A} \right) \end{aligned} \quad (5)$$

where  $p_A$  and  $p_B$  bound the layer in which the mean temperature gradient,  $\nabla \bar{T}$ , is calculated and  $z_A$  and  $z_B$  are the physical heights corresponding to these pressures. Similar equations can be derived for gradient or cyclostrophic balance to deduce the vertical shear for these rotational winds.

It should now be clear how the three-dimensional wind structure can be solved for using the equation for the thermal wind along with the horizontal distribution of the surface wind.

### 10.2.3 Details of the Core

The clear region in the center of a mature tropical storm is known as the eye and is relatively calm with light winds and the lowest surface pressure. An organized band of thunderstorms immediately surrounds the calm, storm center. This region is the eyewall and the strongest winds are to be found on the inner flank of this thunderstorm annulus (Fig. 10.11).

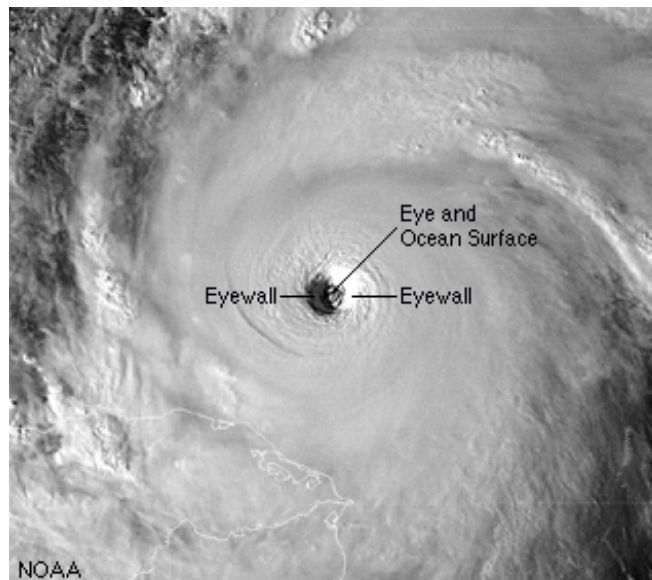


Fig. 10.11. Visible image of the eye and eyewall of a mature tropical cyclone. Notice that eyewall slopes outward from the surface, creating the “stadium effect”.

Boundary layer convergence occurs in the gust front region (due to the thunderstorms) below the eyewall, so air ascending in the eyewall convection comes both from the eye and the outer regions of the storm. For a steady state storm (one that is not changing with time), mass conservation requires subsidence in the eye to compensate for the air rising in the convection. The clear eye results from this subsidence (Fig. 10.12). In weaker storms, the eye may not be evident from visible and infrared satellite images.

The following animation of the evolution of Hurricane Isabel (2003) demonstrates the development of the clear eye as the storm intensifies; eyewall vortices and development of an asymmetric eye, which then resymmetrizes are also evident.



#### **Animations of the eye of Hurricane Isabel from 2003**

A close-up satellite view of Isabel’s eye,

[http://cimss.ssec.wisc.edu/tropic/Isabel\\_Ancillary/java\\_loops.html](http://cimss.ssec.wisc.edu/tropic/Isabel_Ancillary/java_loops.html) (click on the 11<sup>th</sup> first)

Fly through the storm, [http://www.aoml.noaa.gov/hrd/Storm\\_pages/isabel2003/eye\\_small.mov](http://www.aoml.noaa.gov/hrd/Storm_pages/isabel2003/eye_small.mov)

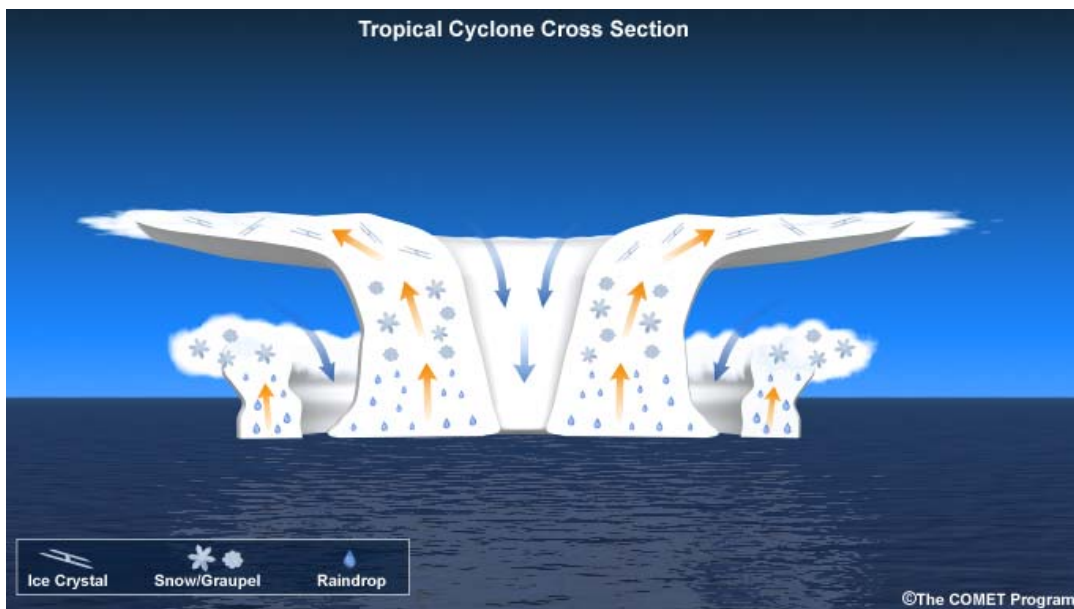


Fig. 10.12. Schematic of the cross-section through a tropical cyclone showing the vertical airflow and microphysics in the eyewall and rainbands.

#### 10.2.4 Post-landfall Structure

With rare exceptions (loss of ships at sea, oil platforms and other structures), the major impacts from a tropical cyclone are felt when the storm makes landfall. Thus, it is particularly important to consider post-landfall structure changes (e.g., Fig. 10.13).

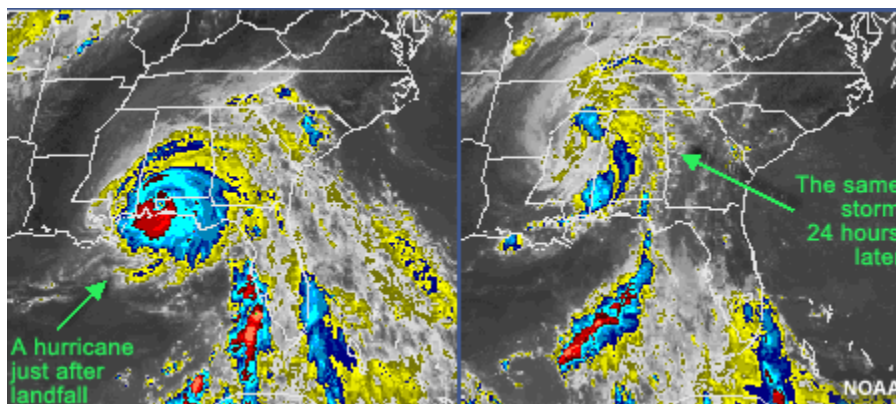


Fig 10.13. An example of post-landfall structural changes.

Three major changes happen at landfall: loss of the ocean energy source causes the storm to weaken, increased friction causes the storm to weaken, and the changing storm structure causes a redistribution of the significant weather associated with the storm. Let us consider each in turn.

The warm, tropical ocean provides energy for the tropical cyclone. Evaporation (latent heat flux) and heat transfer (sensible heat flux) from the ocean surface warm and moisten the



tropical storm boundary layer. Hence, when the storm loses this energy source it begins to weaken. This can be thought of in terms of thermal wind balance of a symmetric vortex in gradient wind balance: the loss of the convection and associated subsidence in the eye weakens the upper tropospheric warm core, raising the central pressure of the storm, which leads to weaker pressure gradient and weaker gradient wind.

Surface friction effects on the atmosphere increase significantly after landfall. The ocean surface has less drag on the air than the solid land so the storm is able to sustain stronger peak surface winds over water. Land surfaces have a greater “roughness” (due to topography and natural and man-made structures) which leads to greater frictional drag and weaker winds.

These two mechanisms for slowing the surface winds take time to act. Any change in surface roughness (landfall or change in land use) will result in the formation of a new “internal” boundary layer that is in balance with the new surface. The new boundary layer will form in the timescale of an inertial period of the storm (about an hour in the strong wind part of the storm).

The ultimate impact of landfall on the surface winds depends on a variety of factors. For example, if the storm comes ashore in the coastal plains and river deltas of the Gulf of Mexico, the frictional effects will be much less than if it makes landfall in a mountainous place like Taiwan or Central America. Land use also matters: all else being equal, a heavily built-up or forested area will have a larger frictional effect than a swamp—and evaporation of moisture from the swamp may even delay weakening or (if the swamp water temperatures are comparable to the SST) even cause the storm to temporarily reintensify<sup>29</sup>, as occurred with Tropical Storm Helene (2000) and Hurricane Gaston (2004).

You might expect islands to have different effects on storms than a continental land mass. For example, the loss of surface energy source and the increased friction will have less impact for a tropical cyclone moving over an island than if it moved completely over land. The size of the island and its topographic scale will cause a range of impacts on the storm.

While post-landfall structure changes generally lead to a decrease in the near-surface wind speeds as described above, the roughness of the terrain can contribute to regions in which the winds experienced are stronger, but for shorter periods. While the storm still has convection, stronger winds from above the surface can be mixed down into the boundary layer causing local wind bursts.<sup>19</sup> Horizontal convective rolls in the boundary layer are similar to well known phenomenon in other fluids, e.g., lake flows. The convective rolls could also contribute to organized regions of preferred higher and lower surface winds. Another local effect can come from the winds being accelerated through narrow channels, whether these are mountain passes or buildings. None of the mechanisms for local increases in surface winds described here will increase the actual wind speed intensity on the storm scale: they are sources of local wind speed increases that may occur even as the storm weakens.



**Examples of Atlantic tropical cyclones observed to intensify over land**

Helene (2000), <http://www.nhc.noaa.gov/2000helene.html>

Gaston (2004), <http://www.nhc.noaa.gov/2004gaston.shtml>

The final effect of landfall on the tropical cyclone is the redistribution of its significant weather. The weakening pressure gradient causes a shift outwards in the region of boundary layer convergence, an associated redistribution of the convection and development of broad regions of stratiform rain feeding off the moisture transported onshore with the storm. At the edge of the rain shield, local regions of strong wind gusts may be associated with the outflow boundaries (the cool downdraft air accompanying the rain) leading to regions of damage far from the storm center. Other dangerous weather phenomena associated with landfall are tornadoes and lightning. The strong moisture gradient between the storm and its landfall environment and the vertical wind shear profile can create the ideal conditions for tornadic thunderstorms. Tornadoes generated with the passage of Hurricane Ivan (2004) caused major damage in Florida, even though the storm made landfall much further west. Lightning generated in the unstable coastal zone can also create a hazard (generally just offshore) to boating and the population near the coast.<sup>30</sup>

As with the frictional weakening of the storm, topography can play a role in these weather-related impacts: the topographic enhancement of the already intense rainfall associated with the storm. Hurricane Mitch (1998) is a terrible example of this combination of very intense rain with unstable mountain slopes leading to large-scale mudslides and loss of life (Box 10-12).

### 10.2.5 The Cyclone Phase Space (CPS) as a Measure of Storm Structure

To describe the structure of a cyclone in a concise way we often just label them “cold core” or “warm core” and give some indication of their intensity. While this is useful, it is a minimal description of the storm structure. After all, Tropical Storm Arlene and Hurricane Katrina were both warm-cored Atlantic storms in 2005 – but Arlene is barely remembered.

The *Cyclone Phase Space (CPS)*, developed by Robert Hart<sup>12</sup> is a concise, three-parameter summary of the structure of a storm. It can be used to describe the structure of any synoptic or meso-synoptic cyclone.

The purpose of the CPS is to distinguish between different types of cyclones. Key structural features that we commonly use to discriminate between different cyclones are symmetry and whether the system is warm cored (strongest winds near the surface) or cold cored (strongest winds near the tropopause).



Realtime CPS diagnostics for operational models and microwave satellite data (where available), <http://moe.met.fsu.edu/cyclonephase/>

#### **Applications suitable for CPS analysis**

Hurricanes Canadian Style, <http://www.meted.ucar.edu/norlat/ett/index.htm>

Diagnosing and Forecasting ET: Hurricane Michael (2000), <http://www.meted.ucar.edu/norlat/ett/michael/>

The three-parameters of the CPS are:

- **Lower-tropospheric symmetry,  $B$**  has this symbol since it indicates the baroclinicity in the region of the cyclone.
- **Lower-tropospheric thermal wind,  $-V_T^L$**  is *proportional* to the thermal wind in the 900-600 hPa layer. This parameter is plotted on the  $x$ -axis in both of the CPS standard views readily available on the web. The negative sign in the parameter name indicates that warm-core is to the right of the diagram (the opposite sign to that expected from the thermal wind calculated).
- **Upper-tropospheric thermal wind,  $-V_T^U$**  is calculated in the same way as  $-V_T^L$  but over the 600-300 hPa layer. This gives a measure of the upper-tropospheric strength of the system. The negative sign in the parameter name indicates that warm-core is to the right of the diagram as above.

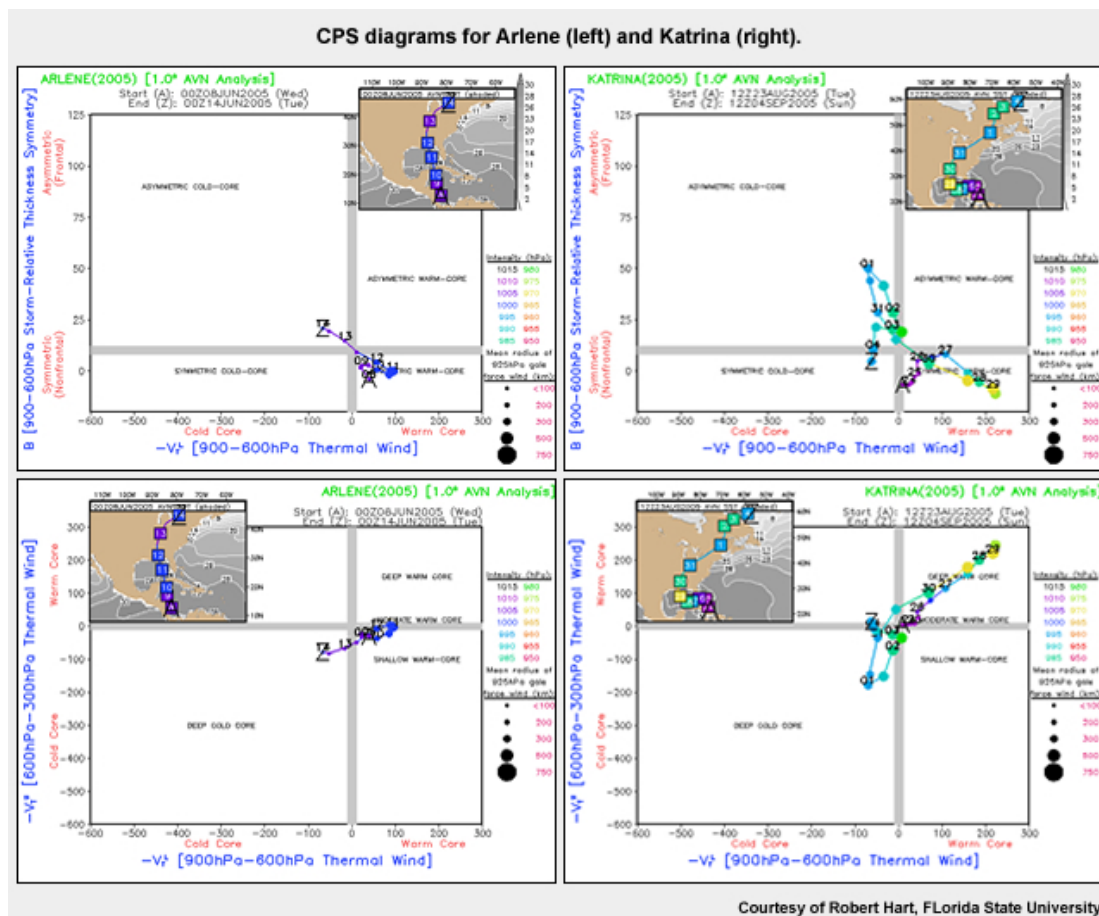


Fig. 10.14. CPS diagrams for Arlene (left) and Katrina (right). Top panels are  $B$  versus  $-V_T^L$  and lower panels are  $-V_T^U$  versus  $-V_T^L$  (see text for discussion of these parameters).



Background on the choice and meaning of the CPS parameters,  
<http://moe.met.fsu.edu/cyclonephase/help.html>

Phase space diagrams for these two hurricanes are provided in Fig. 10.14. Arlene is a weak warm core (signified by the short distance of her CPS path from the origin in the top figure and confirmed by a minimum central pressure 30 hPa higher than Katrina). Once Arlene moved over land, decreasing intensity is signified by the weak cold core and decreasing storm size in both panels. In contrast, Katrina became a very intense warm core (far right in both panels) before undergoing a rapid extratropical transition (ET) over land then attaining symmetric cold core structure in Canadian waters.

The utility of the CPS has been demonstrated for identifying the onset and completion of the transitions from subtropical to tropical cyclones<sup>31</sup> (Section 10.3.3.1) and from tropical to extratropical cyclones<sup>32</sup> (Section 10.7).

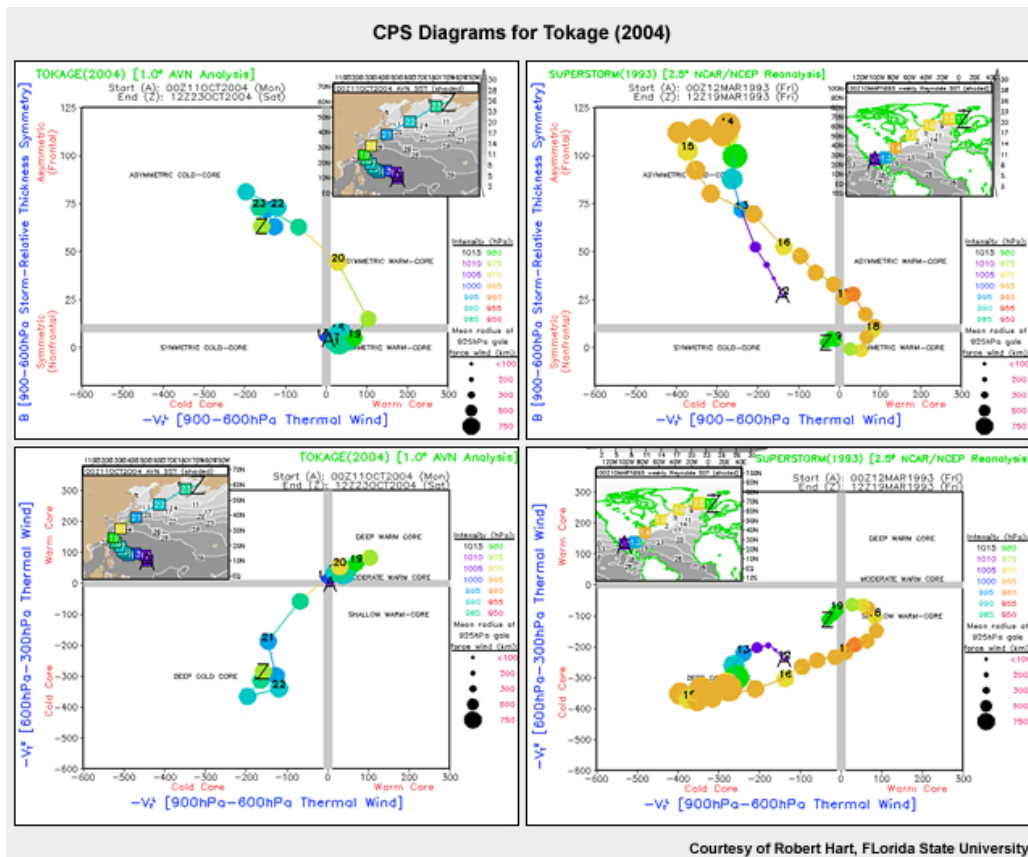


Fig. 10.15. CPS diagrams for Tokage (2004), a typhoon that underwent extratropical transition (left), and the extratropical Blizzard of 1993 (right). Top panels are B versus  $-V_T^L$  and lower panels are  $-V_T^U$  versus  $-V_T^L$ .

An example of the CPS representation of an extratropically transitioning tropical cyclone contrasted with an intense extratropical cyclone is given in Fig. 10.15. Notice that the ET Tokage event begins as warm core and transitions to cold core, while the super storm blizzard event begins as cold core and becomes warm cored as it occludes.

## 10.3 Tropical Cyclogenesis

What is tropical cyclogenesis? Surprisingly, there is no single answer to this question. Operational forecast centers responsible for issuing tropical cyclone watches and warning define genesis as observed sustained mean surface winds (averaging time is dependent on region) in excess of tropical storm force ( $17 \text{ m s}^{-1}$ ;  $60 \text{ km h}^{-1}$ ; 33 knots). While this is a readily applied and unambiguous criterion for tropical storm formation, it is not particularly helpful in understanding the processes leading to genesis. However, implicit in this operational genesis criterion is the expectation that the tropical storm will continue to develop from this point forward; that is, *that the storm will become self-sustaining*. This is the definition of genesis that we will use here: tropical cyclogenesis has occurred when the tropical storm has become self-sustaining and can continue to intensify without external forcing.

### 10.3.1 Necessary Conditions for the Formation of a Tropical Cyclone

Six features of the large-scale tropics were identified by Gray (1968)<sup>33</sup> as *necessary, but not sufficient* conditions for tropical cyclogenesis:

- (i) sufficient ocean thermal energy [SST  $> 26^{\circ}\text{C}$  to a depth of 60 m],
- (ii) enhanced mid-troposphere (700 hPa) relative humidity,
- (iii) conditional instability,
- (iv) enhanced lower troposphere relative vorticity,
- (v) weak vertical shear of the horizontal winds at the genesis site, and
- (vi) displacement by at least  $5^{\circ}$  latitude away from the equator.

The first three thermodynamic parameters measure the ability to support deep convection—criteria that have been identified as seasonal indicators of genesis potential. The latter, dynamical parameters, such as vertical wind shear (Fig. 10.16), measure the daily likelihood of genesis.<sup>34</sup> In recent years, a number of tropical cyclones have remained within  $5^{\circ}$  latitude of the equator, suggesting a need to relax this constraint. Many, but not all, of those near-equatorial systems had very small spatial scale. Locations where conditions (i) and (v) are satisfied are highlighted in Fig. 10.17.

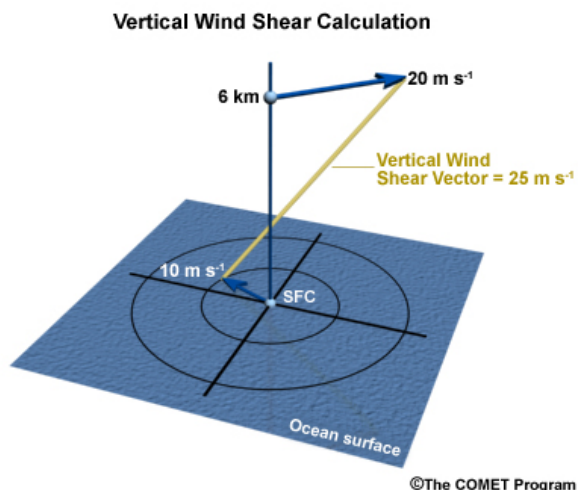
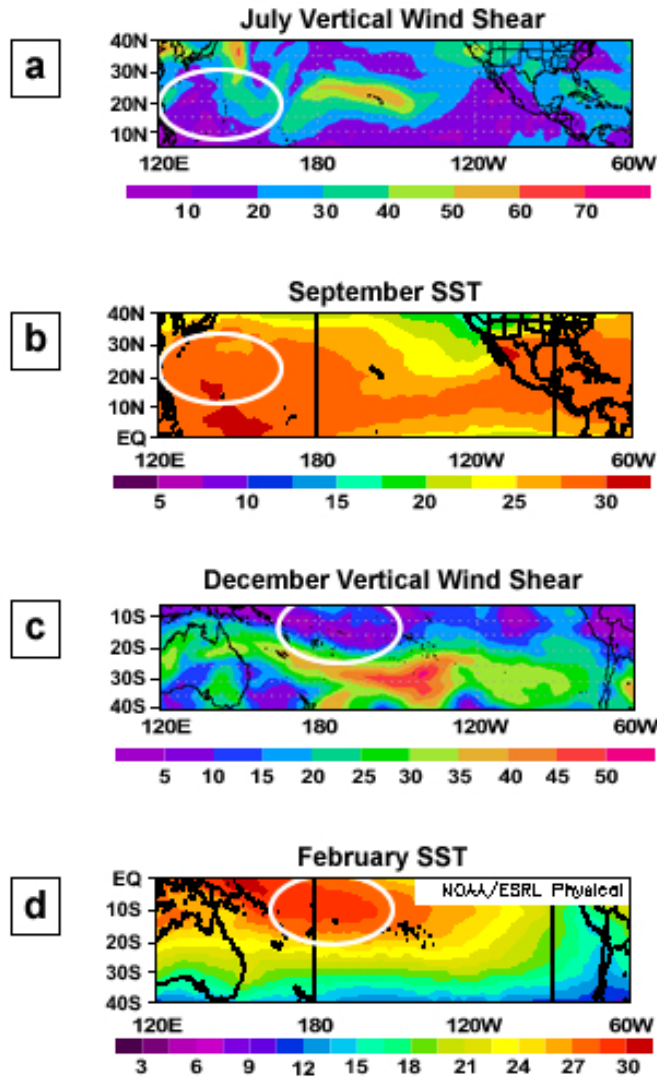


Fig. 10.16. Example of vertical wind shear calculation.

Monthly diagnostics of 850-200 hPa vertical wind shear (1958-2002 in  $m s^{-1}$ ) and sea surface temperature (1977-2006 in  $^{\circ}C$ )



NOAA/Data courtesy of ECMWF ERA-40

Fig. 10.17. Monthly diagnostics of vertical wind shear and sea surface temperature — parameters that are used to identify regions where tropical cyclogenesis is likely. White ovals mark locations where the vertical wind shear and SST favor tropical cyclogenesis.

“Necessary but not sufficient” means that all of these conditions must be present simultaneously before tropical cyclogenesis can occur, but even if all of these conditions are met, tropical cyclogenesis may not occur. *Thus, the necessary, but not sufficient, criteria for tropical cyclogenesis may be summarized as the ability to support deep convection in the presence of a low-level absolute vorticity maximum. The low-level vorticity maximum reduces the local Rossby radius of deformation<sup>d</sup> focusing the convective heating locally.*

The ability of the initial convection to survive for many days depends on its vorticity, stability, and depth—defined by the *Rossby radius of deformation*,  $L_R$ . The Rossby radius,  $L_R$ , is the critical scale at which rotation becomes as important as [buoyancy](#). When the disturbance size is wider than  $L_R$ , it persists; systems that are smaller than  $L_R$  will disperse (Fig. 10.18).  $L_R$  is inversely proportional to latitude so it is very large in the tropics. However, the high vorticity in tropical cyclones reduces the Rossby radius and enables tropical cyclones to last for many days and even weeks.

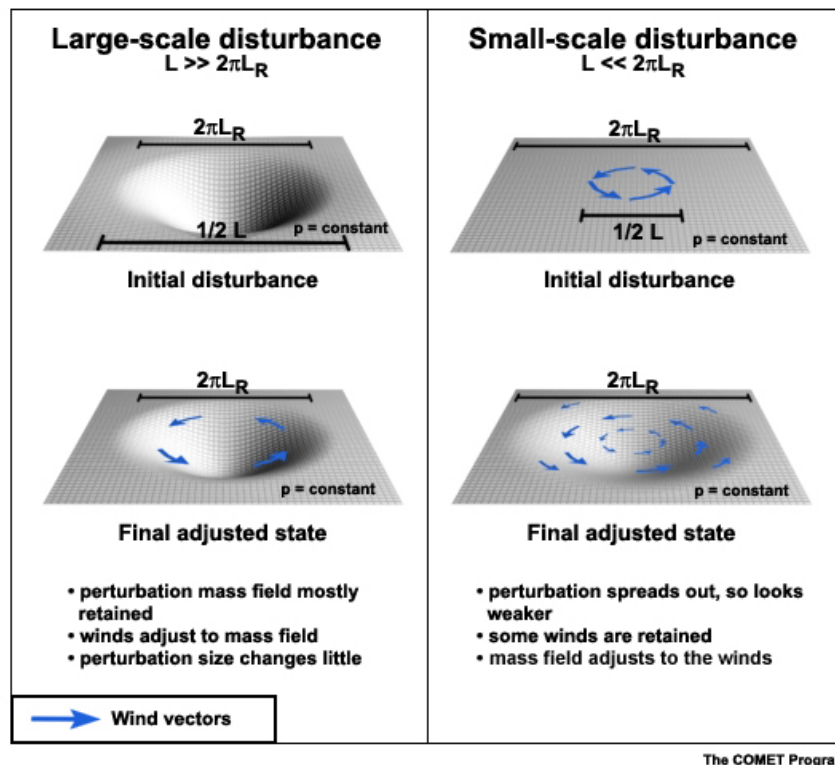


Fig. 10.18. Adjustments based on size relative to the Rossby radius of deformation,  $L_R$ .

<sup>d</sup> The Rossby radius of deformation for a continuously stratified fluid,  $L_R = \frac{NH}{f_0}$

where  $N$  is the Brunt Väisälä frequency,  $H$  is the depth of the system and  $f_0$  is the Coriolis parameter. For a weather system with large relative vorticity, such as a tropical cyclone,  $L_R$  can be generalized as

$$L_R = \frac{NH}{\zeta + f_0} \text{ where } \zeta \text{ is the vertical component of the relative vorticity.}$$

For more information on the Rossby radius of deformation, see the COMET module, The Balancing Act of Geostrophic Adjustment, [http://www.meted.ucar.edu/nwp/pcu1/d\\_adjust/](http://www.meted.ucar.edu/nwp/pcu1/d_adjust/).

This broad description of tropical cyclone development forms the basis of the *Conditional Instability of the Second Kind (CISK)*,<sup>35,36</sup> *Wind-Induced Surface Heat Exchange (WISHE)*,<sup>18</sup> and “*free ride*” *CISK*<sup>37</sup> theoretical models.

While improved observations and field campaigns allow for better resolution of the mesoscale details of formation, the question remains as to whether it is possible to identify an individual incipient disturbance that will develop into a tropical storm, or if larger scale environmental forcing is the crucial factor for development.<sup>38,39</sup> A number of synoptic- and meso-scale influences on tropical cyclogenesis have been newly identified and documented in recent years. As the finer scale features of genesis become better understood and simulated, we can assess our potential for identifying an incipient disturbance that will develop into a tropical storm.

Why are the numerical models unable to help us forecast genesis? While anecdotal evidence for skill in operational model simulations of tropical cyclogenesis is beginning to emerge, we need to find ways to test the accuracy of numerical model genesis forecasts quantitatively (carefully checking how many storms are forecast and missed). Advances in theoretical understanding and observational analysis of tropical cyclogenesis suggest new diagnostics of genesis potential applicable to analysis of the operational models. So we can combine our new understanding of the processes leading to genesis in the atmosphere with measures of forecast skill to assess our progress in genesis forecasting.



### 10.3.2 Dynamic Controls on Genesis in the Monsoon Trough Environment

In most basins, the monsoon trough is the most common region for genesis, so we begin with a review of the controls on tropical cyclogenesis in the monsoon trough environment. A new way of looking at the tropical western North Pacific<sup>40</sup> is to partition its large-scale tropical environment into a monsoon trough zone and an ITCZ zone, separated by a confluence zone (Fig. 10.19). The monsoon trough zone is characterized by the near-equatorial seasonal westerly winds and enhanced rainfall. Lower tropospheric vorticity in the monsoon trough zone is derived from the cyclonic circulation that results from the incursion of the monsoon westerlies. In contrast, the ITCZ zone is dominated by trade easterlies throughout; these low-level easterlies converge in the ITCZ convective trough. The transition zone between the near-equatorial monsoon westerlies and ITCZ trade easterlies is known as the confluence zone. This combination of features—monsoon trough, confluence zone, and ITCZ—will be referred to here as the monsoon region.

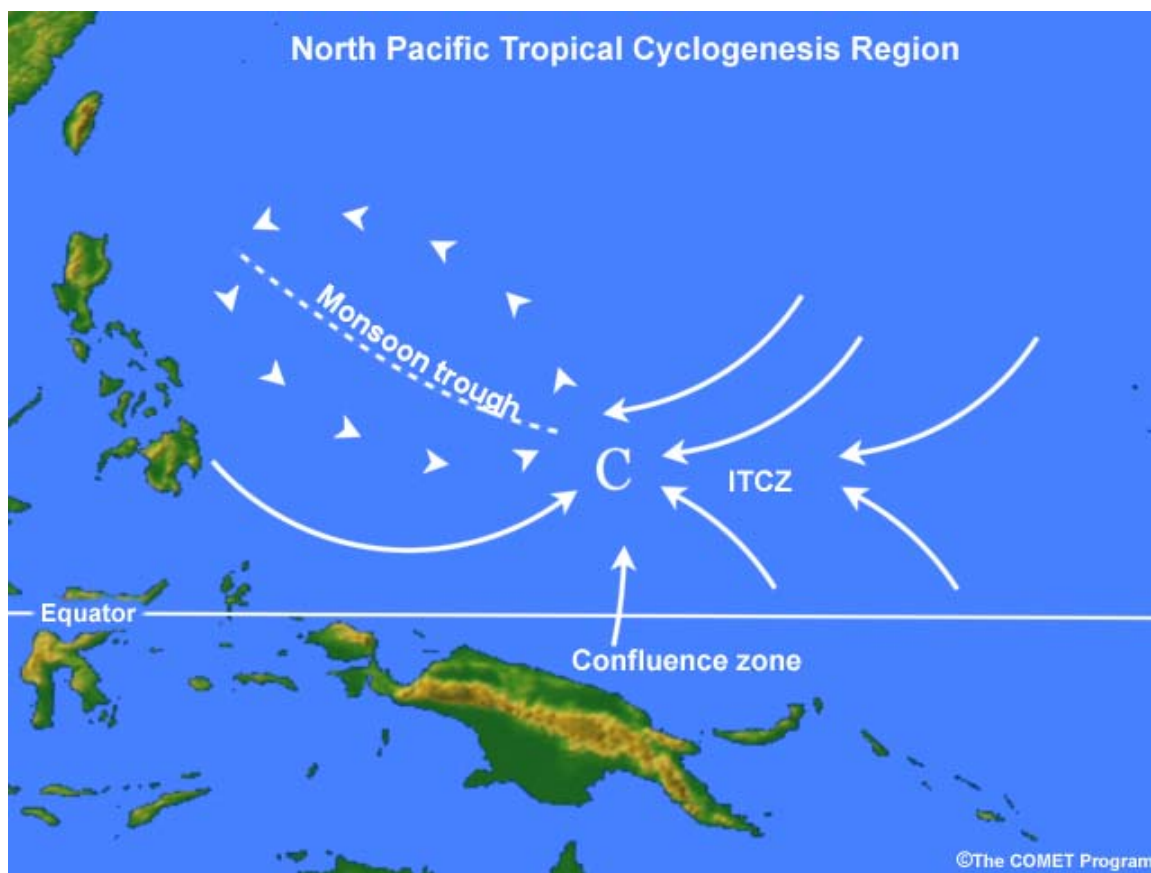


Fig. 10.19. Schematic of the western North Pacific tropical cyclogenesis region partitioned into a monsoon trough zone and the near-equatorial ITCZ, meeting at a confluence zone (following Briegel and Frank 1997).<sup>40</sup>

We have known for over thirty years that the monsoon region provides an ideal environment for tropical cyclogenesis,<sup>41</sup> but recent elucidation of different modes of genesis has led us to re-examine our understanding of genesis in the monsoon region. The new modes of genesis to be discussed here are summarized graphically in a flow chart (Fig. 10.20). After familiarizing ourselves with these different modes of genesis, we will look at two competing studies that assessed the relative importance of all of the known paths to genesis in the monsoon region.

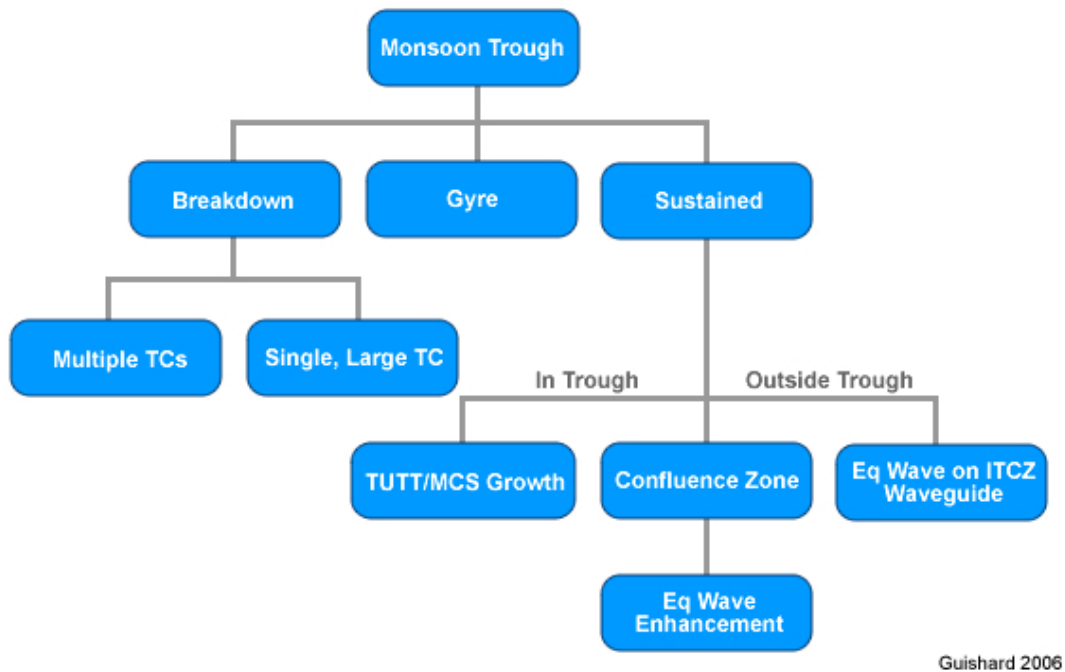


Fig. 10.20. Flow chart delineating pathways to tropical cyclogenesis associated with different modes of the monsoon trough.<sup>40</sup>

### 10.3.2.1 Tropical Cyclogenesis Associated with the TUTT

Mesoscale convective systems (MCS) are organized clusters of convection. We know from the six necessary (but not sufficient) conditions for genesis that organization of convection is one step on the path to tropical cyclone formation, so we are interested in MCS in the tropics. Increasing organization of MCS in the 72 h prior to genesis is observed in monsoon region developments and supports the hypothesis of mutual interaction between a mesoscale vortex and large-scale flow.<sup>38,42,43</sup> In the confluence zone (Fig. 10.21), genesis may be initiated through easterly waves that propagate into the region, possibly interacting with a Tropical Upper Tropospheric Trough (TUTT). The TUTT is a meso-synoptic upper cold low that has been identified as an aid to genesis in the western North Pacific. It can be identified on satellite imagery as a clear region with widely scattered, small convective cells. Both the presence of the equatorial wave<sup>44,45,46,47</sup> and the possible interaction with the TUTT<sup>48,49</sup> will locally enhance low-level convergence and thus moist convection, providing a favorable environment for tropical cyclogenesis. Some investigations of tropical cyclogenesis<sup>42</sup> do not link the TUTT to tropical storm formation, however the geographically-fixed compositing technique used may have resulted in a washing out of any TUTT signature. Tropical cyclones have also been proposed as a mechanism for the *formation* of TUTT cells<sup>43</sup> and that this formation is preconditioned by the large-scale environmental shear. Thus, the TUTT could be a consequence, rather than a driver, of the tropical cyclogenesis.

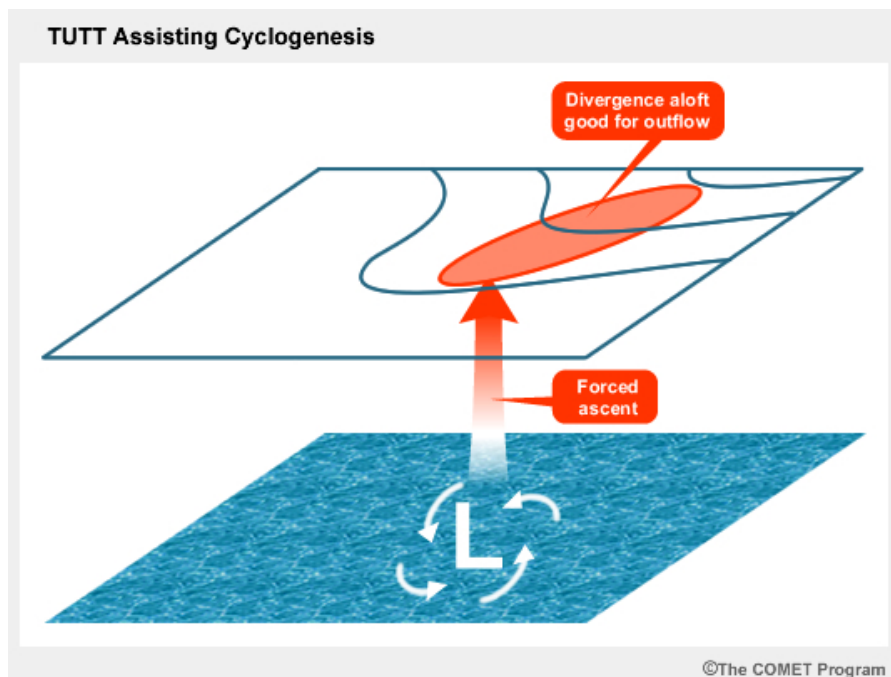


Fig. 10.21. Contribution of the TUTT to tropical cyclogenesis. The TUTT forces ascent in the region of the developing tropical cyclone, but provides very little vertical wind shear increasing the storm convection and strengthening the upper-level outflow of the storm. This can enhance the tropical cyclone development.

### 10.3.2.2 Alternative Monsoon Trough Modes

Three potential paths to tropical cyclogenesis in the monsoon region of the western North Pacific have been newly identified:<sup>40</sup> two distinct modes of monsoon trough breakdown<sup>50</sup> and monsoon gyres.<sup>51</sup>

A straightforward potential vorticity (PV) model for the Hadley cell provides ample evidence that the continuous PV source associated with convection in the ITCZ will act to destabilize and break down the ITCZ periodically<sup>50</sup> through combined barotropic-baroclinic instability. Two outcomes can result from the barotropic mode of ITCZ instability and associated monsoon trough breakdown: formation of a group of several tropical cyclones, or re-symmetrization and development of one, larger, tropical cyclone<sup>52</sup> (Fig. 10.22). As the figure shows, the shape of the initial PV strip used to characterize the ITCZ, as well as the presence of another cyclone, affect which mode of breakdown occurs. The presence of an additional cyclonic vortex in the ITCZ sped its breakdown.

The monsoon gyre is defined as a closed, symmetric circulation at 850 hPa with horizontal extent of 25° latitude that persists for at least two weeks.<sup>51</sup> This circulation is accompanied by abundant convective precipitation around the south-southeast rim of the gyre. The gyre has similar scale and structure to the second mode of the barotropic monsoon trough breakdown and genesis just described (Fig. 10.22b). We cannot yet say whether the gyre is this monsoon breakdown or a distinct path to genesis, however two studies<sup>40,42</sup> of the frequency of different paths to genesis in the monsoon regime suggest that the gyre is a rare path to genesis. One study found formation in the gyre occurred about 6% of the time—and the other did not even classify separately! However, once the gyre was present, six cases of genesis occurred in a three-week period,<sup>40</sup> so it is worth knowing about the gyre.

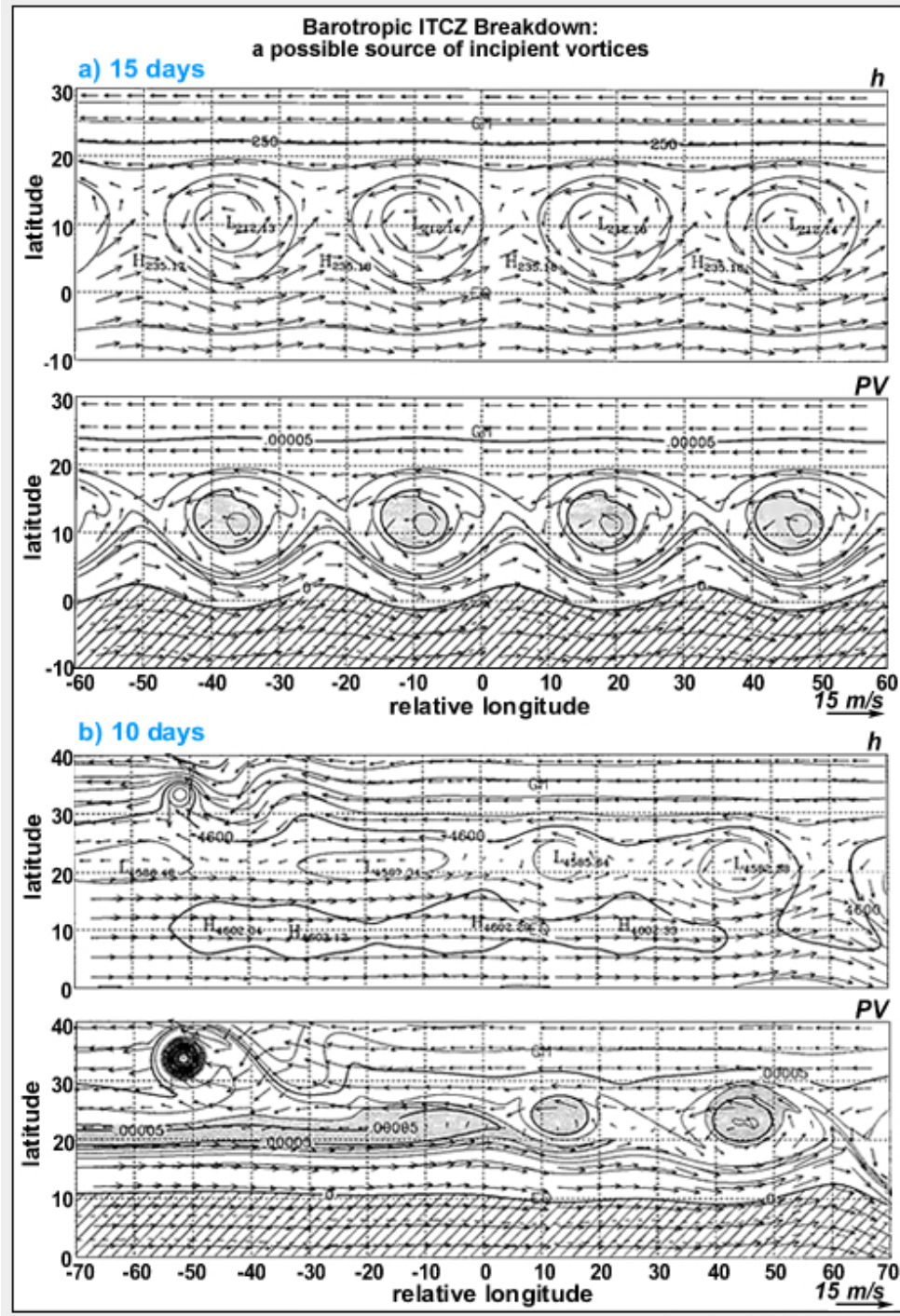


Fig. 10.22. Barotropic ITCZ breakdown simulations from (top two panels) breakdown of the convective ITCZ in isolation; and (lower two panels) accelerated breakdown of the convective ITCZ in the presence of an existing tropical cyclone. The top panel in each pair is equivalent depth and the lower panel is potential vorticity. (Ferreira and Schubert<sup>52</sup>).

### 10.3.2.3 Equatorial Waves

Twin tropical cyclones that straddle the equator<sup>53</sup> at formation have a flow structure suggestive of equatorial Rossby waves<sup>54,55</sup> (Fig. 10.23).

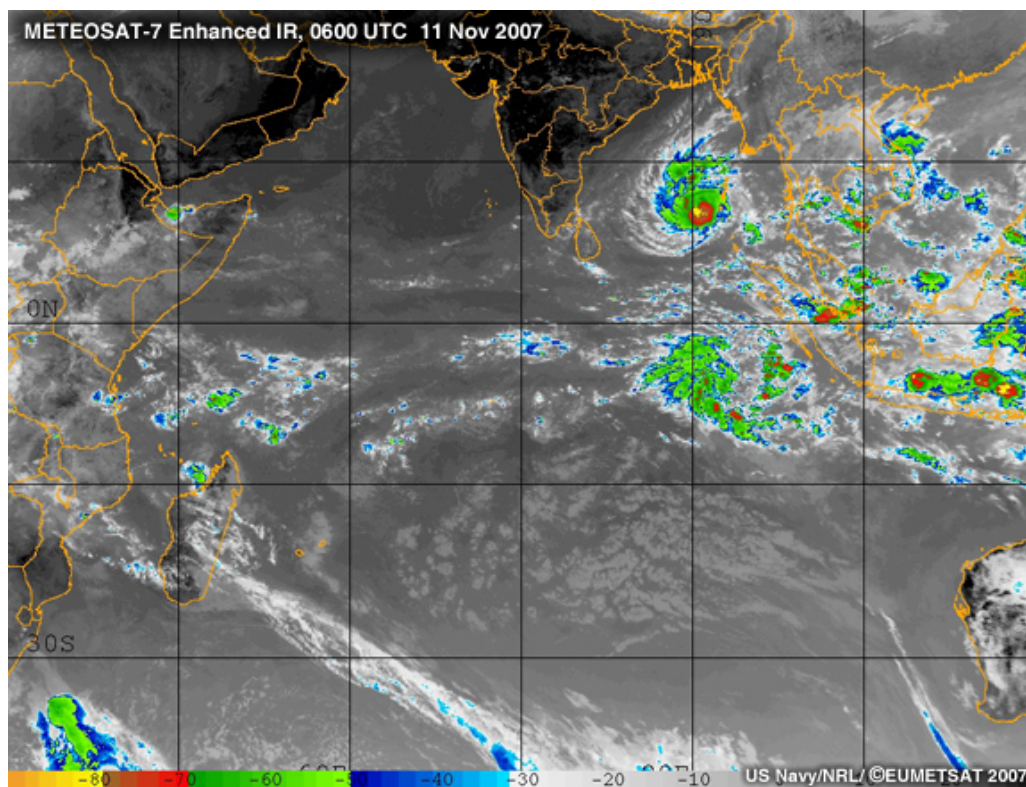


Fig. 10.23. Enhanced IR image at 0600 UTC 11 Nov 2007 of NH and SH twin tropical cyclones, indicative of equatorial Rossby wave genesis.



[Animation of twin tropical cyclogenesis](#)

While the case depicted in Fig. 10.23 is evidence that equatorial Rossby waves may initiate genesis, others argue that the shorter wavelength mixed Rossby-gravity waves are also important. In one study<sup>44</sup> a mixed Rossby-gravity wave packet with slow eastward group velocity (and westward phase speed of individual waves within this wave packet) was demonstrated to be a fertile environment for genesis.

The easiest way to spot the difference between equatorial Rossby and mixed Rossby-gravity waves in satellite imagery is that Rossby waves mirror themselves across the equator (Fig. 10.23) while mixed Rossby-gravity waves alternate (Fig. 10.24). We see the waves marked by convection in the satellite images, so the effects of convection on these waves must be taken into account if we are going to use these ideas in the real world.

Let us consider evolution of the mixed Rossby-gravity waves: a dry mixed Rossby-gravity wave packet (Fig. 10.24, upper panel), will be modified by moist convection (middle). Moist convection interferes directly with the dry mixed Rossby gravity wave

dynamics contributing to the longitudinal asymmetries evident in the satellite image (Fig. 10.24, lower panel).

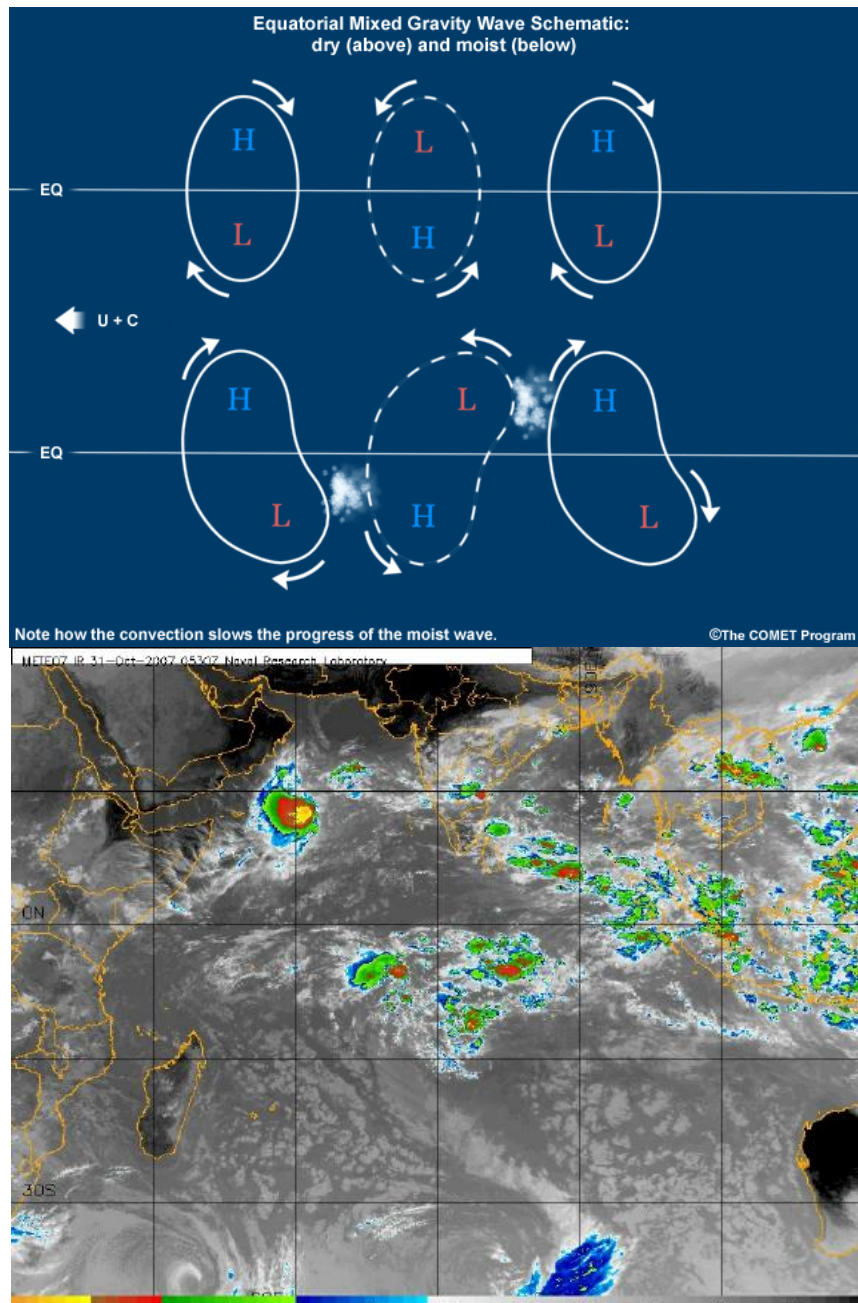



Fig. 10.24. Equatorial mixed Rossby-gravity waves: a) schematic of pressure and wind anomalies for an idealized dry (upper) and moist (lower) MRG wave. Convergence zones are indicated by the clouds. Convection distorts the wave signature and slows its movement. (b) Satellite imagery of an equatorial MRG wave at 1800 UTC 31 Oct 2007 illustrates the impact of the convection on the wave structure. The animation (linked below) shows the westernmost convection center of the wave moving northwards east of Somalia as weakening Tropical Cyclone 05A.

 [Animation of MRG wave](#)

One important feature that we need to remember is that the dry theory tells us that these waves are trapped at the equator due to conservation of PV—the equator is a region of maximum PV gradient.

So we know that mixed Rossby gravity waves will alternate across the equator, but why should they look different at different longitudes (Fig 10.24)? The waves in the eastern part of the domain remain equatorially trapped and symmetric across the equator, but the pattern changes further west. The pattern of convection in the tropics reveals another source of modification to the classic mixed Rossby-gravity wave solution: the presence of a “dynamic equator”, the ITCZ.

In our discussion of the monsoon region modes of genesis, we described the monsoon region as having high PV and convective activity. The dynamic equator, the ITCZ, is part of this monsoon region. Particularly in the western North Pacific, the dynamic equator is well north of the geographic equator. As a result, the highest PV is in the narrow strip of the ITCZ. This means that the highest PV gradients will also be in this region. So, rather than moving along the actual equator, “equatorial” mixed Rossby-gravity waves can undergo a transition in the western part of the basin and track northwestward along the “dynamic equator” associated with convectively-forced PV development in the western Pacific ITCZ. A region of active convection forms on the northwest side of a near-equatorial wave trough (in the region of maximum low-level convergence for a mixed Rossby-gravity wave). This convective region moves away from the equator and may eventually develop into a tropical storm. The ultimate formation of a tropical depression is attributed to enhanced Ekman pumping<sup>56</sup> in the evolving depression (consistent with CISK or free ride development).<sup>35,36,37</sup>

Numerical modeling studies using barotropic models have examined the non-linear evolution of wave activity over the western North Pacific in association with the background confluent flow (recall the confluence zone in Fig. 10.19). If waves with wavelengths near 2000 km are continuously generated upstream (to the east in the deep tropics), their energy will accumulate in the confluence zone. This results in a scale contraction of short Rossby waves contributing to the formation of an incipient vortex that may become a tropical cyclone. This process may contribute to a sequence of vortex formations in the confluent eastern end of the western North Pacific monsoon region.

The western North Pacific does not hold the monopoly on equatorial waves: preferential wave growth also occurs in the dynamically unstable and convectively active eastern Pacific ITCZ.<sup>44</sup> Two hypotheses have been advanced to explain the maintenance of the mean meridional PV gradient here: either convectively-forced PV generation; or cross-equatorial advection of absolute vorticity driven by high cross-equatorial pressure gradients in the ITCZ region.<sup>57</sup> In the second scenario, convection is a consequence of the dynamic instability, rather than its driver, consistent with the temporal lag between the convective heating and the peak in the PV gradient.<sup>58</sup>

The seasonality of tropical cyclogenesis has been related to the convective potential of the region being considered, while dynamical factors contribute to the daily potential for genesis.<sup>34</sup> Regions of observed tropical cyclogenesis are associated with preferred wave



growth (along the equator or the “dynamic equator” associated with the ITCZ) or the monsoon region. The unifying dynamical characteristic of these regions is a sign reversal of the meridional gradient of the large-scale PV. This PV gradient reversal satisfies the Charney-Stern condition for dynamic instability.<sup>59</sup>

#### 10.3.2.4 African Easterly Waves (AEW)

African easterly waves (Fig. 10.25) initiate tropical cyclogenesis in both the North Pacific and North Atlantic Oceans. They form over the African continent during the monsoon season. Easterly waves are well defined wave perturbations with periods of roughly 3–5 days and spatial scale about 1000 km. They occur as waves with maximum amplitude close to the level of the African Easterly Jet (AEJ) and low-level maximum amplitude north of the jet. They move westward at speeds of 7–8 m s<sup>-1</sup>.

Mesoscale convective systems move with and through the synoptic-scale AEWs (Fig. 10.25b). Some tropical cyclones, such as Alberto (2000), began as AEW-MCS systems that initiate near the mountains of East Africa (the Darfur Mountains and Ethiopian Highlands) and move westward while undergoing cycles of regeneration of convection. A few of these systems evolve into tropical cyclones close to the African coast, e.g., Cindy (1999) and Helene (2006); (see Fig. 10.25b for images of Helene). The swirling cloud pattern at 1200 UTC 8 September and 1800 UTC 10 September (Fig. 10.25b) indicate the presence of a mesoscale convective vortex, a feature that sometimes forms in the stratiform region of decaying MCSs. The pre-Helene vortices appear to amplify over the continent within the AEW structure, a strong vortex emerges from the continent, and tropical cyclogenesis occurs soon after. The observations support the notion that mesoscale convection is a source of potential vorticity for tropical cyclogenesis. The interaction of the vorticity associated with AEWs and the mesoscale vorticity associated with MCSs is being studied in order to differentiate between strong and weak AEWs and the implications for tropical cyclogenesis. Mesoscale influences on tropical cyclogenesis are explored further in Section 10.3.3.

While African easterly waves tend to weaken and lose their convection in the central Atlantic, they are often reinvigorated as they pass through the Caribbean, gaining sufficient energy to complete their trek into the eastern Pacific. Indeed, tropical cyclone developments for the 1991 eastern Pacific season were preferentially downstream of inertially unstable zones (such as the Caribbean) consistent with the continued progression of equatorial waves across the Western Hemisphere tropics.<sup>58</sup>

Easterly waves form in an environment similar to the first “multiple storm formation” mode of genesis pictured in Fig. 10.22 (upper panels), giving us confidence that this barotropic model captures the important physics of genesis here. So the multiple storm formation mode of genesis appears to be present in the African monsoon. Since other monsoon regions have very similar PV and convection structures,<sup>60</sup> we expect that Africa should not be a unique region for easterly wave formation.<sup>50</sup> This suggests that similar disturbances could also be generated in the Australian monsoon. Are easterly waves African then, or are they an international phenomenon?

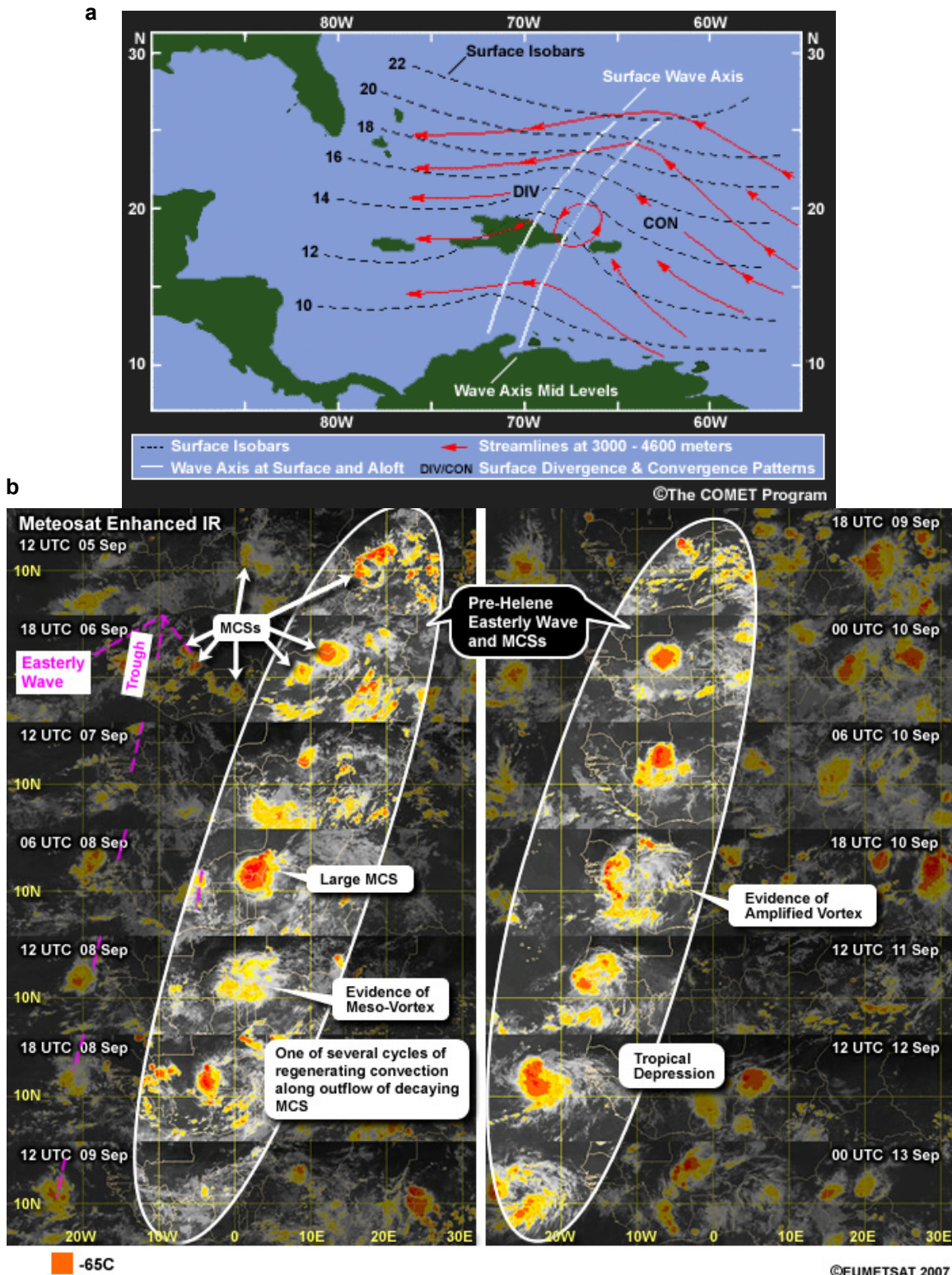


Fig. 10.25. (a) Schematic of an African easterly wave illustrating: the “inverted V” structure; surface isobars (dark dash); 700 hPa streamlines (red); regions of surface convergence and divergence; and eastward tilt of the wave with height (white lines with upper trough axis to east). (b) Enhanced IR images of waves and MCSs between 1200 UTC 5 Sep and 0000 UTC 13 Sep 2006.

A study assessing the potential for easterly wave formation in Australia compared to Africa<sup>60</sup> found a 2–6 day peak in the variance of the African monsoon [outgoing longwave radiation (OLR) and low-level winds] consistent with easterly wave activity,<sup>61</sup> but no corresponding peak in the Australian data even if the criteria were relaxed.




What could cause the lack of easterly wave activity in Australia?



[Satellite animation of easterly waves and tropical cyclones in the North Atlantic 2005](#)



COMET webcast, Conceptual Models of Tropical Waves,  
<http://www.meted.ucar.edu/meteoforum/tropwaves/>

 Three possible reasons for the lack of easterly waves in Australia have been suggested so far:<sup>60</sup> (1) the extent of Australian monsoon (PV gradient) region is only 60% of the African; (2) the lack of topography in Australia could lead to a weaker easterly jet; (3) or the stability of the Australian flow pattern damping out the waves.

So it looks, for now, like Africa is unique as a source for easterly waves.

### 10.3.2.5 Surveys of Observed Mechanisms for Tropical Cyclogenesis in the Monsoon Region

Two studies surveying the genesis locations and associated mechanisms for western North Pacific tropical cyclogenesis were somewhat inconclusive (Fig. 10.26). In agreement with previous studies,<sup>41</sup> genesis in the monsoon trough was dominant with 42–44% of storms forming there (Fig. 10.26). The influence of the confluence zone was another dominant factor in regional tropical cyclogenesis with 29–34% of storms identified as forming there (Fig. 10.26). Genesis in the confluence zone may be separated by as little as 5–7 days. This repeated genesis in the confluence zone was attributed to preconditioning of the low-level flow (increased convergence of tropical moisture) by the maturing storm as it moves away. An alternative explanation for this repeated genesis is the wave energy accumulation in a region of confluence on the dynamic equator described above. In either case, the confluence zone implicated here as a critical region for tropical cyclogenesis. The contribution of easterly waves in western North Pacific remained unclear: as few as 2% and as many as 18% of genesis events were attributed to this mechanism (Fig. 10.26). A second study<sup>42</sup> included a variety of additional mechanisms for tropical cyclogenesis including wave energy dispersion and monsoon gyres (Fig. 10.26).

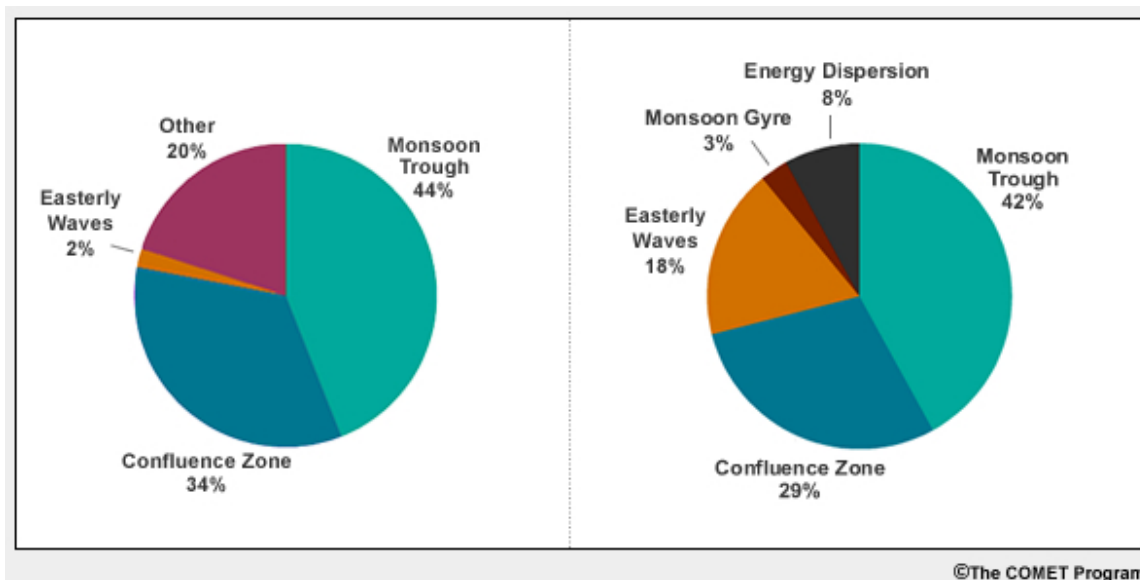


Fig. 10.26. Pie charts outlining the different pathways to tropical cyclogenesis identified by Briegel and Frank<sup>40</sup> (left) and Ritchie and Holland<sup>42</sup> (right).

It is likely that there are real and significant differences between these two surveys: they encompass largely independent time periods: 1988–1989<sup>40</sup> and 1984–1992 (excluding 1989).<sup>42</sup> Much of this discrepancy may be due to interannual variability, such as impacts of the *El Niño Southern Oscillation (ENSO)* on tropical cyclogenesis.

### Box 10-4 They Lived to Tell the Tale!

The roots of this story are a little unclear, but one version states that a group of pilots, including Lt Col Joe Duckworth, were comparing the abilities of their planes. At that time, Duckworth was on assignment training pilots to fly AT-6 aircraft in bad weather. Duckworth maintained that his aircraft could even survive a hurricane. On a dare, he and navigator Ralph O'Hair flew into a hurricane in the Gulf of Mexico. This was the first recorded *intentional* flight into a tropical cyclone!

According to National Weather Service records, Duckworth and O'Hair must have flown into the first recorded storm for 1943 (storms were not named until 1950). This storm later made landfall in Texas as a Category 2 hurricane.

The tradition begun by Duckworth and O'Hair continues to this day: the 53<sup>rd</sup> Weather Reconnaissance Squadron of the Air Force Reserve (commonly known as the "Hurricane Hunters") and the NOAA Corps continue operational and research flights into hurricanes today.



#### Observing hurricanes

Hurricane Hunters, <http://www.hurricanehunters.com/>

(Air Force Reserve 53<sup>rd</sup> Weather Reconnaissance Squadron, [403rd Wing](#), [Keesler Air Force Base](#))

NOAA Aircraft Operations Center, <http://www.aoc.noaa.gov/index.html>

NOAA Corps, <http://www.noaacorps.noaa.gov/>

### 10.3.3 Mesoscale Influences on Tropical Cyclogenesis

In this discussion, we examine the mesoscale features in the environment that can generate an incipient tropical cyclone vortex and sustain it until genesis takes place. Mesoscale influences on tropical cyclone formation include effects contributing to (or limiting) the creation of the incipient vortex or disturbance and the eventual survival of that vortex.

Monsoon depressions,<sup>62</sup> African easterly waves,<sup>46</sup> and subtropical cyclones<sup>63</sup> have long been understood to provide source disturbances from which, under appropriate thermodynamic conditions, a tropical cyclone could develop. While the tropical eastern Pacific is widely recognized as being a very active region of tropical cyclogenesis, explanations for many of the paths to tropical cyclogenesis in this region have only been forthcoming in the last decade.

#### 10.3.3.1 Development of Mesoscale Incipient Vortices from Subtropical Storms

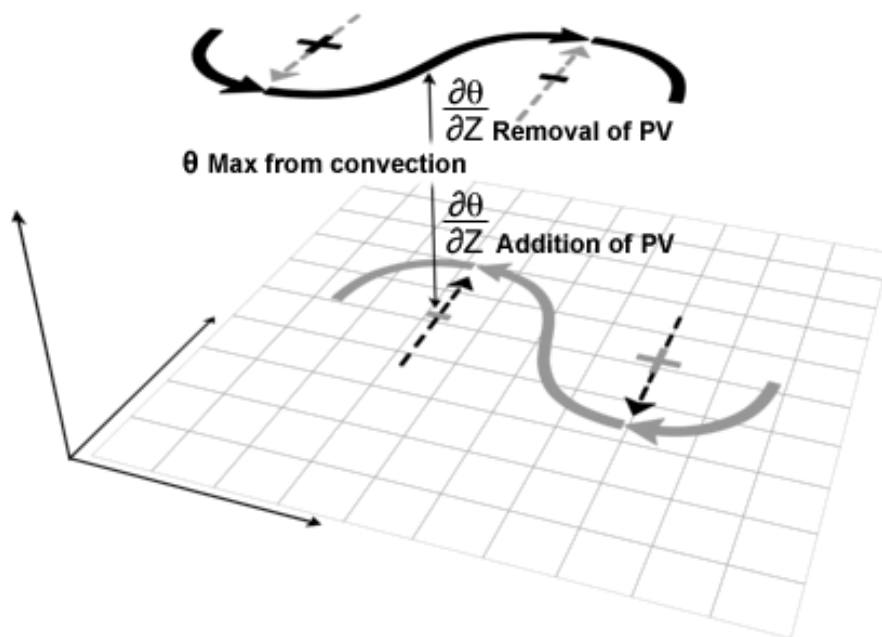
The mechanisms responsible for tropical cyclone formation from mesoscale convective systems (MCS) have only recently been elucidated. In this process, a deep warm-cored cyclone must be created from a shallow, mid-level vortex (cold-cored in the lower-troposphere).<sup>38,64,65</sup>

The mid-level vortex must build down toward the surface to generate the surface inflow and increased surface fluxes needed for subsequent development.<sup>18,37</sup> One hypothesis is that the vortex builds downward through buoyantly-driven, flow relative to the vortex, which advects high PV air downward along isentropic surfaces.<sup>65</sup> Once the surface winds respond to the downward building vortex, surface fluxes can increase the  $\theta_e$  of air inflowing towards the nearly saturated core of the developing system, and provide source air for the “hot towers” of the eyewall.<sup>64</sup> The system is now self-sustaining and can develop independent of its environment.

The need for moistening in the region of the incipient mid-level vortex provides a clue to the large-scale condition of low vertical wind shear. Minimal vortex-relative flow allows for local moistening to be most efficient, promotes more rapid development of the initial disturbance, and minimizes the chance that negative environmental influences will destroy the system.<sup>38,65</sup> Thus, the development of a mid-level vortex into a tropical cyclone requires weak vertical wind shear in a convective and moist environment—in the presence of a relative vorticity maximum. So, the necessary but not sufficient conditions for tropical cyclogenesis<sup>66</sup> must still be satisfied in this more unusual path to genesis.

Three phases of internal development were identified in studies<sup>67,68,69</sup> of the development of Hurricane Diana (1984) from an initially subtropical system. First, a subtropical vortex initially spun up at the equatorward extreme of a quasi-stationary front; second, the transformation from cold to warm core occurred through interactions with an upper-level trough-ridge couplet forcing convectively-generated PV anomalies on the poleward side of the vortex and these PV anomalies mixed into the vortex center; and third the storm intensity was sustained immediately after transition to warm core as the convective

structure [spiral bands] became organized. At last the storm intensified as a tropical system, developing a clear eye.



Guishard 2006

Fig. 10.27. Schematic of upper and lower PV perturbation waves undergoing baroclinic growth as an initially subtropical system with convective heating between the layers modifying the system by diabatic rearrangement of PV. Adapted from Fig. 47 of Guishard (2006).<sup>72</sup> Based on the results of Guishard<sup>72</sup> and Davis and Bosart.<sup>67,69</sup>

These three stages must be related to the physics of the evolution of the baroclinically-induced mesoscale vortex into fully warm core tropical cyclone.<sup>70,71</sup> This PV rearrangement is illustrated in Fig. 10.27.

First, a deep cold core trough (black +) in the upper westerlies moves into the region, causing a sign reversal in the vertical PV gradient to its poleward side. This PV sign reversal satisfies one condition for baroclinic instability, and the approach of the trough from the west fulfils the criterion that the vertical offset of the PV anomalies is opposite to that of the vertical shear of the system.<sup>59</sup> In the event that the upper and lower systems are phase locked, the third criterion for baroclinic instability is satisfied, and a reflection of the upper PV anomaly may develop near the surface (grey +). This may be accomplished by the upper trough breaking off from the westerlies, i.e., a Rossby wave break.<sup>72</sup> The resulting low-level baroclinic wave may serve to organize and focus the convection prevalent over warm (SST > 26°C) water.

The subsequent diabatic import of low-level cyclonic PV (“Addition of PV” in Fig. 10.27), and export of upper tropospheric cyclonic PV (“Removal of PV” in Fig. 10.27) causes a reduction in vertical shear, by displacing the point of inflection between the

upshear upper trough (black +) and the downshear upper ridge (black -) westward, further from the transitioning cyclone. The resultant reduction in vertical shear allows the convection to continue to heat the column above the surface cyclone (“ $\theta$  max from convection” in Fig. 10.27) and build an upper anticyclone, characteristic of tropical cyclone structure.<sup>70,71,73</sup>

The uncertainty in forecasts of subtropical cyclogenesis, also referred to as “tropical transition”, is illustrated by the fact that subtropical cyclones have often been used as a ‘catch-all’ category for different types of ambiguous storms, with forecasters calling them many different things including names like “neutercane”. As a result of impacts from subtropical cyclones in the Atlantic, in 2002, the US National Hurricane Center began naming those storms from the same list as tropical cyclones are named. However, there is much disagreement as to the lifecycle evolution of such storms in the operational forecast and academic communities. The reason for this is that subtropical processes and baroclinic structures may combine to produce hybrid cyclone structures in a variety of locations. In the NH these include the Kona-type cold season Pacific storms, Mediterranean cyclones, and rapid developments over the Great Lakes of North America during boreal autumn. South Pacific cyclones near Australia and Indian Ocean cyclones near southeastern Africa may be Southern Hemisphere examples of these hybrid phenomena. In addition, a South Atlantic storm, which briefly resulted in a tropical cyclone in March 2004, also formed from baroclinic cyclogenesis processes, much like the subtropical storms of the North Atlantic.

With the ongoing improvements in observation capability in the tropics, largely from remotely sensing, it is becoming possible to survey the tropics and to determine the frequency of such genesis events. In addition, state-of-the-art numerical simulations may allow for a close investigation of this process. Current global operational forecast models are able to forecast the baroclinic cyclogenesis of such storms adequately, but often the thermodynamic parameterizations are insufficient to capture the hybrid thermal structure accurately prior to the onset of gale force winds.<sup>31</sup>



### 10.3.3.2 Development of Mesoscale Incipient Vortices from MCS

Tropical cyclogenesis can also result from the merger of two or more MCSs. Tropical Cyclone Oliver (1993) provided the first documented case of genesis from the accumulation of mesoscale vorticity.<sup>38</sup> Oliver evolved from a cluster of weak mesovortices that merged to become two MCS (Fig. 10.28a and b). Subsequently, one of these MCS developed an eye structure (Fig. 10.28c) and sheared the other system, which became the tropical cyclone rainband (Fig. 10.28d). As these processes were occurring, the low-level relative vorticity of the large-scale monsoon trough was strengthening through diabatic processes. This resulted in a reduction of the Rossby deformation radius (Fig. 10.18) of the broader genesis environment, further concentrating the effects of the convective heating locally. Studies of vortex intensification in the presence of an asymmetric PV anomaly for barotropic<sup>74,75</sup> and balanced baroclinic vortices<sup>76</sup> provide theoretical support for this type of genesis.

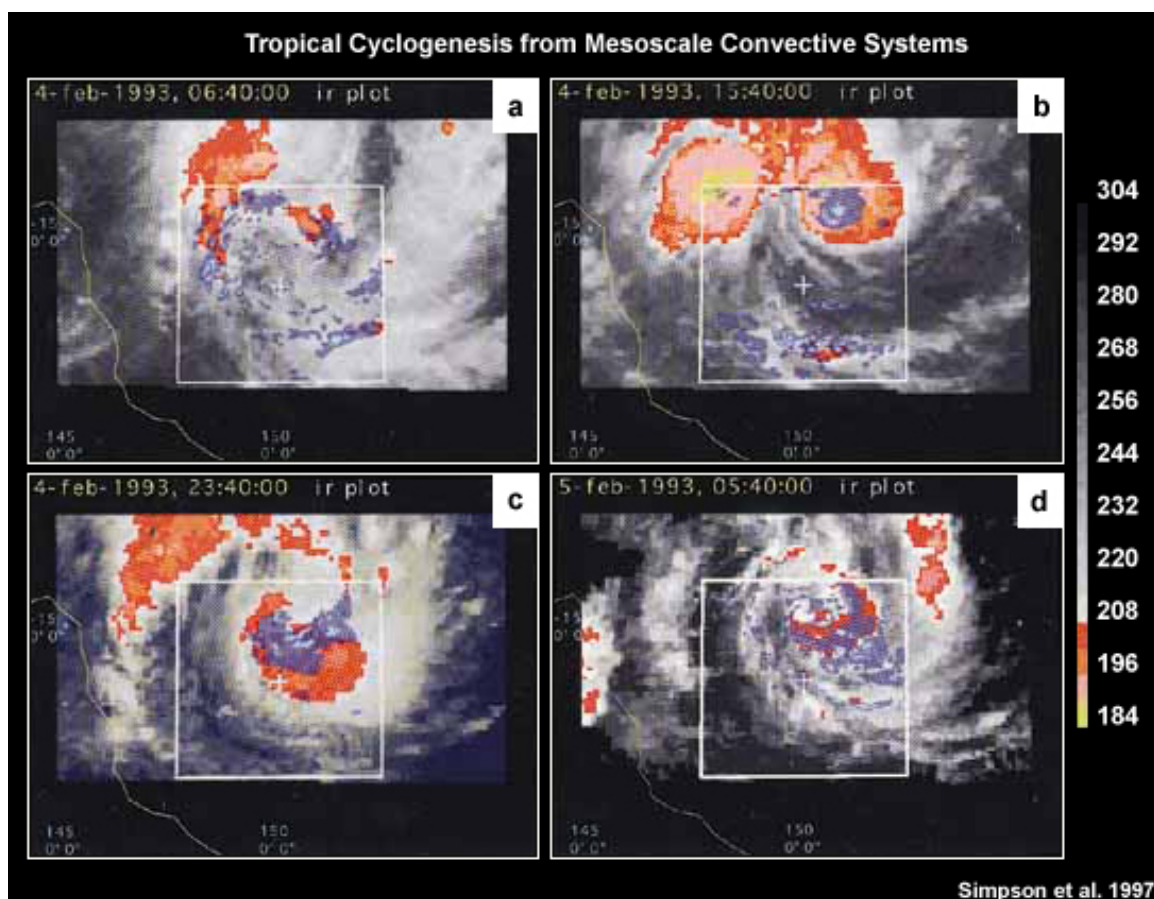


Fig. 10.28. Development of Tropical Cyclone Oliver from the merger of mesoscale convective systems (Simpson et al.<sup>38</sup>).



Review the Rossby Radius of Deformation at [http://www.meted.ucar.edu/nwp/pcu1/d\\_adjust/](http://www.meted.ucar.edu/nwp/pcu1/d_adjust/)  
 Realtime microwave satellite data, <http://cimss.ssec.wisc.edu/tropic/real-time/tpw/mainTPW.html>

An unexpected path to genesis was revealed in an idealized study of the evolution of a Rossby wave advected in easterly flow across a mountain range (representing the northwest-southeast oriented Sierra Madres of Mexico). The interaction led to the development of a lee trough and a secondary vorticity maximum that propagated downstream with period about 5 days.<sup>46</sup> Both the lee trough and secondary vorticity maximum are potential locations for tropical cyclogenesis.<sup>47</sup>

### 10.3.3.3 Vortex Survival and Evolution

Regardless of how the incipient vortex develops, it must remain coherent until it is in a favorable environment for tropical cyclogenesis to occur and for the storm to intensify. Thus, the response of the mesoscale incipient vortex to environmental forcing will also determine its likelihood of genesis.

An incipient tropical cyclone with weak convection will be more susceptible to weakening even in regions of very low vertical wind shear. The shear will tilt the vortex in the vertical, suppressing vertical motion in the region of the convection, and so weakening the storm.<sup>77,78</sup> However, if this vortex experiences only a brief period of vertical wind shear, the vortex can recover from the shear-induced tilt through development of vortex asymmetries.<sup>78,79,80</sup> The return of the tropical cyclone to a symmetric storm is sensitive to the radial gradient of storm vorticity.

Strong vertical wind shear [ $>10\text{-}15\text{ m s}^{-1}$  over 850-200 hPa] is often observed to weaken a developing tropical cyclone through suppression of its core convection. However, in some cases, even a weak storm can act to organize itself against the shear, so that it may persist and even intensify in a region of strong vertical wind shear.<sup>64,81,82,83</sup> Pre-Hurricane Danny (1997) is one storm that likely benefited from the presence of moderate vertical wind shear ( $5\text{-}11\text{ m s}^{-1}$  over 850-200 hPa).<sup>82</sup> The shear acted to promote convection downshear of Danny, creating additional cyclonic vorticity in that region (Fig. 10.29). This newly formed cyclonic vorticity became organized into a low-level vortex, and then ingested the vorticity associated with the original storm, becoming the primary “Danny” (Fig. 10.29). Increased evaporation due to the strengthening surface vortex enhanced the convection and led to the intensification of Danny into a hurricane.

The case of Danny (1997) suggests that the original thermodynamic environment was unable to support tropical cyclone formation. Although detrimental to the original vortex, shear acted in concert with this vortex to modify the thermodynamic environment (through generation of convection, convergence and moistening of the atmosphere), so that when the Danny vortex reformed, it could intensify (further details of this process are given in Section 10.4.2.2). Thus we see that there is “good shear” and “bad shear” when we think about tropical cyclone development. Whether the shear is either good or bad depends on the intensity and size of storm it encounters, as well as the ocean temperatures and atmospheric moisture.

**Hurricane Danny 1997**

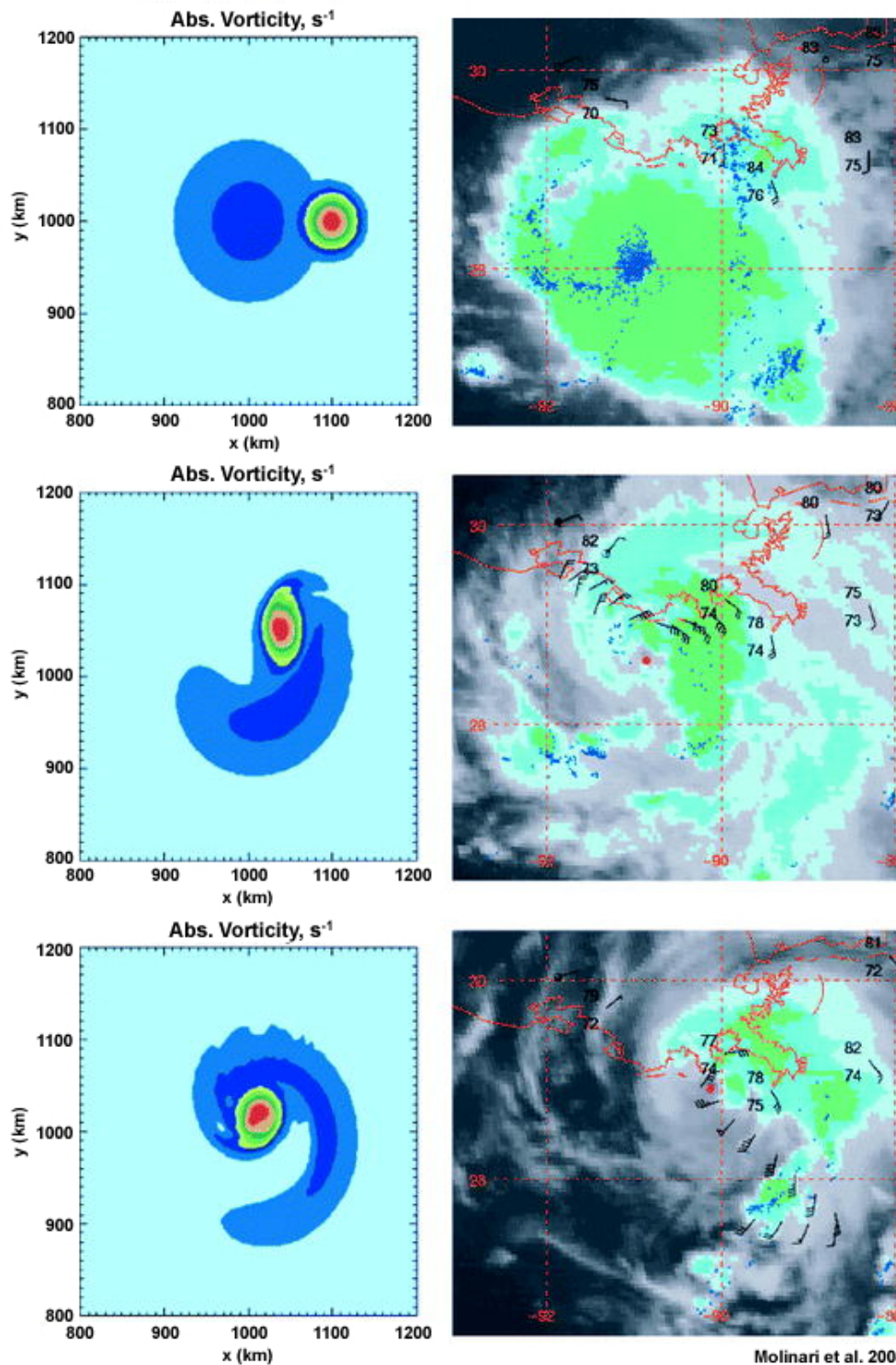


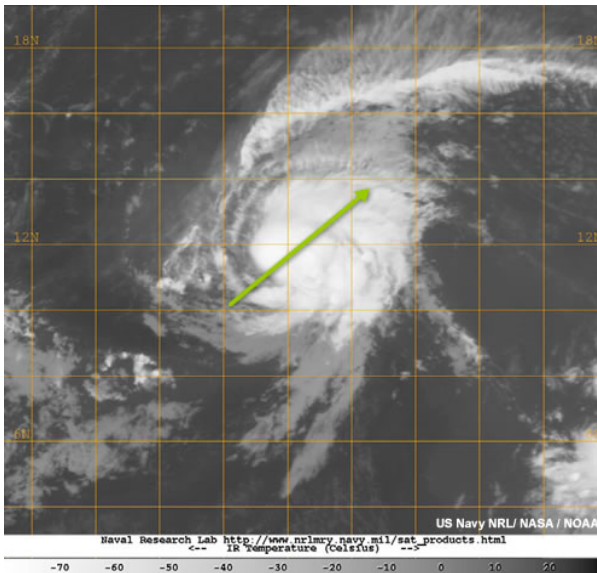
Fig. 10.29. Idealized model (left) and satellite imagery (right) depicting the development of Hurricane Danny (1997) from weak tropical storm (top) to marginal hurricane (bottom).



Now let us try forecasting storm development based on our understanding of the impacts of shear and other environmental factors.

Given vertical wind shear and SST information for the tropical cyclones shown below, what do you think will happen in the next 36 hours? Make your forecast for each storm:

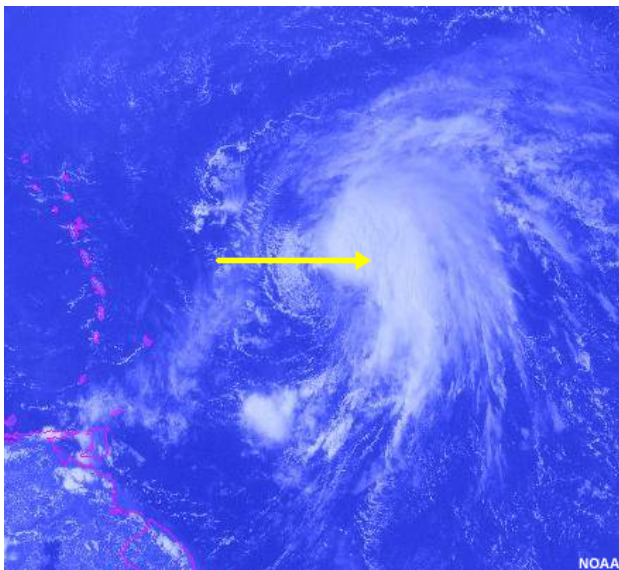
- The storm intensifies
- The storm intensity is essentially unchanged
- The storm weakens



**Storm 1:** SST = 26.5°C

Shear magnitude = 15 m s<sup>-1</sup>/(650 hPa)

Shear direction given by arrow



**Storm 2:** SST = 28.0°C

Shear magnitude = 10 m s<sup>-1</sup>/(650 hPa)

Shear direction given by arrow



Using the materials we have covered, you should have been able to devise some simple forecast rules to guide your forecasts of the next stage of development for these two storms. For example:

- (i) strong vertical wind shear is generally bad;
- (ii) vertical wind shear can help the storm intensify if the SST are warm and there are no other negative factors (such as dry air) to slow intensification.

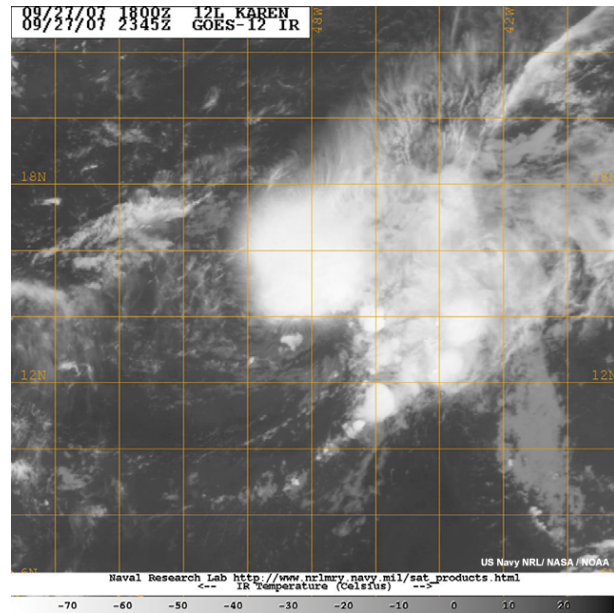
**The correct forecasts for our storms are:**

**For Storm 1, the answer is (c)**

The storm weakened.

**Why?** In this situation the combination of strong shear and cool (for the tropics) SST both acted against intensification.

This satellite image is for the same storm 36 hours later. Clearly it is disorganized and has lost most of the active convection around its eye (we see the cirrus shield here).

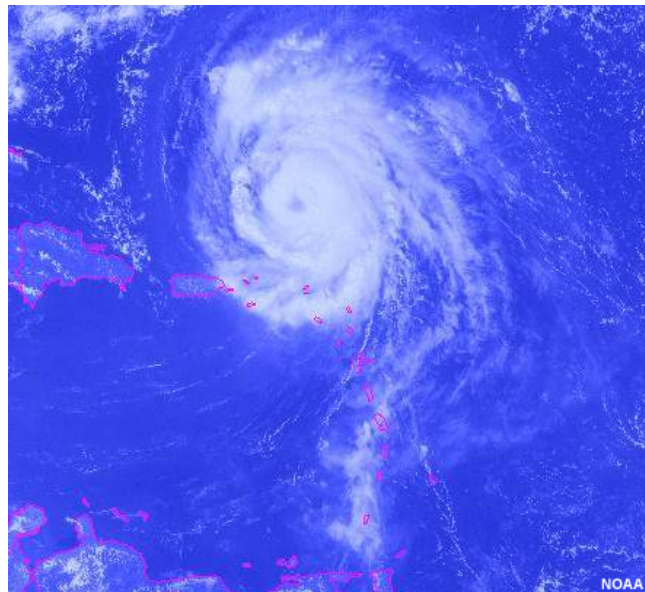


**For Storm 2, the answer is (a)**

The storm intensified.

**Why?** While the shear is weaker than for storm 1, it is still relatively strong. Thus, the warmer SST must have provided a strong enough moisture source so that the storm was able to resist the shear, increase its convection, and intensify.

This satellite image is for the same storm 72 hours later. The storm has developed a symmetric structure with a closed eyewall and a clear eye.



As demonstrated with the case of Hurricane Danny just discussed, inclusion of moisture into consideration of the cyclone evolution introduces the possibility that moist convection could act to reduce the impacts of vertical wind shear, possibly through vertical momentum transports. However, as we shall see, all moist convection is not created equal – and not all convection is immediately good for the storm.

The spatial distribution of convection within the vortex can have a large impact on the early evolution of a tropical cyclone.<sup>84</sup> If the distribution of convection within the vortex can have such a large impact, let us explore the factors governing this distribution.

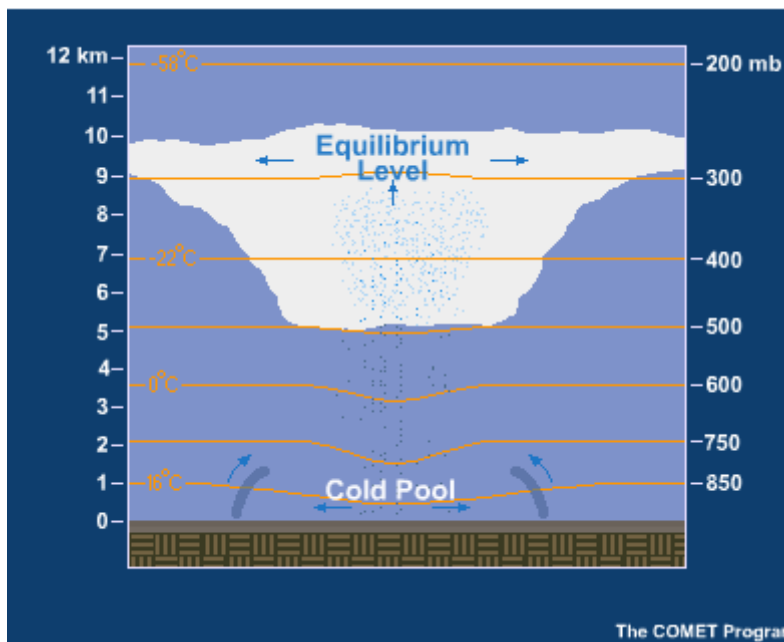


Fig. 10.30. Suppression of convection due to stabilization of the boundary layer by the cool downdrafts.



[Animation of convective updrafts and downdrafts in an airmass thunderstorm](#)

Convection developing in a sub-saturated environment will entrain dry air which evaporates the rain in the downdraft, and so delivering cool and dry downdraft air into the boundary layer under the convection. Clearly, this will dry and stabilize the boundary layer locally,<sup>18</sup> suppressing further convection (Fig. 10.30). Conversely, high mid-tropospheric relative humidity will suppress the entrainment of dry air into the convective downdrafts, maintaining a moist boundary layer and facilitating continued core convection in the developing storm. Should the eyewall convection be cut off, “peripheral” convection at large radius outside the radius of maximum winds may become established.<sup>65,84</sup> This outer ring of active convection spins up the tangential wind and associated radial pressure gradient locally. This reduces the radial pressure gradient closer to the storm center so weakens the low-level inflow to the core. The secondary circulation (in-up-and-out) of the storm now feeds this outer convection, resulting in subsidence in the vicinity of the old eyewall. The subsidence weakens the eyewall

convection, suppressing mid-troposphere moisture buildup in the core and weakening the peak surface winds. The peripheral ring of convection is now dominant and modulates the location of subsequent convection.<sup>84</sup> Should the original eyewall collapse completely, the ring of peripheral convection may contract to form a new eyewall. Conservation of absolute angular momentum suggests that the storm should eventually reintensify through this process.<sup>28,85</sup>

Observational analyses of the distribution of lightning data with respect to the storm track provide insights into the interaction of the moist storm vortex and its environment.<sup>30</sup> Stratification by vertical wind shear [ $r \leq 500$  km, 850-200 hPa] reveals a slight preference for downshear left convection in the storm core ( $r < 100$  km) and a strong signal for downshear right convection in the outer band ( $100 \text{ km} < r < 300$  km). This distribution of convection is consistent with the development of deep divergent circulations in the evolving storms that act to oppose the vertical wind shear and minimize the tilt of the storm center.<sup>77</sup> These results were less consistent for weaker storms, indicating that tropical depressions were less able to respond to vertical wind shear than stronger storms.

Figure 10.31 depicts the impact of vertical wind shear on tropical cyclones of different intensity.<sup>29</sup> The distribution of lightning flashes within 300 km of the storm center (located at the origin in each case) is illustrated for (a) Hurricane Bertha from 1996 and (b) a post-landfall weakening Tropical Storm Alberto (1994). The images have been rotated so that the vertical wind shear vector points upwards. The figures illustrate the greater lightning activity in the rainbands and eyewall in weaker tropical storms even though the magnitude of the vertical wind shear impacting Bertha was almost twice that experienced by Alberto.

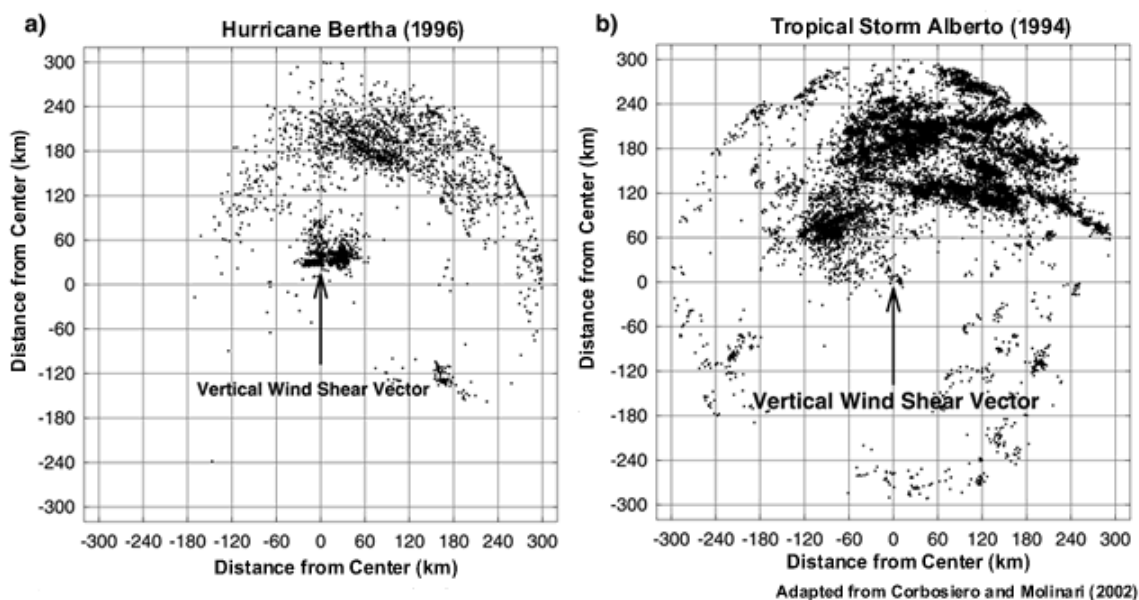


Fig. 10.31. Demonstration of the impact of vertical wind shear on tropical cyclones of different intensity. The figure shows the distribution of lightning flashes around (a) Hurricane Bertha (1996) and (b) weakening Tropical Storm Alberto (1994). Adapted from Corbosiero and Molinari (2002).<sup>30</sup>

Consideration of a dry, baroclinic vortex in a region of westerly shear may provide some useful insights on the impacts of shear on a tropical cyclone. Due to the environmental vertical shear, the vortex tilts, modifying vertical and horizontal wind shear at all levels<sup>86</sup> and creating a wavenumber one<sup>c</sup> asymmetry in the potential temperature<sup>87</sup> to balance the vortex windfield changes. These vertical motion and potential temperature anomalies are consistent with observations of Hurricane Danny (1997).<sup>82</sup> The vortex is more resistant to deformation (has stronger inertial stability) in the lower troposphere compared to the upper troposphere. As a result, the vortex begins to break down in the upper troposphere first in the region of downshear ascent (cool potential temperature anomaly). The storm mixes out the asymmetries (a process known as resymmetrization), returning once more to a symmetric, balanced structure.

#### 10.3.3.4. Using Eddy Angular Momentum Fluxes to Describe TC Development

Since we are used to picturing tropical cyclones as symmetric rotating vortices (e.g., Fig. 10.4 and 10.11), let us try to understand the impact of environmental interactions on a tropical cyclone in a storm-centered way. Note that we are not discussing new processes for storm development, just a new way to think about the information we have already discussed.

We are going to describe changes in a symmetric tropical cyclone due to eddy momentum fluxes. The symmetric tropical cyclone is a pure circle so that, if you are standing at the storm center, the storm's rotational winds and its in-up-and-out secondary circulation look the same in every direction.

This means that everything that is not purely symmetric compared to the storm location is labeled the "environment." So we are thinking about the changes in the symmetric storm due to everything else. If we write this mathematically, then the horizontal winds can be written

$$u = \bar{u} + u' \qquad v = \bar{v} + v' \qquad (6)$$

where  $(\bar{u}, \bar{v})$  are the symmetric averages and  $(u', v')$  represent asymmetric horizontal motion. To change the symmetric rotating wind speed at a chosen radius, we can advect winds from another radius. We write this as

$$\begin{aligned} -\overline{ruv} &= -\overline{r(\bar{u}\bar{v} + u'\bar{v} + \bar{u}v' + u'v')} \\ &= \overline{-ruv} - \overline{ru'\bar{v}} - \overline{r\bar{u}v'} - \overline{ru'v'} \\ &= -\overline{r\bar{u}\bar{v}} - \overline{ru'\bar{v}} - \overline{r\bar{u}v'} - \overline{ru'v'} \\ -\overline{ruv} &= -\overline{r\bar{u}\bar{v}} - \overline{ru'v'} \end{aligned} \qquad (7)$$

<sup>c</sup> A wavenumber one asymmetry consists of one positive and one negative anomaly on the mean flow. These anomaly maxima are "opposite" each other across the center of the vortex.



We have now derived a simple mathematical expression to quantify the impact of “everything else” on the symmetric storm. This expression is the definition of the eddy angular momentum fluxes.<sup>28,88,89</sup> Since the inertial stability of the tropical cyclone is very large in the lower troposphere (Fig. 10.10, Section 10.2.2.2), the tropical cyclone will be very resistant to radial transports here. This means that eddy angular momentum fluxes in the upper troposphere can have the greatest impact on the symmetric tropical cyclone.

From the tropical cyclone-centered perspective, a *positive* eddy angular momentum flux results from the *inward* transport of cyclonic momentum by the asymmetric radial flow. Alternately, changing all of the signs, *outward* transport of anticyclonic angular momentum by the asymmetric radial flow also corresponds to a *positive* eddy momentum flux. The asymmetrical radial flow also affects eddy heat fluxes. Since these fluxes exclude symmetric transports, they provide a concise way of summarizing environmental (or asymmetric storm) impacts on the symmetric storm evolution.

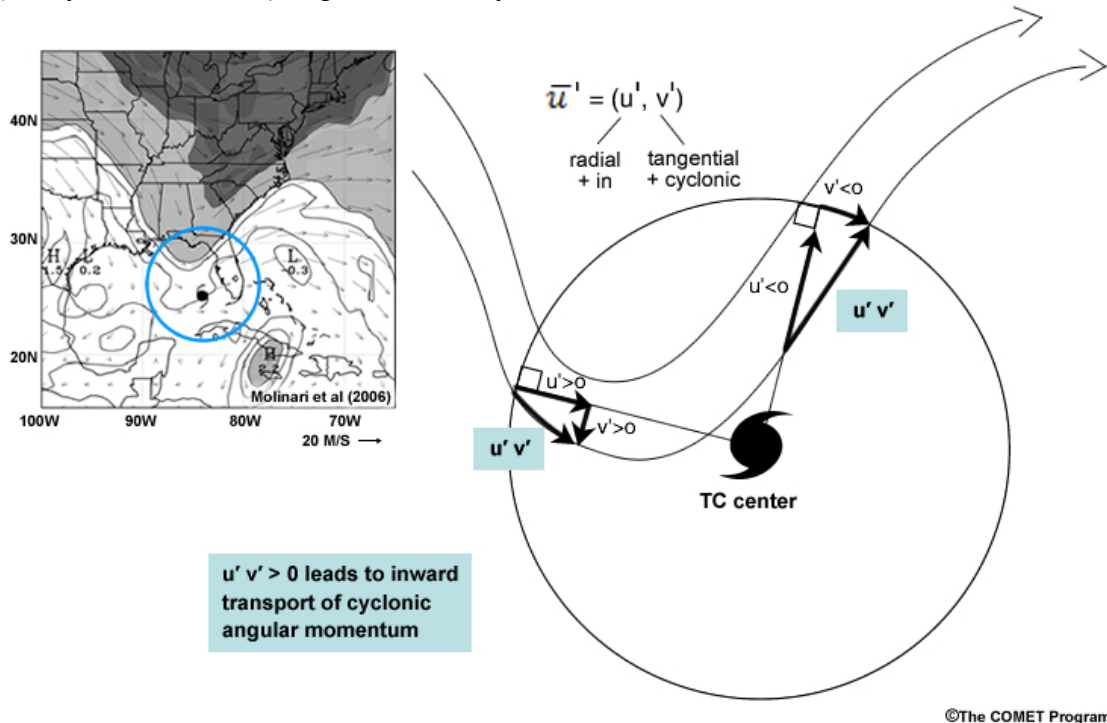


Fig. 10.32. Schematic of the transport of eddy angular momentum flux in a cyclone-relative framework. Inset shows winds vectors and PV (contours, shaded  $> 1.5$  units) on a constant potential temperature surface in the upper troposphere. The storm central pressure was 997 hPa.

Focusing on the circle centered on the storm in Fig. 10.32, we see that the interaction with the trough leads to both outward flux of anticyclonic momentum to the northeast of the tropical cyclone and import of cyclonic angular momentum to the southwest. The combined effect of these fluxes,  $\overline{u'v'}$ , results in a net outward flux of anticyclonic angular momentum from the storm outflow. This corresponds to a *positive* eddy angular

momentum flux and is equivalent to saying that we have *inward* transport of cyclonic momentum.

However you say it, the eddy fluxes are weakening the upper level anticyclone of the tropical cyclone. How could this cause the tropical cyclone to intensify? Although the anticyclone aloft has weakened, the rest of the tropical cyclone has yet to feel the impact of the eddy angular momentum fluxes, so the in—and up—parts of the secondary circulation are in balance with the cyclonic vortex below, but the “out-” part is not.

Think back to our discussion of inertial stability: flow that is out of balance is easier to change than strongly rotating flow. So the out of balance anticyclone will change due to the secondary circulation being driven from below. The readjustment of the anticyclone forces a stronger secondary circulation, driving more ascent, increasing the convection near the storm center, and intensifying the storm.<sup>90</sup>

Realistic eddy fluxes have been derived from observations of developing and non-developing tropical disturbances.<sup>34,91</sup> Idealized studies of genesis have demonstrated that an incipient vortex in a quiescent (thermodynamically marginal) environment can be made to intensify under the influence of eddy fluxes from a developing system. Left alone, this system would not intensify. Equally, intensification of an otherwise viable incipient vortex can be suppressed through application of realistic eddy fluxes derived from observations of non-developing tropical disturbances<sup>88</sup>. In the case of Hurricane Diana (1984), eddy fluxes at upper levels induced a surface radial inflow<sup>89</sup> that enhanced surface moisture fluxes, driving low-level moisture convergence and ultimately, storm development.<sup>68,69</sup>

### 10.3.4 Saharan Air Layer (SAL)

Another large scale modulator of tropical cyclone development in the eastern Atlantic is the Saharan Air Layer (or SAL), first identified in the 1970s.<sup>92</sup> From late spring to early autumn the enhanced warm season solar radiation causes deep mixing over the Saharan Desert that results in a dry, well-mixed boundary layer that can extend up to 500 hPa. At its southern end, this Saharan boundary layer air is bounded by the African Easterly Jet, which has peak amplitude of 10-25 m s<sup>-1</sup> near 700 hPa. Sand storms created in this dry environment result in suspended particles throughout the layer. Advection of this desert boundary layer over the Atlantic Ocean (often in association with an African easterly wave progression) results in its being undercut by a moist marine layer and creates the SAL. The SAL is thus an elevated layer of very dry, well-mixed air embedded in the Atlantic marine environment (Fig 6.20, Chapter 6).

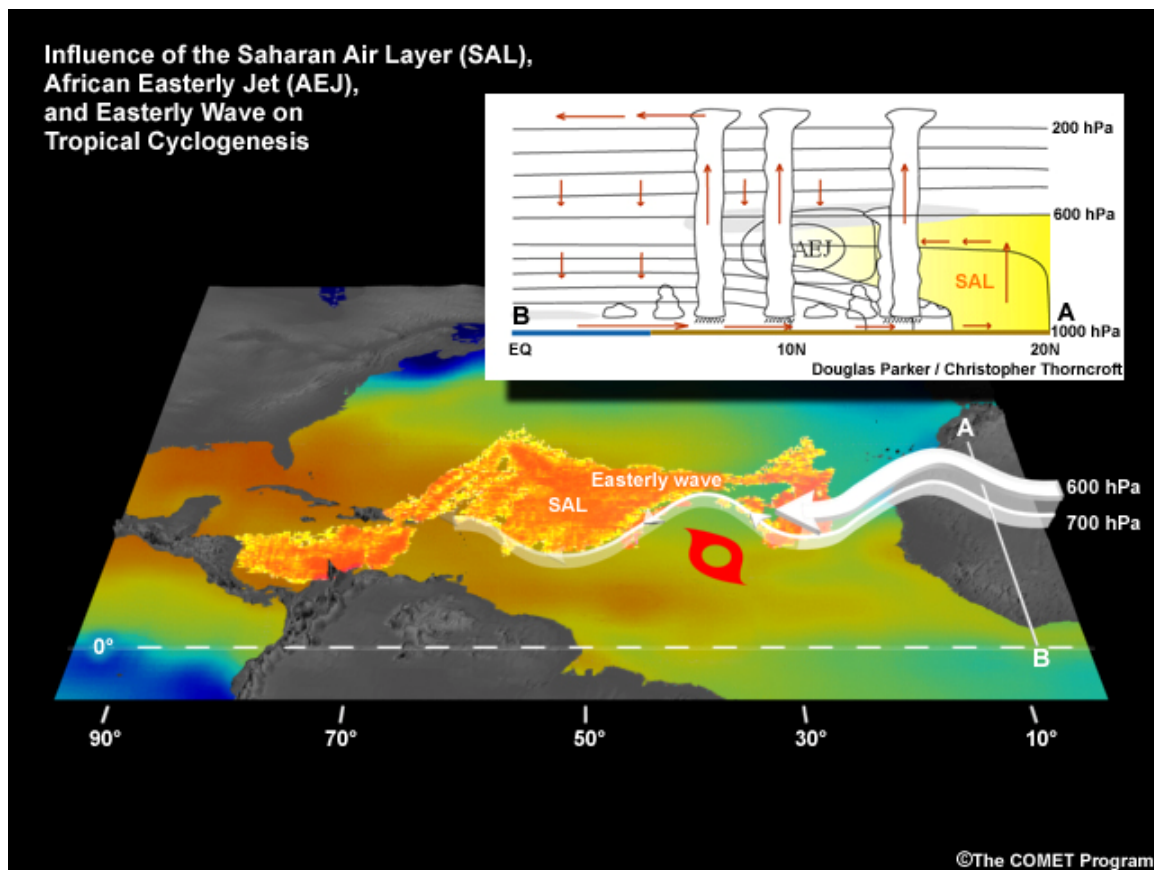


Fig. 10.33. Schematic of the Saharan Air Layer, and influences on genesis, as described by Dunion and Velden<sup>95</sup> and Karyampudi and Pierce<sup>93</sup>. The African easterly jet (AEJ) at the southern bound of the SAL and an African easterly wave are shown. The cross-section is a conceptual model of the SAL, AEJ, and convective weather systems based on the JET 2000 field program.

As a SAL outbreak moves off the west coast of Africa, the 700 hPa African easterly jet also elongates offshore due to the meridional temperature gradient between the SAL air and the tropical air to the south.<sup>93</sup> Cyclonic shear vorticity south of this mid-level jet accompanied by a mid-level disturbance (the easterly wave) can generate cross-contour flow in the vorticity field, leading to cyclonic vorticity advection and the enhancement of a nearby surface disturbance south of the mid-level easterly jet (Fig. 10.33). Eventual coupling of low- and mid-level disturbances can then lead to tropical depression formation.

This positive relationship between the SAL and tropical cyclone formation is not ubiquitous however. Large SAL outbreaks can weaken any mid-level disturbances in the flow through the generation of a stronger mid-level easterly jet, which causes a more zonally oriented mid-level flow, thus eliminating this tropical cyclogenesis mechanism. As expected then, over-forecasting of genesis by North Atlantic operational numerical models has been attributed to inadequate characterization of the SAL elevated dry layer and accompanying jet.<sup>94</sup> A recently developed satellite algorithm for tracking the SAL<sup>95</sup> (e.g., Fig. 10.34) provides promise for improving such biases. More information on tracking the SAL is available in [Chapter 3, Section 3.8](#).



CIMSS SAL background, <http://cimss.ssec.wisc.edu/tropic/real-time/wavetrak/sal-background.html>  
NOAA Hurricane Research Division SAL project, <http://www.aoml.noaa.gov/hrd/project2006/sal.html>  
Real-time diagnostics of the SAL, <http://cimss.ssec.wisc.edu/tropic/real-time/wavetrak/winds/m8split.html>

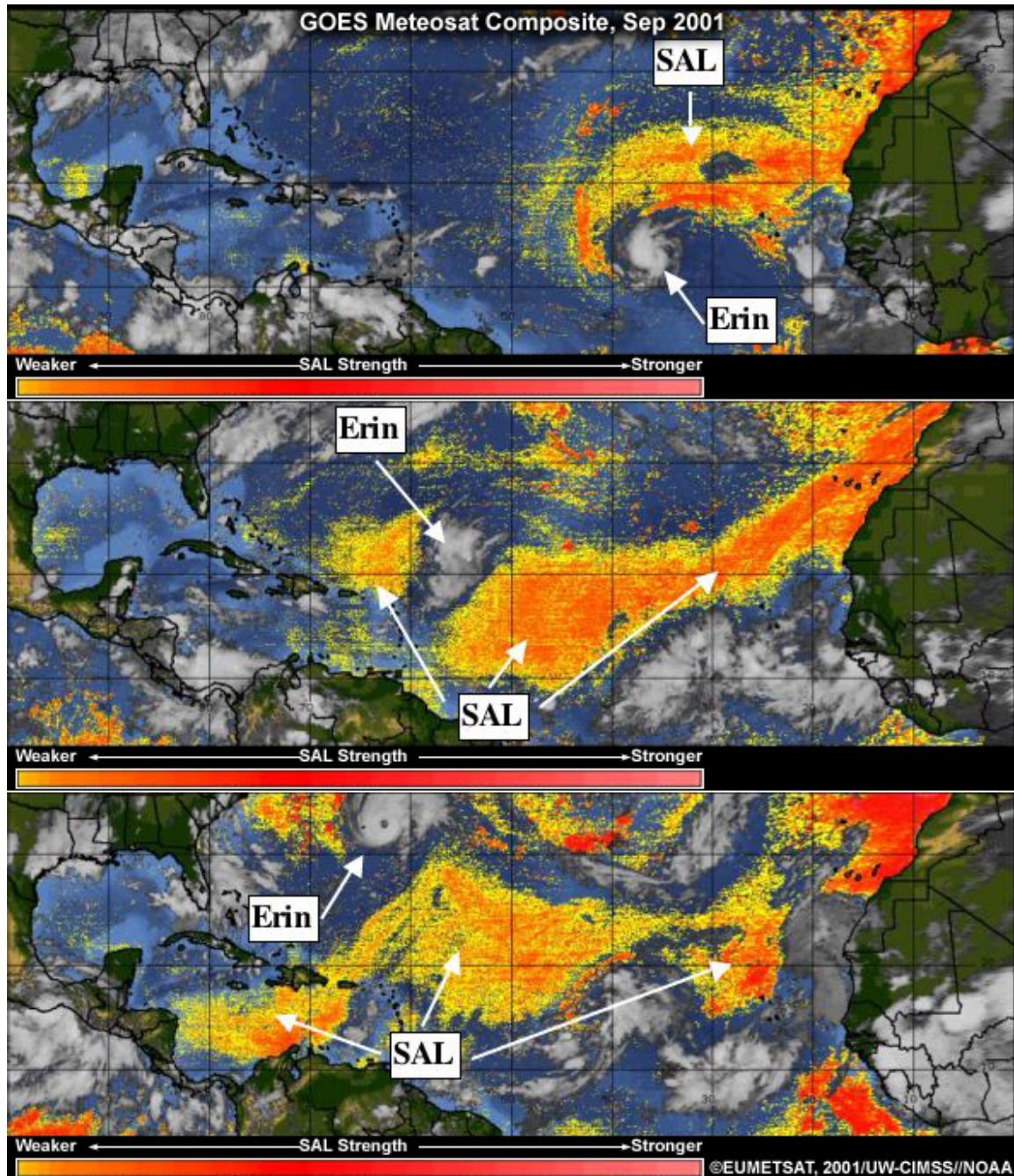


Fig. 10.34. Time series of GOES SAL-tracking imagery for the interaction of Hurricane Erin (2001) with a SAL event. Time moves forward from top (0000 UTC 2 Sep) to middle (1800 UTC 5 Sep) to bottom (1800 UTC 9 Sep).

### 10.3.5 Summary of Possible Tropical Cyclogenesis Mechanisms

In the last 10 to 15 years, a much broader range of systems have been recognized as potential candidates for the incipient vortices leading to a tropical depressions, and the associated mechanisms for tropical cyclogenesis have been elucidated. The most recently identified mechanisms contributing to tropical cyclogenesis in each of the affected ocean basins are given in Fig. 10.35.

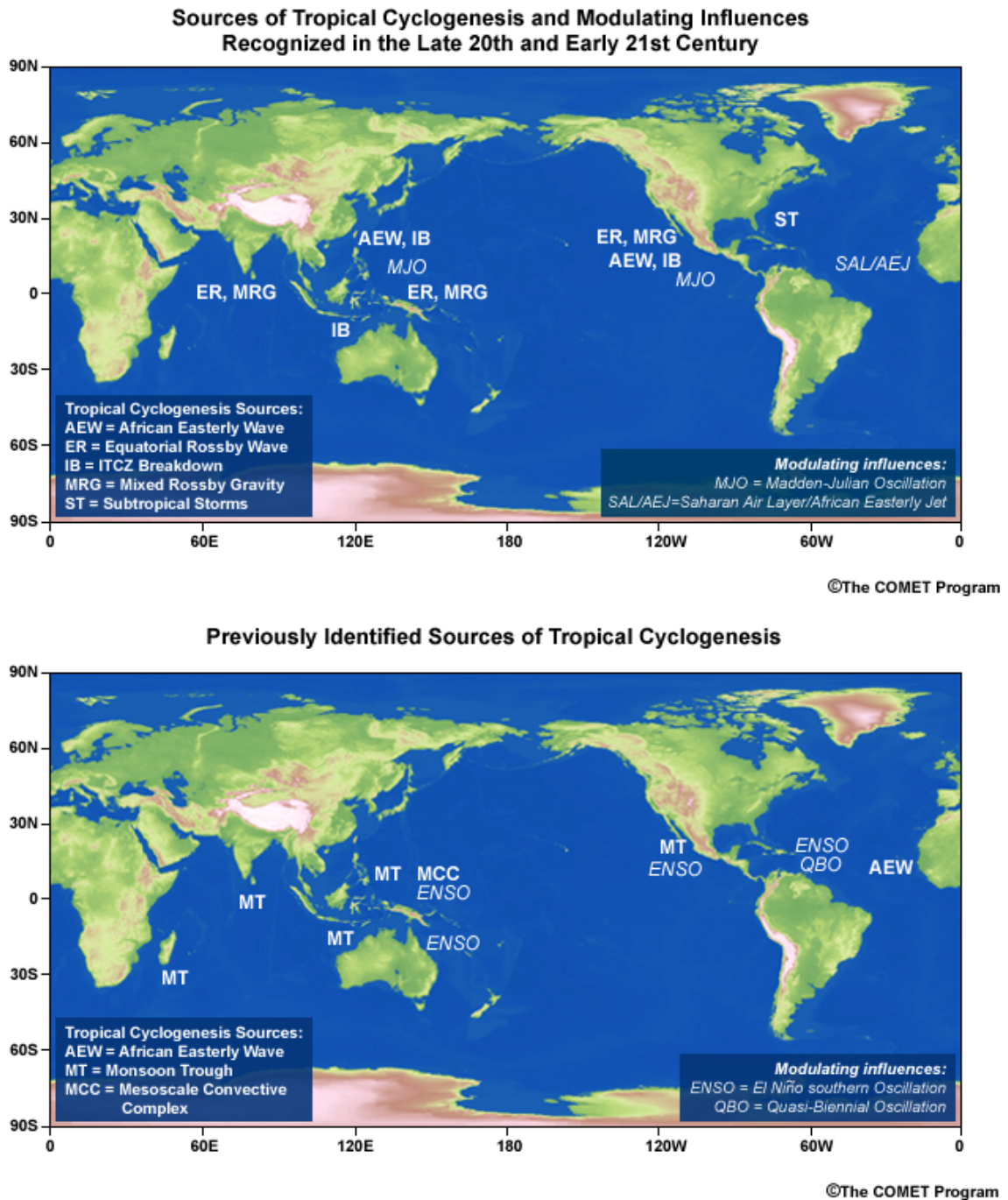


Fig. 10.35. Recognized sources of tropical cyclogenesis identified for each ocean basin.

On the large scale, impacts of the environmental dynamical structure on tropical cyclogenesis include clarification of the positive role of shear in the baroclinic development of subtropical precursor disturbances and the basin-wide increase in convective organization through the evolution of the MJO. Diabatically-forced PV enhancement in the monsoon trough zone has been shown to result in different modes of trough breakdown and persistence of easterly waves into the western North Pacific has been demonstrated. Also, satellite observations have been useful in confirming the role of equatorial Rossby and mixed Rossby gravity waves as precursor disturbances ultimately resulting in tropical cyclogenesis.

On the system scale, new mechanisms for the development of the incipient vortex disturbance have been identified. Internal system dynamics relevant to PV mixing and convective distribution/feedbacks on storm evolution have been better clarified.

Operational forecasts of tropical cyclogenesis have been developed on two fronts: seasonal forecasts of tropical cyclone activity, expressed in terms of storm and hurricane numbers or storm days; and deterministic simulations of the genesis of individual storm events.

One message comes out of all of these genesis mechanisms: each component of Gray's genesis parameter<sup>33</sup> plays a physical role in preconditioning the environment for genesis, thus modulating storm genesis frequency.

Alternative approaches to developing daily genesis parameters<sup>33,34,96,97</sup> highlight the importance of the large-scale dynamical environment. Each study cited in these references, obtained their best results from a combination of multiple synoptic parameters. All of the large-scale parameters employed in each study must be favorable for genesis to occur; however, no currently available set of predictors results in a sufficiency criterion for genesis. Thus the search for the sufficiency condition and for the mechanisms for generating the incipient vortex continues.

## 10.4 Intensity

When a tropical cyclone is bearing down on land, the first question that people ask is “Will it hit me?” followed shortly thereafter by “How intense is it?” Both questions amount to “How will it affect me?”

In this section, we will review (i) the stages of the typical lifecycle for a tropical cyclone, (ii) use of satellites in estimating the intensity of systems, (iii) the concept of Potential Intensity (PI) and its relationship to actual intensity, (iv) modulation of storm intensity by its environment, (v) inner core impacts on storm intensity and (vi) satellite estimation of tropical cyclone intensity.

### 10.4.1 Key Stages of a Typical Tropical Cyclone Lifecycle

The key stages in the lifecycle of a typical tropical cyclone are incipient disturbance, tropical storm, tropical cyclone (hurricane, typhoon), and possibly severe tropical cyclone (major hurricane, supertyphoon). Having reached its peak intensity at one of these stages (see Box.10.3) for storm intensity classifications), the storm will either decay or undergo extratropical transition. These stages are associated with changes in the storm intensity and structure. In this section, we review the physical stages of the storm lifecycle as illustrated by the stages of Hurricane Rita (Figs. 10.36–10.40).

#### 10.4.1.1 Incipient Disturbances

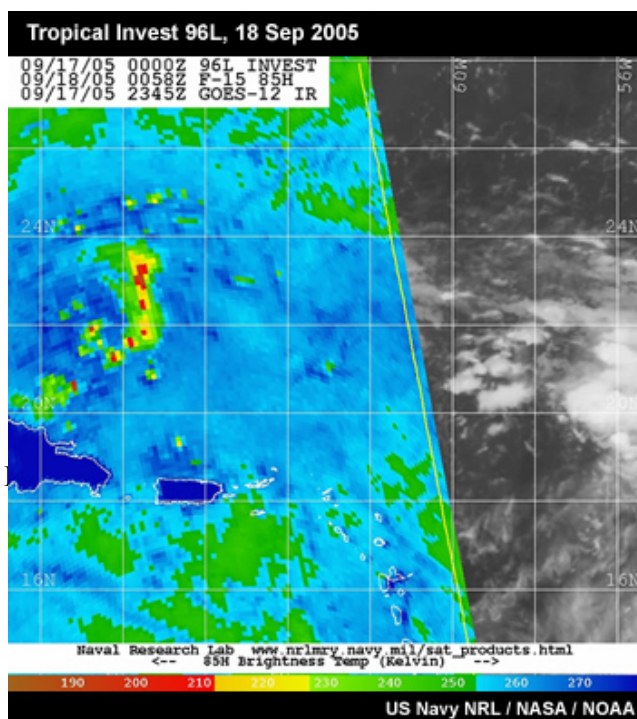


Fig. 10.36. Combined infrared and SSM/I satellite image for Tropical Invest 96L, the disturbance that became Hurricane Rita (2005). Images are taken near 0000 UTC 18 Sep 2005. Note the “hook” of intense convection near the western edge of the image. The peak surface winds associated with this disturbance were estimated to be  $12 \text{ m s}^{-1}$  with minimum surface pressure of 1012 hPa.



A tropical cyclone will not develop instantaneously: some intermediate, weaker disturbance is needed to provide the “seed” from which a tropical cyclone can develop (Fig. 10.36). In contrast to our expectations for a tropical cyclone, the incipient disturbance can be very asymmetric. A detailed discussion of the sources of disturbances is presented in Section 10.3, so only a few key points are reviewed here.

A promising incipient disturbance is one that satisfies all of the necessary, but not sufficient, conditions for tropical cyclogenesis (Section 10.3.1); these can be summarized as a low-level cyclonic vorticity maximum in weak vertical wind shear and associated with deep convection. Disturbances meeting these criteria differ in their own formation histories in the different tropical ocean basins:

- Western Pacific and Indian Oceans: The monsoon trough is the dominant location for tropical cyclogenesis in the Pacific<sup>41</sup> and Indian Oceans, but equatorial Rossby (Fig. 10.23) and mixed Rossby gravity waves (Fig. 10.24b) are increasingly being recognized as potential initiators of tropical cyclogenesis in these basins (Fig. 10.35a). Further, merger of a number of smaller (weaker vorticity) mesoscale systems has also been identified as a mechanism for tropical cyclogenesis in the North Pacific<sup>38</sup> (Section 10.3.3.2).
- Eastern Pacific: Tropical storms forming in the eastern North Pacific have been identified with both instabilities in the ITCZ<sup>44,50,52</sup> (Section 10.3.2.2) and with moist easterly waves intruding from the Atlantic<sup>46</sup> (Section 10.3.2.4).
- Atlantic Ocean: The monsoon in the Atlantic basin is mainly confined to West Africa. Easterly waves forming here are influenced by local convection and mesoscale systems that initiate near the Aïr Mountains, Jos Plateau, and Guinea Highlands. As illustrated in Fig 10.25b, they are typically less symmetric than the classic inverted-V satellite signature first reported by Frank.<sup>98</sup> Another source of Atlantic tropical cyclogenesis is subtropical cyclones (Section 10.3.3.1); the potential importance of subtropical cyclones to tropical cyclogenesis has yet to be documented in other basins. Subtropical cyclones typically form at the equatorward extreme of a midlatitude frontal zone.<sup>31</sup>

### 10.4.1.2 Tropical Storm

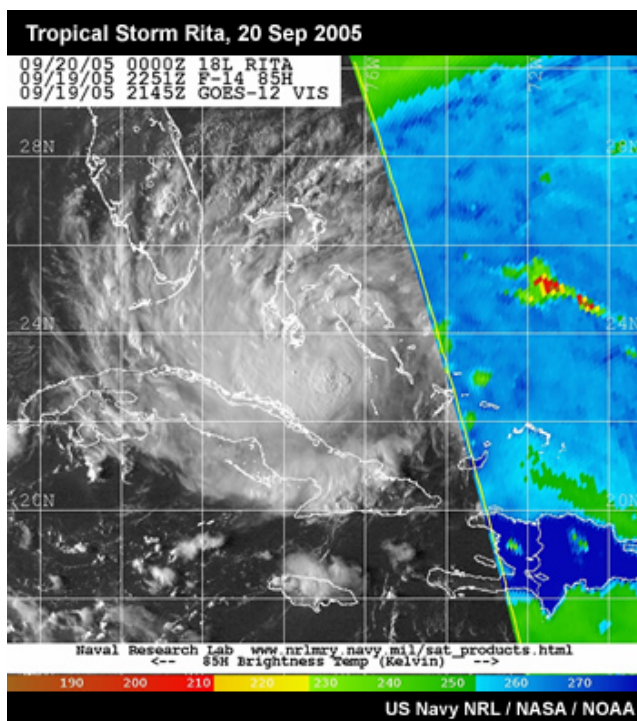


Fig. 10.37. Combined infrared and SSM/I satellite images of Tropical Storm Rita. Images are taken near 0000 UTC 20 Sep 2005 when Rita had central pressure of 993 hPa and peak winds of  $30 \text{ m s}^{-1}$ .

Given a favorable environment, an incipient disturbance may organize into a tropical storm. Maintenance of these favorable environmental conditions for tropical cyclogenesis is ideal for further intensification to the tropical storm stage (Fig. 10.37). The warm ocean waters of the tropics provide the energy source for the tropical cyclone. Evaporation (latent heat flux) and heat transfer (sensible heat flux) from the ocean surface warm and moisten the tropical storm boundary layer. The heat and moisture fluxes and the potential energy comprise the moist static energy of the air ([Chapter 6, Section 6.2.3](#)). Conversion of this moist static energy into kinetic energy via convection is the mechanism by which a tropical cyclone intensifies. Later in this chapter we will explore theories for the potential intensity ( $PI$ ) possible for a storm (Section 10.4.2.3) based on this mechanism and the reasons why every storm does not achieve its potential intensity (Section 10.4.3).

Operational centers require a consistent definition – peak surface wind speed – to decide when a system has become a tropical storm, but this is not always the most helpful definition for explaining the storm evolution. Tropical disturbances require external forcing to be sustained. Thus, a physically-based definition of the transition from a tropical disturbance to a tropical storm is that *the system has become a tropical storm once it is self-sustaining*. This means that, while external forcing might help or hurt the evolution of the tropical storm, it does not *need* external forcing to remain a coherent system, or even to intensify.

### 10.4.1.3 Tropical Cyclone (typhoon, hurricane)

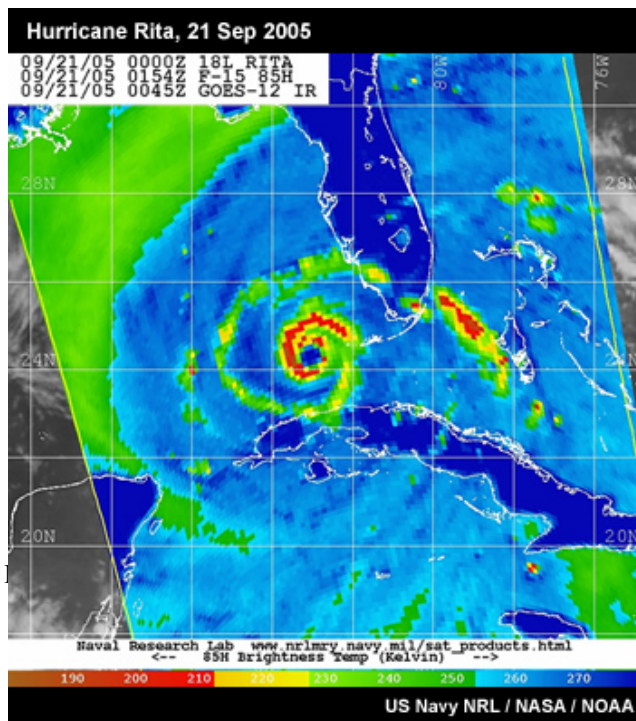


Fig. 10.38. Combined infrared and SSM/I satellite images of Hurricane Rita. Images are taken near 0000 UTC 21 Sep 2005. At this time, Rita had peak winds of  $45 \text{ m s}^{-1}$  and central pressure of 967 hPa, making it a Category 2 on the Saffir-Simpson scale. Note the intense eyewall convection and clear eye.

Continuing maintenance of the favorable environmental conditions for tropical cyclogenesis and intensification leads to further intensification into a more intense tropical cyclone with a symmetric structure and a clear eye (Fig. 10.38). Traditionally, vertical wind shear has generally been considered to have a negative effect on tropical cyclone intensification. An exception to this rule is the role of the TUTT in intensifying western North Pacific storms. New research is now challenging this view: vertical wind shear has been shown to intensify storms in a marginal thermodynamic environment.<sup>88,89,99</sup> These storms must already be sufficiently intense to survive the initial disruption of their convection by the vertical wind shear, explaining why shear is still considered to be a negative effect on tropical cyclogenesis.

Regional differences also may provide the source of the forcing leading to this further intensification. For example, storms forming on the Northwest Shelf off the west coast of Australia may track parallel the coast for hundreds of kilometers. The warm waters of the “Northwest Shelf” provide the ideal environment for continued intensification of these storms until they either encounter the midlatitude westerlies (and their associated strong vertical wind shear) or a dry air intrusion from the Australian deserts disrupts the convective organization of the system.

### 10.4.1.4 Severe Tropical Cyclone (*supertyphoon, major hurricane*)

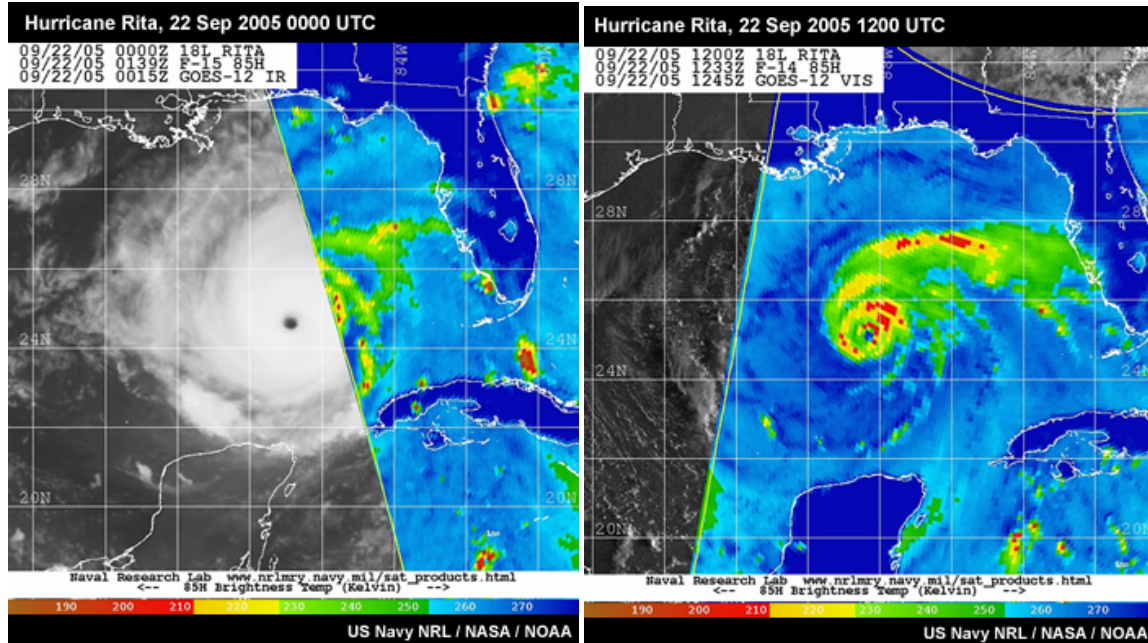


Fig. 10.39. Combined infrared and SSM/I satellite images of Hurricane Rita at about 0000 UTC 22 Sep 2005 (left) and twelve hours later (1200 UTC; right). Rita was a Category 5 hurricane over this period, with peak surface winds of  $75 \text{ m s}^{-1}$  and minimum central pressure around 898 hPa (left). In the left panel, note the clear eye and symmetry of the storm. The intense eyewall convection, spiral rainbands (green/red) with subsidence between (light to dark blue) and clear eye are evident in the right panel.

Relatively few tropical cyclones reach this status, characterized by peak sustained surface winds in excess of  $50 \text{ m s}^{-1}$  (Box 10-3, Fig. 10.39). Intensification to severe tropical cyclone requires that the storm remain over the open ocean, so storms forming close to land are less likely to reach such intensities. However, there are exceptions to every rule: the tropical cyclones off the Western Australian coast, described in the previous section, form and track relatively close to land; further, storms in the Bay of Bengal, Gulf of Mexico, and Western Caribbean have been observed to intensify rapidly into severe tropical cyclones. Wilma (2005, Box 10-5) is one such storm.

One limit on the intensity of storms in the SH is the relatively zonal nature of the mean flow. The SH has much smaller land masses and mountain ranges than the NH, providing less obstruction to the atmospheric flow. The result is more zonal mean midlatitude winds with the mean westerly zone being closer to the equator. In contrast, the many mountain ranges and large extents of the NH continents result in a large meridional component to the mean flow, which can steer tropical cyclones to much higher latitudes. The relative susceptibility of Japan (roughly  $36^\circ\text{N}$ ) to tropical cyclone landfalls compared to, say, New Zealand (about  $42^\circ\text{S}$ ) illustrates this point.

A subset of historically significant severe tropical cyclones is reviewed in Boxes 10-5, 10-11, and 10-12.

### 10.4.1.5 The End of the Tropical Cyclone Lifecycle: Decay or Extratropical Transition (ET)

When a tropical cyclone moves into a hostile environment it will either decay (Fig. 10.40) or undergo extratropical transition. As might be expected, a hostile environment includes at least one of the following: strong vertical wind shear (in excess of  $10\text{--}15\text{ m s}^{-1}$  over a deep layer), cool ocean temperatures under the storm core (less than  $26^\circ\text{C}$ ), dry air intrusion, or landfall. Cool SST and strong shear are typical of a midlatitude environment, explaining why this region is generally thought to be a tropical cyclone graveyard.

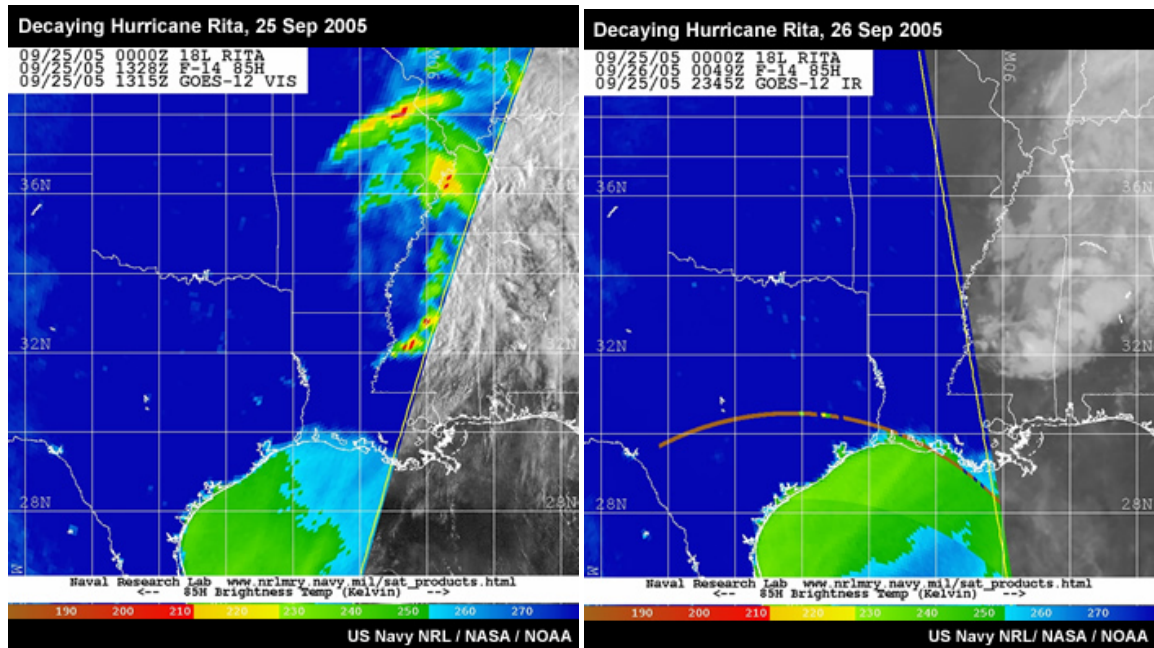


Fig. 10.40. Combined infrared and SSM/I satellite images of the decaying Hurricane Rita between 1200 UTC 25 Sep (left) and 0000 UTC 26 Sep (right). Rita had decayed to  $18\text{ m s}^{-1}$  peak surface winds and minimum central pressure of  $983\text{ hPa}$ . The eyewall is no longer symmetric (left) and the eye is again overcast (right).

The hostile environment may unbalance the storm so that it ceases to be self-sustaining—and will decay—but intense storms may instead undergo transition into an extratropical cyclone (Section 10.7).

## Box 10-5 Record Tropical Cyclone Intensity in the Eastern and Western Hemispheres

### Supertyphoon Tip (1979) – The Most Intense Tropical Cyclone on Record

Supertyphoon Tip was legendary for its spatial extent as well as its intensity – most of the North Pacific basin appeared to be rotating! At its most intense, the minimum sea level pressure of Tip was measured at 870 hPa at 0353 UTC on 12 October 1979.<sup>100</sup> The estimated maximum sustained (1-minute) surface wind was  $85 \text{ m s}^{-1}$  ( $305 \text{ km h}^{-1}$ ).

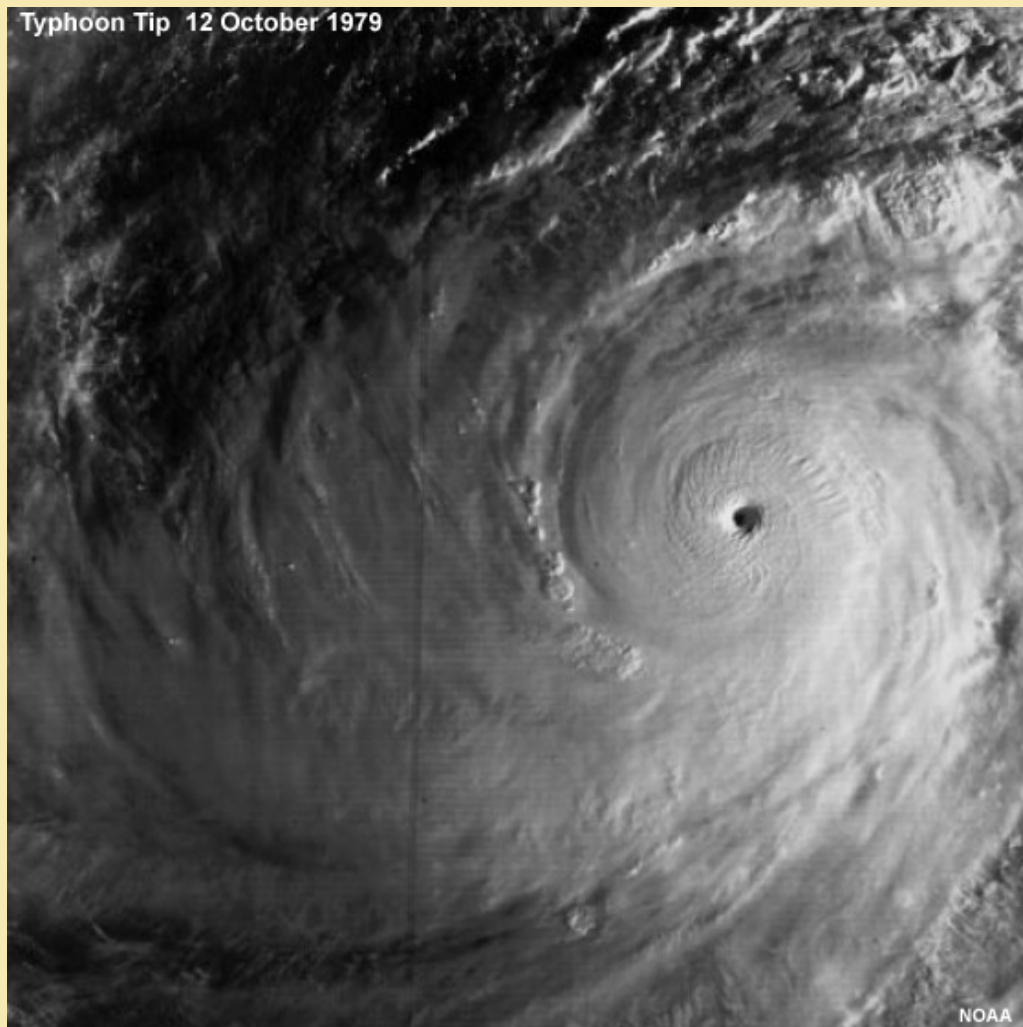


Fig. 10B5.1. Image of Supertyphoon Tip at 0353 UTC on 12 October 1979.<sup>100</sup>



<http://agora.ex.nii.ac.jp/digital-typhoon/summary/wnp/s/197920.html>

## Box 10-5 continues

Major Hurricane Wilma (2005) – The Most Intense in the Western Hemisphere

Three days after forming in the northwestern Caribbean Sea and gradually intensifying, Wilma went through an unprecedented intensification cycle from 953 hPa to 901 hPa between 2310 UTC 18 October and 0433 UTC 19 October 2005: a rate of almost 10 hPa h<sup>-1</sup>! Around 1200 UTC 19 October 2005, Wilma attained its record-setting Category 5 intensity with maximum 1-minute 10-meter winds of 82 m s<sup>-1</sup> (295 km h<sup>-1</sup>) with 882 hPa minimum central pressure—6 hPa lower than the previous record of 888 hPa in Hurricane Gilbert (1988). At peak intensity, Air Force reconnaissance measured its eye diameter to be only 3.7 km – likely a record for the smallest eye in an Atlantic hurricane. Wilma was a Category 5 hurricane for a day. On 20 October the eye diameter expanded to 74 km and the peak winds dropped to 67 m s<sup>-1</sup>. Wilma maintained this now very large eye for most of the remainder of its lifecycle. Twenty-two fatalities were directly attributed to Wilma: 12 in Haiti, 1 in Jamaica, 4 in Mexico, and 5 in Florida.

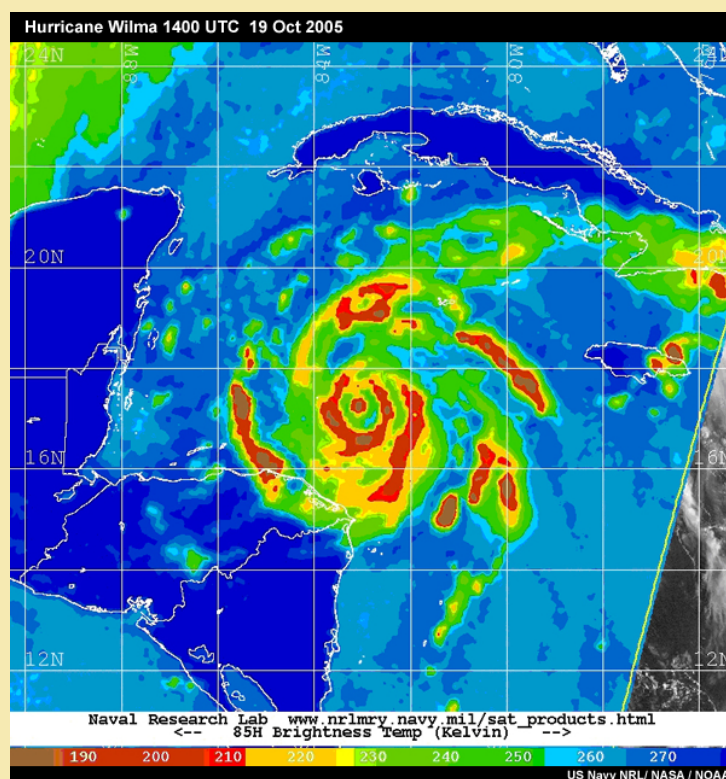


Fig. 10B5.2. Major Hurricane Wilma at peak intensity at 1400 UTC 19 Oct 2005. At this time, Wilma had a central pressure of 882 hPa and peak 1-minute surface wind speed of 80 m s<sup>-1</sup>, making it a strong Category 5 on the Saffir-Simpson scale.

## Box 10-5 continues

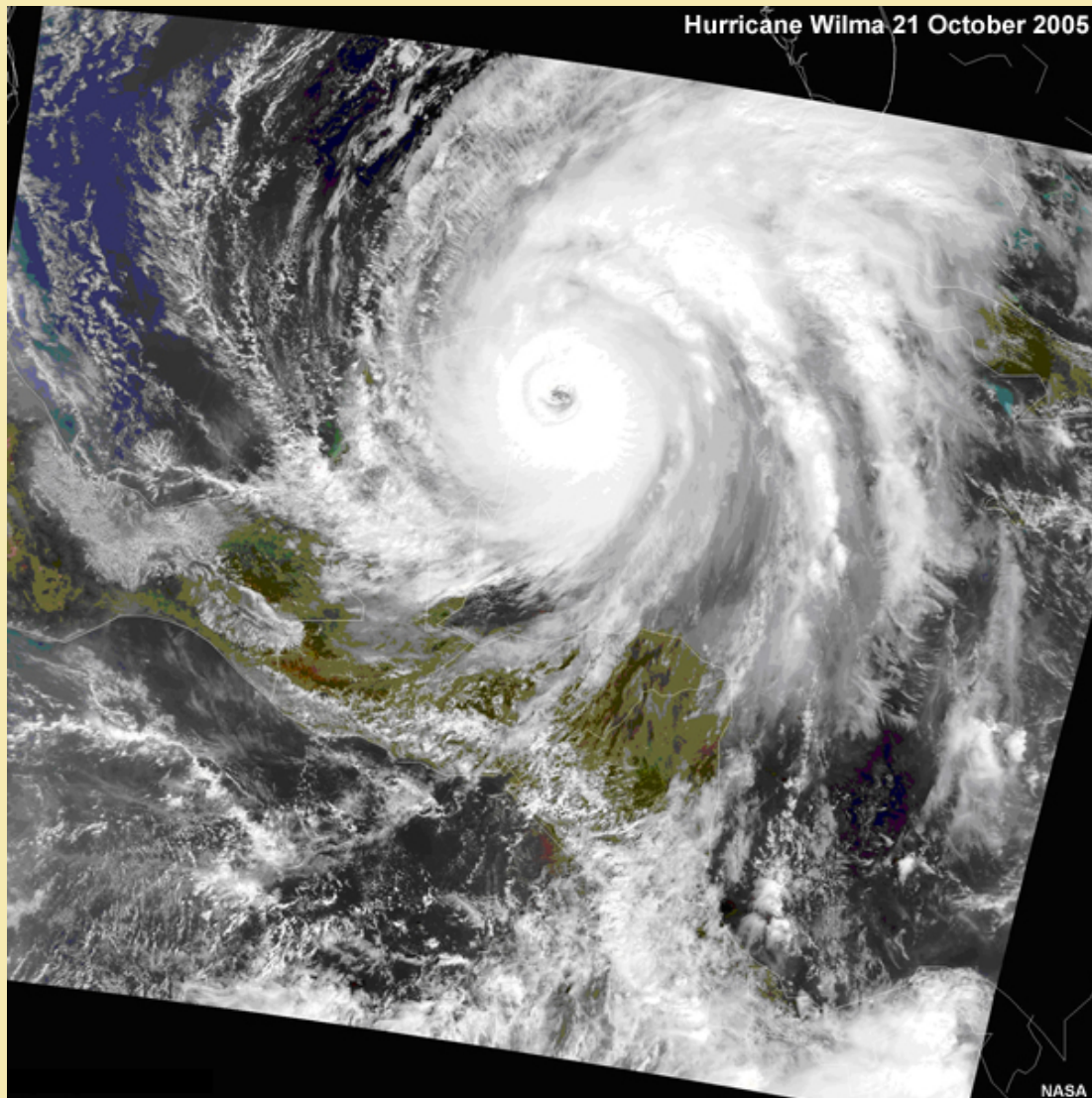


Fig. 10B5.3. Major hurricane Wilma at 1630 UTC 21 Oct 2005. At this time Wilma had a central pressure of 926 hPa and peak 1-minute surface winds of  $60 \text{ m s}^{-1}$ , making it a Category 4 hurricane on the Saffir-Simpson scale.



## 10.4.2 Potential Intensity (PI)

In 1948, Palmén<sup>101</sup> explained the 26-27°C lower SST bound for tropical storm formation in terms of the boundary layer equivalent potential temperature ( $\theta_e$ ) needed to sustain deep convection in the tropics. Through this analysis, Palmén provided insight into the source of the empirically determined lower bound on SST for tropical cyclogenesis. But how intense can a tropical cyclone become? What explains the maximum intensity a storm achieves? The development of a method for estimating the *Potential Intensity* (PI), the maximum possible surface wind speed or minimum central pressure attainable by an individual storm – has long been a goal for tropical cyclone specialists. Considering the impacts of SST and other weather systems that we have discussed, we expect the potential intensity to depend on the storm environment. Indeed, we will see that the PI is a function of the storm environment in each of the approaches discussed in this section.

### 10.4.2.1 Early Theories of Potential Intensity: CISK

Banner Miller developed a theoretical model for hurricane intensity in 1958.<sup>102</sup> He related the maximum intensity of a tropical cyclone to the (i) SST at the center of the storm, (ii) relative humidity of the surface air in the storm; (iii) lapse rates in the environment of the storm, and (iv) potential temperature at the top of the storm and its height above the surface. He reasoned that the surface temperature and humidity (and thus, to the equivalent potential temperature,  $\theta_e$ , of the surface air) determined the temperatures attained aloft in convection—and thus, the potential temperature at the top of the eyewall. Miller calculated the hydrostatic pressure drop due to the potential temperature anomaly associated with the eyewall convection, concluding that subsidence warming in the eye must be included to attain the range of observed minimum central pressures.

Miller's model of the mature hurricane is consistent with *Conditional Instability of the Second Kind* (CISK), a theory for tropical cyclone maintenance and intensification that was proposed, in the early 1960s, by two groups simultaneously.<sup>35,36</sup> According to the “CISK view”, the frictional convergence of warm, moist (high  $\theta_e$ ) boundary layer air into the tropical cyclone determines the amount of latent heat release in the eyewall convection (Fig. 10.41). In this view, boundary layer convergence provides all of the moisture available to ascend into the convection and condense as rain—thus providing the latent heat release that is converted to mechanical energy: the winds of the tropical cyclone. However, friction has two roles in CISK: (1) deceleration of surface winds (below gradient wind balance) is the cause of (2) frictional convergence that imports the moist, boundary layer air. *Thus, to intensify the storm, latent heat release must provide mechanical energy in excess of that lost to the frictional deceleration creating the convergence.* Hence, if the energy from the latent heat release balances the energy lost to surface friction, the storm will maintain its current intensity. If the mechanical energy due to latent heat release exceeds the energy lost to surface friction, the tropical cyclone will intensify.<sup>37</sup> One important component of the CISK theory is that it relies on the existence of an incipient disturbance to create the convergent inflow. Many tropical disturbances

exist, but only a few develop into tropical cyclones.<sup>34</sup> The success of an individual disturbance depends upon its environment.<sup>66,103</sup>

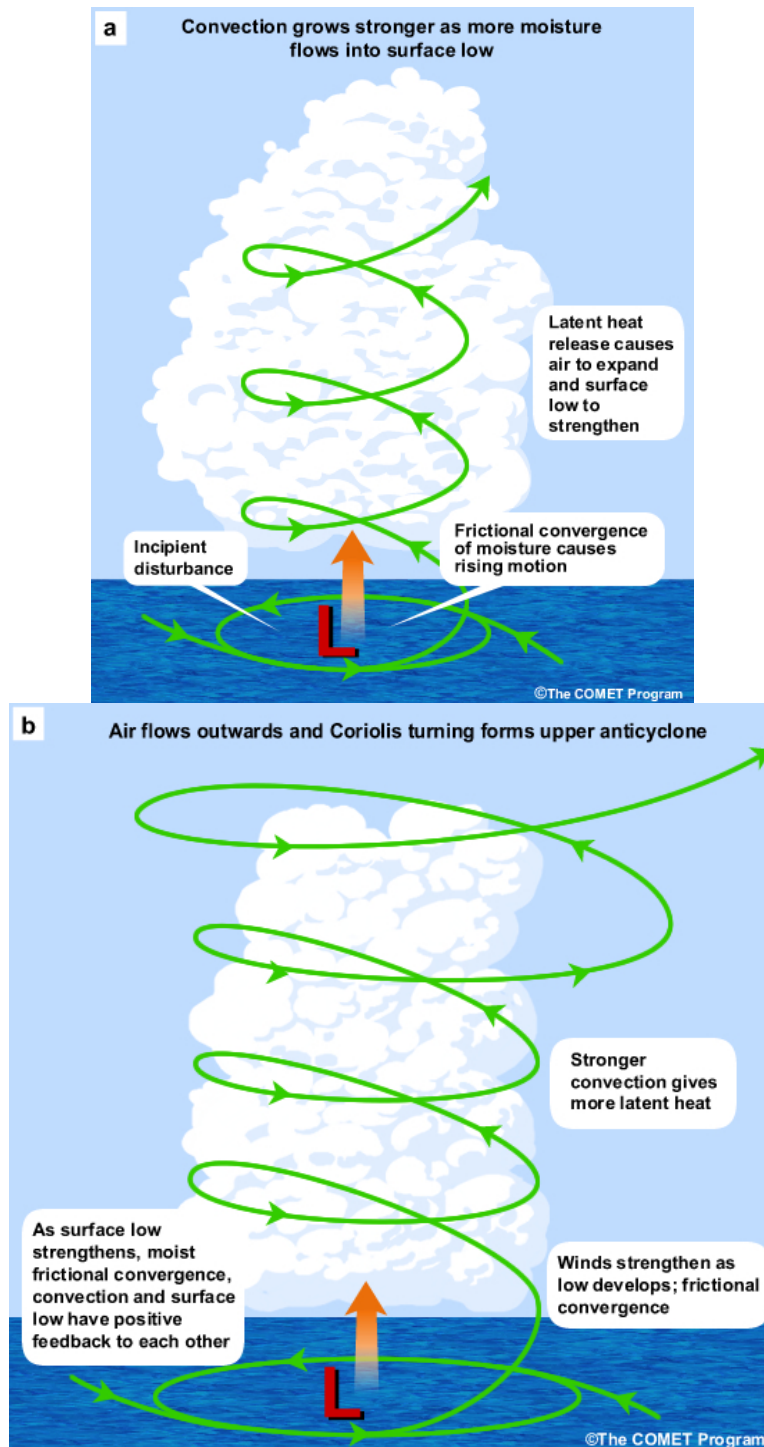


Fig. 10.41. Schematic of CISK: (a) given an incipient low-level cyclone with a moist boundary layer, frictional convergence of moisture, and forced ascent drive convection; (b) latent heating due to convection reduces surface pressure, strengthens the low-level cyclone, and enhances moisture convergence and convection in a positive feedback loop.

### 10.4.2.2 WISHE: A Carnot Cycle Theory of Potential Intensity

An alternative view of a tropical cyclone is to consider it to be a closed system, a “Carnot engine”<sup>17,104</sup> (Fig. 10.42), rather than the moist, frictionally driven convective “chimney” of CISK. As with the CISK theory, this WISHE tropical cyclone intensity theory relies on the presence of a finite amplitude incipient disturbance.<sup>16</sup>

Those familiar with thermodynamics may recall that a Carnot engine is a closed system in which heat energy is converted to mechanical energy. Our discussion of the Carnot cycle model of a tropical cyclone here will be descriptive. For a more complete, mathematical discussion of this theory, the reader is referred to the source papers.<sup>17,18,105,106</sup>

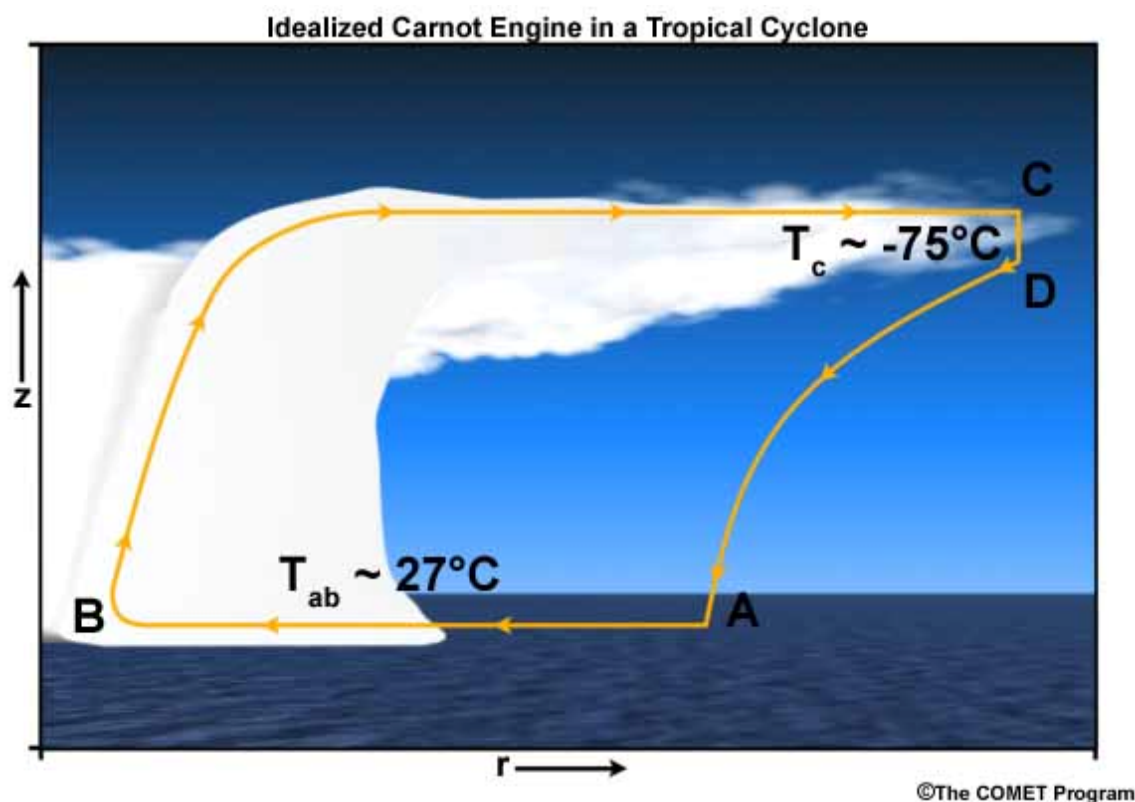


Fig. 10.42. Schematic of the energy flux in a tropical cyclone idealized as a Carnot engine. Air in the atmospheric boundary layer (bottom right to left) flows in isothermally, rises up adiabatically in the eyewall convection, flows out to great distance isothermally near the tropopause, then sinks far from the storm. See the text for details of this conceptual model.

The four “branches” of the Carnot cycle (Fig. 10.42) are: (1) isothermal inflow of near-surface air<sup>f</sup> (A-B); (2) moist adiabatic ascent in the eyewall convection and outflow just below the tropopause (B-C); and (3) sinking of cooled air in the environment far from the tropical cyclone center (C-D). To close the system, (4) the cooled air is assumed to return to the tropical cyclone environment adiabatically (D-A).

Flow from B to C and D to A is along angular momentum surfaces, although the model assumes that surfaces of angular momentum have constant saturated equivalent potential temperature ( $\theta_e^*$ ) above the boundary layer that is equal to  $\theta_e$  of the boundary layer air. Variations of moisture and frictional effects cause these surfaces to diverge in the boundary layer itself.

While the tropical cyclone is drawn as a closed system in the conceptual model pictured here, the link between the branch sinking far from the storm center and the boundary layer inflow is not supportable from observations. Further, a downwards flux of heat through the top of the boundary layer also warms it. This process is absent in all of the PI models described. Tropical cyclones exist in a complex fluid system (the atmosphere) and are not truly isolated systems. However, in spite of this and other approximations in the Carnot cycle theory of potential intensity, it provides a reasonable estimate of the upper limit for tropical cyclone intensity in a given environment, although not for the actual intensity at any given time.

Let us now consider the first two branches of the Carnot cycle: the inflow and transport of air aloft in the eyewall and outward near the tropopause. Inflow in the atmospheric boundary layer is assumed to be isothermal, even though the air is moistening due to evaporation from the sea surface and the surface pressure is dropping (since the need for an incipient disturbance discussed in Section 10.3 means that air is already flowing towards the center of a low pressure system). This means that heat must be being added to the inflowing air, otherwise the dry adiabatic expansion (due to the surface pressure drop) and evaporative cooling would both decrease the surface air temperature. In the strict formulation of the Carnot model, the heat added to keep the surface air isothermal can come from two sources: sensible heat flux at the ocean surface (warm water heating the air via conduction) and heat release due to the frictional deceleration of the winds as they flow over the ocean surface.

Air transported by moist adiabatic ascent from the surface to the top of the eyewall has the same saturation equivalent potential temperature,  $\theta_e^*$  (an approximation of the moist static energy). As a result, we can calculate the temperature difference between the air at the surface and the top of the tropical cyclone if we know (i) the value of  $\theta_e^*$  for the boundary layer air directly under the eyewall and (ii) the height of the tropopause (the maximum height of the outflow layer). This gives us the characteristics of the moist adiabatic outflow of the Carnot engine (Fig. 10.42). As we will discuss below, it is this

---

<sup>f</sup> Recall that recent analyses<sup>15</sup> of the tropical cyclone boundary layer have concluded that it is not isothermal. The impact of this result on this PI model (through changes in the inflow properties) has yet to be tested.

temperature difference between the surface and tropopause that tells us how much energy we can get from the system.

To a good approximation, as the air ascends, it is flowing along constant angular momentum surfaces, so there is an inherent assumption in this model that angular momentum surfaces have constant  $\theta_e^*$ . Angular momentum is calculated from a combination of wind speed and distance from the center of the coordinate system (in this case, the center of the tropical cyclone), and the winds in a tropical cyclone rotate more slowly as we look higher above the surface and as we move to larger radii. This means that surfaces of constant angular momentum must slope outward with height, in agreement with the schematic in Fig. 10.42. This is consistent with the sloping nature of the eyewall evident in the photograph from Hurricane Ivan (2004) (Fig. 10.43).

The reasons for the slope of constant absolute angular momentum surfaces in a tropical cyclone and the link to the eyewall structure are discussed in Box 10-6.



Fig. 10.43. Photograph of the sloping eyewall of Hurricane Ivan (2004). Photograph taken by Jenni Evans from the NOAA WC-130 mission flying into Ivan the night before it made landfall on the Gulf of Mexico coast.

We have seen that the source of energy for the theoretical Carnot cycle tropical cyclone is the underlying ocean. Evaporation, sensible heat flux and heat from friction combine to maintain an isothermal and increasingly moist boundary layer inflow to feed the deep convection of the eyewall. In the traditional CISK view of tropical cyclone lowering,<sup>35,36,102</sup> frictional convergence of moist boundary layer air, which provides fuel for latent heat release in the eyewall, and subsidence within the eye combine to create and maintain the warm core of the tropical cyclone, lowering the surface pressure. In the Carnot cycle view, the air rises nearly moist adiabatically in the eyewall, conserving  $\theta_e^*$  while becoming increasingly dry due to rain.<sup>18,104</sup> The net result is much cooler

temperatures in the outflow layer (just below the tropopause) than the boundary layer inflow temperatures (which are taken to be the same as the SST) (Fig. 10.42). This temperature difference between the ocean surface and the tropopause provides the thermodynamic energy to drive the system.

We calculate the efficiency,  $\varepsilon$ , of the tropical cyclone Carnot engine to determine the fraction of the heat energy that can be converted into mechanical energy. Using typical values for the SST and tropopause temperatures (Fig. 10.42), we solve for  $\varepsilon$ :

$$\varepsilon = \frac{(T_{IN} - T_{OUT})}{T_{IN}} \cong \frac{(SST - T_{TROP})}{SST} = \frac{(300 - 200)}{300} = \frac{1}{3} \quad (8)$$

So we see that approximately one third of the available heat energy can be converted into mechanical energy.

How does this translate to TC winds? Emanuel assumed gradient wind balance for the tropical cyclone. As we have already seen, observations (Fig. 10.8) and balanced flow diagnostics (Section 10.2.2.1) support gradient balance as a reasonable assumption,<sup>22,107</sup> especially in the strong wind region of the storm. Given the drop in the central pressure under the eye (which is solved for in the Carnot cycle model) and assuming a distance to the undisturbed environment and an environmental pressure (model parameters that must be assigned), the gradient wind distribution for the three-dimensional wind field can be calculated.<sup>17,104</sup>

More recent elaborations on this Carnot cycle theory of tropical cyclones have explored the impacts on PI of other important features of tropical cyclones such as (1) an explicit, subsident eye,<sup>108</sup> (2) frictional dissipation,<sup>105</sup> (3) the partition of latent and sensible surface heat fluxes,<sup>18</sup> (4) the feedback on intensity due to tropical cyclone modulation of SST, (5) the storm environment,<sup>106</sup> and (6) the role of sea spray in modulating tropical cyclone intensity.<sup>109</sup> Each of these studies highlights the sensitivity of the symmetric Carnot cycle model of tropical cyclone potential intensity to the underlying assumptions. Changes to the assigned model input parameters (environmental humidity and pressure, for example) can impact the estimated PI by up to one Saffir-Simpson category,<sup>108</sup> so we expect variations in PI due to the treatment of these aspects of the tropical cyclone. Thus, uncertainties in the estimation of the PI of a given storm remain. These uncertainties give us insight as to why forecasts of current intensity remain a challenge.

### 10.4.2.3 Utility of Potential Intensity in Understanding Tropical Cyclones

Four applications of PI illustrate its utility for understanding the evolution and impacts of real tropical cyclones.<sup>110</sup>

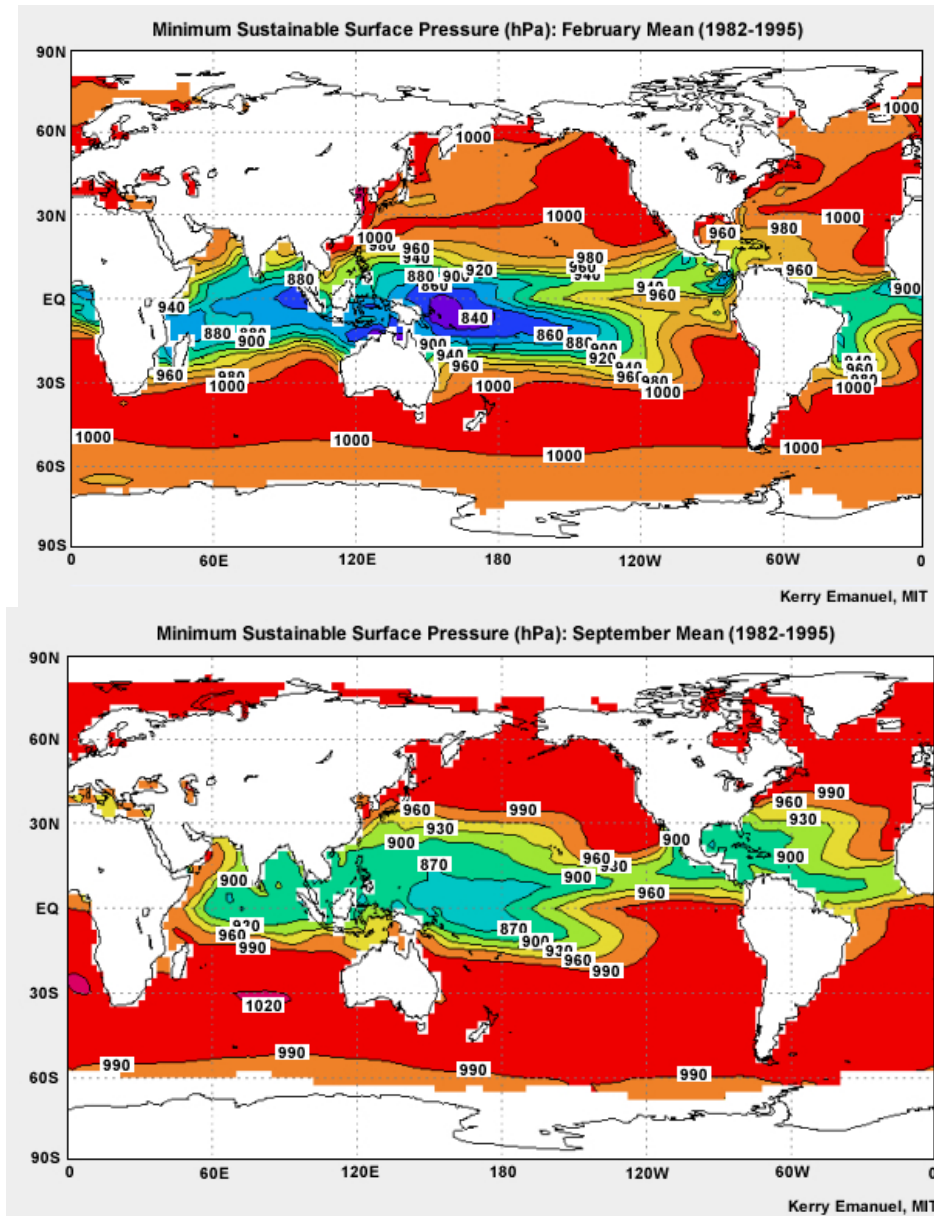


Fig. 10.44. Maps of the mean minimum sustainable surface pressure, a measure of potential intensity, in February (upper) and September (lower). Maps obtained from <http://wind.mit.edu/~emanuel/pmin/climo.html>.

The WISHE theory for tropical cyclone intensity we reviewed in Section 4.2.2.2 assumes the tropical cyclone is like a Carnot engine, so that the maximum thermodynamic energy ( $\epsilon$ , defined in Eq. (8) above) is available for conversion to mechanical energy. Hence, the WISHE theory predicts the PI of the tropical cyclone – the maximum intensity possible if only thermodynamic processes were acting – rather than the actual intensity expected for the storm at any time. Although WISHE does not predict actual storm intensity, it is useful for understanding the global distribution of tropical activity (Fig. 10.44).

Our second application of PI is in real-time intensity forecasting. Estimation of the evolving PI of active tropical cyclones provides guidance on the possible impacts of these storms.

The *Statistical Hurricane Intensity Prediction Scheme (SHIPS)*<sup>111,112</sup> is an empirically-derived intensity model that was developed using the historical North Atlantic tropical cyclone database. Since its implementation, SHIPS has provided guidance for operational forecasts of both Atlantic and eastern North Pacific hurricane intensity. SHIPS employs a simplified PI calculation that relies only on SST.<sup>111</sup> From 1993-2005 (the last published evaluation of this forecast model)<sup>111</sup> the difference between this PI and the observed storm intensity was one consistently useful predictor for the SHIPS intensity forecasts. So our second application of PI is to assist in operational forecasts of *actual* intensity.

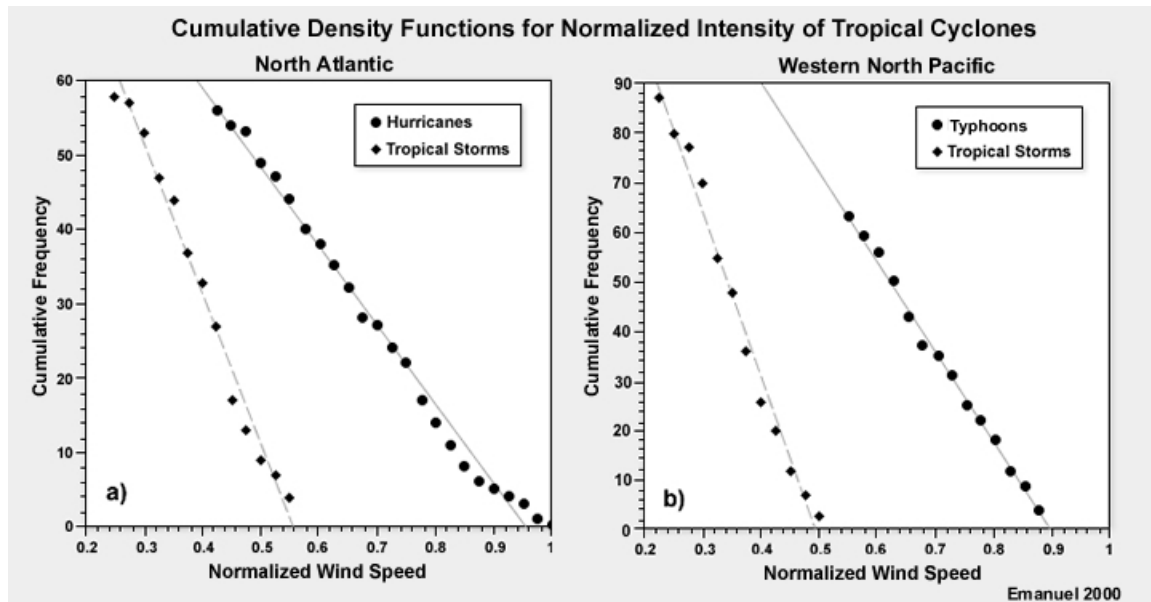


Fig. 10.45. Cumulative density functions (CDFs) for normalized intensity (actual/PI) for tropical cyclones in the North Atlantic and western North Pacific. Data are stratified by storm intensity. Only storms whose PI is not decreasing are included.

A third application of PI is to compare the observed intensity for a tropical cyclone with its PI based on the conditions on that day. Diagrams of the cumulative frequency for North Atlantic and western North Pacific tropical cyclones, presented in Fig. 10.45, show



that a tropical cyclone sampled at any random time is equally likely to have any intensity between the tropical cyclone threshold intensity and the storm PI.

The fourth application of potential intensity is in the study of the climatological impact of tropical cyclones.<sup>110</sup> The PI is assumed to be a measure of tropical cyclone impacts at a fixed location. The PI anomaly (relative to a 17-year climatology) can be tracked over time (Fig. 10.46 and Fig. 10.47). The impact of the tropical cyclone is assumed to be gone when the PI anomaly is no longer detectable.

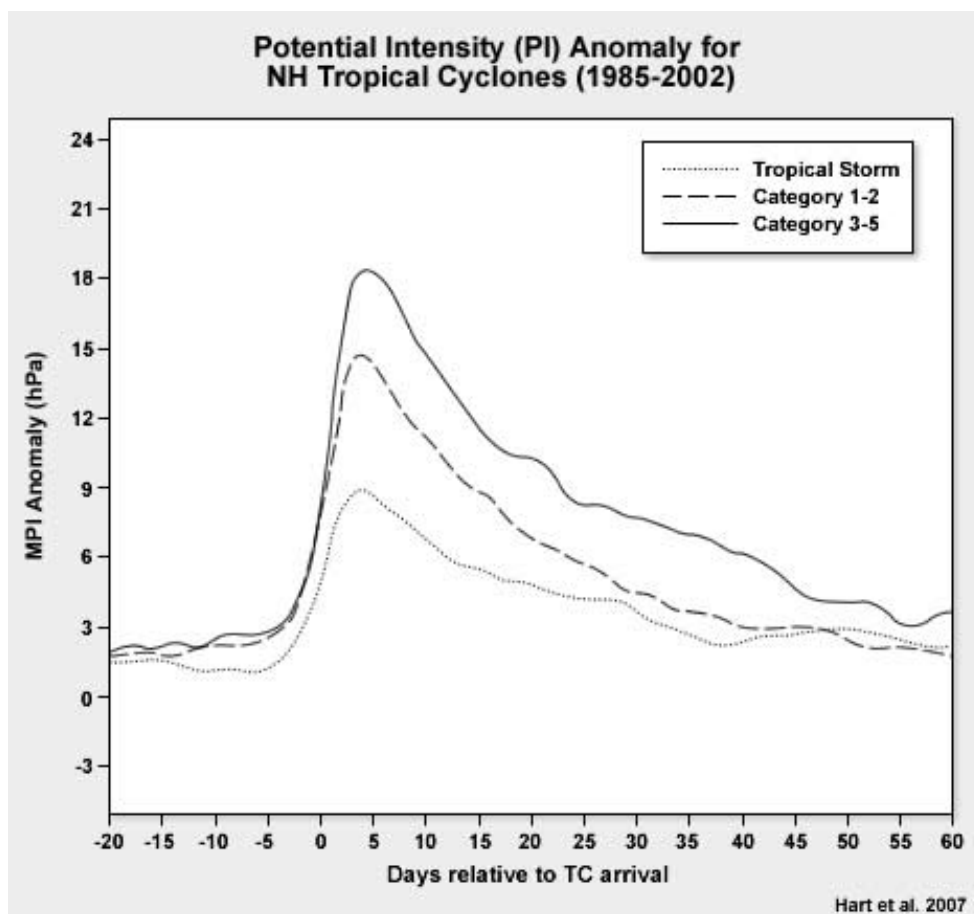


Fig. 10.46. Evolution of potential intensity (PI) anomaly for all NH tropical cyclones from 1985-2002. MPI anomaly is relative to a 17-year mean PI calculated over 1985-2001; this mean PI reflects the climatological spatial variation in SST and tropopause base states. All times for all storms south of 35°N and of at least tropical storm intensity are included. Climatological and anomalous PI are calculated on a 5°×5° grid. “Days relative to TC arrival” refers to the passage of a tropical cyclone into the 5°×5° gridbox over which the PI anomaly is calculated.

This analysis—plotted in Fig. 10.46—demonstrates that the impact of a tropical cyclone (measured by its PI anomaly) is obvious for over a month after its passage: the MPI anomaly increases dramatically near “days relative=0” then slowly drops in value, returning to its original value between 30 days (grey) to 60 (black) days after this. The

diagnostics plotted in Fig. 10.47 tell us that this impact of the tropical cyclone on its environment derives both from the expected SST anomaly resulting from the storm passage, but also from a long-lived atmospheric anomaly.

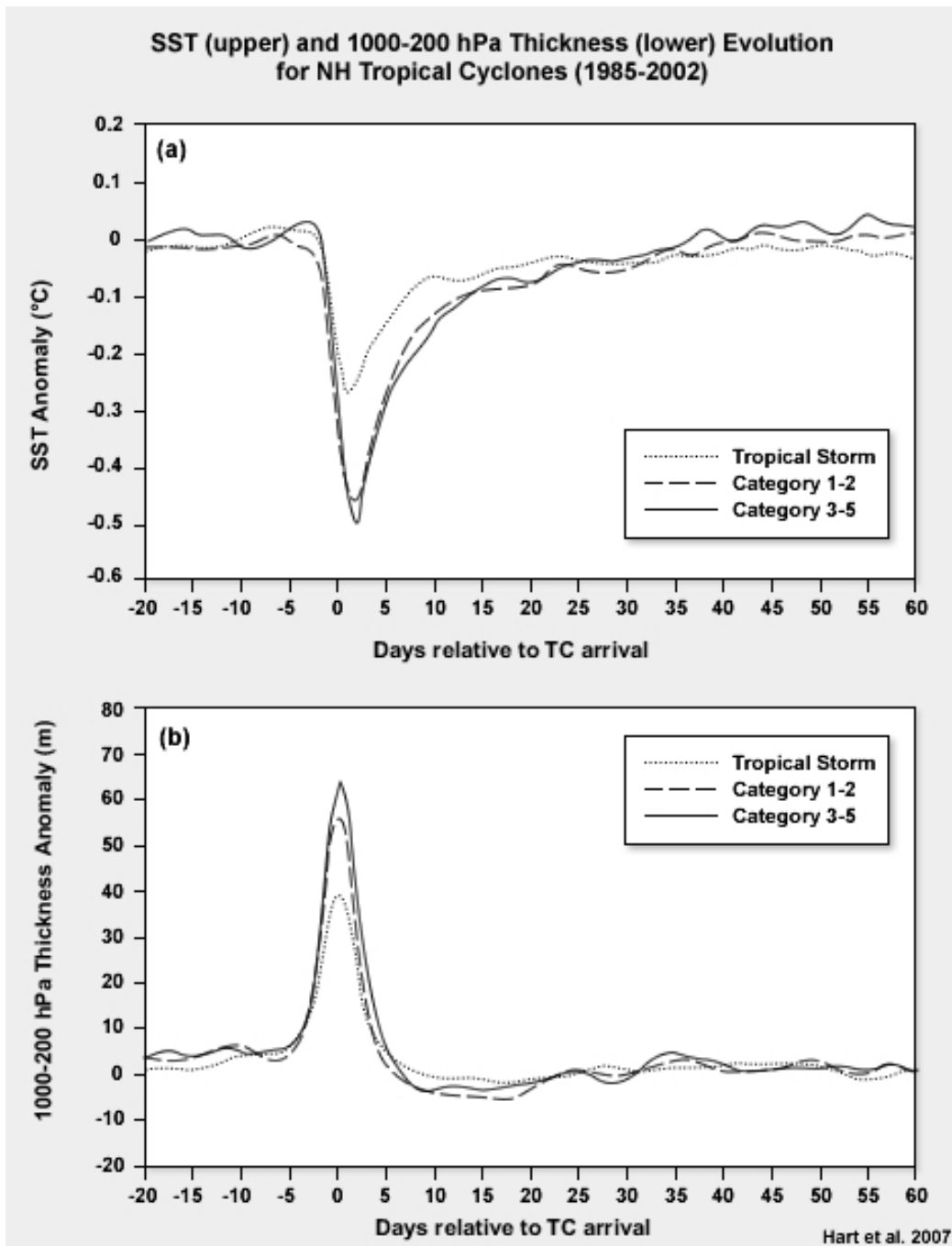


Fig. 10.47. Evolution of anomalies of (a) SST and (b) 1000-200 hPa thickness corresponding to the MPI anomaly evolution pictured in Fig. 10.46.

### Box 10-6 Sloping Angular Momentum Surfaces and Their Link to the Eyewall

In meteorology, it is conventional to refer to “*specific*” quantities<sup>g</sup>. This is because we do not define individual parcels of the atmosphere and so we are not concerned with the mass or other properties of a parcel, but rather with properties of the atmosphere in general. *With this in mind, we will discuss absolute angular momentum, remembering that we are discussing specific absolute angular momentum.*

Recall that the (specific) absolute angular momentum,  $\vec{M}$ , is defined as

$$\vec{M} = \vec{r} \times \vec{v}_a, \quad (B10-6.1)$$

where  $\vec{r}$  is the position vector (relative to the axis) and  $\vec{v}$  is the absolute velocity of the parcel whose angular momentum is being calculated.

If we are only interested in the azimuthal rotation about the vertical axis, we only need the vertical component of the relative angular momentum:

$$M = rv + \frac{f_o r^2}{2}, \quad (B10-6.2)$$

where  $M$  is now the magnitude of this vertical component of the absolute angular momentum,  $r$  is the scalar radial distance to the location where the rotational wind has speed  $v$ , and  $f_o$  is the value of the Coriolis parameter at the center of the storm. Since  $\frac{\partial v}{\partial z} < 0$  (the rotational wind speed decreases with height),  $\left. \frac{\partial M}{\partial z} \right|_{r=\text{constant}} < 0$ , so angular momentum decreases as you go upwards at a constant radius from the center. The contribution of the second term,  $\frac{f_o r^2}{2}$ , to the angular momentum gives  $\frac{\partial M}{\partial r} > 0$  increases as radius increases since  $f_o$  is constant and  $r^2$  increases rapidly with radius. The winds increase, then decrease with radius, so  $\frac{\partial M}{\partial r} > 0$  inside the radius of maximum winds and  $\frac{\partial M}{\partial r}$  is small at large radii (since the decreasing winds and increasing radii oppose).

Combining this information on  $M(r,z)$  leads us to outward and upward sloping surfaces of constant absolute angular momentum. Since a fluid will flow along surfaces of constant absolute angular momentum in an adiabatic system, this confirms the near-moist adiabatic nature of this ascent. So now that we agree that (i) the sloping eyewall is a constant angular momentum surface and (ii) for our isolated, symmetric tropical cyclone air flowing along this surface must remain moist adiabatic, let us continue our exploration of the remaining aspects of the Carnot cycle theory.

<sup>g</sup> “*Specific*” quantities are *quantities that are normalized per unit mass*. For example, mass is represented by the inverse density,  $\rho$ , which equates to volume per unit mass.

### 10.4.3 Why is Every Storm not a Cat 5? Environmental Factors Governing Intensity

The conditions assumed in the CISK and WISHE conceptual tropical cyclone models – warm ocean waters,<sup>101</sup> much cooler outflow temperatures,<sup>102</sup> boundary layer convergence, and high relative humidity and accompanying convection<sup>35,36</sup>—are all present for every tropical storm. So why does every tropical cyclone not intensify to  $100 \text{ m s}^{-1}$ ? Because reality is not the ideal! The large-scale environment changes under the influence of other weather systems.

Variations in the same environmental factors governing intensification can also limit the intensity of a storm: insufficient humidity, cooler SST or warmer tropopause, dry air intrusion, a region of strong baroclinicity are all inhibitors of intensification. “Potential” intensity is only achievable when these factors combine favorably. While these environmental characteristics can inhibit intensification, taking these factors to the other extreme, for example, no vertical wind shear and very warm waters, does not provide the ideal environment for a storm to reach its PI.

The actual intensity of a tropical cyclone that is moving rapidly out of the tropics can even exceed its PI! These storms are most likely undergoing extratropical transition (Section 10.7). Since the environment for this storm is changing so rapidly, its intensity cannot adjust quickly enough to the current environment of the storm so the current intensity tells you more about where the storm has just been (the SST and tropopause temperatures it has experienced earlier in its track) than where it is now.

Figure 10.48 is reproduced from a study<sup>113</sup> of the observed distribution between intensity and SST. The 20-year period chosen was predominantly in the satellite era (1967-1986). The SST range plotted is from 15-35°C. All times for all storms in the dataset were included in the analyses depicted in both Figs. 10.48 and 10.49, so we should interpret these results in terms of the storm lifecycle.

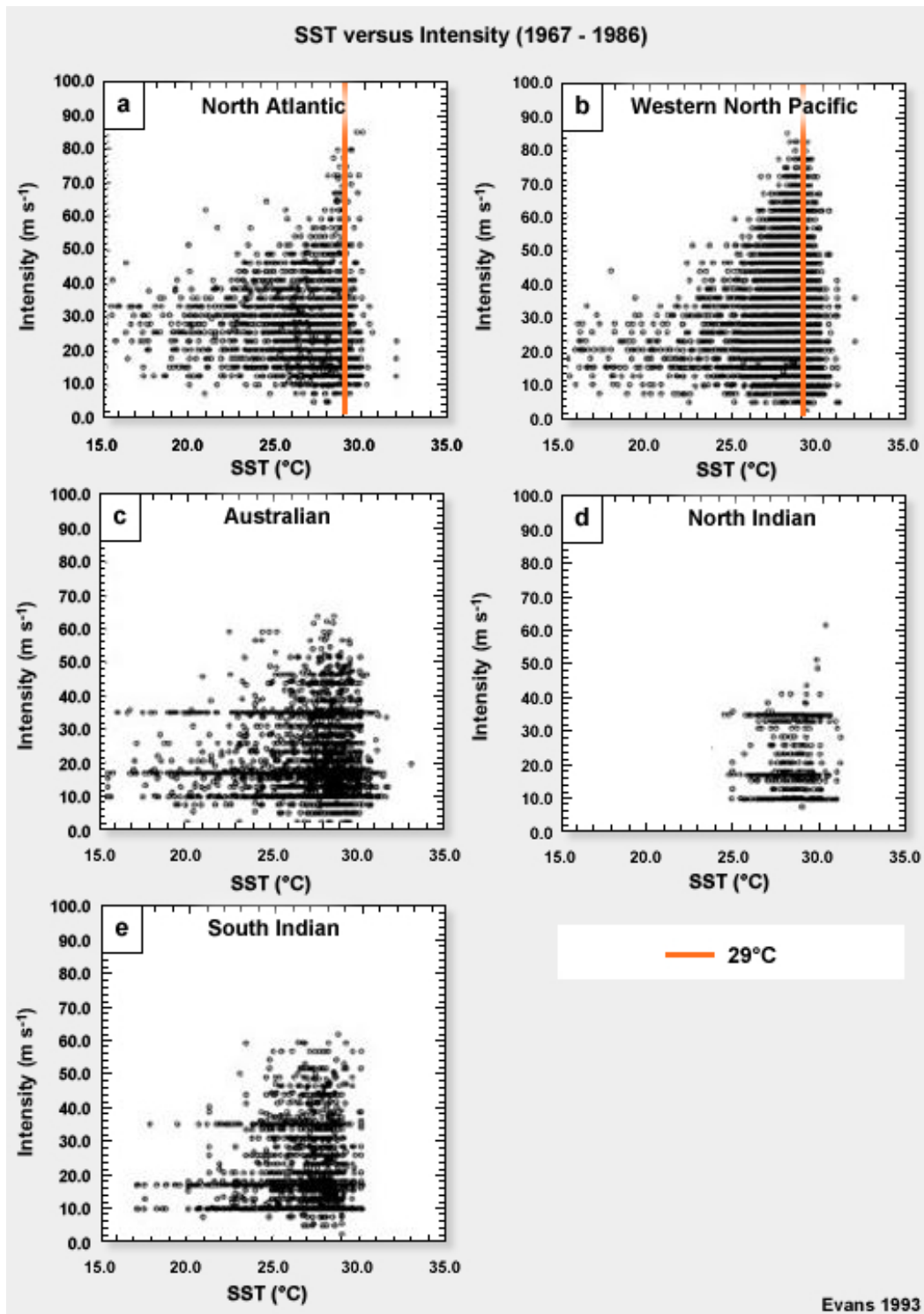


Fig. 10.48. Intensity ( $\text{m s}^{-1}$ ) against SST ( $^{\circ}\text{C}$ ) for (a) North Atlantic, (b) western North Pacific, (c) Australian, (d) North Indian, and (e) South Indian basins. All storm observations for the 20 year period 1967-1986 are included. Figure is from Evans (1993).<sup>113</sup>

Three conclusions can be drawn from Fig. 10.48:

1. Basins without regular reconnaissance flights (panels (c)-(e)) have intensity distributions that emphasize key intensity values (likely reflecting a dependence on satellite-based algorithms to estimate intensity)
2. Storm intensity increases dramatically for “tropical” SST > 25°C or so
3. The two basins with reconnaissance (panels (a) and (b)) show a uniform distribution of intensity across the observed SST range applicable. This means that stronger storms are restricted to a smaller, warmer range of SST.

To think about conclusion (3) in another way, picture a vertical line running through SST=29°C in both scatter plots in Fig. 10.48. In panels (a) and (b) — the two basins with regular reconnaissance flights during this 20 year period — storm intensities are distributed evenly along that line. This relatively uniform distribution of storm intensity at each SST is consistent with the result pictured in Fig. 10.45: that actual intensity normalized by potential intensity is uniformly distributed.

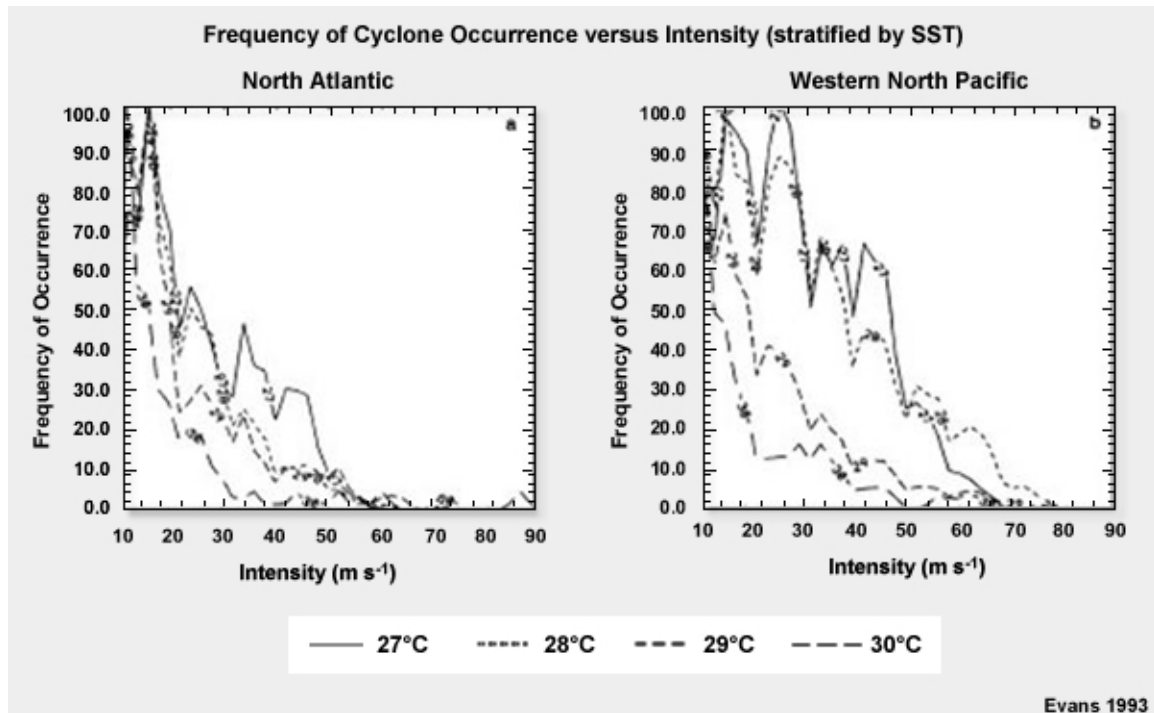


Fig. 10.49. Frequency of occurrence of storms of a particular intensity stratified by SST for North Atlantic and western North Pacific for 1°C SST bands: 27 (solid), 28 (dot), 29 (short dash), and 30 (long dash). Since there are many fewer TC observations over 30°C than 29°C etc., frequencies are scaled so that the maximum frequency for each SST is 100. This maximum frequency always coincides with the weakest intensity explored. All time periods for all storms occurring in the 20-year window are included.

Frequency distributions of intensity for 1° SST bands (Fig. 10.49) were obtained from the data used in Fig. 10.48. The mean lifecycle of a tropical cyclone is revealed by this analysis: systems over the warmest SST (30°C) of the deep tropics have the weakest intensity, indicating that this group is dominated by systems that have recently formed.<sup>113</sup> As each storm intensifies (moving towards right in each panel of Fig. 10.49), it moves over progressively cooler SST, suggesting that the intensifying storm is gradually moving poleward towards cooler (but still tropical) SST.



What factor(s) might make the warm near-equatorial waters unfavorable for tropical cyclone development? Why might a storm not intensify if it was in an environment with warm SST, no land or dry air, and no vertical shear? Hint #1: the wind speed right at the ground must be very slow. Hint #2: the warm temperatures of the ocean surface do not extend all the way to the bottom of the ocean.



The warm near-equatorial SST are unfavorable for tropical cyclone development since this is also a region of vanishing Coriolis parameter and a region where the sign of cyclonic potential vorticity changes. As a result, it is difficult to create a balanced, cyclonic incipient disturbance to intensify into a tropical cyclone. There are a few exceptions to this where storms form within 5° or so of the equator – for example, Hurricane Ivan (2004). These are usually very small (“midget”) cyclones while they are close to the equator.<sup>114</sup>

Now why could weak vertical wind shear limit storm intensity? Given the weak environmental winds near the surface, some vertical wind shear is needed to advect the storm along.<sup>115,116</sup> Without this environmental advection, a storm will have relatively slow motion. The side-effect of this slow motion over water is that the storm will mix cooler ocean water from below the thermocline.<sup>h</sup> A small contribution to this surface ocean cooling may also come from the storm rainfall. Thus, a storm that stays in the same location will cool the waters below it – and thus limit its own peak intensity.<sup>117</sup> The shear inherent in the advection of the storm may delay intensification, but if all other factors are favorable it is possible for the storm to ultimately reach its PI.<sup>83</sup>

#### 10.4.4 Links between Inner Core Dynamics, Cyclone Structure and Intensity

As we have discussed, the key to a storm maintaining its current intensity or intensifying further is the maintenance of the deep convection surrounding its core. Maintenance of intensification by the WISHE process (described in Section 10.4.2.2) requires a very moist boundary layer.<sup>84</sup> Sub-saturated convective downdrafts will lower the relative humidity (and thus, the moist static energy) of the boundary layer,<sup>18</sup> limiting the energy

---

<sup>h</sup> The thermocline is the inversion separating the near-surface warm waters from the deeper cool waters for oceans and lakes. In the oceans, the (same) thermocline also separates the fresher waters near the surface from the saltier waters below.

available to the storm. It will take a number of hours for evaporation to recover the boundary layer moisture before intensification can resume. These arguments can readily be extended to understand why dry air intrusions (from dry – even desert – land masses or from the SAL in the case of the Atlantic Ocean) negatively impact intensifying tropical cyclones: the dry tropospheric air weakens the convection, creating sub-saturated downdrafts, which subsequently cools the boundary layer and lowers its relative humidity.

In thinking about why every tropical cyclone does not become a  $100 \text{ m s}^{-1}$  behemoth, we argued that a minimum level of vertical wind shear is necessary for a storm to maintain its intensity or to intensify further. While this is true, the strong vertical wind shear that leads a storm to begin recurvature causes the majority of storms to weaken.<sup>118,119</sup> This weakening can be understood in terms of the reorganization of the storm in adjusting to this new environment.<sup>77,87</sup> The tropical cyclone is a fluid vortex and so it is not separate from its environment: the cyclone and environment are part of one system. Thus, we cannot think of the environment blowing past the storm or blowing it over. The environmental wind shear will cause the storm to reorganize through induced convection on the downshear side of the storm that will initially create an asymmetry. Ultimately the storm will either re-intensify in the vertical wind shear (possibly undergoing ET; Section 10.7) or it will decay.

These arguments do not apply uniformly across all tropical cyclone intensities. As we discussed in Section 10.2.2.2, the inertial stability of a tropical cyclone increases with increasing intensity. Since inertial stability is a measure of the resistance of a tropical cyclone to external influences, increasingly intense tropical cyclones should be more resistant to adverse environmental effects. For example, a storm rotating with peak surface windspeeds of  $50 \text{ m s}^{-1}$  would be less disrupted by strong vertical wind shear than a storm of  $20 \text{ m s}^{-1}$ . Equally well, a storm whose strong winds extend further from its center will also be more resilient, since this storm will have large values of inertial stability out to larger radius.<sup>120</sup> However, the inertial stability of the tropical cyclone decreases dramatically aloft (Fig. 10.10), so the tropical cyclone is susceptible to upper-tropospheric environmental forcing.

There is one environmental exception to this argument of inertial stability providing the tropical cyclone with increased protection against adverse environmental effects: the SST. Since the ocean surface impacts the tropical cyclone from below, no amount of inertial stability will “protect” the tropical cyclone from adverse impacts due to cool SSTs.



### 10.4.5 Estimation of TC Intensity by Remote Sensing

Remote-sensing is the primary method of observing tropical cyclones, which spend most of their lifetime over the ocean, outside of the network of *in situ* instruments. In addition to estimates of intensity, remotely-sensed observations help scientists to understand the large-scale environment and TC internal instabilities, factors which influence tropical cyclone intensity.<sup>76,121,122</sup> Instruments include satellite radiometers (IR, visible, and microwave), precipitation and cloud radars (ground, airborne, and satellite), satellite scatterometers, and synthetic aperture radars (SAR). Figure 10.50 illustrates recent advances in satellite radar and microwave observations of tropical cyclone structure.

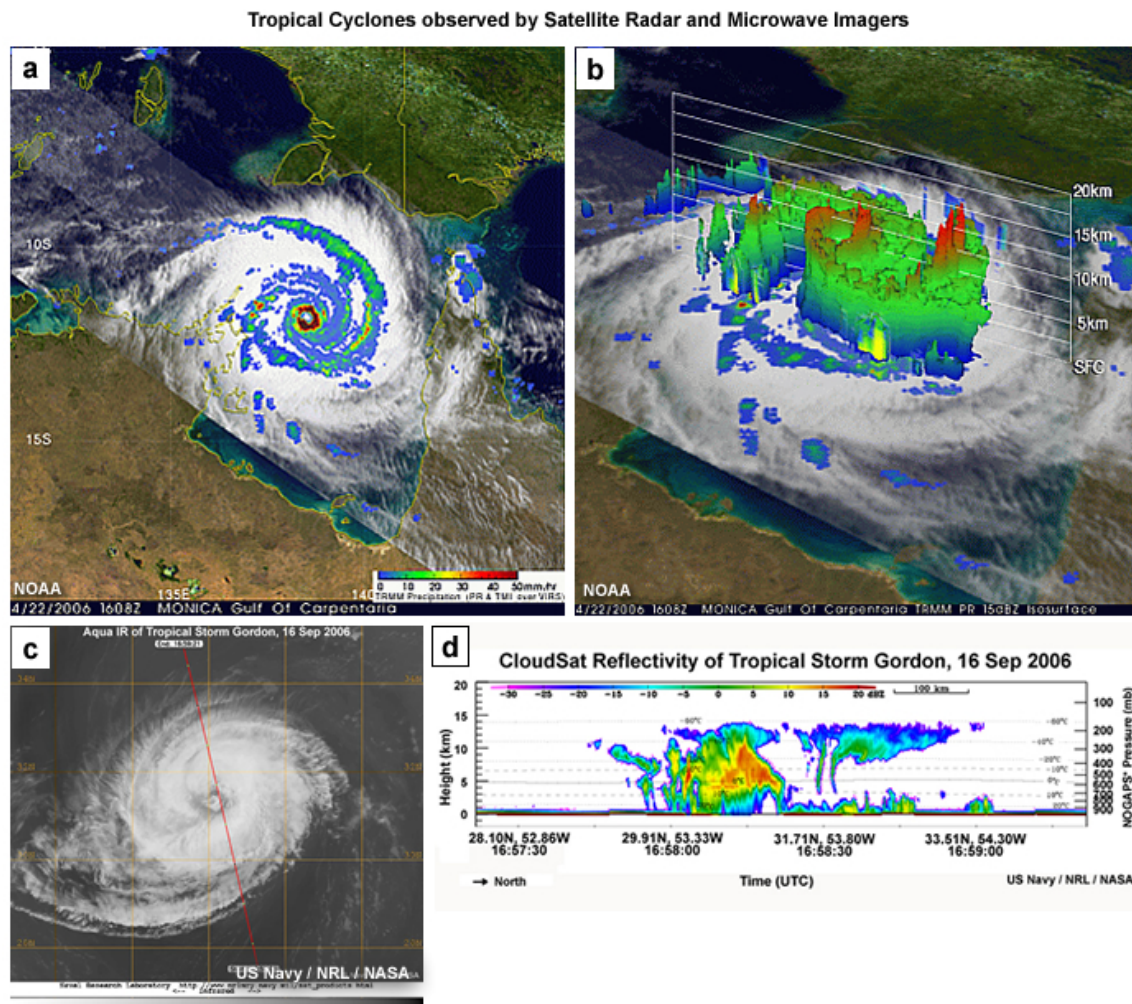


Fig. 10.50. Tropical cyclone satellite observations: (a) the Tropical Rainfall Measurement Mission (TRMM) Precipitation Radar (PR), TRMM Microwave Imager (TMI), and Visible Infrared Scanner (VIRS); (b) 3D radar reflectivity from the TRMM PR; (c) Aqua-EOS IR; and (d) CloudSat reflectivity profile along the red line in (c).



TRMM Radar Animations, [http://trmm.gsfc.nasa.gov/publications\\_dir/multi\\_resource\\_tropical.html](http://trmm.gsfc.nasa.gov/publications_dir/multi_resource_tropical.html)  
 US Navy NRL, CloudSat TC images, [http://www.nrlmry.navy.mil/tc\\_pages/tc\\_home.html](http://www.nrlmry.navy.mil/tc_pages/tc_home.html)  
 (Click on CloudSat button in upper right)

### 10.4.5.1 Satellite-IR Estimates

Satellite sensors are the most suitable instruments for observing the full lifecycle and intensity changes of TCs across the globe. The analysis of geostationary longwave (IR) images is the standard method of estimating TC intensity, with the exception of the North Atlantic and Northeast Pacific, where aircraft reconnaissance flights are routine.

In 1975, Vern Dvorak introduced a classification scheme for estimating the intensity of TCs from satellite imagery.<sup>123</sup> The “Dvorak Technique”, which was developed using empirical data, relates a numerical index (called the current intensity or CI) to an estimate of the maximum sustained winds (MSW)<sup>123</sup> at the surface (Table 10.2). With frequently available geostationary IR images (15-30 minutes routinely and 5 minutes in rapid-scan mode), the intensity can be updated for continuous operational forecasting.

The Dvorak Enhanced IR technique uses a special enhancement, known as the IR-BD curve, to identify intense convection and changes in the cloud top pattern around the eye. It identifies four basic TC pattern types, the:

- **Eye pattern**
- **Curved band pattern**
- **Shear pattern**
- **Central dense overcast (CDO) pattern**

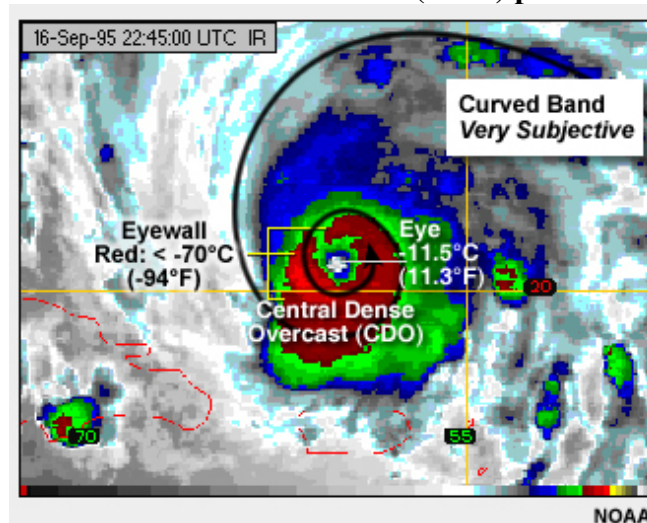


Fig. 10.51. Sample identification of the Dvorak eyewall pattern, subjective curved band pattern, and CDO.

The eye pattern identifies the temperature contrast between the warmest part of the eye and the coldest surrounding convection within 55 km (e.g., Fig. 10.51). The greater the temperature contrast, the stronger the system. The curved band pattern is based on the idea that the more wrapped around the rainbands, the greater the system vorticity. The curved band pattern is often easier to follow in visible images than in IR images. The CDO is the area covered by the cirrus clouds that extend from thunderstorms in the eyewall and rainbands of a TC. The shear pattern examines the distance from the

low-level center to the CDO with the principle being that greater involvement of the low level center with the deep convection indicates a stronger system. The CDO appearance is judged on its size and degree of banding.

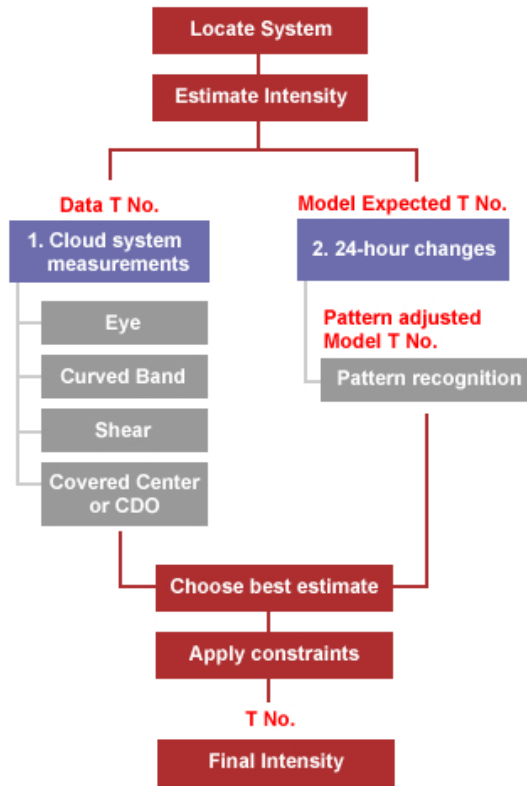
Table 10.2 Summary of the Dvorak Atlantic and western North Pacific wind–pressure relationships.

CI	MSW (kts)	MSLP (hPa)	
		Atlantic	WestPac
1.0	25		
1.5	25		
2.0	30	1009	1000
2.5	35	1005	997
3.0	45	1000	991
3.5	55	994	984
4.0	65	987	976
4.5	77	979	966
5.0	90	970	954
5.5	102	960	941
6.0	115	948	927
6.5	127	935	914
7.0	140	921	898
7.5	155	906	879
8.0	170	890	858

(From Velden et al.<sup>124</sup>)

The following basic steps in the Dvorak Technique are illustrated in a decision tree in Fig. 10.52:

- (1) Find the cloud system center, which is the point towards which the cloud bands spiral. Center location is fairly easy if the low-level circulation is exposed, otherwise, the center is identified by other features such as cirrus outflow, animation, or extrapolation;
- (2) Make two-quasi-independent estimates of the intensity of the TC. Assign a T or “tropical” (T No.), which is related to storm intensity (Fig. 10.53);
- (3) Choose the best estimate;
- (4) Apply selected rules to determine final intensity.



Adapted from Velden et al. 2006

Fig. 10.52. The basic steps in the Dvorak Technique.

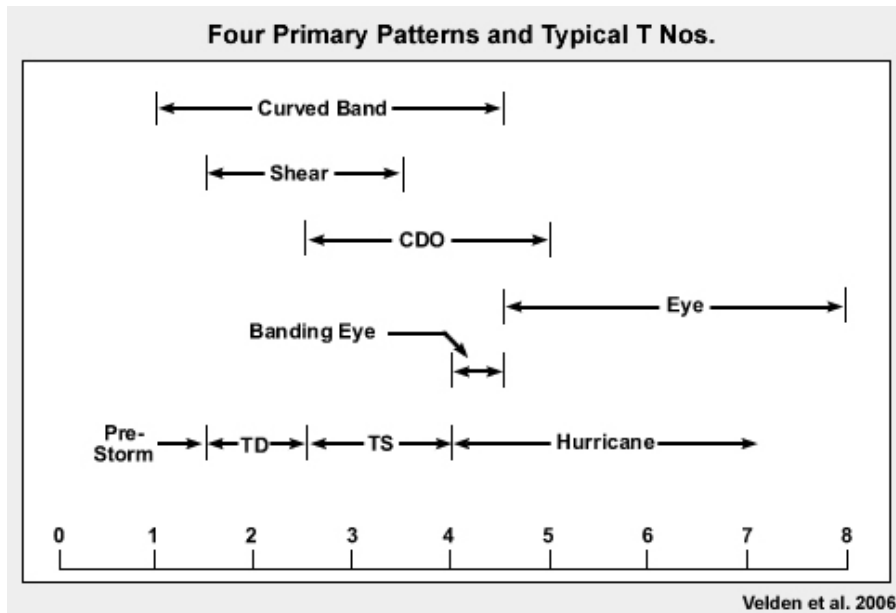


Fig. 10.53. Primary Dvorak cloud patterns relative to T No. and typical TC intensity range assignments (Velden et al.<sup>125</sup>).

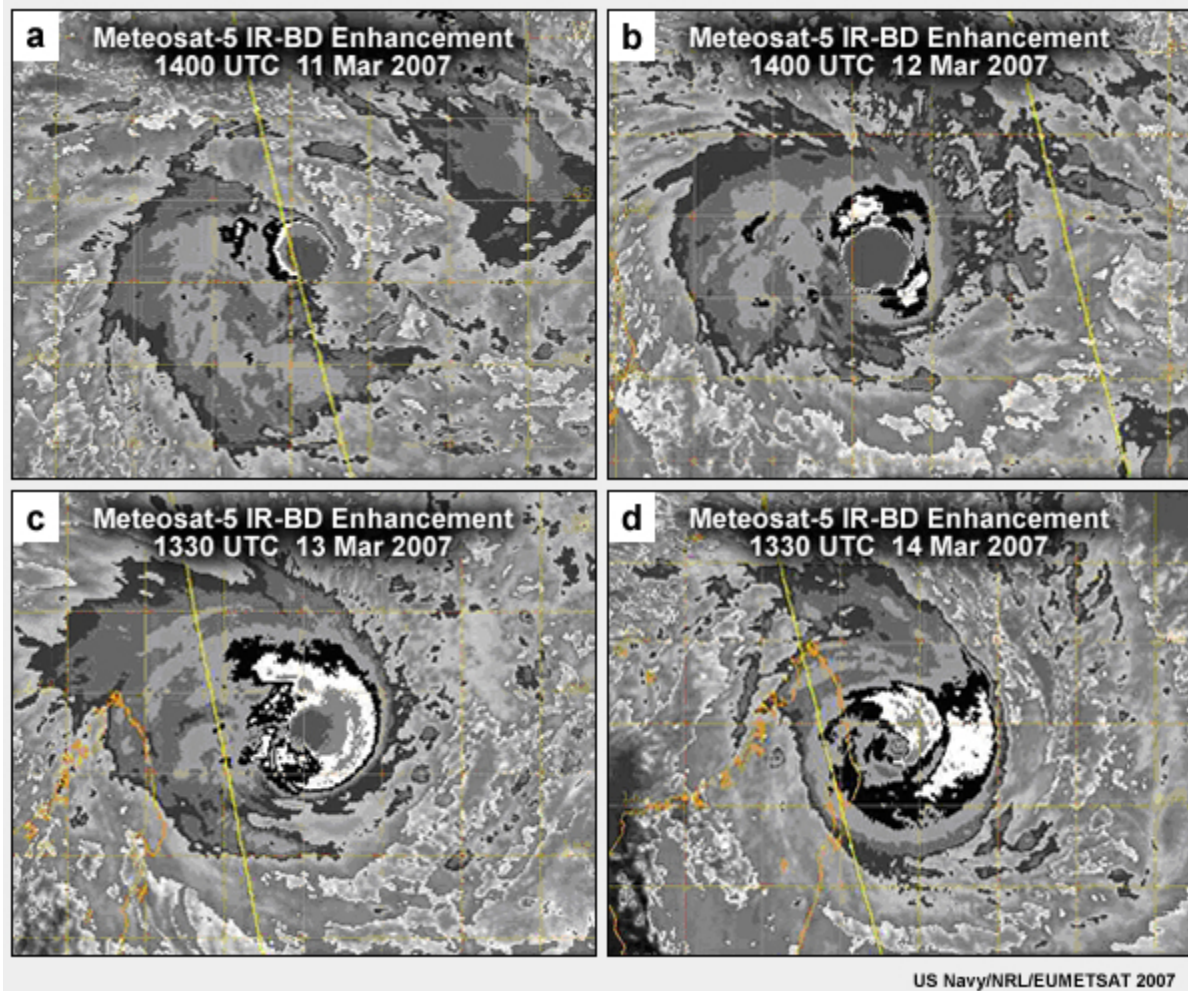


Fig. 10.54. IR-BD enhanced images of Tropical Cyclone Indlala (2001) with central pressure of (a) 994 hPa, (b) 984 hPa, (c) 967 hPa, and (d) 927 hPa.

 [Animation of Indlala images](#)

Figure 10.54 shows changes in the cloud organization, central area of the cyclone, and rain bands as Tropical Cyclone Indlala intensified. Between 11 and 12 March, no eye is observed in the IR but the CDO expands and the bands become more curved. During 13 and 14 March, the formation of a small eye (with warmer temperatures relative to the eyewall), the expanded area of very cold cloud in bands around the eye, and a more symmetric cold cloud pattern indicate the increased intensity of Indlala.

The Dvorak Technique has been updated<sup>124</sup> and automated<sup>126</sup> through the use of digital IR data and objective algorithms that are based on the original empirical relationships. First was the Objective Dvorak Technique (ODT), then the Advanced Objective Dvorak Technique (AODT), and, as of 2006, the Advanced Dvorak Technique (ADT). An example of comparison between aircraft reconnaissance observations of the intensity of Hurricane Ivan (2004) with both the ODT and ADT is presented in Figure 10.55.

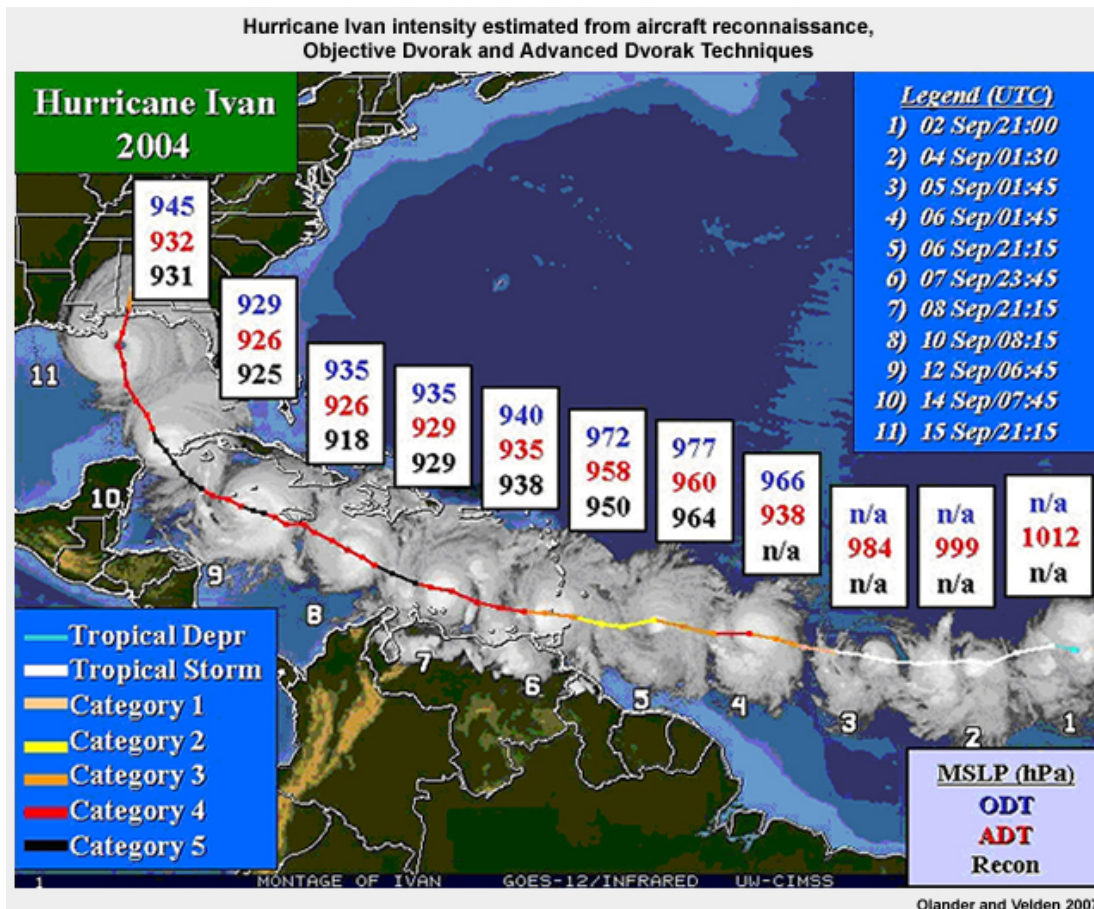


Fig. 10.55. Comparison of the TC intensity estimates from aircraft reconnaissance, ODT, and ADT.

IR analysis has expanded beyond the Dvorak techniques. Knaff et al. (2004)<sup>126</sup> created an objective technique for identifying annular hurricanes. An annular hurricane is “distinctly more axisymmetric with a large circular eye surrounded by a nearly uniform ring of deep convection and a curious lack of deep convective features outside this ring.”<sup>127</sup>



**Tutorials on the Dvorak Technique**

CIMSS, University of Wisconsin, Advanced Dvorak Technique,

<http://cimss.ssec.wisc.edu/tropic2/misc/adt/info.html>

Tutorial on the use of satellite data to define tropical cyclone structure

<http://severe.worldweather.org/iwtc/pptFile/Topic1/Topic1a/IWTC6-rz.ppt>

NOAA Regional and Mesoscale Meteorology Branch (RAMMB) Tropical RAMDIS Online,

<http://rammb.cira.colostate.edu/ramdis/online/tropical.asp>

### 10.4.5.2 Satellite Microwave Observations

Infrared-based techniques have the disadvantage of observing only the cloud tops. Often, thick cirrus can hide the underlying structure of the TC. Microwave radiometers have improved the detection of internal cyclone structure, such as the location of the eye, because microwave wavelengths are strongly attenuated by hydrometeors (droplets or ice crystals) inside of the eyewall and rainbands. For example, in Fig. 10.56, it is difficult to identify the eye of Tropical Cyclone Indlala from the IR images (upper panels). However, in the 85 GHz microwave images, the eye is prominent (Fig. 10.56, lower panels), providing a reliable indication of a strengthening tropical cyclone. Moreover, the region of cold cloud to the right of the eye, in the IR image, is not associated with deep convection; it shows up as blue in the microwave image. Unfortunately, microwave instruments fly on low-earth-orbiting (LEO) satellites which observe the same cyclone at most twice per day ([Chapter 3, Section 3.1.2.2](#)). Multiple daily views of the same tropical cyclone have become more common as the network of LEO satellites continues to expand.

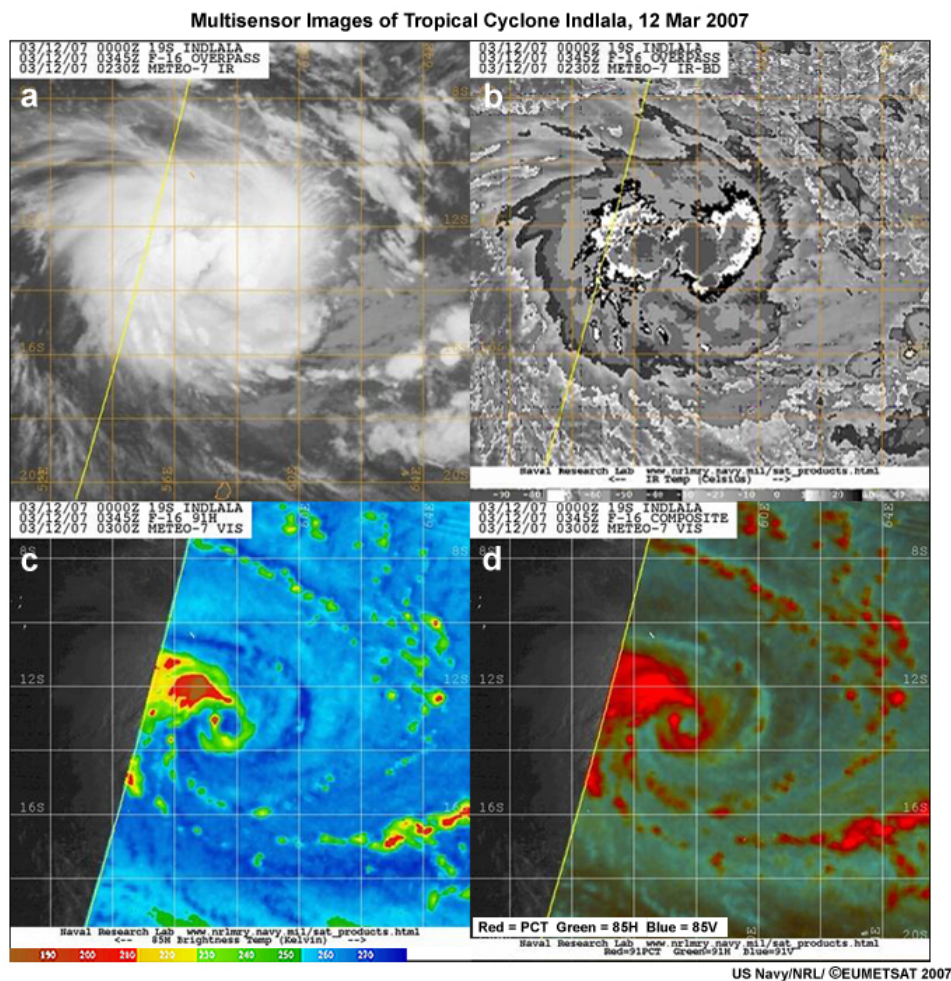


Fig. 10.56. Tropical Cyclone Indlala (2007) observed by geostationary grayscale IR and enhanced IR-BD (upper left, right) and polar-orbiting microwave 85GHz sensor (lower).

Because they show the internal structure of TCs, microwave images are helping to identify intense cyclones (Fig. 10.57), many of which display concentric eyewall structures.<sup>85</sup>

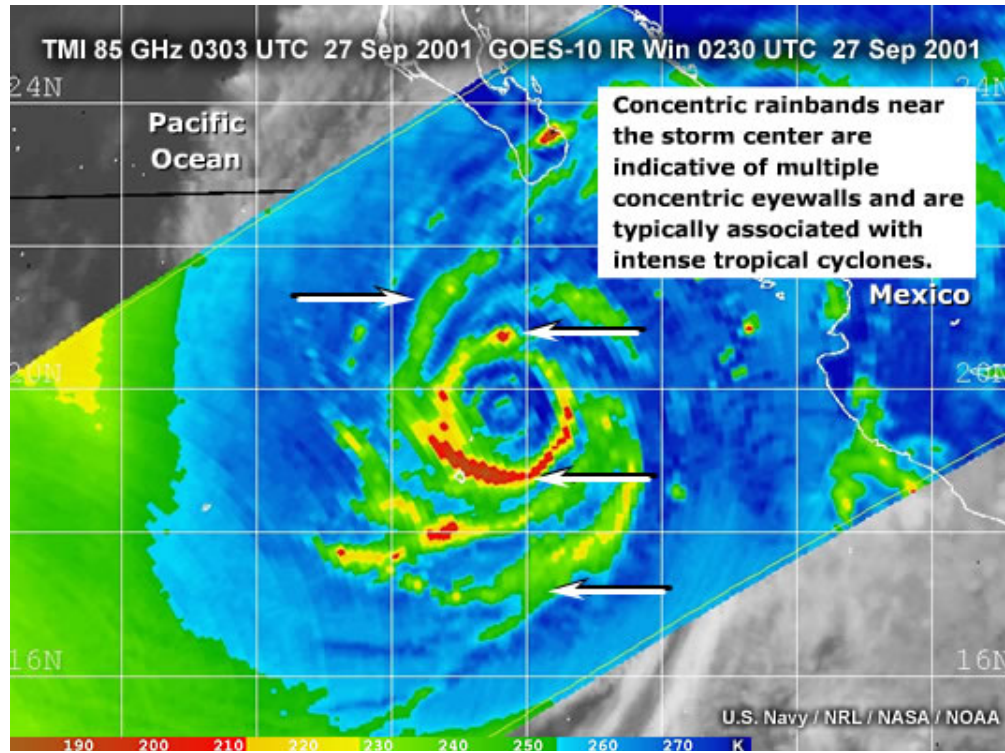


Fig. 10.57. TRMM TMI 85GHz image of Hurricane Juliette (2001). The greens, yellows, and reds indicate heavy precipitation.



A recent innovation, entitled, The Morphed Integrated Microwave Imagery at CIMSS (MIMIC) developed by Anthony Wimmers and Chris Velden of CIMSS, tries to fill the microwave temporal gap.<sup>128</sup> MIMIC creates a sequence of synthetic TC microwave images for the periods between actual satellite microwave observations by four LEO microwave instruments: the [DMSP-13/14 SSM/I \(85 GHz channel\)](#), the [TRMM TMI \(89 GHz channel\)](#) and the [Aqua AMSR-E \(85 GHz channel\)](#). The technique is based on the general expectation that tropical cyclones are roughly axially symmetric in terms of wind speed. The motion of features is the result of interpolation of images, advection, and rotation as the interpolated images are blended. The morphed images are produced every 15 minutes to match the geostationary-IR routine and are available in real-time for five ocean basins. A sample image, for Hurricane Ivan (2004), is shown in Fig. 10.58.

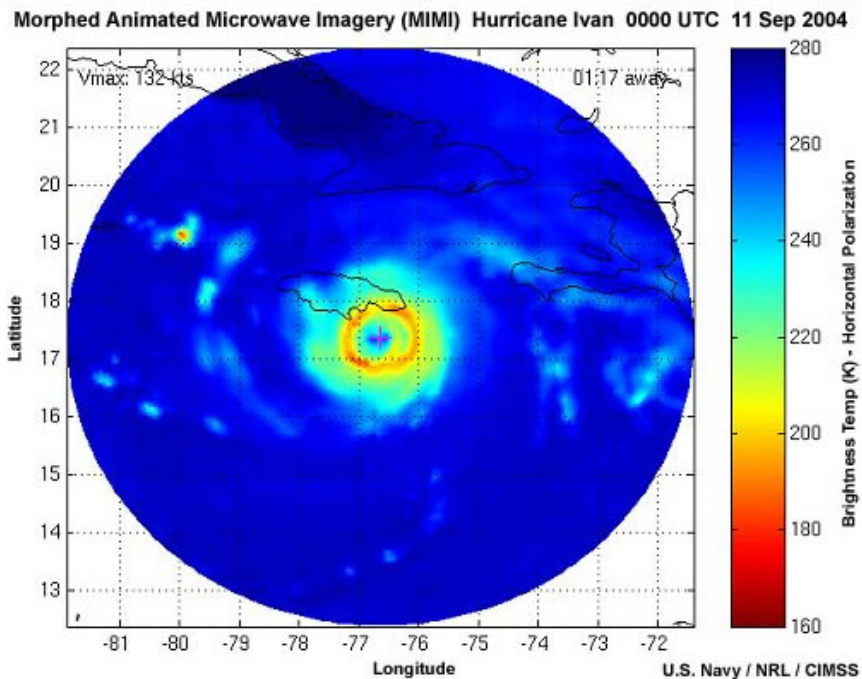


Fig. 10.58. MIMIC sequence of morphed and observed microwave images of Hurricane Ivan, September 2004.



MIMIC animation of Hurricane Ivan,  
[http://www.meted.ucar.edu/npoess/tc\\_analysis/s8p3a.htm](http://www.meted.ucar.edu/npoess/tc_analysis/s8p3a.htm)



MIMIC Home, <http://cimss.ssec.wisc.edu/tropic/real-time/marti/marti.html>  
 US Navy NRL Microwave Image Interpretation Training,  
[http://www.nrlmry.navy.mil/sat\\_training/tropical\\_cyclones/ssmi/composite/index.html](http://www.nrlmry.navy.mil/sat_training/tropical_cyclones/ssmi/composite/index.html)

While microwave instruments provide superior TC feature identification, one caveat must be considered in locating the eye of a TC; the effect of parallax. Parallax errors occur when a satellite's slanted viewing angle places features away from their actual location. Figure 10.59 illustrates how parallax errors differ at 85GHz, which is sensitive to ice scattering at high altitudes, and 37GHz, which is sensitive to emissions from liquid drops at low altitudes. The parallax error is about 5 km at 37GHz compared with 10-20 km for 85GHz. The latter frequency has higher resolution (compare Fig. 10.59, b and d) and is the preferred channel for observing tropical cyclone structure and intensity changes.

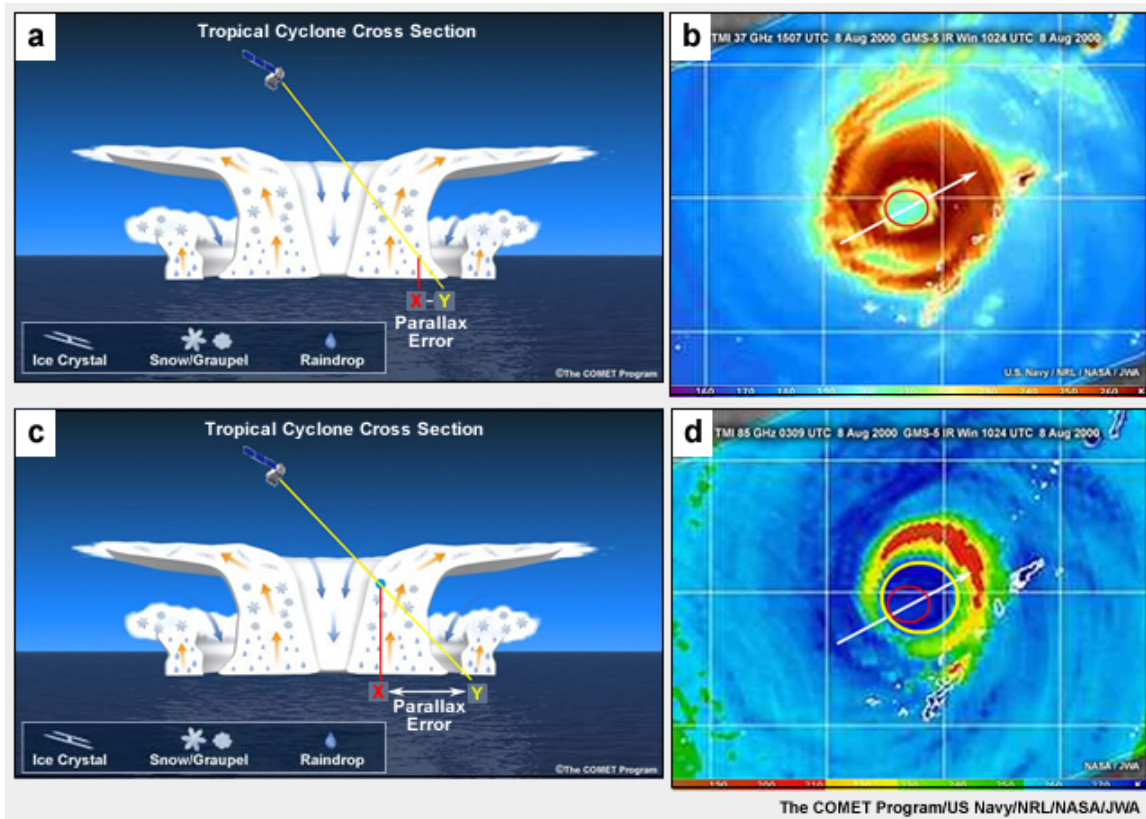


Fig. 10.59. Conceptual model of the relative parallax errors in satellite microwave images of (upper) 37GHz liquid droplet emissions and location of the eye of Typhoon Jelawat (2000) and (lower) same as upper except for 85GHz ice scattering. The red circle is the 37GHz eye position and the yellow circle is the 85GHz position.

### 10.4.5.3 Eyewall Replacement Cycles

The concentric eyewall phenomenon or eyewall replacement cycle<sup>107</sup> is often observed during periods of intensification or weakening of intense TCs (those with winds greater than  $50 \text{ m s}^{-1}$ , 115 mph). In general, TC eyewalls contract as they strengthen to the intense TC threshold. After the existing eyewall has contracted to its minimum size for that threshold intensity, the TC enters a weakening phase. All other factors being equal, the TC weakens when an outer eyewall forms; some of the moisture and momentum is taken from the existing eyewall, which dissipates. The outer eyewall contracts gradually and the TC regains its original strength or becomes stronger. For example, major Hurricane Ivan weakened, from a category 5 to a category 4, as it approached Jamaica from the southeast, in part because of an eyewall replacement cycle. Two concentric eyewalls are evident in the radar image from Kingston, Jamaica (Fig. 10.60). The case of Hurricane Georges on 19 September 1998 illustrates the intensification phase of the eyewall replacement cycle. Fig. 10.61 shows TMI images of Hurricane Georges during a period of intensification when the concentric eyewalls were replaced by a single eyewall.

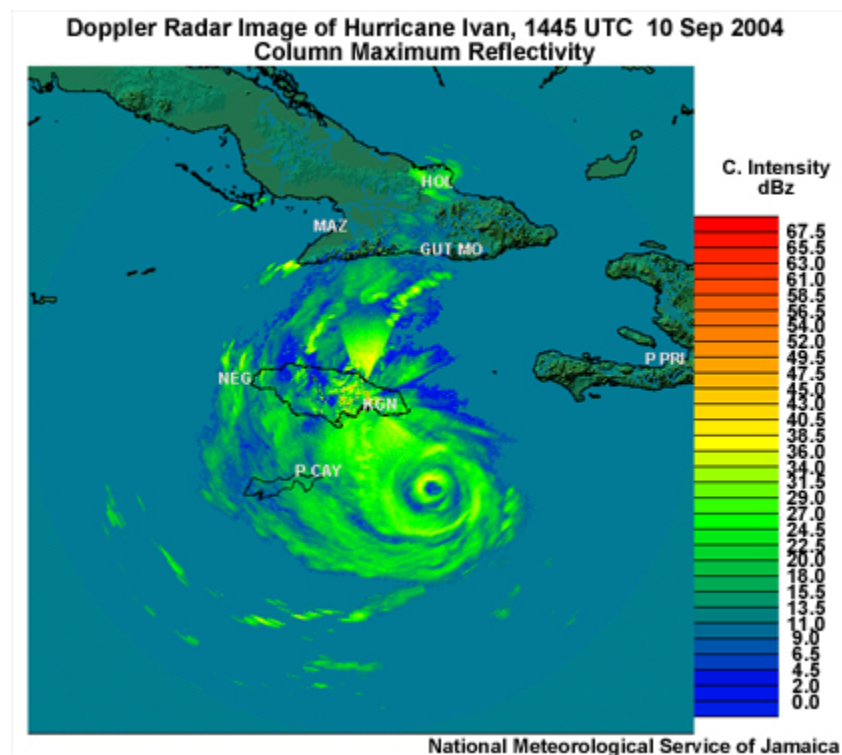


Fig. 10.60. Radar reflectivity image from Kingston, Jamaica at 1445 UTC 10 Sep 2004. Note the two concentric eyewalls that were likely the cause of short term weakening in Ivan. At this time, Ivan had weakened from category 5 to category 4 with sustained winds of  $65 \text{ m s}^{-1}$  (125 knots; image courtesy of the National Meteorological Service of Jamaica).

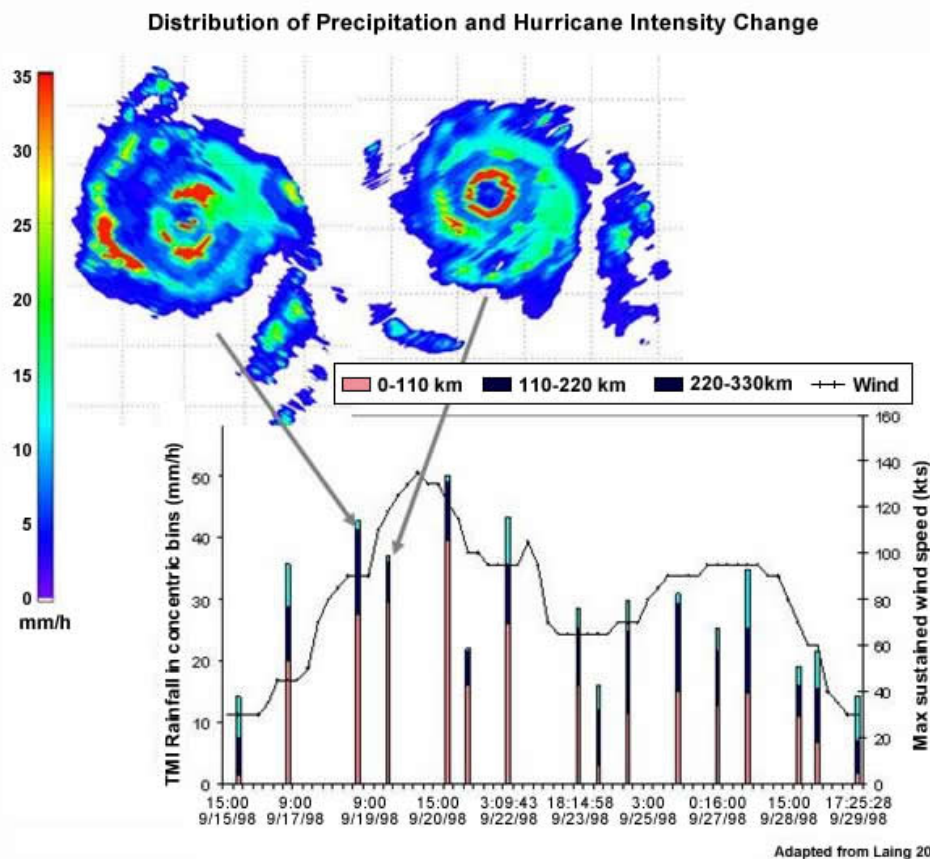


Fig. 10.61. Spatial distribution of surface rain rates ( $\text{mm hr}^{-1}$ ) in Hurricane Georges via TRMM TMI, best track maximum sustained wind speed (knots, solid black line), and rainfall in concentric bins around the center of the cyclone ( $\text{mm hr}^{-1}$ , vertical bars).

Eyewall replacement cycles can last as short as 12-18 hours to as long as 2-3 days (Figs. 10.61 and 10.62<sup>129</sup>). Some intense TCs, such as Hurricane Ivan (2004), undergo multiple eyewall replacement cycles. The West Pacific has the largest percentage of intense storms which exhibit double eyewall structure because many can travel longer distances before encountering land, cool SSTs, or other unfavorable environmental conditions.

New satellite analyses are being developed to objectively identify eyewall replacement cycles. By enhancing the signal to noise ratio of the images, Kossin and colleagues (J. Kossin, personal communication) found that IR imagery does contain information about the onset of eyewall replacement cycles. The IR information, when combined with microwave image data, is being used to create an objective index to calculate the probability of secondary eyewall formation.



Development of a Secondary Eyewall Formation Index, 60<sup>th</sup> Interdepartmental Hurricane Conference  
<http://www.ofcm.gov/ihc06/Presentations/02%20session2%20Observing%20the%20TC/s2-11kossin.ppt>

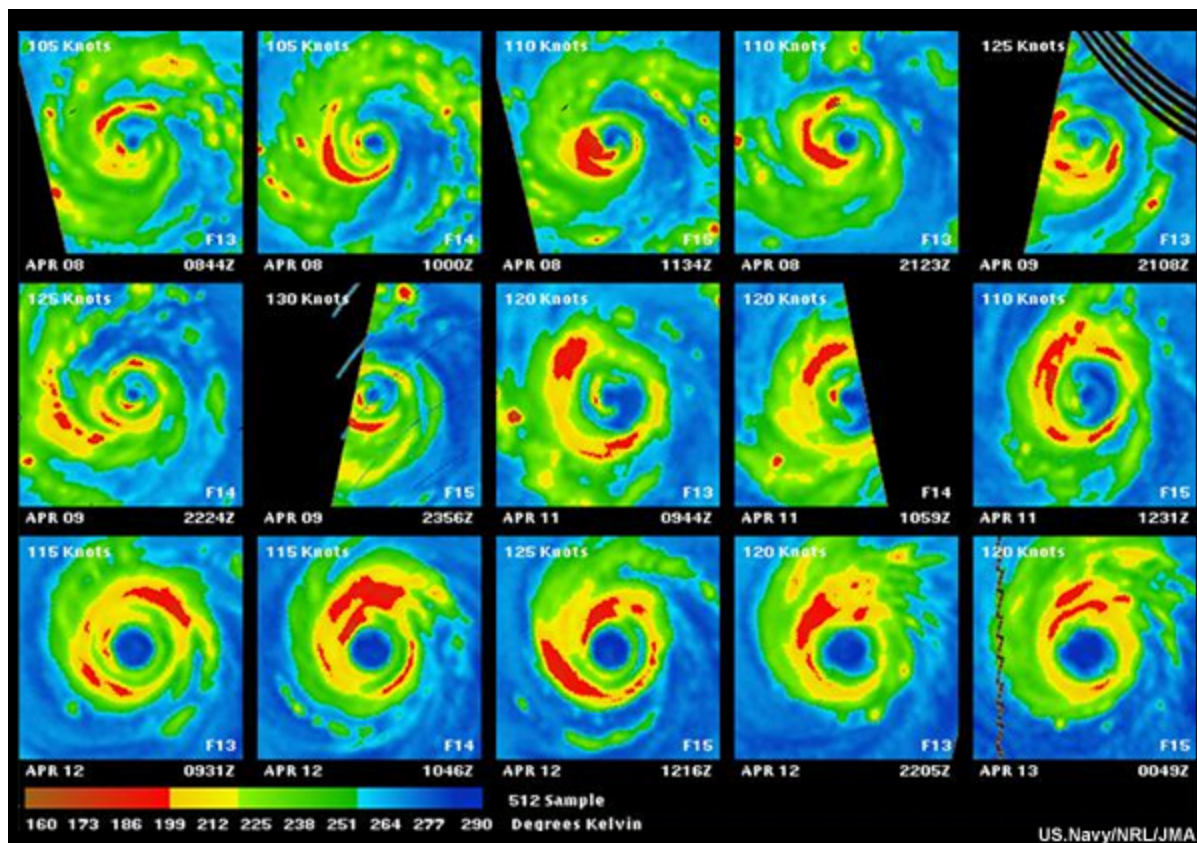


Fig. 10.62. Eyewall replacement cycle in Typhoon Sudal in the West Pacific, seen in SSM/I 85 GHz H-Polarized image from 8-13 April 2004 (image courtesy of Dr. Jeff Hawkins, NRL Monterey).

#### 10.4.5.4 Satellite-derived Winds

It is important to consider TC intensity not only in terms of the central pressure or the radius of maximum winds but in terms of other wind speed radii that are critical to decision makers. The width of evacuation zones is based on thresholds such as the radius of gale force winds (1-minute sustained surface winds between 34 and 47 knots or 17 and 24 m s<sup>-1</sup>). Wind velocity estimates are also critical to forecasting of storm surge. TC sizes range from Cyclone Tracy (1974), whose radius of gale force winds was only 48 km, to Super Typhoon Tip, which had a gale force wind radius of 1110 km.

Prior to landfall, near surface wind speed and direction are observed by satellite-based microwave scatterometers, which measure the backscatter from small-scale waves on the ocean surface and relate the backscatter to wind velocity. Microwave scatterometers generally perform best in moderate-wind and low-precipitation environments,<sup>130</sup> outside of the high-wind and high precipitation region of the eyewall. Microwave sensors such as TMI estimate wind speed away from heavy precipitation regions. Cloud drift winds, although limited by inaccuracies in height assignments, also provide estimates of winds outside of intense convection.<sup>124</sup> Figure.10.63 provides examples of satellite-derived winds in and around TCs.

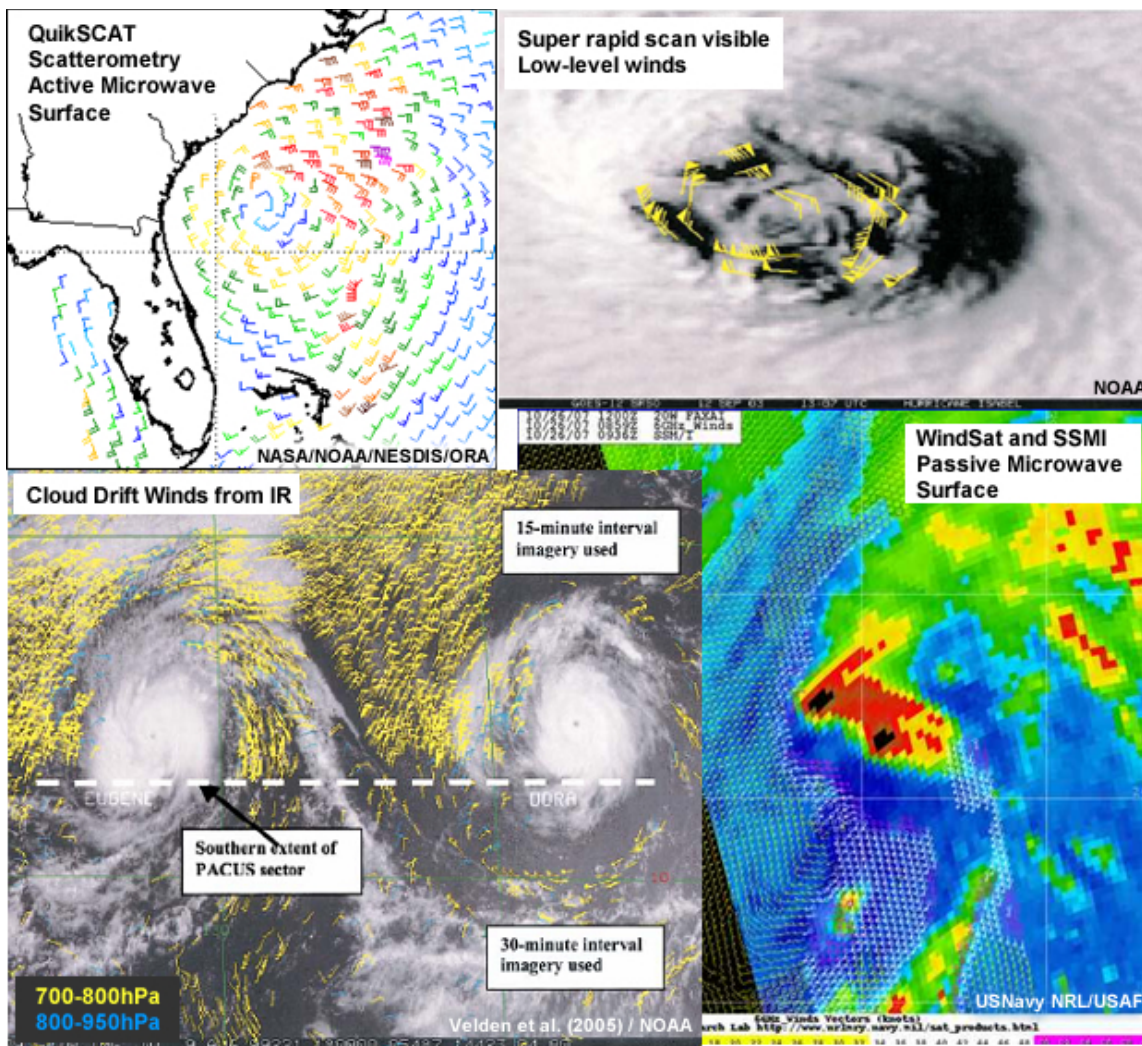


Fig. 10.63. Satellite wind estimates from scatterometer, cloud drift IR images, rapid scan visible images, and passive microwave sensors.

#### 10.4.5.5 TC Intensity and 34-kt Wind Speed Radius

Statistical relationships between TC intensity estimates from aircraft reconnaissance and satellite IR imagery indicate that the radius of the 34 knot winds could be used to estimate TC intensity. A strong relationship has been found between core intensity and the radius of 34 knot winds<sup>130</sup>. Note that relationship between the 34 knot ( $17 \text{ m s}^{-1}$ ) wind radii and intensity is not applicable in all situations as the radius of 34 knot winds is also affected by latitude and number of hours since the TC reached tropical storm intensity.<sup>131</sup> As TCs move to higher latitudes, they tend to become larger.<sup>132</sup>



Best track critical wind radii data, [http://www.ssec.wisc.edu/~kossin/sharedfiles/ReadMe\\_Kossin.pdf](http://www.ssec.wisc.edu/~kossin/sharedfiles/ReadMe_Kossin.pdf)

#### 10.4.5.6 Remote Sensing of Inner Core Dynamical Features

While eyewalls are often observed to be nearly circular, they are occasionally observed to adopt polygonal shapes. Based on theoretical dynamics, numerical simulations, and liquid water experiments<sup>133,134,135</sup> the polygonal structures were hypothesized to be associated with mesovortices. Recent observational studies<sup>136</sup> show pentagon-shaped reflectivity patterns (Fig. 10.64a, c) associated with mesovortices within the eye (Fig. 10.64c), confirming their existence. These eyewall mesovortices are deep vortex structures in the eyewall convection and so have much smaller horizontal scale than the eye. Wind speed in eyewall vortices can be 10% greater than the rest of the eyewall. Addition of the flows associated with the mesovortices to the flow in the eye results in the polygonal shape observed in the cloud pattern.

The 2005 *Hurricane Rainband and Intensity Change Experiment (RAINEX)* made targeted observations in the inner core of Hurricanes Katrina, Rita, and Ophelia in order to understand how changes in their inner core influenced and were influenced by intensity changes. Fig. 10.65 shows a number of interesting features hitherto unobserved, such as filaments of very high reflectivity that are oblique to the concentric eyewall and rainbands. These structures are affected by varying winds as they move around the eyewall and provide clues about how eyewalls transform during rapid changes in intensity. They appear to be similar to structures predicted in theoretical studies and numerical models.<sup>132,137 133,138</sup>

How do these mesovortices affect TC intensity? Theoretical models and evidence in the new observations suggests that the mesovortices contribute cyclonic vorticity which is mixed into the eye. This increase in the local vorticity spins up the eye. In addition, the low-level mesovortices create a secondary circulation that transfers air from the eye to the eyewall and provides additional power to the hurricane heat engine.<sup>136</sup> Polygonal eyewalls can also be explained by the vortex asymmetry theory<sup>74,75</sup>. Vortex Rossby waves, analogs of the synoptic-scale waves, transport wave energy, momentum, and heat in the eyewall region. In rapidly intensifying TCs, counter-rotating vortex Rossby waves grow, while straddling the relative vorticity maximum between the eye-wall and the center of rotation. The vortex Rossby waves help to mix high  $\theta_e$  air into the eyewall updrafts.

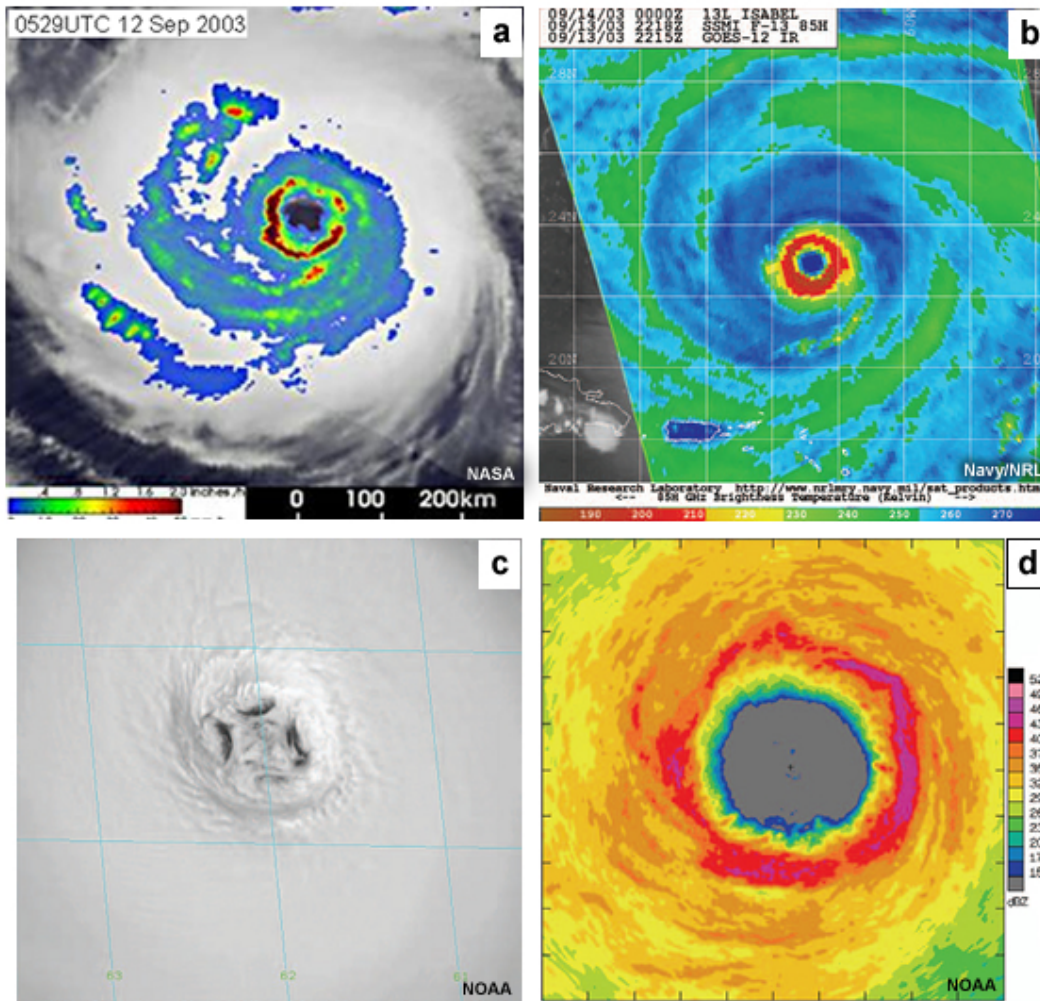


Fig. 10.64. Satellite and airborne radar imagery of Hurricane Isabel. (a) TRMM PR image at 0529 UTC on 12 September 2003; (b) SSM/I 85-GHz brightness temperature at 2218 UTC; (c) visible image at 1745 UTC from GOES super-rapidscan operations; and (d) radar reflectivity (dBZ) from lower-fuselage (5 cm) radar onboard NOAA aircraft while flying inside the eye at  $\sim 2$  km altitude. The time of the radar image (1747 UTC) is 2 min after the visible image shown in (b). The horizontal scales (km) are approximately 1400 in (b), 300 in (c), and 180 in (d). Panels b, c, and d are from Montgomery et al.<sup>135</sup>



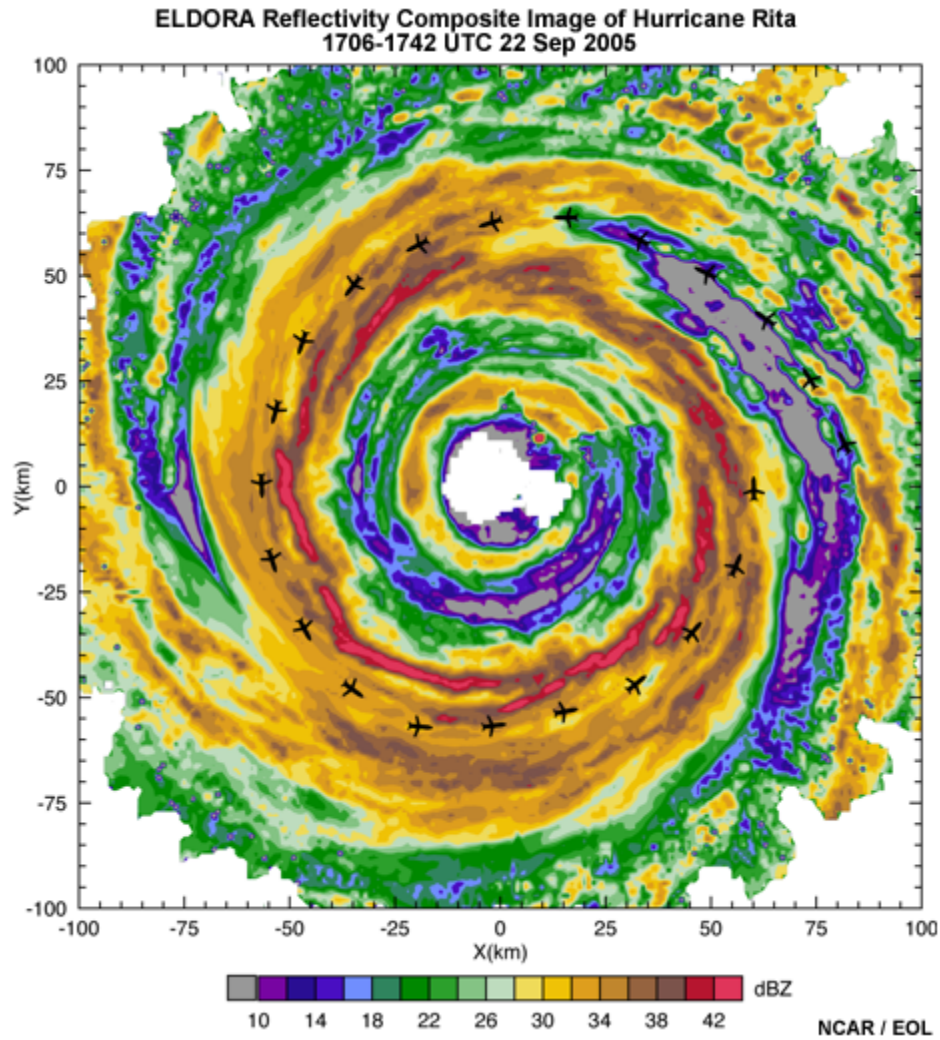


Fig. 10.65. Radar reflectivity composite image of Hurricane Rita taken by ELDORA, 22 Sep 2005, during the Hurricane Rainband and Intensity Change Experiment (RAINEX). The flight track is marked by airplane icons. (Image courtesy of Mr. Michael Bell and Dr. Wen-Chau Lee).

## 10.5 Climatology of Tropical Cyclones

Tropical cyclones are a natural part of the climate system, forming in all tropical ocean basins with the possible exception of the South Atlantic (Fig. 10.1), although rare storms with tropical characteristics are observed in the South Atlantic (Box 10-7). Another location rarely considered as a tropical cyclone center is the Gulf of Oman, so the intrusion of Tropical Cyclone Gonu into this region was an unexpected event (Box 10-8).

### 10.5.1 Seasonality of Tropical Cyclone Formation

Environmental conditions favorable for tropical cyclone formation vary geographically and by season. Broadly speaking, warm ocean temperatures and weak vertical wind shear are two of the necessary, but not sufficient, conditions for tropical cyclogenesis.<sup>33</sup> The wind shear tends to be weaker early in the local summer, increasing as the tropical and subtropical oceans warm and the winter Hadley cell strengthens through the local summer and into autumn (Fig. 10.66). Thus, the SH seasonal cycle is out of phase with the NH and generally follows the seasonal monsoon variations (see Section 10.3 for discussion of the large-scale factors governing tropical cyclogenesis).

While tropical cyclones are common in most of the global tropics, the western North Pacific is the only basin in which they have been observed in every month of the year (Fig. 10.67). The formation of Tropical Storm Ana in April 2003 and the 2005 Atlantic storms, concluding with Tropical Storm Zeta—for which warnings were issued until 6 January 2006, mean that tropical cyclones have been recorded in the North Atlantic in all months except February and March. Based on long-term statistics of tropical cyclones in the North Atlantic; the “hurricane season” for that basin is defined from 1 June through 30 November. The Eastern North Pacific hurricane season begins on 15 May and also extends to 30 November. In the North Indian Ocean tropical cyclones tend to occur in the monsoon transition months of early (May-June) and late in the wet season (October-November), when the large-scale conditions for genesis are most favorable over that ocean. In the Southern Hemisphere, the tropical cyclone seasons typically extend from November through April, although early and late season storms (October and May) have been observed.



NHC Summary of 2005 Atlantic Hurricane Season, <http://www.nhc.noaa.gov/2005atlan.shtml>  
NHC Archive of Hurricane Seasons, <http://www.nhc.noaa.gov/pastall.shtml>  
Japan Meteorological Agency (JMA),  
<http://www.jma.go.jp/jma/jma-eng/jma-center/rsmc-hp-pub-eg/trackarchives.html>  
NOAA NWS Climate Prediction Center, Expert Assessments (assessments, advisories, outlooks),  
[http://www.cpc.ncep.noaa.gov/products/expert\\_assessment/](http://www.cpc.ncep.noaa.gov/products/expert_assessment/)



NASA visualizations of 2005 hurricane season, IR clouds, SST, storm tracks, name labels,  
<http://svs.gsfc.nasa.gov/goto?3354> (list of all movies with and without audio)

Video interview with Dr. Jenni Evans, Penn State University Weather World,  
[http://www.met.psu.edu/dept/images/videos/Evans\\_interview.mp4](http://www.met.psu.edu/dept/images/videos/Evans_interview.mp4)

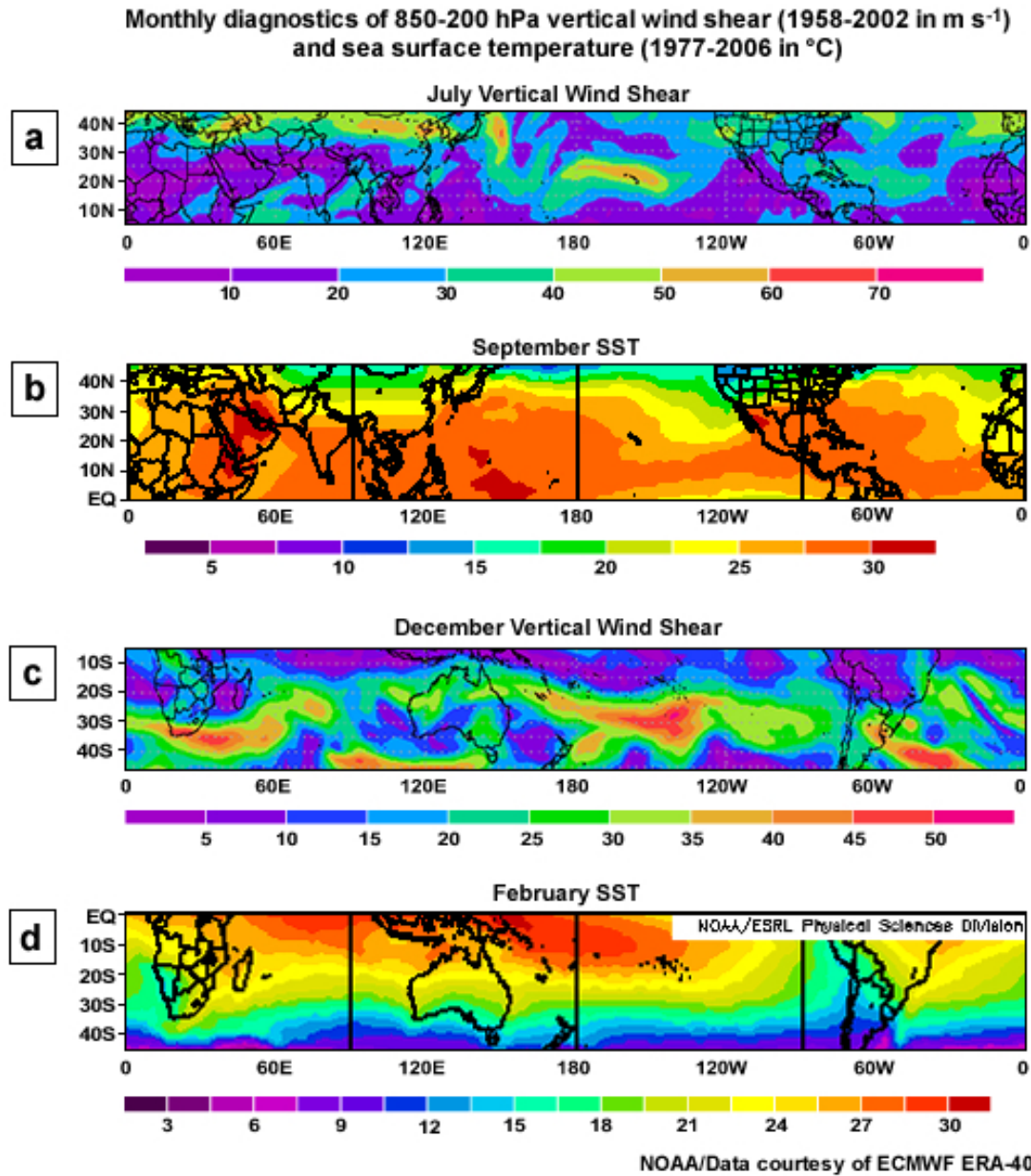


Fig. 10.66. Monthly diagnostics of 850-200 hPa vertical wind shear (1958-2002 in  $\text{m s}^{-1}$ ) and sea surface temperature (1977-2006 in  $^{\circ}\text{C}$ ). (a) July shear and (b) September SST for the NH; (c) December shear and (d) February SST for the SH. Wind shear values are in  $10 \text{ m s}^{-1}$  bands from  $< 10 \text{ m s}^{-1}$  in light purple then dark purple, blue, teal, green, orange, red, and  $> 70 \text{ m s}^{-1}$  in pink. The SST color scheme follows the same order in  $3^{\circ}\text{C}$  increments from  $3^{\circ}\text{C}$  to  $30^{\circ}\text{C}$ . Shear and SST are from ERA-40 analyses available at <http://www.ecmwf.int/products/data/archive/descriptions/e4>.

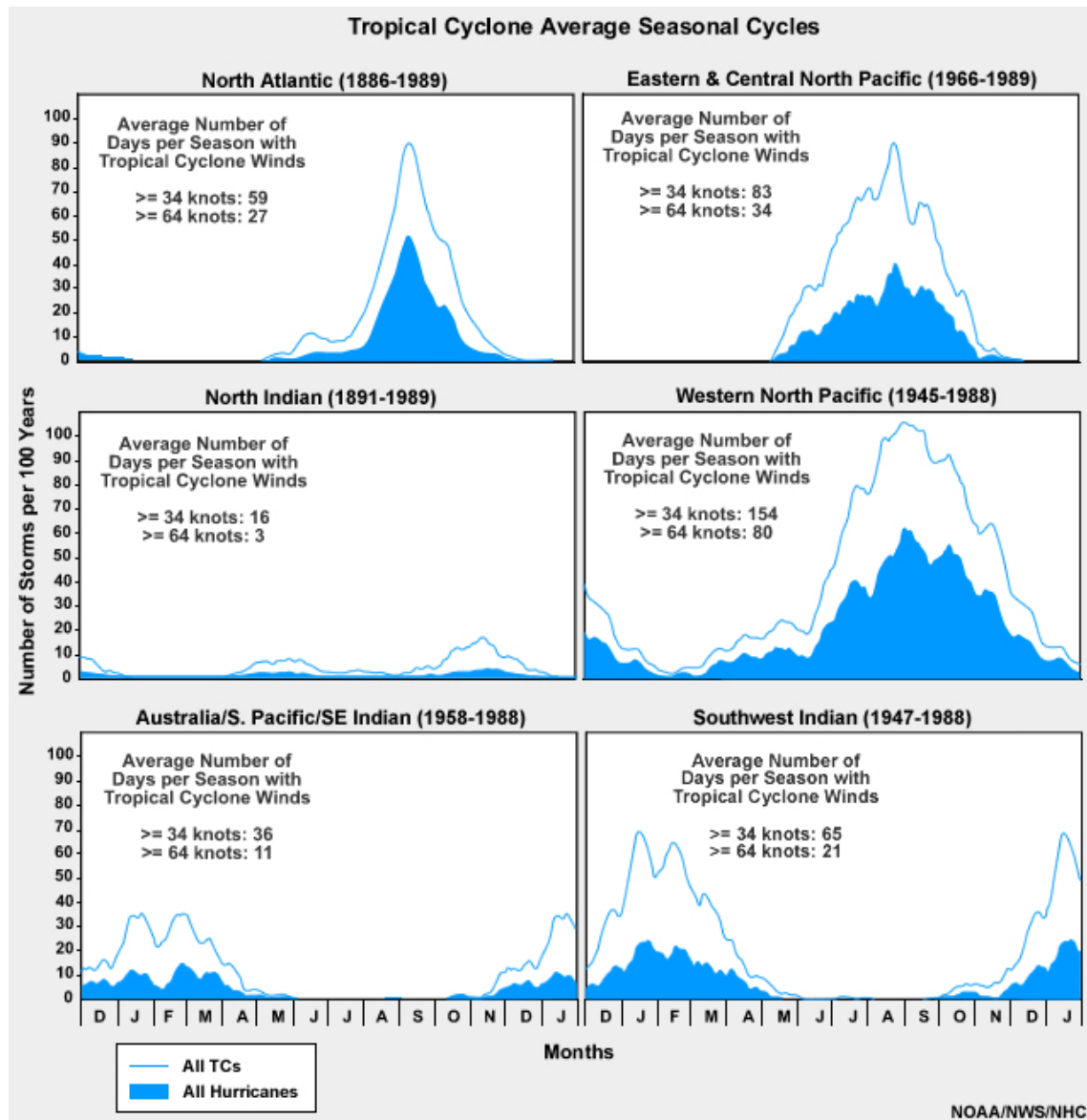


Fig. 10.67. Average annual cycle of tropical cyclone occurrence for each ocean basin. The abscissa spans the 13 months December through January of the following year; the ordinate is the number of storms per hundred years. The blue line represents all tropical cyclones (surface winds greater than  $17 \text{ m s}^{-1}$  or 34 knots); shading represents tropical cyclones of hurricane strength (surface winds greater than  $33 \text{ m s}^{-1}$  or 64 knots). The averaging time for the mean surface wind speeds varies across basins (Box 10-3).

### Box 10-7 South Atlantic Tropical Cyclone Catarina (2004)

No tropical cyclones have been observed in the South Atlantic since the beginning of the satellite era over 40 years ago – that is, until “Tropical Cyclone Catarina” made landfall in Brazil on 28 March 2004! Because the South Atlantic was thought to be unfavorable for tropical cyclone formation, there was no list of WMO-sanctioned names for this basin. So why Catarina? Because Tropical Cyclone Catarina came ashore near the small town of Torres (about 800 km south of Rio de Janeiro) in the Brazilian state of Santa Catarina. This rarest of tropical cyclones left its mark: at least two people lost their lives, 11 were reported missing and 75 severely injured. Roughly 32,000 homes were damaged and almost 400 of these were destroyed, giving a total damage estimate of about US \$350M.

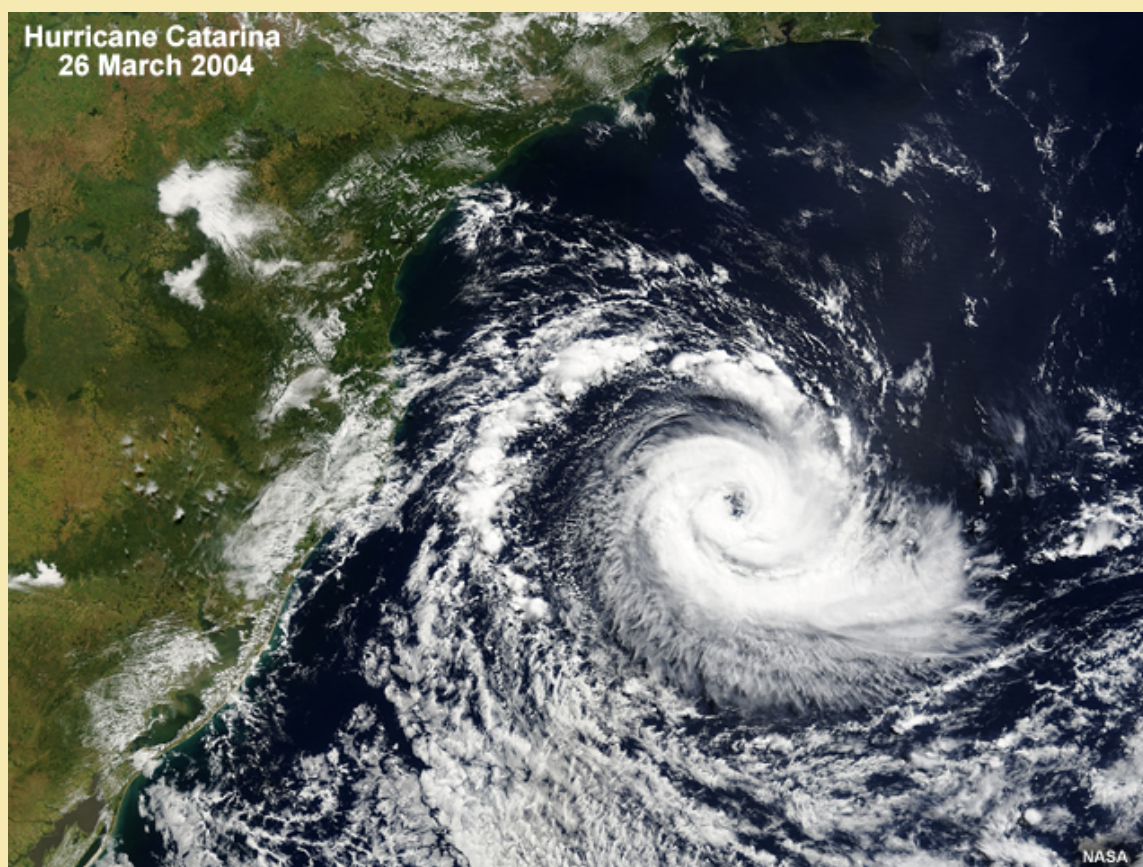


Fig. 10B7.1 Tropical Cyclone Catarina on 26 Mar 2004. At this time, Catarina was estimated to have surface winds of  $35 \text{ m s}^{-1}$  (70 knots; Category 1 on the Saffir-Simpson scale). Image taken by the MODIS (Moderate Resolution Imaging Spectro-radiometer) instrument on the Terra satellite.



[Satellite animation of Catarina's landfall in Brazil](#)

## Box 10-7 continues

Why was Catarina such a surprise?

Until Catarina, the cooler SST of the tropical South Atlantic and the strong vertical wind shear were thought to preclude tropical cyclone formation. The warmest waters in this region are usually near 26°C, thought to be the minimum SST needed for tropical cyclone formation in the present climate. But Catarina was not a typical tropical cyclone: its genesis was not in the tropical ITCZ, but near latitude 29°S, far poleward of typical genesis latitudes. The storm meandered roughly along this latitude until making landfall. Catarina began as a subtropical storm that formed at a frontal boundary over waters that were thought to be too cool for tropical cyclone formation. Recently, Guishard et al. (2007)<sup>30</sup> have shown that subtropical cyclones in the North Atlantic are found to be precursors to tropical cyclogenesis on average once or twice per season. Hurricane Michael (2000) is another recent example of a hurricane forming from a subtropical cyclone.<sup>139</sup> So we see that, storms forming under the right conditions farther from the equator *can* become tropical cyclones. Another piece of the Catarina puzzle comes from theory; if the tropopause *and* surface are cool, it is still possible to achieve hurricane intensity.<sup>17</sup> Hence, although rare, we know that the formation and intensification of Catarina can be explained by our current understanding of tropical cyclones in other regions.

How do we know that Catarina achieved hurricane status (at least 33 m s<sup>-1</sup>)? The most comprehensive information on Catarina came from the TRMM<sup>140</sup> TMI which sensed the warm core of the system that is typical of a tropical cyclone and the spiral band structure (Fig. 10B7.2), QuikSCAT recorded the surface winds (Fig. 10B7.3).

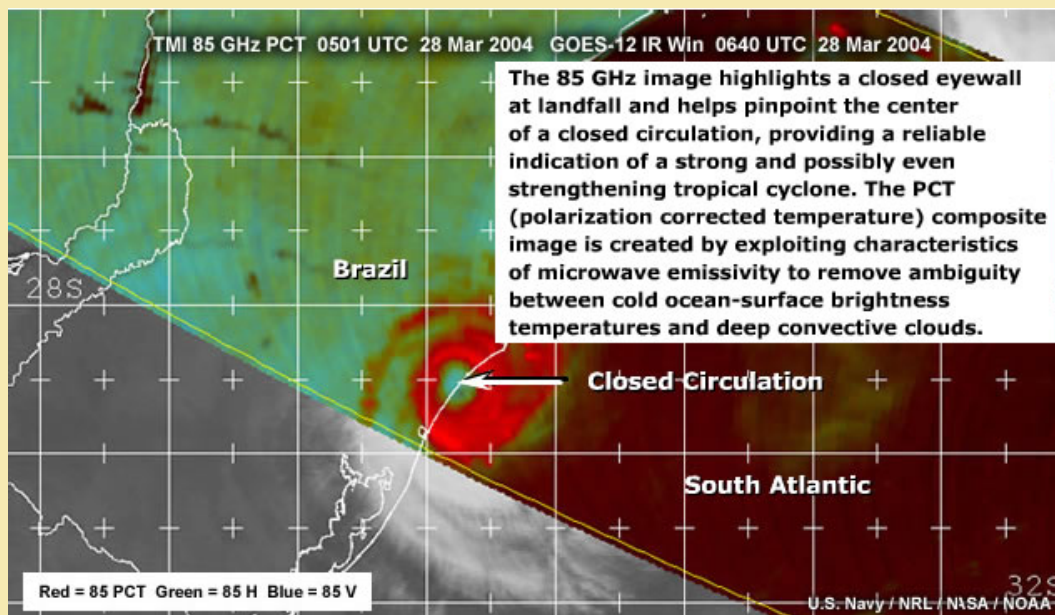


Fig. 10B7.2 85GHz microwave image of Tropical Cyclone Catarina taken by the TMI at 0501 UTC 28 Mar 2004.

## Box 10-7 continues

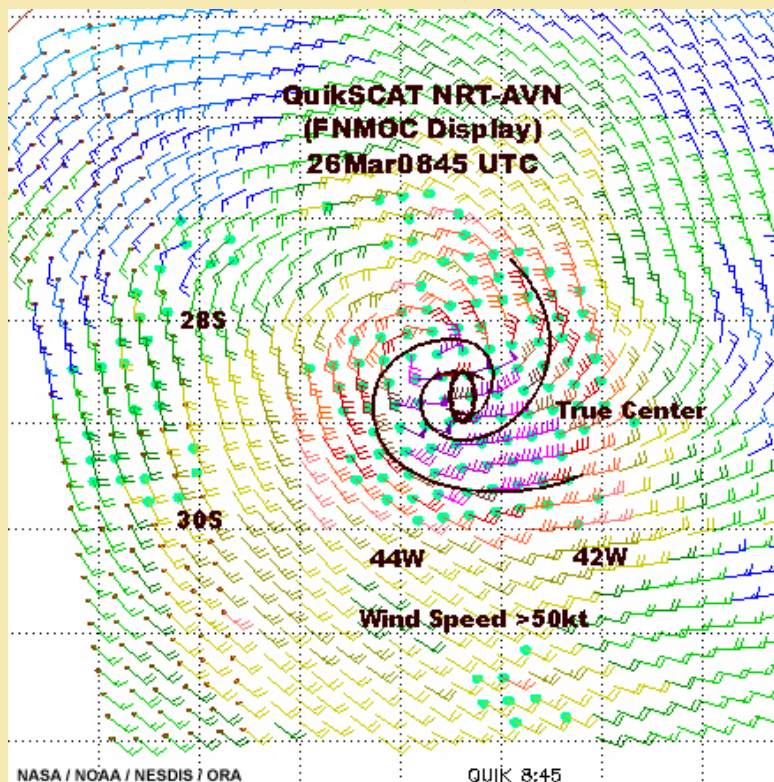


Fig. 10B7.3 QuikSCAT scan of Tropical Cyclone Catarina at 0845 UTC 26 Mar 2004.

Wind barbs are in knots ( $1 \text{ knot} = 0.51 \text{ m s}^{-1}$ ); green dots indicate winds that may be inaccurate due to rain interfering with the measurement. At this time, Catarina was still intensifying.



More information and images of Catarina

<http://australiasevereweather.com/cyclones/2004/summ0403.htm>

[http://trmm.gsfc.nasa.gov/publications\\_dir/south\\_atlantic\\_cyclone.html](http://trmm.gsfc.nasa.gov/publications_dir/south_atlantic_cyclone.html)

<http://cimss.ssec.wisc.edu/tropic/brazil/brazil.html>

<http://www.ssd.noaa.gov/PS/TROP/catarina.html>

### Box 10-8 Tropical Cyclone Gonu (2007)

Where in the world would you feel safe from tropical cyclones? How about the deserts of the Middle East? No – even this region can be impacted by tropical cyclones! Tropical Cyclone Gonu<sup>1</sup> entered the Gulf of Oman as a “Severe Cyclonic Storm” (Box 10-3) with 1-minute maximum sustained winds of  $43 \text{ m s}^{-1}$  (83 kts,  $153 \text{ km h}^{-1}$ , or 95 mph). As the storm moved across the Gulf towards the Iranian coast, it weakened to a tropical storm with winds of around  $23 \text{ m s}^{-1}$  (45 kts,  $83 \text{ km h}^{-1}$ , or 51 mph,) at landfall on 7 June 2007.

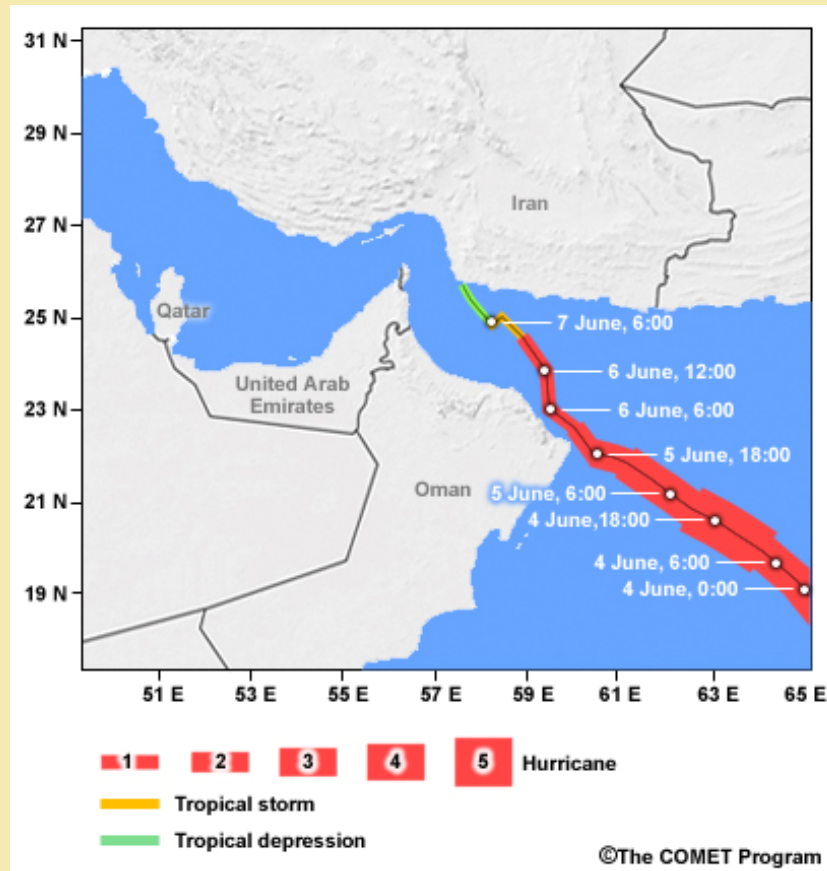


Fig. 10B8.1 Track and windspeed of super cyclonic storm Gonu (2007).

Although Gonu made landfall in Iran, its major effects were in Oman. The Omani capital, Muscat, was impacted by severe winds and associated waves, as well as the torrential rain. Topographic enhancement of the storm rainfall compounded the flooding in Muscat. Gonu was blamed for only three fatalities in Iran; in contrast 25 fatalities were reported in Oman, with about the same number of people reported missing.

<sup>1</sup> Gonu is the word for a bag made of palm leaves in the Maldives.



## 10.5.2 Intraseasonal Variability

Variation of the necessary conditions for tropical cyclogenesis can lead to clustering of formation events within a storm season. These intraseasonal variations in tropical cyclogenesis frequency are driven by a variety of factors; some, such as the 30-60 day oscillation of tropical rainfall, also known as the *Madden-Julian Oscillation (MJO)*,<sup>141,142</sup> are tropics-wide phenomena, while others are regional modulators of genesis, such as the *Saharan Air Layer (SAL)* in the North Atlantic (Section 10.3.4).

### 10.5.2.1 Intraseasonal Modulation by the Madden-Julian Oscillation (MJO)

The passage of the “active” phase of the MJO through a region enhances the convective activity locally;<sup>143,144</sup> conversely, the “inactive” phase of the MJO suppresses convective activity. At the onset of the MJO, convective activity is disorganized and relatively short lived. As the MJO approaches, the convective systems become increasingly more organized<sup>145</sup> (more symmetric and longer mean lifetimes). By the peak of the MJO, tropical cyclogenesis is likely; Fig. 10.68 shows phases of the MJO and the origins of disturbances that developed into tropical cyclones.

**Composite evolution of 200hPa velocity potential anomalies ( $10^5 \times \text{m}^2/\text{s}$ ) and points of origin of tropical systems that developed into hurricanes/typhoons**

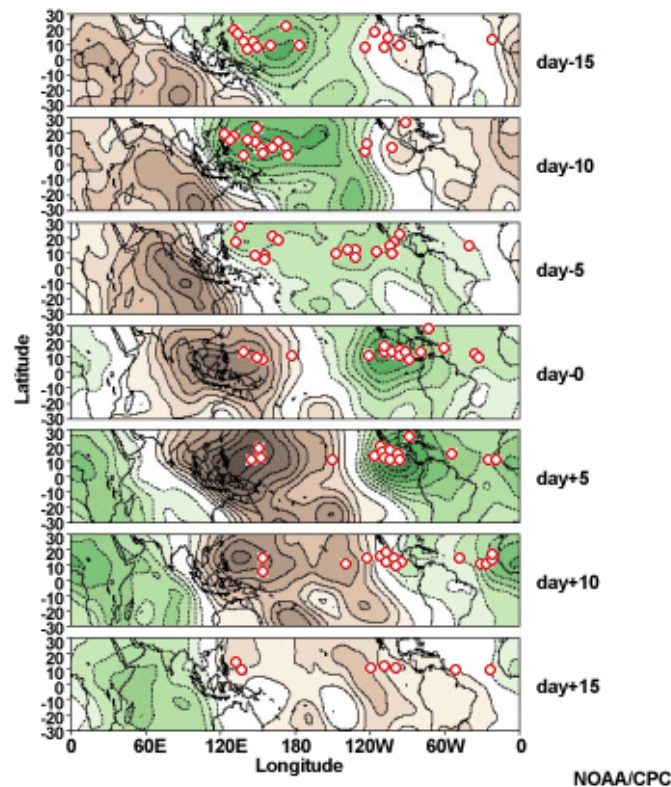


Fig. 10.68. Points of origin of tropical systems that developed into tropical cyclones (red circles) relative to phases of the MJO. The MJO cycle is identified here by the 200 hPa velocity potential anomalies ( $10^5 \times \text{m}^2 \text{s}^{-1}$ ); green is the peak and dark brown is the lull.

Modulation of tropical cyclogenesis potential by the MJO agrees with the three week active/three week inactive periods of tropical cyclogenesis proposed much earlier.<sup>33</sup>



Is the role of the MJO here simply to increase or decrease the likelihood that an incipient disturbance could develop adequate convection to intensify further,<sup>45,146,147</sup> or is the question more complex?



Different hypotheses have been presented for why and how the MJO modulates tropical cyclogenesis. One perspective is that the increasing convective organization moistens the free troposphere through detrainment of moisture from the clouds. The moisture above the boundary layer provides a favorable environment for sustaining deep convection and for forming larger convective complexes. These organized convective complexes have associated lower tropospheric PV maxima, reducing the local Rossby radius in the presence of convection—one path we have discussed for tropical cyclogenesis<sup>145</sup> (Section 10.3.1). An alternative perspective,<sup>148</sup> is that genesis is more likely for western Pacific storms not because the MJO acts an inherent control on genesis, but rather that the general increase in convective activity in the enhanced phase of the MJO produces many more seed systems from which a tropical storm could develop. However, that hypothesis was contradicted by another study that found that the fraction of systems developing from convective cluster to tropical storm is unchanged between “favorable” [convection active] and “unfavorable” [convection suppressed] phases of the MJO.<sup>143</sup> Since the vast majority of tropical cyclones in the Australian region form near the axis of the Australian summer monsoon,<sup>41</sup> modulation of this feature by the MJO has been linked to tropical cyclone activity in that region.

Deep convection in the eastern Pacific has been credited with maintaining the PV gradient reversal<sup>60</sup> associated with the off-equatorial movement of Rossby and mixed Rossby-gravity waves into the Pacific confluence zone (Fig. 10.24a). This process is now regarded as a potential source of tropical cyclogenesis (Fig. 10.35a). Maintenance of the dynamic equator by convection highlights the potential importance of convection as a modulator to the dynamic genesis environment, not just a seasonal tracer. Since the MJO is a strong modulator of tropical convection, it has been linked to modulation of the dynamical controls on tropical cyclone genesis too.

MJO modulation of near-equatorial easterly waves over the eastern Pacific affects intraseasonal variations in tropical cyclogenesis in that region.<sup>58,146,149,150</sup> Provided these easterly waves remain coherent in their passage from Africa to the eastern North Pacific, their likelihood of forming tropical cyclones depends on timing rather than initial strength. For cyclogenesis, the easterly wave must interact with the convectively active cycle of the MJO in regions of dynamic instability over the warm tropical waters. As the MJO moves through the region, favorable genesis locations progress eastward and northward, moving with the deep convection in the ITCZ.<sup>149</sup> The need for all of these complementary factors helps to explain why eastern Pacific cyclogenesis is suppressed in the “unfavorable” phases of the MJO.<sup>149</sup>

A study<sup>151,152</sup> of the easterly wave-MJO system confirmed that barotropic dynamics are an important contributor to coupling the convectively active phase of the MJO with a potential increase in tropical cyclogenesis in both the western and eastern Pacific. The anomalous westerly jet associated with the westerly phase of the MJO is thought to be crucial in the barotropic formation of incipient disturbances across the entire tropical Pacific. The suggestion is that the convectively active phase of the MJO may create a large scale environment in the eastern North Pacific conducive to tropical cyclogenesis even in the absence of upstream contributors<sup>151</sup> (e.g., easterly waves).

### 10.5.2.2 Intraseasonal Modulation by the Saharan Air Layer (SAL)

The relationship of the SAL and tropical cyclogenesis was explored briefly in the 1970s<sup>92,153</sup> and 1980s.<sup>154</sup> Since the early 2000s, a special satellite retrieval algorithm<sup>95</sup> ([Chapter 3, Section 3.8](#)) and targeted field measurements have increased our knowledge of the structure of the SAL and its role as a modulator of tropical cyclogenesis<sup>155</sup> (Section 10.3.4, Fig. 10.33, Fig. 10.34).

The SAL is most prevalent off the West African coast in the *Main Development Region (MDR)* for Atlantic tropical cyclogenesis. Active convection may persist on its southern and western boundaries, but low relative humidity in the SAL suppresses convection elsewhere. The dry and dusty SAL creates an elevated warm anomaly, reversing the usual meridional temperature gradient over the tropical Atlantic, and results in the formation of the African Easterly Jet (AEJ). Strong vertical wind shear, associated with the jet, extends westward with the movement of the SAL and stifle development<sup>95,156</sup>. While the SAL may inhibit development of African easterly waves into tropical storms,<sup>95</sup> the waves have been proposed as transportation for Saharan dust<sup>157</sup> and so may be implicated in their own demise!

Western Sahel rainfall has also been linked to North Atlantic tropical cyclone activity.<sup>158</sup> Whether the SAL is involved in any intraseasonal modulation of Atlantic storm activity related to western Sahel rainfall—or whether Sahel rainfall is a straightforward proxy for easterly wave genesis frequency—remains an open question.



Daily monitoring of MJO, NOAA

[http://www.cpc.noaa.gov/products/precip/CWlink/daily\\_mjo\\_index/mjo\\_index.html](http://www.cpc.noaa.gov/products/precip/CWlink/daily_mjo_index/mjo_index.html)

Real-time diagnostics of the SAL, CIMSS, University of Wisconsin (Madison)

<http://cimss.ssec.wisc.edu/tropic/real-time/wavetrak/winds/m8split.html>

### 10.5.3 Interannual Variability

Before discussing interannual variability, it is important to understand the difference between annual cyclone activity (frequency and intensity) and the severity of cyclone impacts (landfall frequency, fatalities, and damage). For example, the 2004 western North Pacific and Atlantic tropical storm seasons were not exceptionally active seasons. Yet, Japan suffered a total of ten landfalls and the US state of Florida had three landfalls and suffered the effects of a fourth storm that made landfall in the adjacent state of Alabama (Box 10-9). Furthermore, Hurricane Andrew (1992), a Category 5 hurricane, made landfall near Miami during an inactive season. Thus, commonly-used activity parameters are not necessarily good indicators of impacts, which can be influenced by other, less well defined, modulators of tropical cyclogenesis and track. For instance, one potential explanation for the impact of the 2004 North Atlantic season is that the large-scale steering flow and equatorial trough<sup>159</sup> allowed storms to develop at low latitudes in the eastern Atlantic and to track westward, while remaining unusually close to the equator, before curving poleward as they approached or entered the Gulf of Mexico.

On interannual timescales, tropical cyclone variability can stem from global patterns of atmosphere or atmosphere-ocean variation, such as the *El Niño Southern Oscillation (ENSO)*<sup>160,161,162</sup> or the *Quasi-Biennial Oscillation (QBO)*<sup>162,163,164,165</sup> of the lower stratospheric wind. Rainfall in the western Sahel has also been associated with variations in the seasonal frequency and intensity of Atlantic tropical cyclones.<sup>166,167</sup>

The active 2005 season in the North Atlantic was attributed to extraordinarily warm ocean temperatures in that basin,<sup>168,169</sup> however the Atlantic and Gulf of Mexico were similarly warm in 2006 (Fig. 10.69), which was an average year for tropical cyclone activity. Further, the patterns of Atlantic SST in 2004 and 2006 were very similar (Fig. 10.69), yet 2004 was a relatively active year with 15 named storms (9 hurricanes).

Increased understanding of interannual modulators of tropical cyclone activity has inspired seasonal forecasts of likely season severity.<sup>160,170,171,172,173</sup> While these forecasts have skill they have largely failed to identify shifts in activity that may be associated with multidecadal variability or, possibly, with global climate change.<sup>159,174</sup> To provide context for such shifts in tropical cyclone activity, longer term records of these storms<sup>175</sup> and variations in environmental factors modulating genesis<sup>176</sup> are necessary. Conventional observational methods cannot provide such records. Thus, proxy records are the mechanism that provide a window on tropical cyclone activity in the distant past. Tropical cyclone variations on decadal timescales are discussed in Section 10.5.4.



#### **Seasonal summaries**

Japan Meteorological Agency (JMA),

<http://www.jma.go.jp/jma/eng/jma-center/rsmc-hp-pub-eg/trackarchives.html>

Joint Typhoon Warning Center (JTWC), <https://metocph.nmci.navy.mil/jtwc/atcr/2004atcr/>

NHC Archive of Hurricane Seasons, <http://www.nhc.noaa.gov/pastall.shtml>

NHC 2004 Atlantic Tropical Cyclone Reports, <http://www.nhc.noaa.gov/2004atlan.shtml>

ENSO monitoring: Real-time data, <http://www.pmel.noaa.gov/tao/jsdisplay/>

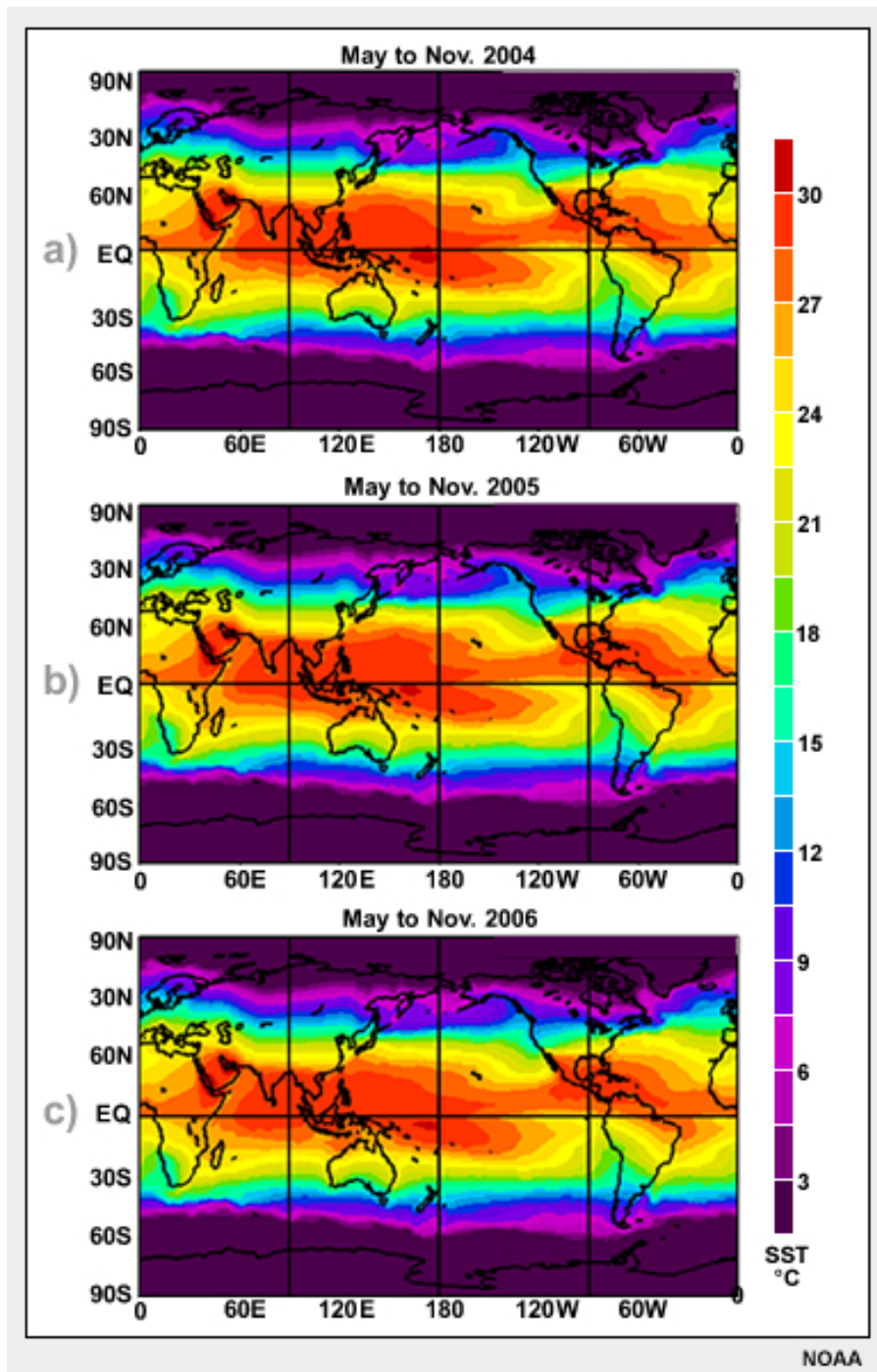


Fig. 10.69. Global NOAA optimum interpolation sea surface temperature maps May through November inclusive for (a) 2004, (b) 2005, and (c) 2006.

### 10.5.3.1 Interannual Modulation Due to the El Niño Southern Oscillation (ENSO)

Variation in basin-scale annual tropical cyclone activity can derive from a range of spatial and temporal forcings.<sup>33,160,162</sup> One of the dominant, multi-year influences of interannual tropical cyclone activity is the El Niño Southern Oscillation (ENSO).

The large-scale atmospheric and oceanic changes accompanying a *warm event* (El Niño) or a *cold event* (La Niña) result in shifts in the tropical regions most favorable to tropical cyclogenesis (e.g., Fig. 10.70). For example, the suppression of convection in the Maritime Continent, and extension of the deep convective zone into the central Pacific and Indian Ocean basins during a warm event, is accompanied by changes to the vertical wind shear and sea surface temperature patterns across the tropics. The result is cooler SST and stronger vertical wind shear in the tropical western Pacific and Atlantic basins as well as warmer SST and weakened vertical wind shear in the central Pacific, eastern North Pacific and the central Indian Oceans. Consequently, tropical cyclone activity in the central Pacific, eastern North Pacific and the central Indian Oceans is generally enhanced during a warm event and tropical cyclones are less prevalent in the central ocean basins in neutral or cold event years. The inverse is true for the western Pacific and North Atlantic Oceans: cold events are more favorable for tropical cyclogenesis and so are typically accompanied by more active tropical cyclone seasons than neutral or warm event years.<sup>160,162,166,173,177</sup>

Caution should be used when considering interannual variability and ENSO. Although 1992 was a warm event year (part of a multi-year sustained warm event), it was the year that a Category 5 hurricane made landfall in Miami, Florida. Hurricane Andrew was the first storm—and a very late start—of a relatively quiet season, yet it was the most devastating storm to hit the US mainland in almost twenty years. This demonstrates that links between seasonal activity and landfall frequency, storm intensity, or storm impacts are tenuous.

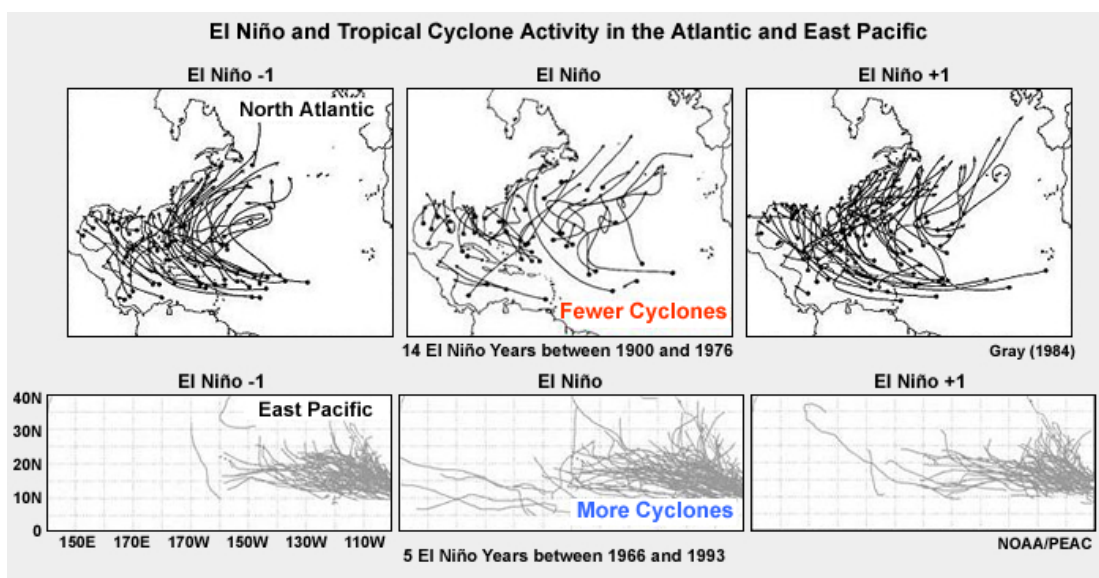


Fig. 10.70. Tropical cyclone activity in the Atlantic (upper) and East Pacific (lower) the year before, during, and after El Niño.



NHC report (updated) for Hurricane Andrew (1992), <http://www.nhc.noaa.gov/1992andrew.html>

### 10.5.3.2 Interannual Modulation by the Quasi Biennial Oscillation (QBO)

The second multi-year modulator of interannual tropical cyclone activity is the Quasi Biennial Oscillation of the stratospheric zonal wind (Fig. 10.71).<sup>162,163,164,165</sup> As with ENSO, the effects of the QBO on tropical cyclone activity are regionally dependent.

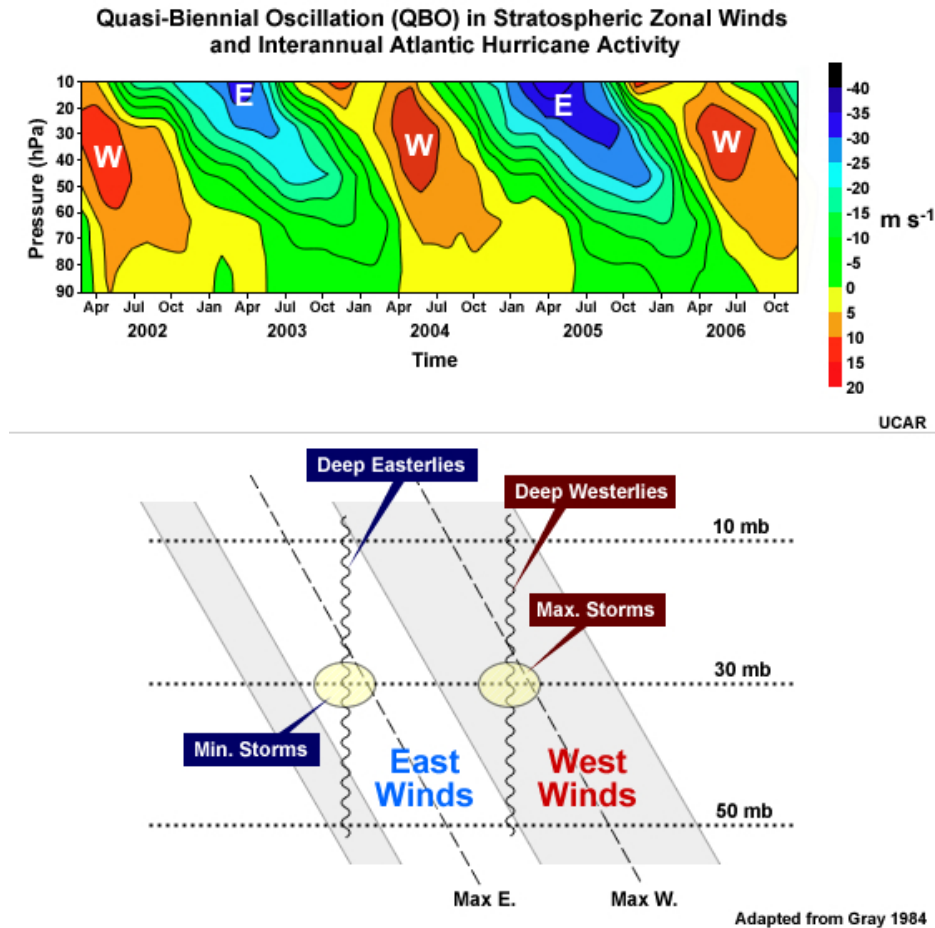


Fig. 10.71. The 10-50hPa stratospheric zonal wind (upper) and typical variation when the 30hPa westerly winds are becoming stronger (wavy lines in grey shaded region) and Atlantic hurricane activity is enhanced. Hurricane activity is suppressed during the easterly wind phase of the QBO (lower, unshaded region). Lower panel is adapted from Gray (1984).<sup>162</sup>

The link between the phasing of the QBO and tropical cyclone activity in the western North Pacific and North Atlantic Oceans<sup>160,165,171</sup> lies in the associated changes in the local vertical wind shear. The phases of the QBO tied to more (less) active hurricane seasons result in decreased (increased) vertical wind shear in the lower stratosphere. In the western North Pacific this decrease (increase) in vertical wind shear occurs in the easterly (westerly) phase of the QBO and is linked to enhanced (suppressed) seasonal tropical cyclone activity.<sup>164</sup> A westerly QBO (westerly anomaly in the equatorial zonal wind at 30 hPa) during Atlantic hurricane season typically results in a more active season than normal; in contrast, an easterly QBO suppresses seasonal activity with similar effectiveness to a warm event (Fig. 10.71).<sup>19</sup>

### 10.5.4 Decadal Cycles and Influences

While very long-time (multi-century) changes in the tropical climate have been investigated for decades, tropical cyclone variability on timescales longer than a few years has only recently been recognized.<sup>178,179,180,181</sup> Variations in the ENSO phenomenon on decadal timescales have been analyzed from surface pressure and SST records extending back to the mid-19<sup>th</sup> century or even earlier.<sup>182,183</sup> These data have been recovered from observation archives such as ship logs<sup>184,185</sup> or from proxy records.<sup>175</sup> These ENSO variations have been proposed to impact typhoon and tropical cyclone activity in the Pacific, and possibly Indian Ocean basins. Long-term records of tropical cyclone activity—such as the six century landfall record for China<sup>181</sup>—may be used to test this link.

Three possible physical mechanisms have been proposed to explain decadal modulation of ENSO: (i) a coupled internal oscillator in the equatorial Pacific;<sup>186</sup> (ii) tropical forcing from midlatitude variability;<sup>186</sup> or (iii) slowing of the global meridional overturning circulation leading to decadal SST fluctuations in the Pacific.<sup>187</sup> It is not yet clear whether one of these mechanisms or a different mechanism not yet considered will explain this phenomenon.<sup>27,28</sup>

The third proposed mechanism for interdecadal variability of ENSO builds upon the concept of the *Ocean Conveyor Belt* which links the global ocean currents (see Fig. 10.72).<sup>188</sup> The surface ocean currents are driven by formation of “deep water” which sinks deep into the ocean in the northern Atlantic and in the Southern Ocean.

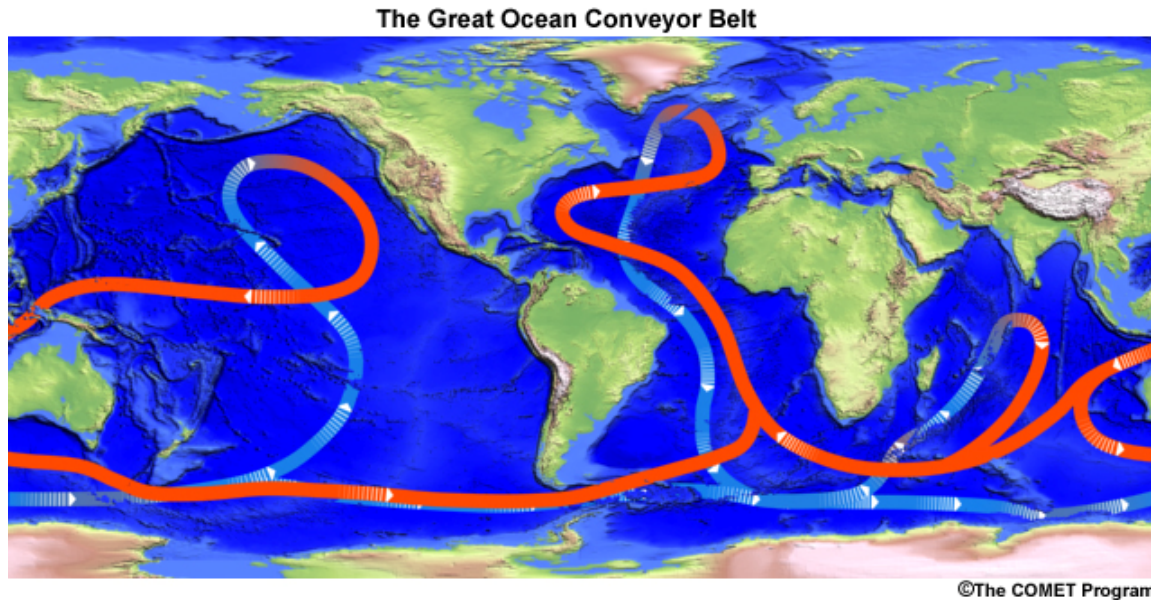


Fig. 10.72. The Great Ocean Conveyor Belt. Adapted from Broecker.<sup>188</sup>

The correspondence between monsoonal rains (drought) over the Sahel region of West Africa, circulation changes in the tropical Atlantic<sup>189</sup> and enhanced (reduced) incidence of intense Atlantic hurricanes<sup>158,167,190</sup> provides evidence of the link between African easterly wave activity and intense hurricane activity in the basin on multidecadal timescales. Variations in the number of easterly waves are only weakly related to the total number of



North Atlantic tropical cyclones in a season. Rather, fluctuations in easterly wave activity contribute to variations in the frequency of *intense hurricanes* (peak winds in excess of  $50 \text{ m s}^{-1}$ , corresponding to Saffir-Simpson Cat 3-5).<sup>191</sup> This reflects the longer passage over warm ocean waters typical of storms reaching such intensities.

Multidecadal variations in Atlantic hurricane activity have been associated with long-term changes in the ocean temperatures and vertical shear of the horizontal winds in that ocean basin.<sup>180</sup> These coupled variations have been termed the *Atlantic Multidecadal Oscillation (AMO)*, which has also been linked to decadal-scale variations in the Ocean Conveyor Belt. If the Ocean Conveyor Belt is accelerated, the tropical Atlantic is warmer than climatology and hurricanes activity increases. By this theory, warm (cool) phases of the tropical Atlantic correspond to transport of waters through the global ocean currents that is faster (slower) than climatology.

Since ocean temperatures and vertical wind shear have been strongly tied to the likelihood of tropical cyclogenesis, the link between these environmental fields and hurricane variability should be unsurprising. The periodic cycling of the ocean “conveyor belt”<sup>188</sup> has been tied to long-term variations in Atlantic Ocean temperatures and extended West African droughts,<sup>192,193</sup> apparently making a good case for multidecadal fluctuations in the ocean currents as the source of ocean surface temperature changes, the resultant variations in West African monsoon rainfall and, by implication, easterly wave frequency. It would seem that the case is closed – but science is rarely that straightforward!

Recent work has cast doubt on the multidecadal modulating influence of the oceans on Atlantic hurricanes, opting for an alternative explanation for the 20<sup>th</sup> Century ocean warming. In this scenario, global climate change combined with the cooling then warming due to the temporal variation in sulfate aerosols through the course of the 20<sup>th</sup> Century governed the evolution of Atlantic Ocean temperatures.<sup>194</sup> This global change (non-AMO) interpretation of Atlantic SST variations raises such fundamental questions as “What is the role of tropical cyclones in the climate?” and “What are the mechanisms through which variations in the base state of the climate affect tropical cyclones?” and “Could changes in tropical cyclone characteristics feedback and influence the evolution of the base state of the climate?”

Theories for the influence of global warming have proposed increases in tropical cyclone intensities linked to the expected continued warming. Newly created datasets<sup>131,195</sup> can be used to test these theories and may perhaps provide some insight into the dominant forcing of multidecadal tropical cyclone variations. In the meantime, the tropical cyclone community has prepared a consensus statement on the current understanding of global warming. This statement should be expected to be revised as the science evolves.



#### **Official statements on tropical cyclones and climate change**

WMO statement (long version) [http://www.wmo.ch/pages/prog/arep/tmrip/documents/iwtc\\_statement.pdf](http://www.wmo.ch/pages/prog/arep/tmrip/documents/iwtc_statement.pdf)

WMO statement executive summary [http://www.wmo.ch/pages/prog/arep/tmrip/documents/iwtc\\_summary.pdf](http://www.wmo.ch/pages/prog/arep/tmrip/documents/iwtc_summary.pdf)

AMS endorsement of this WMO statement <http://www.ametsoc.org/POLICY/wmo.html>

### 10.5.5 Seasonal Forecasting of Tropical Cyclone Activity

The first systematic, statistically-based seasonal forecasting methodology for tropical cyclone activity dates back to the late 1970s<sup>172</sup> and focused on the Australian region. It was not until 1984 that scientists from Colorado State University began publishing regular forecasts of annual tropical cyclone activity for the North Atlantic basin.<sup>162,170</sup>

Table 10.3. List of groups currently issuing seasonal forecasts of tropical cyclone activity. The group, their basin(s) of interest, the modeling approach used and the website location of their forecast products are provided. Adapted from Camargo et al.<sup>202</sup>

Group	Basins	Type	Website
City University of Hong Kong, China (CityU)	Western North Pacific	Statistical	<a href="http://aposf02.cityu.edu.hk">http://aposf02.cityu.edu.hk</a>
Colorado State University, USA (CSU)	Atlantic	Statistical	<a href="http://hurricane.atmos.colostate.edu">http://hurricane.atmos.colostate.edu</a>
Cuban Meteorological Institute (INSMET)	Atlantic	Statistical	<a href="http://www.insmet.cu/">http://www.insmet.cu/</a>
European Centre for Medium-Range Weather Forecasts (ECMWF)	Atlantic Australian Eastern North Pacific North Indian South Indian South Pacific Western North Pacific	Dynamical	<a href="http://www.ecmwf.int">http://www.ecmwf.int</a> (collaborating agencies only)
International Research Institute for Climate and Society (IRI)	Atlantic Australia Eastern North Pacific South Pacific Western North Pacific	Dynamical	<a href="http://iri.columbia.edu/forecast/tc_fcst/">http://iri.columbia.edu/forecast/tc_fcst/</a>
Macquarie University, Australia	Australia/Southwest Pacific	Statistical	<a href="http://www.iges.org/ellfb/past.html">http://www.iges.org/ellfb/past.html</a>
National Meteorological Service, México (SMN)	Eastern North Pacific	Statistical	<a href="http://smn.cna.gob.mx">http://smn.cna.gob.mx</a>
National Climate Centre, China	Western North Pacific	Statistical	<a href="http://bcc.cma.gov.cn">http://bcc.cma.gov.cn</a>
NOAA Hurricane Outlooks	Atlantic Eastern North Pacific Central North Pacific	Statistical	<a href="http://www.cpc.noaa.gov/index.php">http://www.cpc.noaa.gov/index.php</a> <a href="http://www.cpc.noaa.gov/index.php">http://www.cpc.noaa.gov/index.php</a> <a href="http://www.prh.noaa.gov/hnl/cphc/">http://www.prh.noaa.gov/hnl/cphc/</a>
Tropical Storm Risk (TSR)	Atlantic Western North Pacific Australian region	Statistical	<a href="http://www.tropicalstormrisk.com/">http://www.tropicalstormrisk.com/</a>

Table 10.4. Predictors and predictands used for each statistically-based seasonal forecast model identified in Table 10.3. OLR is outgoing long-wave radiation (Chapter 3), MDR is the Main Development Region of the North Atlantic and PDO is the Pacific Decadal Oscillation. Adapted from Camargo et al.<sup>202</sup>

Group	Predictors	Forecasts Produced
City University of Hong Kong, China (CityU)	<ol style="list-style-type: none"> <li>1. ENSO</li> <li>2. Extent of the Pacific subtropical ridge</li> <li>3. Intensity of India-Burma trough</li> </ol>	<ol style="list-style-type: none"> <li>1. Number of TCs</li> <li>2. Number of named TCs</li> <li>3. Number of typhoons</li> </ol>
Colorado State U.	<ol style="list-style-type: none"> <li>1. SST North Atlantic</li> <li>2. SST South Atlantic</li> <li>3. SLP South Pacific</li> <li>4. ENSO</li> <li>5. Atlantic multi-decadal mode</li> </ol>	<ol style="list-style-type: none"> <li>1. Number of named TCs</li> <li>2. Named of named TC days</li> <li>3. Number of hurricanes</li> <li>4. Number of hurricane days</li> <li>5. Number of major hurricanes</li> <li>6. Named of major hurricane days</li> <li>7. Accumulated cyclone energy</li> <li>8. Net tropical cyclone energy</li> </ol>
Cuban Meteorological Institute (INSMET)	<ol style="list-style-type: none"> <li>1. North Atlantic winds</li> <li>2. ENSO</li> <li>3. Intensity of the Atlantic subtropical ridge</li> <li>4. North Atlantic SST</li> <li>5. QBO</li> </ol>	<ol style="list-style-type: none"> <li>1. Number of named TCs</li> <li>2. Number of hurricanes</li> <li>3. Number of named TCs in the Atlantic MDR, Caribbean and Gulf of Mexico (separately)</li> <li>4. First day with TC genesis in the season</li> <li>5. Last day with a TC active in the season</li> <li>6. Number of named TCs that form in the Atlantic MDR and impact the Caribbean</li> </ol>
Macquarie U.	<ol style="list-style-type: none"> <li>1. SOI index</li> <li>2. Equivalent potential temperature gradient</li> </ol>	<ol style="list-style-type: none"> <li>1. Number of TCs</li> <li>2. Number of TCs in the Coral Sea</li> </ol>
National Meteorological Service, México (SMN)	<ol style="list-style-type: none"> <li>1. SST anomalies</li> <li>2. Equatorial wind anomalies</li> <li>3. Equatorial Pacific OLR</li> </ol>	<ol style="list-style-type: none"> <li>1. Number of TCs</li> <li>2. Number of tropical storms</li> <li>3. Number of hurricanes</li> <li>4. Number of major hurricanes</li> </ol>
NOAA (Atlantic and Eastern Pacific)	<ol style="list-style-type: none"> <li>1. ENSO</li> <li>2. Tropical multi-decadal mode</li> <li>3. Atlantic SST</li> </ol>	<ol style="list-style-type: none"> <li>1. Number of named TCs</li> <li>2. Number of hurricanes</li> <li>3. Number of major hurricanes</li> <li>4. Accumulated cyclone energy</li> </ol>
NOAA (Central Pacific)	<ol style="list-style-type: none"> <li>1. ENSO</li> <li>2. PDO</li> </ol>	<ol style="list-style-type: none"> <li>1. Number of named TCs</li> </ol>
Tropical Storm Risk (TSR)	<ol style="list-style-type: none"> <li>1. Trade winds</li> <li>2. MDR SST</li> <li>3. ENSO</li> <li>4. Central North Pacific SLP</li> </ol>	<ol style="list-style-type: none"> <li>1. Number of named TCs</li> <li>2. Number of hurricanes</li> <li>3. Number of major hurricanes</li> <li>4. Accumulated Cyclone Energy</li> <li>5. Accumulated Cyclone Energy of landfalling TCs</li> <li>6. Number of landfalling named TCs</li> <li>7. Number of landfalling hurricanes</li> <li>8. Number of landfalling major hurricanes</li> </ol>

Early in statistical predictions of North Atlantic seasonal hurricane activity, forecasts (of total number of named storms, named storm days, hurricanes and hurricane days) relied predominantly on the phases of ENSO (either prior to the season or predicted for the peak of the season) and the QBO, as well as Caribbean sea level pressures. For example, more tropical cyclones are predicted for cool events (anti-ENSO), west phase of the QBO<sup>162</sup> or below-normal Caribbean basin sea level pressures<sup>196</sup> — and especially if all three coincide. These relationships with seasonal tropical cyclone (tropical storm and hurricane) activity were explained in terms of the large-scale atmospheric and oceanic changes relevant to tropical cyclogenesis that resulted in the tropical Atlantic. Necessary conditions for tropical cyclogenesis are enumerated in Section 10.3.1.

To illustrate the link between these phenomena and tropical cyclogenesis conditions, consider the example of an ENSO year. In an ENSO year the vertical wind shear is generally increased in the tropical Atlantic (a region of relatively high shear climatologically for tropical storm development). This renders the Atlantic basin less conducive to tropical cyclogenesis. Even though this is the case, devastating storms can occur in the Atlantic in ENSO years—Hurricane Andrew of 1992 is the quintessential storm to illustrate this point.

Clearly the statistical models must be built around combinations of a set of predictors to provide forecasts of each tropical cyclone-based quantity (the *predictands*). The predictors (middle column) and predictands (right column) for each of the statistical models are listed in Table 10.4.

Interestingly, even groups forecasting for the same basin use different predictors for the same predictand. For example, while the Cuban Meteorological Institute uses QBO as a predictor for North Atlantic hurricane activity,<sup>197</sup> neither CSU nor NOAA uses this predictor (Table 10.3).<sup>180,198</sup>

Table 10.5 Forecast methodology for each of the dynamically-based seasonal forecast models identified in Table 10.3. Adapted from Camargo et al.<sup>202</sup>

<b>ECMWF</b>	1. Coupled dynamical model 2. Model tropical cyclones identified and tracked	1. Number of named tropical cyclones 2. Mean location of tropical cyclogenesis
<b>IRI</b>	1. Various SST forecast scenarios 2. Atmospheric models 3. Model tropical cyclones identified and tracked	1. Number of named tropical cyclones 2. Accumulated cyclone energy (northern hemisphere only) 3. Mean location of tropical cyclones (western North Pacific only)

A recent innovation in seasonal tropical cyclone forecasting is dynamically-based forecasts<sup>199</sup> (Table 10.5). In this approach, global forecast models are run out for the season and the number of tropical cyclone-like vortices predicted in these models is counted. Various storm characteristics can be recorded for these modeled storms and predictions can also be issued on these quantities. One example is the accumulated cyclone energy (ACE), a measure of wind energy that is defined as the sum of the squares of the maximum sustained surface wind speed (knots) measured every six hours for all named systems while they are at least tropical storm strength.

A seasonal forecast model must demonstrate skill against a “*no skill*” baseline prediction to be useful.<sup>200</sup> The most common no skill forecast used for operational weather forecast models is a combination of climatology and persistence (known as *CLIPER*). Evaluations of a number of available statistical seasonal forecast models demonstrated that these had skill against this CLIPER benchmark.<sup>201,202</sup> This means that these models have useful information on the likelihood of more or less activity in the upcoming season. Other statistical metrics of forecast skill including root mean square error, Pearson correlation coefficient, Spearman rank correlation coefficient, bias compared to climatology<sup>202</sup> provide different perspectives on forecast skill. For example, the Pearson correlation is sometimes called the rank correlation, since it evaluates the similarity in the ordering of two groups of data such as the actual number of storms in a season and the model forecast. The Pearson correlation will not tell you how close the forecast is each year, but it will tell you if the forecast picks active and inactive seasons well.

For the first 20 years, seasonal tropical cyclone forecasts were restricted to information on basin-wide tropical cyclone activity. A relatively new development in this arena is forecasts of landfall frequencies.

### Box 10-9 Unusual Tropical Cyclone Seasons around the Globe

Every so often a tropical cyclone season will catch the attention of even the most disinterested observers of the tropics. The maps that follow here depict a selection of recent seasons that have caught the imagination of many across the globe.



Fig. 10B9.1. In 2006, the eastern North Pacific seemed to constantly have tropical cyclones forming. The entire season, from Aletta through Sergio, is plotted here.

## Box 10-9 continues

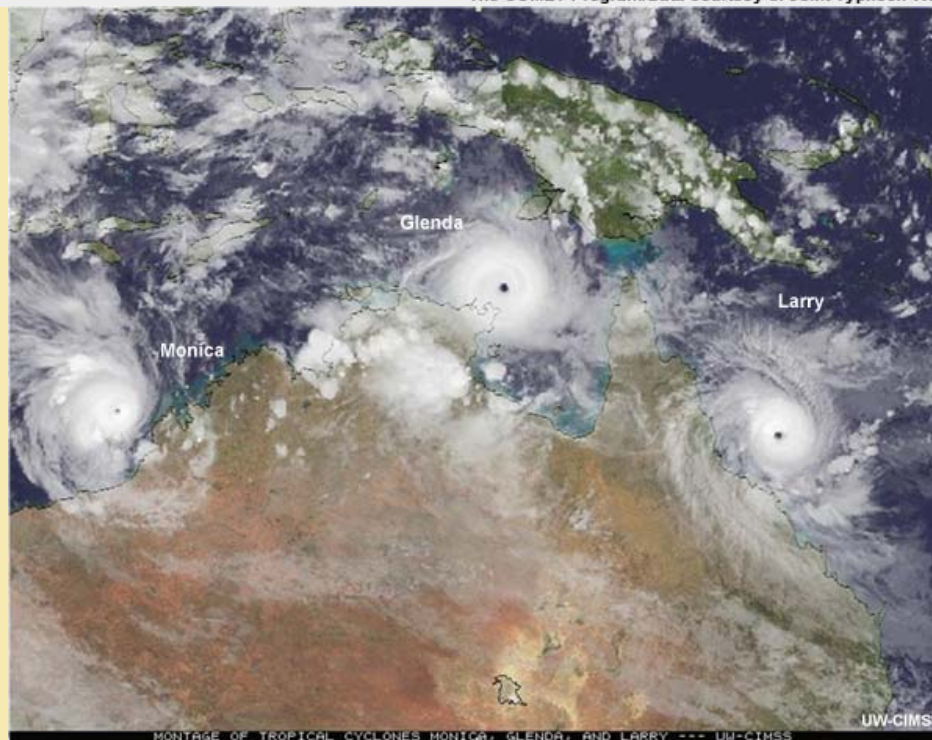
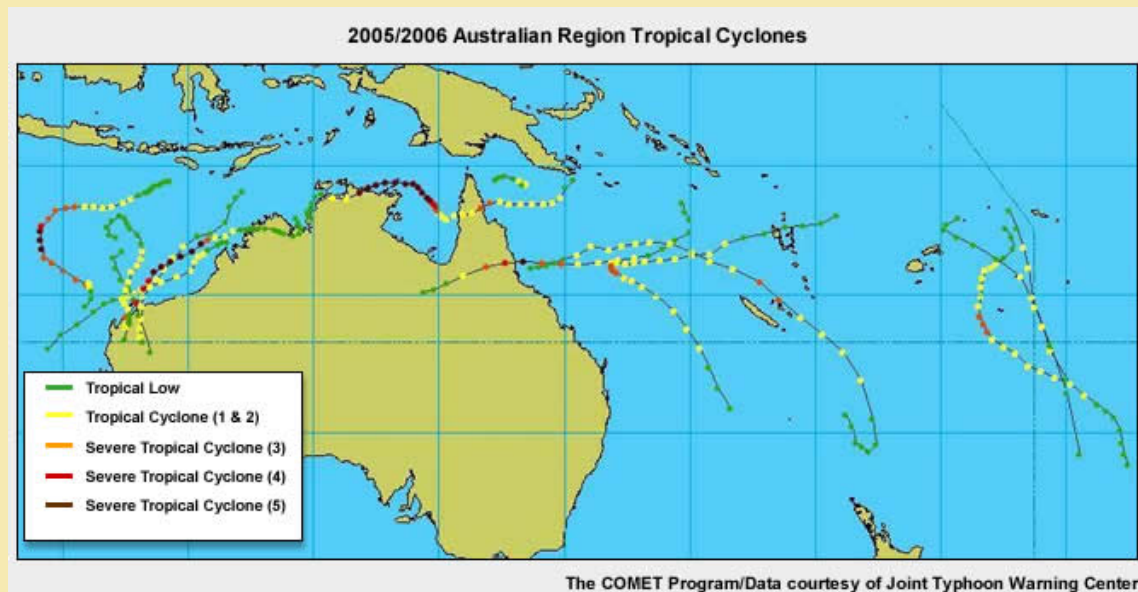


Fig. 10B9.2. (Upper) Tracks of all 2005/2006 Australian region tropical cyclones; and (lower) a satellite montage of severe tropical cyclones Glenda, Monica and Larry. These three storms impacted Australia within a month, but only two storms were active at any time (this artificial image was created to compare them). Montage created by C. Velden and T. Olander (CIMSS/University of Wisconsin).



Cyclone Larry report, [http://www.bom.gov.au/weather/qld/cyclone/tc\\_larry/Larry\\_report.pdf](http://www.bom.gov.au/weather/qld/cyclone/tc_larry/Larry_report.pdf)

Box 10-9 continues

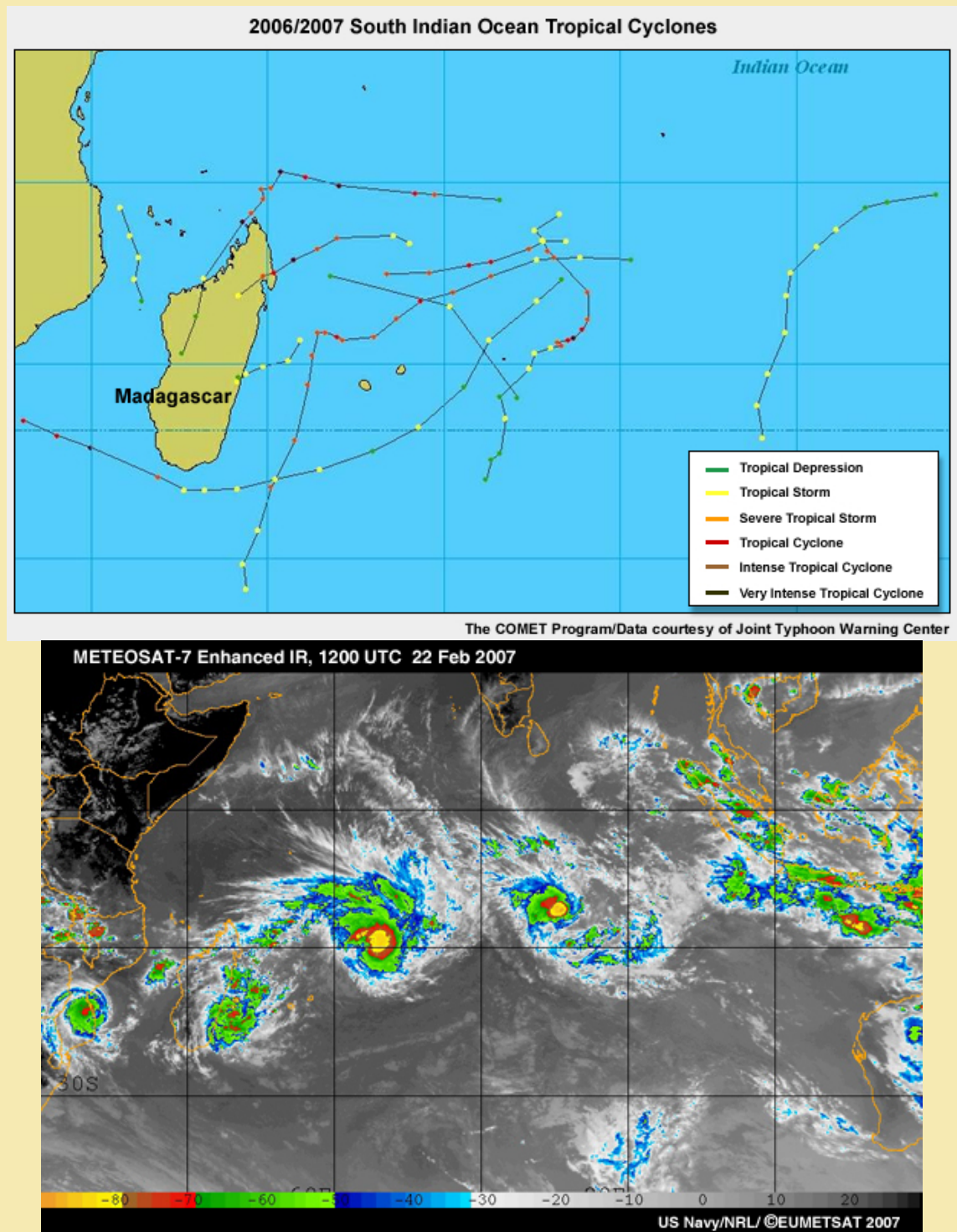


Fig. 10B9.3. (Upper) The 2006/2007 South Indian Ocean tropical cyclone season was extremely active. Madagascar in particular suffered severe impacts, although other parts of southern Africa did not go unscathed. (Lower) Enhanced IR image of tropical cyclones on 22 Feb 2007.



## Box 10-9 continues

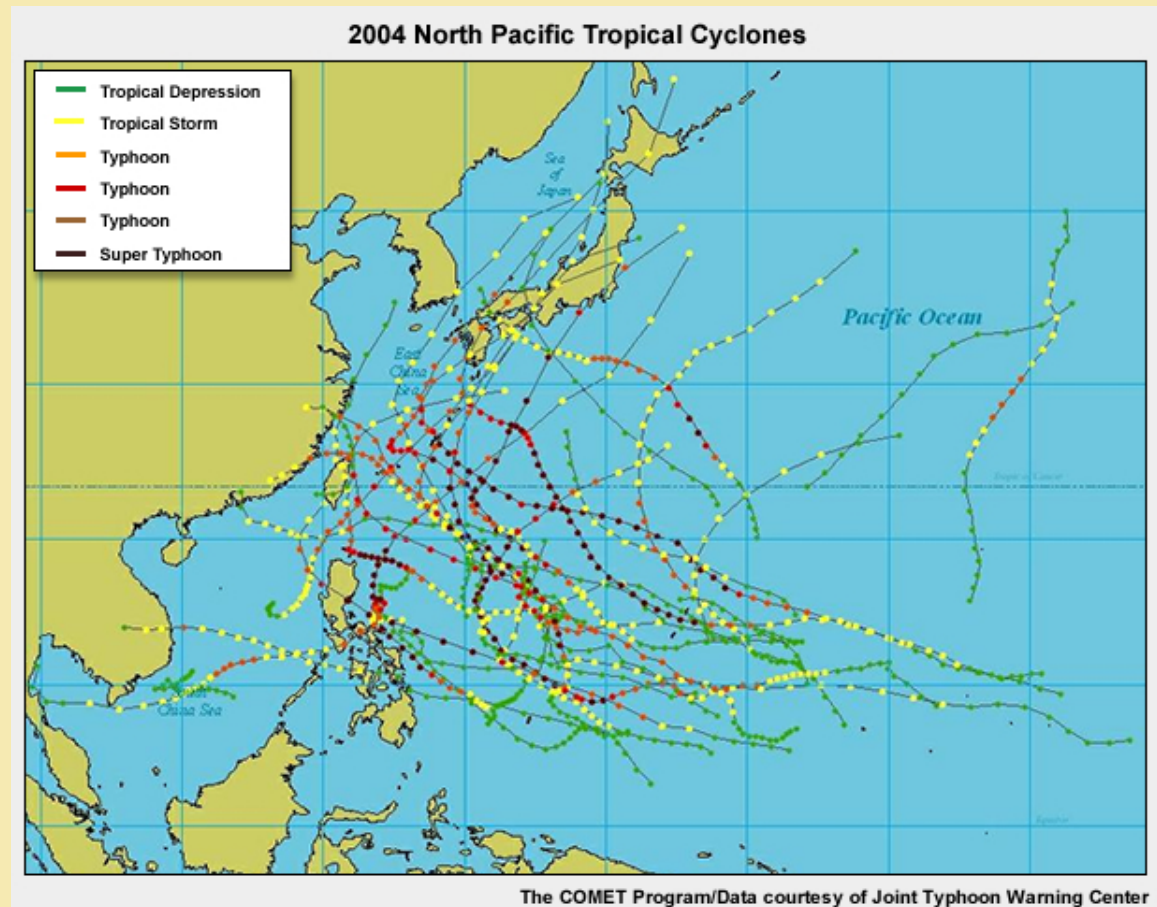
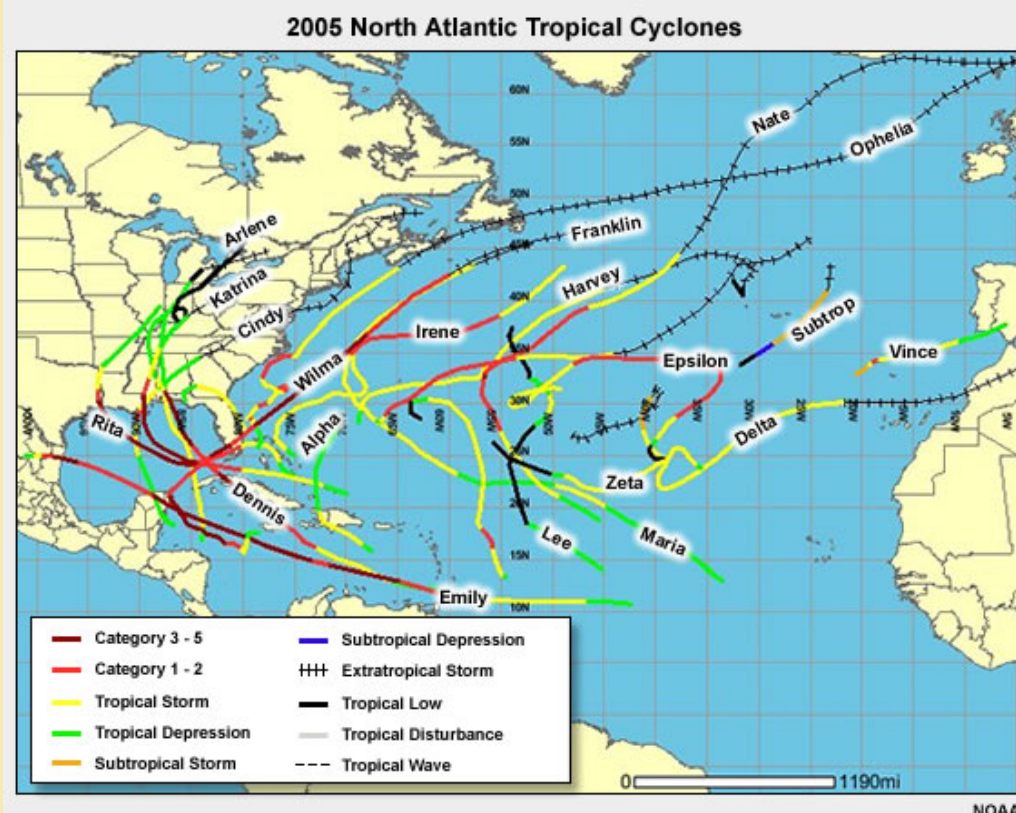
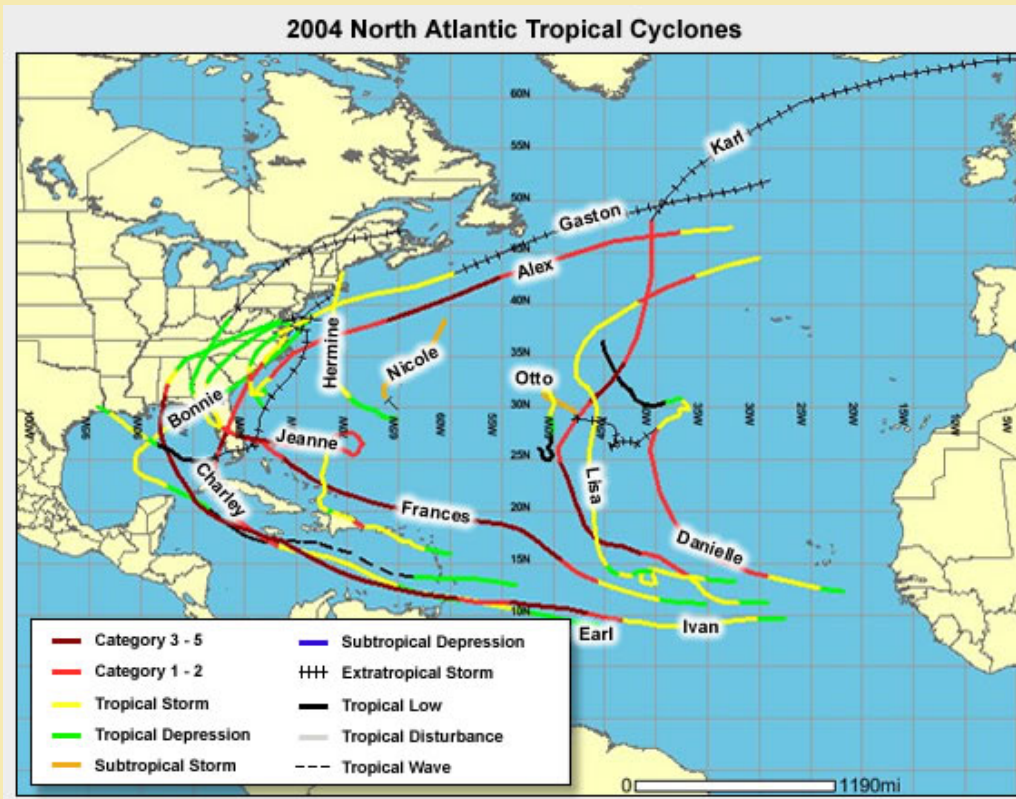


Fig. 10B9.4. Thirty tropical cyclones (including 16 typhoons and five supertyphoons) in the western North Pacific in 2004 ranked this as an active season, even for this very active region of the tropics. Climatologically, the western North Pacific has 25 named systems with 16 of these being typhoons or supertyphoons. For Japan, the season was particularly devastating – ten typhoons made landfall in Japan that year (many of these were either undergoing or having completed extratropical transition).

Box 10-9 continues



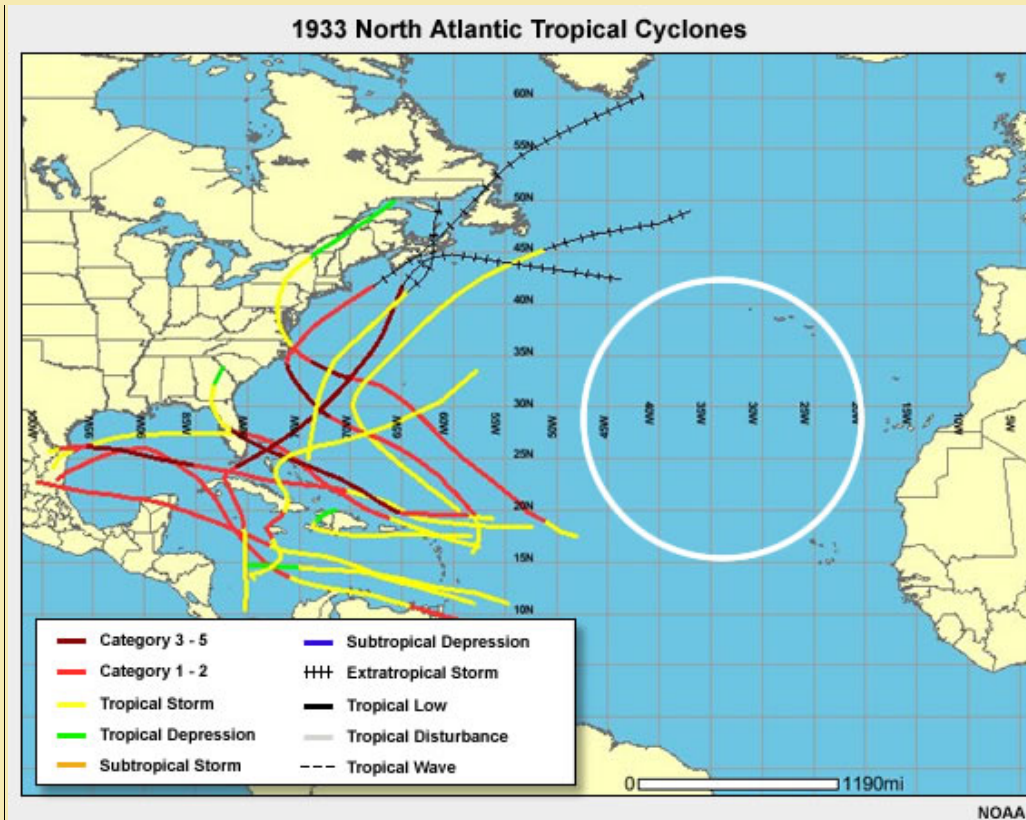


Fig. 10B9.5. Both the 2004 (top) and 2005 (middle) Atlantic hurricane seasons were very active (see table below) – and became notorious for their multiple landfalls in the Caribbean, Central America and North America. But were these seasons unprecedented? Statistics from the 1933 hurricane season (Table 10B.6.1) show that this was also an unusually active season. Further, the map of observed tracks from 1933 (bottom panel) shows that no tracks were recorded in the eastern third of the basin. It is feasible that there were tracks in this region that were missed. Track data and statistics are from NOAA HURDAT database.

Table 10B9.1 Comparison of the 2004, 2005 and 1933 North Atlantic hurricane seasons.

	Climatology	2004	2005	1933
<b>Named storms</b>	<b>10</b>	16	28	21
<b>Tropical Storms</b>	<b>4</b>	5	12	11
<b>Hurricanes</b>	<b>6</b>	9	15	10
<b>Subtropical storms</b>	<b>1-2*</b>	1	1	0

## 10.6 Tropical Cyclone Motion

For over a century it has been known that a tropical cyclone will move in response to the other weather systems in its environment.<sup>203,204</sup> Initially, the tropical cyclone was considered to be a passive “cork in a stream” being “steered” by the other weather systems around it. Certainly, environmental steering (advection) is important to tropical cyclone motion. Advection of the storm by its environment is closely related to the deep-layer mean wind, the average wind calculated through a deep layer of the atmosphere.<sup>205,206</sup> When calculating this wind from standard pressure level data, it is necessary to weight each level by the mass of the layer it represents. For tropical cyclone motion, the average from 850-200 hPa is used most often, however a shallower (say 850-500 hPa) layer can work better for weaker storms. The deep-layer mean wind was often well approximated by the 500 hPa wind averaged over a circle centered on the tropical cyclone.<sup>207</sup> However, the choice of the averaging layer for the advection has been shown to be weakly related to storm intensity.<sup>208</sup> While advection is clearly important, the limited success of forecasts using this approach led scientists to consider more realistic explanations of the storm motion. In this section we review the various mechanisms that contribute to the motion of a tropical storm.

The most straightforward approach to the study of storm motion is to consider the motion due to the flow averaged through a deep layer, so we begin this study with the barotropic, nondivergent potential vorticity equation. The barotropic constraint means that we are assuming that the atmosphere has the same horizontal structure at all levels in the vertical, so it can be represented by the deep layer mean flow. Hence, the barotropic PV reduces to the vertical component of the absolute vorticity ( $\zeta + f$ ).

The barotropic, nondivergent potential vorticity (PV) equation<sup>j</sup> is written

$$\frac{d(\zeta + f)}{dt} \equiv \frac{\partial(\zeta + f)}{\partial t} + \bar{\mathbf{v}} \cdot \nabla(\zeta + f) = 0, \quad (9)$$

where the variables have their usual meaning (these are also defined in Box 10-10 and Appendix B). Equation (9) states that the absolute vorticity is conserved following the flow. Since  $\frac{\partial f}{\partial t} = 0$  (the Coriolis parameter at a fixed location does not change with time),

we can rearrange this equation as:

$$\frac{\partial \zeta}{\partial t} = -\bar{\mathbf{v}} \cdot \nabla(\zeta + f). \quad (10)$$

This equation is a statement that the relative vorticity,  $\zeta$ , at a fixed location on the earth changes in time  $\partial \zeta / \partial t$  due to advection of absolute vorticity ( $-\bar{\mathbf{v}} \cdot \nabla(\zeta + f)$ ).

Scale analysis of this equation<sup>209</sup> shows that the most important term is the advection of relative vorticity,  $-\bar{\mathbf{v}} \cdot \nabla \zeta$ . However, observations show that if advection of Earth vorticity,  $-\bar{\mathbf{v}} \cdot \nabla f$ , is not considered, an error in the motion of a few meters per second

<sup>j</sup> Note the middle two terms are an expansion of the first term  $\frac{d(\zeta + f)}{dt}$ , the Lagrangian time derivative.

with a direction offset from the steering will occur. This error adds up in the course of a 24-hour or longer forecast and so we must consider this term as well.

$-\vec{v} \cdot \nabla f$  is known as the  $\beta$ -effect, since

$$\beta = \frac{1}{a} \frac{df}{d\varphi} = \left( \frac{2\Omega}{a} \right) \cos \varphi \quad (11)$$

is the north-south variation of the Coriolis parameter. In Cartesian coordinates, we write this as  $\beta = \frac{df}{dy}$ .

### 10.6.1 The “ $\beta$ -Effect”

In addition to vortex motion due to steering by the large-scale flow, there is a contribution to tropical cyclone motion resulting from vortex interaction with the Earth's background vorticity gradient,<sup>209,210</sup> known as either the  $\beta$ -effect<sup>k</sup> or as *propagation due to the  $\beta$ -gyres*. This vortex propagation component of the motion is typically smaller than the steering (often only a couple of  $\text{m s}^{-1}$  forward speed), but its impact on the storm direction can sometimes have substantial impacts on the storm evolution. This is because the change in direction can result in the storm interacting with different phenomena (other weather systems, SST anomalies, etc.).

In thinking about how the observed motion of a tropical cyclone differs from the motion expected if it were just blown along by the other weather features around it, we must understand the  $\beta$ -gyres<sup>l</sup>. A straightforward mathematical analysis to demonstrate the physics underlying our list of facts is given in Box 10-10.

- Propagation of a tropical cyclone could not occur without the north-south variation in the Coriolis parameter.
- The rotating winds of a tropical cyclone, combined with the north-south variation in the Coriolis parameter, induce relative vorticity asymmetries in the tropical cyclone (Fig. 10.73). These asymmetries are called the  $\beta$ -gyres.
- Since relative vorticity is calculated by taking spatial gradients of the vector wind, *changes in vorticity must result in changes in the winds*. Hence, *the  $\beta$ -gyres must have winds associated with them*.
- The winds of the  $\beta$ -gyres produce a net flow across the tropical cyclone center. Generally the  $\beta$ -drift is towards the northwest at a few knots; the speed and actual direction is related to the vortex size and strength.<sup>211</sup>

<sup>k</sup>Interestingly, the Earth's vorticity gradient can be regarded as representing a second vortex of much larger scale than the tropical cyclone. In this way, the results in this section can be extended to both a synoptic-scale environment and to the Fujiwhara interaction of two or more tropical cyclones.

<sup>l</sup>The alert student may notice that these arguments are very similar to the conceptual model used to explain the evolution of Rossby waves. Indeed, Rossby wave dispersion has been used to describe  $\beta$ -gyre evolution. However, the traditional treatment of Rossby waves considers a purely zonal background flow that results in westward propagation. It is the feedback of the vortex that provides the additional, poleward motion here.

- In computer modeling studies, the  $\beta$ -gyres initially form at the radius of maximum winds ( $R_{MAX}$ ) of the tropical cyclone and are oriented due east and west of the cyclone center. The cyclonic  $\beta$ -gyre is to the east of the storm center and the anticyclonic  $\beta$ -gyre is to the west. This is true in both hemispheres.
- As the computer simulation evolves, the  $\beta$ -gyres move further out from the storm center and are rotated cyclonically (because of the storm's rotational winds) from their initial east-west orientation.
- This final location and orientation of the  $\beta$ -gyres results in relative vorticity asymmetries with associated winds that cause the tropical cyclone to propagate poleward and westward in both hemispheres. In the NH the tropical cyclone propagates further north and west than would be expected due to steering alone, while SH tropical cyclones propagate further south and west.
- In the real atmosphere we cannot see the  $\beta$ -gyres evolve in this way. *In reality, development of the  $\beta$ -gyres occurs along with the evolution of the tropical cyclone and its environment.*
- It is important to remember that *the tropical cyclone will always propagate to the west compared to the steering flow, no matter which hemisphere it is in.*
- Development of the  $\beta$ -gyres can be demonstrated using the barotropic, nondivergent vorticity equation. This derivation is given in detail in Box 10-10.

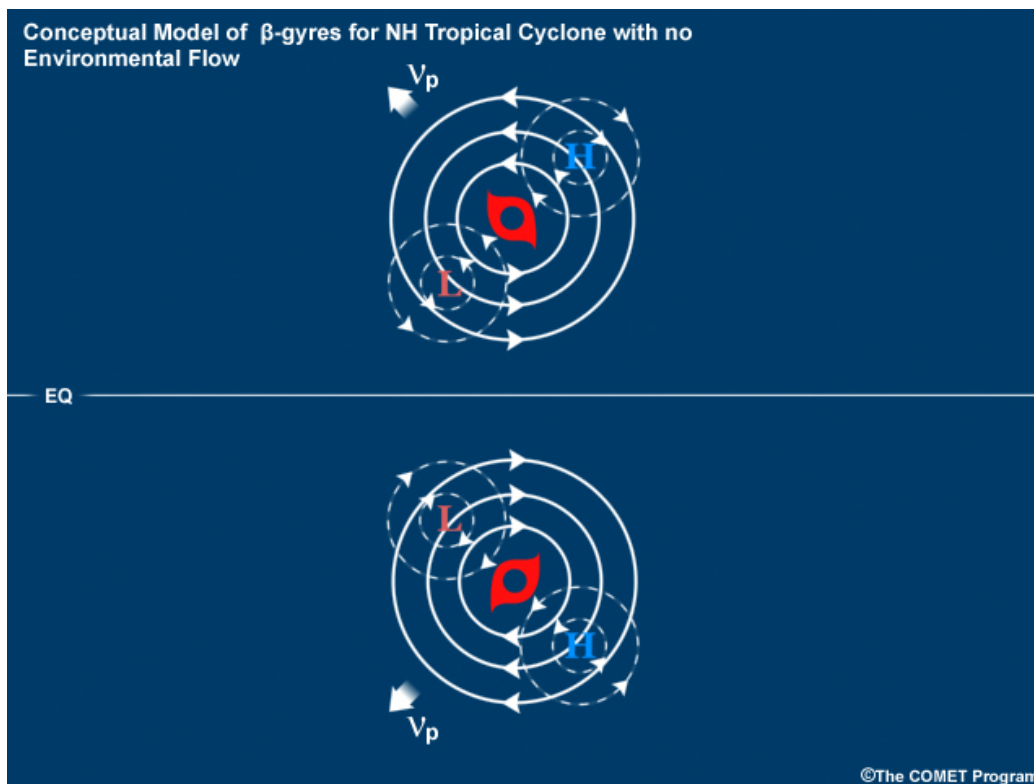


Fig. 10.73. Schematic of the  $\beta$ -gyres resulting for a tropical cyclone in a quiescent environment (i.e., no environmental flow). The gyres are illustrated for both a NH and a SH tropical cyclone.

### Box 10-10 Absolute Vorticity Conservation and the $\beta$ -Effect

#### 1. Conservation of Barotropic, Nondivergent Absolute Vorticity

Barotropic, nondivergent absolute vorticity,  $\zeta_a$ , can be useful for studying some problems in synoptic (or larger scale) meteorology, as demonstrated by a scale analysis of the complete prognostic vorticity equation.

Propagation is the deviation of the tropical cyclone motion from the environmental steering. Conservation of the absolute vorticity,  $\zeta_a$ , provides insight into the source of this propagation component of motion. The barotropic, nondivergent vorticity equation is

$$\frac{d\zeta_a}{dt} = 0 \quad (B10-10.1)$$

In other words, *a parcel moving with the prevailing winds will always have the same value of absolute vorticity.*

Next, we will investigate how this simple concept can be used to explain the propagation of a tropical cyclone.

#### 2. Propagation due to Barotropic Absolute Vorticity Conservation: the $\beta$ -Effect

To solve for the  $\beta$ -gyres, we use perturbation analysis of the barotropic, nondivergent (and, hence frictionless) vorticity equation, Eq. (B10-10.1). We expand the absolute vorticity,  $\zeta_a$ , into its relative vorticity,  $\zeta$ , and earth vorticity,  $f$ , components to get:

$$\frac{d(\zeta + f)}{dt} = 0$$

Expanding the total derivative, remembering that  $f=f(y)$ , and rearranging gives

$$\frac{\partial \zeta}{\partial t} = -\vec{v} \cdot \nabla(\zeta + f) \quad (B10-10.2)$$

Therefore, *at a given location, the relative vorticity,  $\zeta$ , changes with time because of the advection of absolute vorticity,  $(\zeta + f)$ , by the prevailing winds.*

Since you cannot see vorticity, an illustration to help understand this concept is a dust storm. If you are standing at a location with a clear view and dust blows in, the amount of dust that you are breathing changes with time because of the concentration of dust advected to that location by the winds.

We will make a number of assumptions to simplify the analysis, while retaining the key physics. Observations on the consequences of these assumptions help to clarify why we are taking this approach.

## Box 10-10 continues

### Assumptions and observations underlying our thought experiment to solve for the $\beta$ -gyres

- Because of its nearly-circular horizontal structure, cylindrical coordinates are the ideal coordinate frame for studying the structure of a real tropical cyclone.
- In our notation for cylindrical coordinates, the wind components  $(u, v, w)$  correspond to the radial, rotational and vertical directions  $(r, \lambda, z)$ .
- Since we are using the barotropic, nondivergent vorticity equation—which also means no friction—the *simple tropical cyclone in our solution below has only symmetric rotating winds, no radial or vertical wind components*. Therefore, any asymmetries that develop are not part of the original, symmetric tropical cyclone.
- To simplify, we begin our thought experiment with *only the symmetric tropical cyclone on a rotating Earth* (Coriolis parameter varying in the north-south). There are no other weather systems (and so *no steering flow*).
- In this experiment *asymmetries can only result from interactions between the symmetric TC and the Earth vorticity gradient. These asymmetries are the  $\beta$ -gyres*.
- With no steering flow, *any motion of the simple tropical cyclone must be due to the  $\beta$ -gyres*.

### Solving for the $\beta$ -gyres

The observations above suggest that we partition each wind component  $(u, v, w)$  further into a *symmetric, s, (tropical cyclone)* and *asymmetric, a, ( $\beta$ -gyre)* component:

$$\vec{v} = \vec{v}_s + \vec{v}_a, \quad \zeta = \zeta_s + \zeta_a \quad (B10-10.3)$$

Because we can have no vertical motion in this particular vorticity equation, only the horizontal wind components remain. Both the winds and the vorticity, which is derived from the winds, are partitioned into storm and  $\beta$ -gyre components. Substituting the partitioned components into Eq. (B10-10.2) gives

$$\frac{\partial(\zeta_s + \zeta_a)}{\partial t} = -\vec{v}_a \cdot \nabla \zeta_s - \vec{v}_s \cdot \nabla \zeta_a - \vec{v}_s \cdot \nabla f \quad (B10-10.4)$$

where small terms are ignored. The advection of the symmetric vorticity by the symmetric winds,  $-\vec{v}_s \cdot \nabla \zeta_s = 0$  and both  $-\vec{v}_a \cdot \nabla \zeta_a$  (advection of the  $\beta$ -gyres by themselves)  $-\vec{v}_a \cdot \nabla f$  ( $\beta$ -gyre advection of Earth vorticity) are very small. The remaining terms in Eq. (B10-10.4) correspond to the following physical processes:

- $\frac{\partial(\zeta_s + \zeta_a)}{\partial t}$ , the time rate of change of the total relative vorticity at a location.
- $-\vec{v}_a \cdot \nabla \zeta_s$ , the propagation of the symmetric tropical cyclone due to the  $\beta$ -gyres.
- $-\vec{v}_s \cdot \nabla \zeta_a$ , the advection of the  $\beta$ -gyres by the tropical cyclone. This causes the change in their orientation away from the east-west direction.
- $-\vec{v}_s \cdot \nabla f$ , the term that creates the  $\beta$ -gyres, since we begin with only the symmetric tropical cyclone on a rotating Earth.



### Box 10-10 continues

The impact of these processes on the tropical cyclone structure and motion are illustrated in Fig. 10.73 for both NH and SH examples.

### 3. Motion due to a $\beta$ -Effect Modified by Environmental Vorticity Gradients

In the real atmosphere, we cannot ignore other weather systems, so *to make this solution more realistic, we should also include an environmental flow*. This will change two key things: (1) we will also *have steering* to move the tropical cyclone; and (2) the presence of other weather systems will *change the background absolute vorticity gradient*.

Since the other weather systems will not be symmetric around the tropical cyclone, their effect will show up in the asymmetric components of the winds and relative vorticity. Let us partition the asymmetric fields further into environment (*e*) and  $\beta$ -gyres (*g*):

$$\vec{v} = \vec{v}_s + \vec{v}_e + \vec{v}_g, \quad \zeta = \zeta_s + \zeta_e + \zeta_g \quad (B10-10.5)$$

To keep things simple, we will assume that the environment does not change in time:

$$\frac{\partial \vec{v}_e}{\partial t} = 0 \quad \text{and} \quad \frac{\partial \zeta_e}{\partial t} = 0.$$

Substituting expressions (B10-10.5) into Eq. (B10-10.2) leads to

$$\frac{\partial(\zeta_s + \zeta_g)}{\partial t} = -\vec{v}_s \cdot \nabla(\zeta_e + f) - \vec{v}_s \cdot \nabla \zeta_g - \vec{v}_e \cdot \nabla \zeta_s - \vec{v}_g \cdot \nabla \zeta_s - \vec{v}_e \cdot \nabla f \quad (B10-10.6)$$

Including the environment adds extra terms to the simple solution in Eq. (B10-10.4):

- $-\vec{v}_e \cdot \nabla \zeta_s$ , the *steering of the symmetric tropical cyclone* due to other weather systems.
- $-\vec{v}_g \cdot \nabla \zeta_s$ , the propagation of the symmetric tropical cyclone due to the  $\beta$ -gyres (this is the same as  $-\vec{v}_a \cdot \nabla \zeta_s$  in Eq. (B10-10.4)).
- $-\vec{v}_s \cdot \nabla(\zeta_e + f)$ , the term that creates the *environmental  $\beta$ -gyres* since  $\nabla(\zeta_e + f)$  is the background absolute vorticity gradient for the symmetric tropical cyclone.
- $-\vec{v}_s \cdot \nabla \zeta_g$ , the advection of the environmental  $\beta$ -gyres by the tropical cyclone that changes their orientation, the same as  $-\vec{v}_s \cdot \nabla \zeta_a$  in Eq. (B10-10.4).

The biggest impact of including an environment in this case is that  $\nabla(\zeta_e + f)$  may no longer point north-south since  $\nabla \zeta_e$  could be much larger than  $\nabla f \sim 10^{-11} \text{ s}^{-1} \text{ m}^{-1}$  and  $\nabla \zeta_e$  will point towards the strongest weather system nearby. Therefore,  $-\vec{v}_s \cdot \nabla(\zeta_e + f)$  could result in environmental  $\beta$ -gyres that have *any orientation*. Examples of vortex changes due to the creation of the environmental  $\beta$ -gyres are shown in Fig. 10.74.

## 10.6.2 Environmental “ $\beta$ ” Effects

Studies of tropical cyclone motion in environments that vary in the horizontal have generally focused on storm environments characterized by a shear flow representative of observed ridge and trough features.<sup>212,213,214,215</sup> Each of these studies considered a single tropical cyclone-like vortex in a spatially varying environment. The impact of the change to the  $\beta$ -gyres due to the environmental relative vorticity gradient are illustrated in Fig. 10.74, where  $\beta_{env} = \nabla(\zeta_e + f)$ .

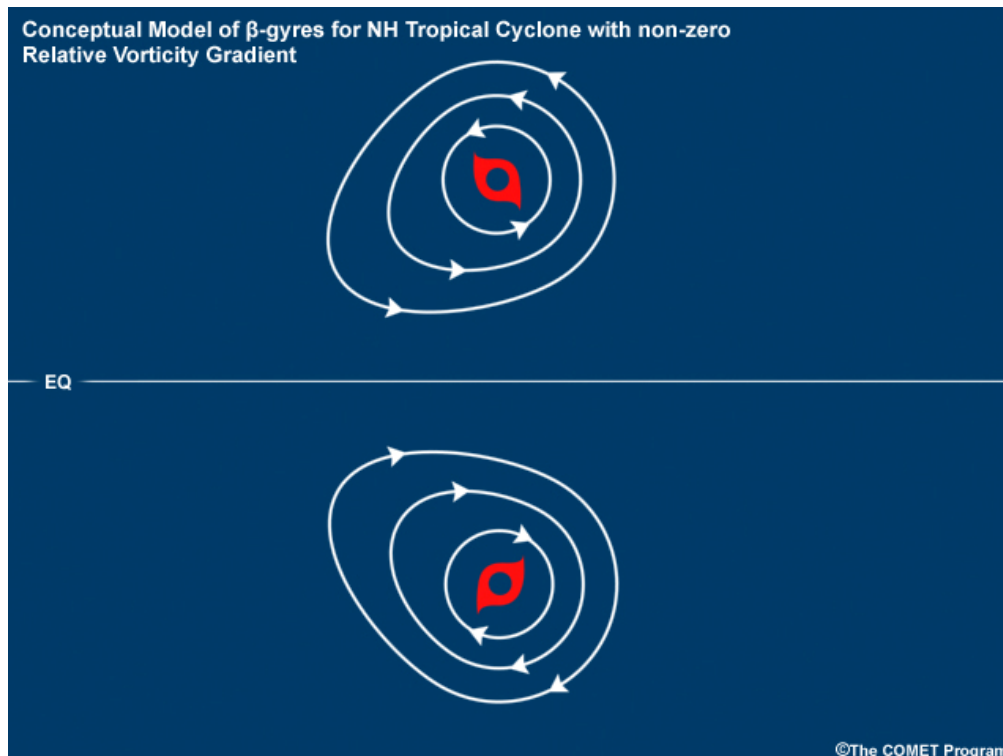


Fig. 10.74. Schematic of the asymmetric (NH and SH) tropical cyclone calculated by summing the symmetric vortex and the  $\beta$ -gyres. The  $\beta$ -gyres here are the result of a symmetric tropical cyclone in a more typical environment with non-zero relative vorticity gradient.



Does the environmental vorticity gradient that led to the  $\beta$ -gyres implied in Fig. 10.74 reinforce or oppose the meridional gradient of the Coriolis parameter,  $\beta$ ? Justify your answer.

Even a relatively weak zonal flow can change the sign of the absolute vorticity. Let us calculate what the spatial gradient of the environmental wind shear,  $\frac{\partial^2 u}{\partial y^2}$ , needs to be to cancel out  $\beta$ .

First, we need to calculate a typical value for  $\beta$ . Recall Eq. (11):

$$\beta = \frac{df}{dy} = \frac{2\Omega}{a} \cos \varphi, \quad (12)$$

where  $\Omega=7.292 \times 10^{-5} \text{ s}^{-1}$  is the rotation rate of the Earth about its axis,  $a=6.37 \times 10^6 \text{ m}$ , and  $\varphi$  is the latitude of interest – let us use  $\varphi=15^\circ$ . Note that this calculation applies for either hemisphere since  $\beta > 0$  everywhere and is symmetric about the equator because of its dependence on cosine.



Solve for the relative vorticity gradient that the environment would need to have to negate  $\beta$ . To do this you should complete the following steps:

1. Calculate  $\beta$ .
2. Deduce the value of  $\frac{\partial^2 u}{\partial y^2}$  needed to negate  $\beta$ .
3. Solve for the simplest functional form for  $\frac{\partial^2 u}{\partial y^2}$ , assuming  $\beta$  is constant. The assumption that  $\beta$  is constant is commonly made in the tropics, since the value of  $\beta$  varies relatively slowly there.
4. Translate your information for  $\frac{\partial^2 u}{\partial y^2}$  and  $\beta$  into a change in the zonal winds between two points.
5. Evaluate whether such a change is realistic.



Solution to the previous exercise:

**1. Calculate  $\beta$ .**

$$\beta = \frac{df}{dy} = \frac{2\Omega}{a} \cos \varphi = \frac{2 \times 7.29 \times 10^{-5}}{6.37 \times 10^6} \cos(15^\circ) = \frac{14.584}{6.37} \times 10^{-11} \times 0.97 = 2.2 \times 10^{-11} \text{ s}^{-1} \text{ m}^{-1}.$$

**2. Deduce the value of  $\frac{\partial^2 u}{\partial y^2}$  needed to negate  $\beta$ .**

To negate  $\beta$ ,  $\frac{\partial^2 u}{\partial y^2}$  must also be  $2.2 \times 10^{-11} \text{ s}^{-1} \text{ m}^{-1}$ .

**3. Solve for the simplest functional form for  $\frac{\partial^2 u}{\partial y^2}$ , assuming  $\beta$  is constant.**

Make one assumption: that  $\frac{\partial^2 u}{\partial y^2} = \frac{d^2 u}{dy^2}$  - that is, the zonal wind only varies in the north-south direction. Now solving for the functional form of  $u$  is straightforward:

$$\frac{du}{dy} = \int \frac{d^2 u}{dy^2} dy = \int \beta dy = \beta y + C_1 \text{ s}^{-1},$$

where  $C_1$  is an integral constant and we recall that we have also assumed  $\beta$  to be constant. Integrating once more gives:

$$u(y) = \int \frac{du}{dy} dy = \int (\beta y + C_1) dy = \beta y^2 + C_1 y + C_2,$$

where  $C_2$  is another integral constant. For simplicity, let us assume that both  $C_1$  and  $C_2$  are zero. This leaves  $u(y) = 2.2 \times 10^{-11} y^2 \text{ m s}^{-1}$ .

**4. Translate your information for  $\frac{\partial^2 u}{\partial y^2}$  and  $\beta$  into a change in the zonal winds between two points.**

A change in the zonal winds between two points is given by

$$\frac{du}{dy} = 2.2 \times 10^{-11} y,$$

So in this simple world, moving north or south by one meter will change the winds by  $2.2 \times 10^{-11} \text{ m s}^{-1}$ . What does that translate to over synoptic scales? A synoptic system has spatial scale of order  $1000 \text{ km} = 10^6 \text{ m}$ . This tells us that we can negate the effects of  $\beta$  with a change in the  $u$ -component on the synoptic scale of  $2.2 \times 10^{-5} \text{ m s}^{-1}$ !

**5. Evaluate whether such a change is realistic.**

Since this is a tiny wind change over synoptic scales, this result tells us that ignoring  $C_1$  and  $C_2$  likely was not appropriate. By matching actual wind speeds from climatology to different latitudes, we can construct a more realistic functional form for  $u(y)$  and  $\frac{du}{dy}$ . Try this now.

### 10.6.3 Interaction of Vortices: The Fujiwhara Effect

For over a century it has been known that each vortex in a multiple vortex configuration will move in response to the other vortices, even in an otherwise quiescent environment.<sup>203,204</sup> Dynamically, this motion results from the mutual advection of the symmetric vorticity associated with each vortex. Two observational studies<sup>216,217</sup> of the western North Pacific and North Atlantic confirm the importance of multiple vortex interactions in these basins (Fig. 10.75). Binary storm interaction occurred 1.5 times per year on average for the western North Pacific and once every three years<sup>216</sup> in the North Atlantic (over the period 1945-1981). Binary interactions (large angular rotation rates) occurred when the tropical cyclone centers were separated by distances of less than 1300-1400 km, with this critical separation distance depending on the sizes of the interacting systems.<sup>217,218</sup> Of these interacting cyclones, 70% orbited cyclonically around one another with orbital speed varying inversely with separation distance.

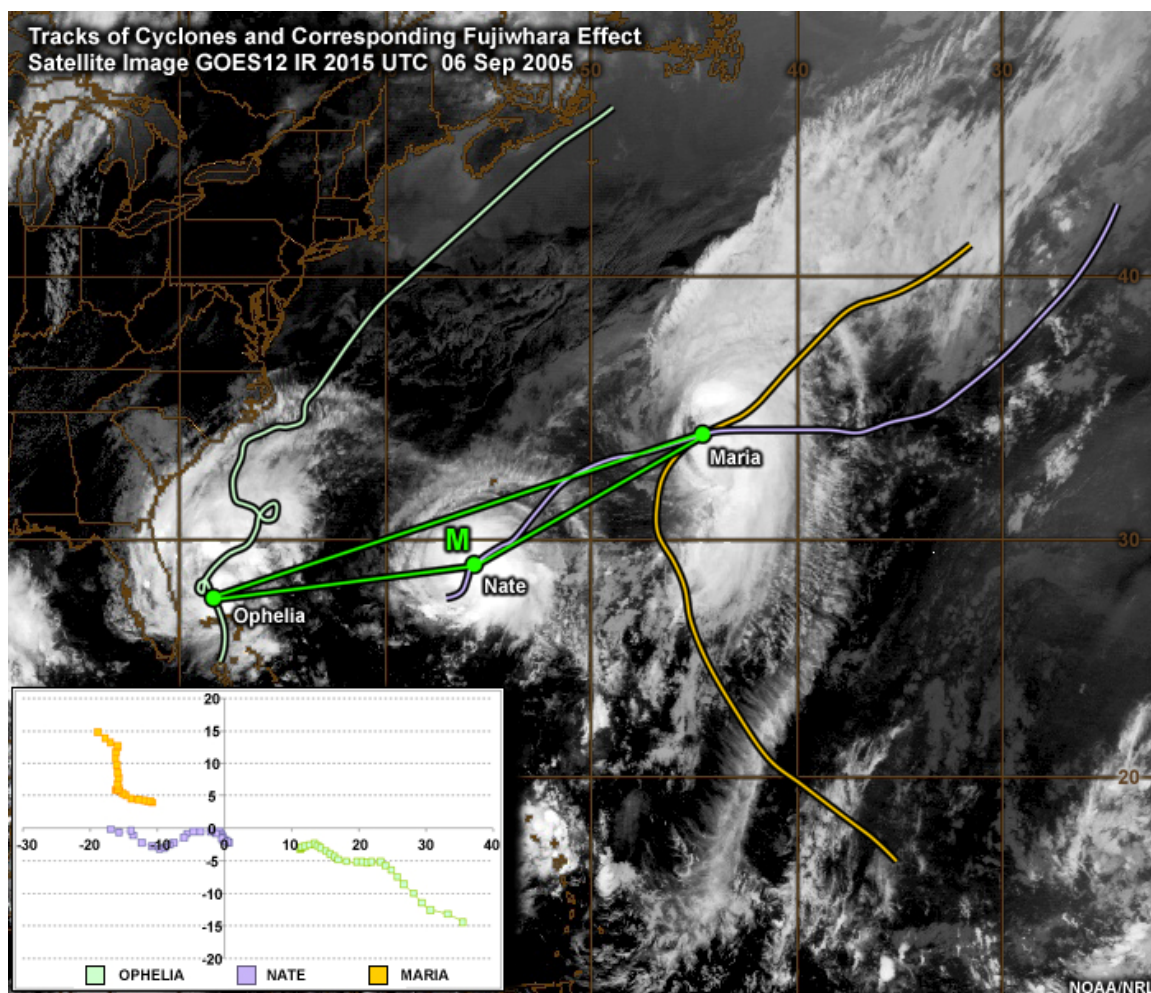


Fig. 10.75. GOES infrared satellite image of four Atlantic tropical cyclones (Maria, Nate, and Ophelia) from 2015 UTC on 6 Sep 2005 and (inset) their movement relative to a centroid point (M). This situation would result in complex Fujiwhara effects of each storm on the motion of the others (inset graph).

A comprehensive analysis of ten cases of tropical cyclone interaction provided a framework for discussion of binary storm interactions.<sup>219</sup> By considering the centroid-relative track of the vortex pair, the storm-storm interactions can be separated into four components: (i) Approach and Capture, (ii) Mutual Orbit, (iii) Merger, and (iv) Escape (Fig. 10.76).

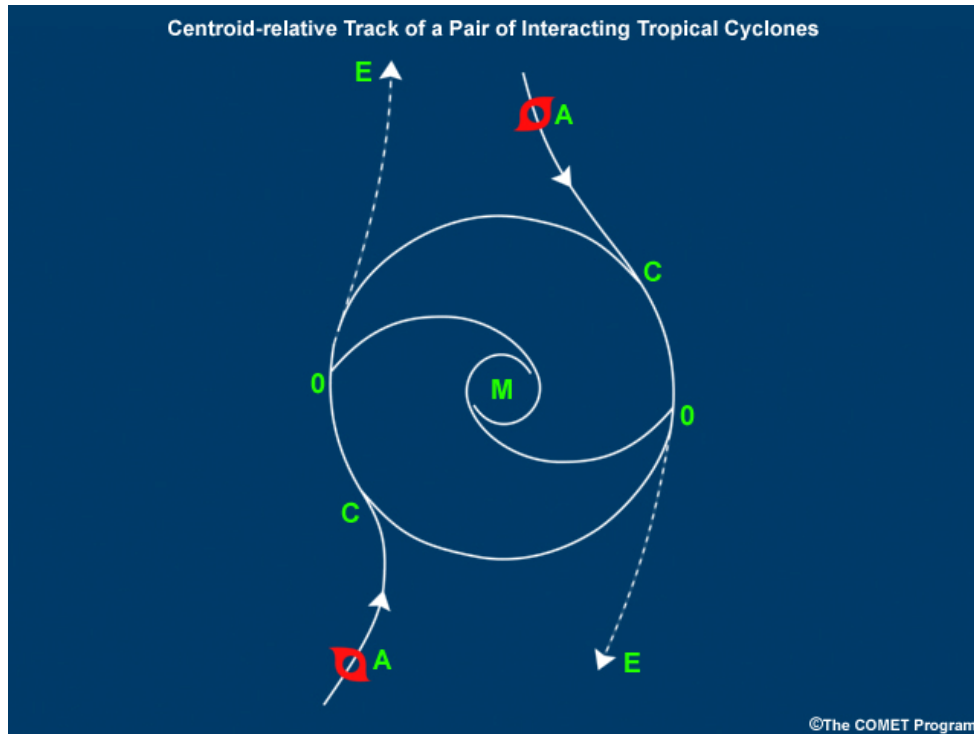


Fig. 10.76. Centroid-relative track of a pair of interacting tropical cyclones illustrating the four stages of storm-storm interactions: (i) Approach (A) and Capture (C), (ii) Mutual Orbit (O), and either (iii) Merger (M) or (iv) Escape (E).



#### [Merger of two tropical cyclones, Zeb and Alex \(1998\)](#)

Pairs of interacting tropical cyclones respond to the environmental vorticity gradient provided by the presence of the second vortex<sup>220</sup> in a similar way to any other environment. Hence, each tropical cyclone in the pair will be both advected by its partner and will propagate on the environmental vorticity gradient resulting from both  $\beta$  and the partner vortex.<sup>221,222,223,224</sup> Attribution of this propagation to one of the two components of the environmental vorticity gradient ( $\beta$  or the second vortex) is not straightforward. A number of studies have shown that Fujiwhara interactions are well simulated by barotropic physics alone.

Consideration of a cyclonic vortex pair on a  $\beta$ -plane and in a range of progressively more complex environmental flows provides a more realistic perspective on storm motion during Fujiwhara interactions. Environmental advection of an identical vortex pair in a zonally sheared environment is modulated by (i) the sense and magnitude of the

environmental shear and vorticity gradient; (ii) the earth vorticity gradient; and (iii) the development of a link between the two vortices that leads them to move as one system for three or more days of their evolution. The link established between the two vortices is the consequence of the distortion of each vortex by the other.<sup>224</sup> All of these effects contribute to the ultimate motion patterns observed for the dual-vortex system however the relative contributions of each of factors (i)-(iii) differ over time. The sign of the environmental shear has a substantial impact upon the centroid propagation<sup>m</sup> of the vortices. Environments with cyclonic horizontal shear produce an enhancement of the  $\beta$ -drift, and an increased westward motion of the centroid. Anticyclonic horizontal shear in the environment opposes  $\beta$ , resulting in decreased westward motion and increased poleward motion of the storm. It is important to note that the impact of the environmental shear here is not direct, but results from variations in the associated vertical component of relative vorticity due to the environmental wind structure.<sup>224</sup>

#### 10.6.4 Structure and Intensity Impacts on Motion

In our discussion of tropical cyclone structure, we explored a number of measures describing the radial structure of the rotational wind field (Fig. 10.9).<sup>27</sup> These are the (1) *intensity* (peak surface winds), (2) *strength* (the average winds in an annulus outside the eyewall), and (3) *size*.

While intensity and size are relatively straightforward to determine, strength is more ambiguous. Strength is designed to capture the variation of the rotational wind with radius: the *shape* of the profile. Intuitively, you know that a storm whose intense winds extend out a very large distance will be more damaging than a storm in which these winds drop off rapidly. These intense winds correspond to larger inertial stability (Section 10.2.2.2), and hence to a tropical cyclone that is more resilient to environmental influences.<sup>120</sup> In extreme cases such as Supertyphoon Tip in 1979 (Box 10-5),<sup>100</sup> this can mean that the storm generates its own steering flow and its motion is not well correlated to flows generated by surrounding weather systems. However, these situations are extremely rare. More commonly, the increase in inertial stability that follows from increased intensity minimizes the impact of strong vertical or horizontal wind shear on the storm.

In studies of tropical cyclone motion<sup>207,225</sup> the relationship between the tropical cyclone motion and strength was generally closest when strength was evaluated between 3-5 degrees latitude radius (so approximately 300-500 km). Indeed, tropical cyclone propagation speed increases and its direction<sup>211</sup> has a more westward component for increasing storm strength. The size of a tropical cyclone also relates to its propagation speed, but not its *direction* of propagation: larger tropical cyclones have a larger propagation speed than smaller storms.<sup>86,87,211,226</sup>

---

<sup>m</sup> The centroid propagation is the difference between the environmental advection and the mean motion of the vortex pair. The centroid of a vortex pair with equal size and intensity is the mid-point between their centers.

So more intense storms must also move more quickly – right? NO! Storm intensity is only weakly, and indirectly, related to its motion. One study of tropical cyclones in the Australian region has demonstrated that tropical cyclone intensity is linked to the layer over which the environmental winds advect the storm,<sup>208</sup> but no significant link has been drawn between propagation and tropical cyclone intensity.<sup>211</sup>

In summary, a tropical cyclone moves through a combination of advection by the average tropospheric winds of its environment and propagation due to the vorticity gradients of the Earth and its environment (including other tropical cyclones in Fujiwhara interactions), as well as variations in motion due to horizontal and vertical wind shear. The structure of the tropical cyclone (its size and inertial stability) will impact how the storm responds to all of these contributors to its motion: larger storms will have a larger propagation component of their motion; stronger storms will have a larger deviation between the direction of the advection and their motion; and the choice of the depth of the troposphere needed to calculate the environmental advection of the storm is weakly related to the storm intensity.



## 10.7 Extratropical Transition

Poleward movement of a tropical cyclone is generally expected to lead to the decay of the system as it encounters the hostile, strongly sheared environment and cooler waters (or land) of the midlatitudes. *The exceptions to this rule are extratropically transitioning tropical cyclones.* The process by which an initially tropical cyclone is transformed into an extratropical cyclone is known as *Extratropical Transition (ET* – not to be confused with evapotranspiration!). Tropical cyclones typically weaken as they recurve,<sup>118,119</sup> but as they move into the extratropics these systems can reintensify into intense midlatitude storms with extensive regions of intense rain and larger gale (and even hurricane) force wind areas than their tropical antecedents.<sup>227</sup> The remnant tropical cyclone can also provide a region of enhanced thermal contrast for the later development of an intense midlatitude storm. The rapid forward speed, the large size of their gale force wind area and intense rainfall region, and extraordinarily large ocean waves of an ET can persist long after its “tropical storm” status has been discontinued.<sup>228</sup>

Extratropical cyclones with tropical roots have been tracked poleward of 50°N in the North Atlantic and western North Pacific, with landfalls of initially tropical storms being recorded in western Europe and Alaska (e.g., Fig. 10.1 and Fig. 10.77)! ET systems carry their past with them (evident in their  $\theta_e$  and PV signatures).<sup>229</sup> This transport of moist warm tropical air to high latitudes provides an atypically large energy reservoir for a warm season midlatitude cyclone.

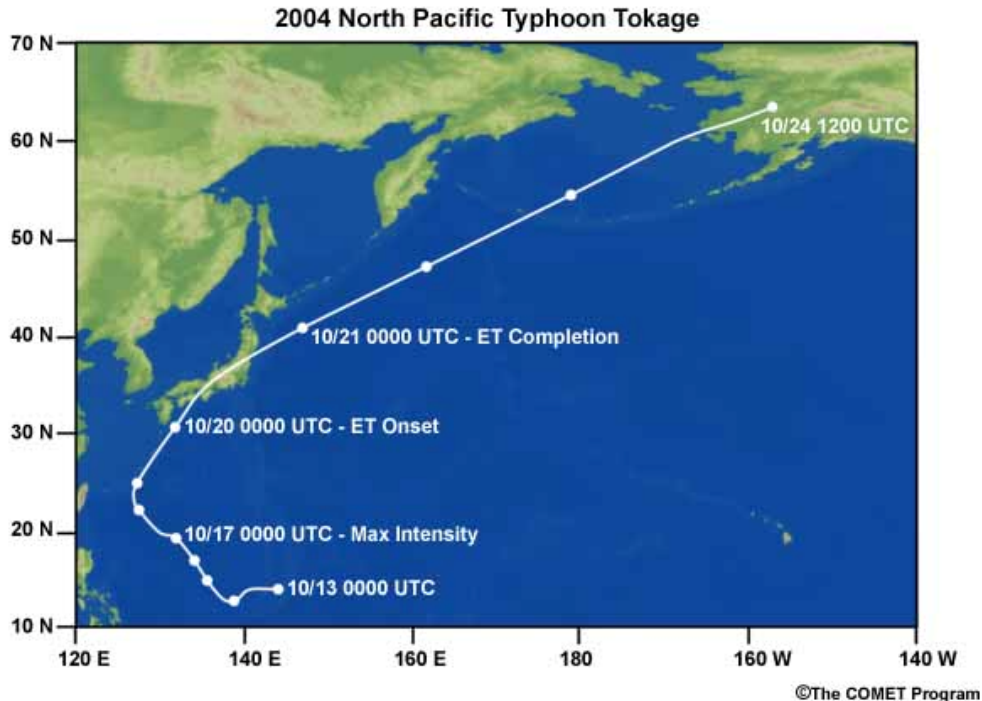


Fig. 10.77. Extended best track of North Pacific Typhoon Tokage (2004).

The role of ET in the tropical cyclone climatology has been documented in all tropical cyclone basins. ET studies up until 1960 were limited to only three sets of case studies,<sup>230,231,232,233</sup> with increasing interest from the 1950s,<sup>3</sup> possibly as a result of Hurricane Hazel's impact on the northeast US and Canada and a spate of typhoon landfalls in Japan. An explosion of research in the 1990s<sup>155</sup> has expanded this field of research across all affected basins.

One important advance in our understanding of ET in recent years has been the recognition that the impacts of ET are not just confined to the storm itself. The energy reservoir provided by the import of moist warm tropical air to high latitudes can actually amplify the midlatitude planetary wave pattern.<sup>234</sup> This amplification can cause intense midlatitude cyclogenesis far from the location of the ET event. It can also feed back onto the longwave pattern, modifying interactions between other tropical cyclones and troughs. There is no systematic impact of this change in the longwave pattern on ET. It does not always increase, or always decrease, the incidence of ET.<sup>235,236</sup>

The likelihood of ET for an individual storm depends on (i) the structure and intensity of the tropical cyclone itself, (ii) its thermodynamic environment (convective forcing), (iii) the structure of the midlatitude trough (especially the spatial extent and strength of its associated vertical wind shear) interacting with the tropical cyclone, and (iv) the relative location of the tropical cyclone in the trough.<sup>236,237</sup>

### 10.7.1 Climatology of ET around the World

While a substantial fraction of the Pacific and Atlantic tropical cyclones undergo ET, it is a relatively rare phenomenon in the Indian Ocean, involving only about 10% of tropical storms in the South Indian Ocean.<sup>238</sup> The relative frequency of ET (percentage of named storms per year) is around 46% in the North Atlantic,<sup>229</sup> 27% in the western North Pacific<sup>22</sup> and 33% in the western South Pacific.<sup>239</sup> Since the annual tropical storm frequency is much higher in the western North Pacific than the North Atlantic, the North Pacific is the most frequent location for ET.<sup>240</sup> In each of these basins, the likelihood of ET increases through the storm season, with the peak in ET frequency lagging the peak month for tropical storm activity. For example, in the North Atlantic, the climatological peak of ET incidence is in October, while September is the peak month for tropical cyclone formation (Fig. 10.78). Fifty percent of October storms undergo ET; this ratio is 48% in September and below 40% in all other months. Transition occurs at lower latitudes at the beginning and end of the season, and at higher latitudes during the tropical season peak in August and September (Fig. 10.79).

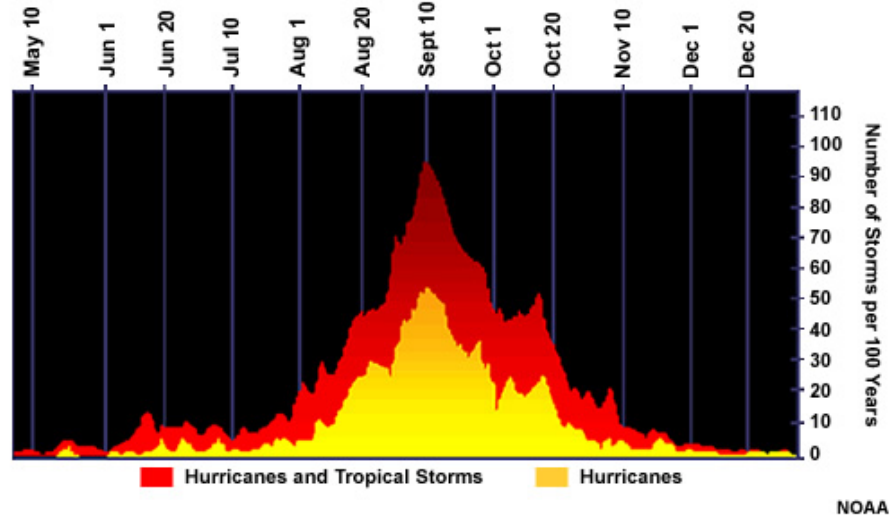


Fig. 10.78. Seasonal cycle of North Atlantic tropical cyclones illustrating the September peak in both tropical storms and hurricanes.

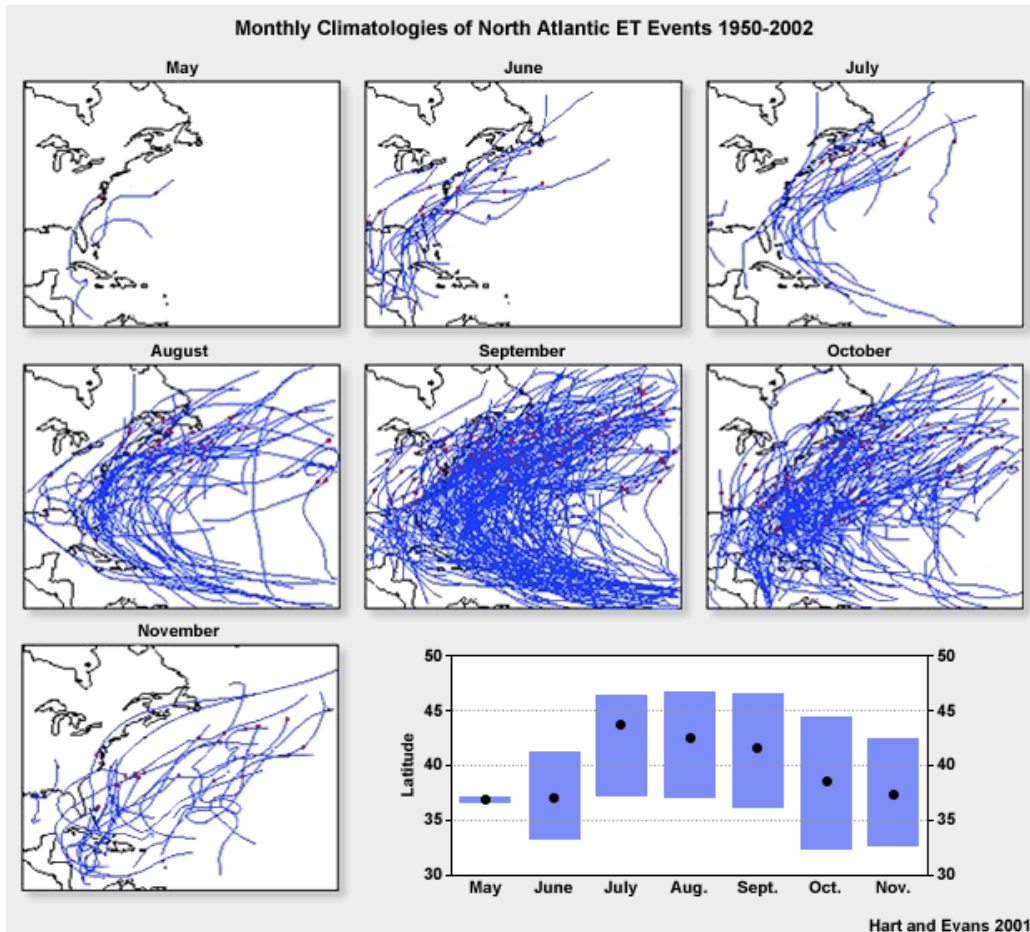


Fig. 10.79. Monthly climatologies of North Atlantic ET events, 1950-2002. Red dots show the transition point as defined by NHC. The latitude range of ET in each month is shown in the box and whisker plot: solid black circles denote the mean transition location for each month. Reproduced from Hart and Evans (2001).<sup>229</sup>

Almost 50% of tropical cyclones making landfall in the North Atlantic undergo ET, with the northeast United States/Canadian Maritimes (1-2 storms per year) and western Europe (once every 1-2 years) being most vulnerable (Fig. 10.80). Ten typhoon landfalls in Japan and five in China during 2004 recently emphasized the susceptibility of higher latitude Asian nations to ET (Box 10-9).

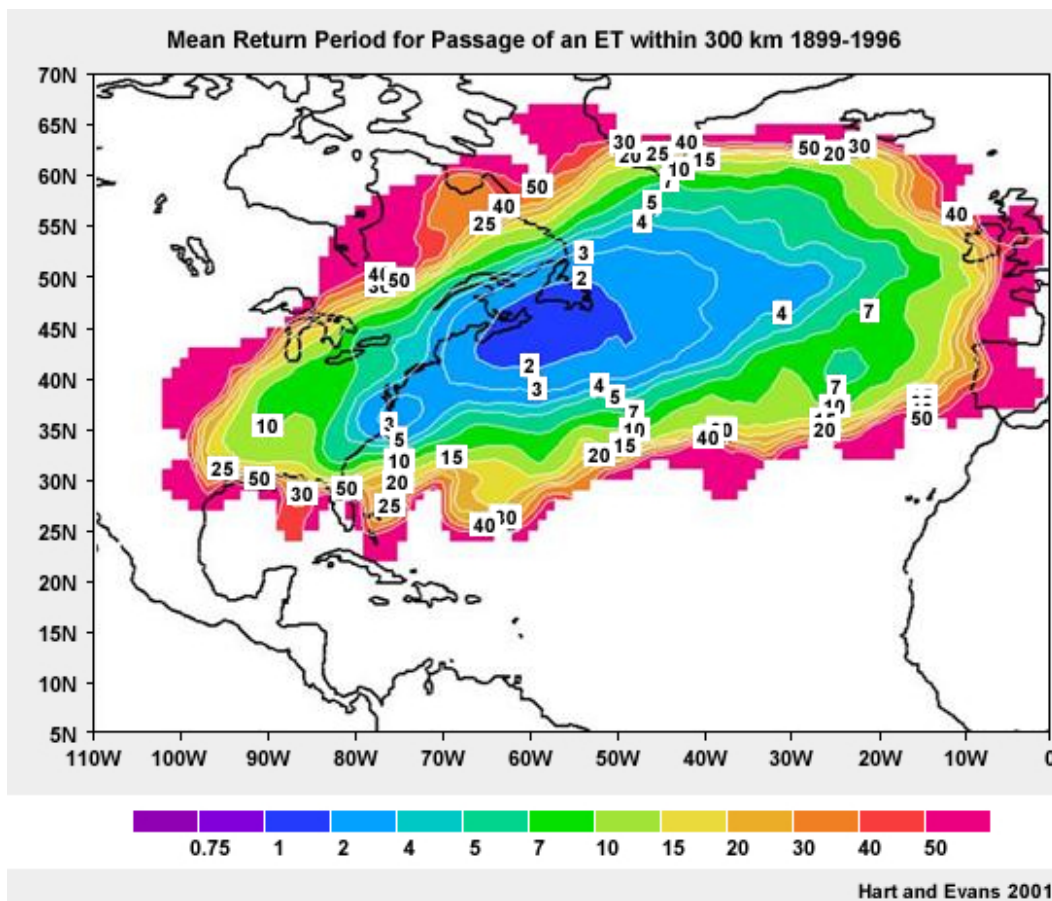


Fig. 10.80. Mean return period (years) for passage of an ET within 300 km. NHC best tracks from 1899-1996 were used to derive these statistics (Hart and Evans 2001).<sup>228</sup>

In the North Atlantic, the observed seasonal peak of ET occurs in September,<sup>229</sup> as could be inferred from the close proximity of the two development zones in the coastal US region, a common location for recurvature in this basin. The patterns for October support its status as another active ET month. These development zones have shifted further south in November, so while they remain in close proximity, the few tropical storms occurring in November are typically too weak to survive recurvature.<sup>229</sup> For the western North Pacific, the ET maximum is typically September<sup>227,240</sup> consistent with the diagnostics in Fig. 10.81. This agreement between the seasonality of ET in these two basins with the diagnostics presented in Fig. 10.81, give us confidence in that the same diagnostics will be useful to infer the expected annual cycle of ET for the remaining basins.

One third of tropical cyclones in the western South Pacific are observed to undergo ET, with March being the most active ET month.<sup>239</sup> This is generally borne out by the development diagnostics, although based on these alone, an April peak might be expected. This highlights the importance of considering the environment *in the region and time of tropical storm activity* when deducing likely ET. Generally, April is only an active month during ENSO years.

Should ET occur in the North Indian Ocean, it should be expected at the extreme ends of the summer monsoon season, as the development zones are only in proximity with each other *and over water* in these transition months. There are not strong indications for ET in the western South Indian Ocean off Africa. Finally, the most likely months for ET off the Western Australian coast (the eastern South Indian Ocean) are November, April and May, the transition months for the monsoon season there.<sup>238</sup>

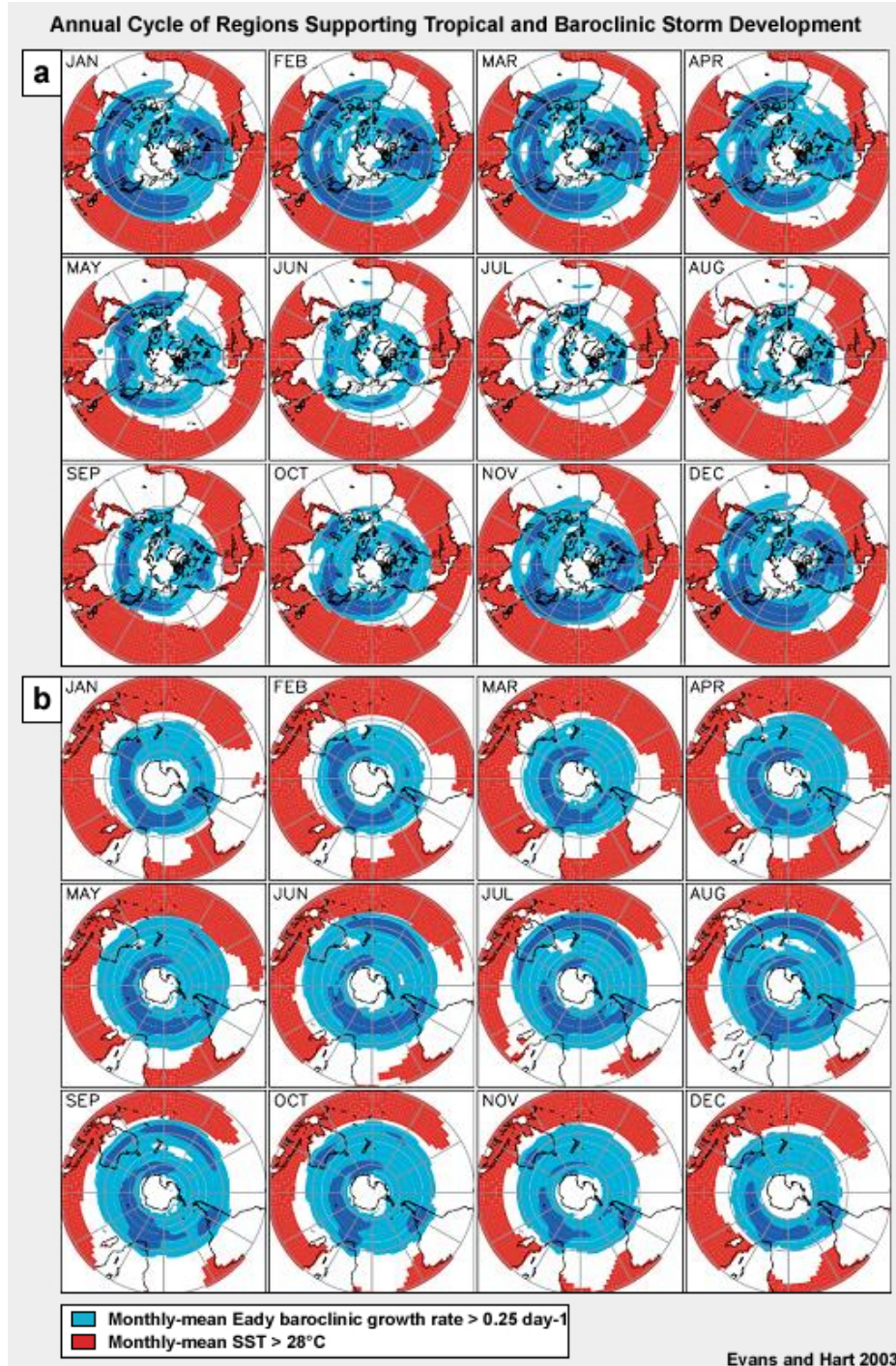


Fig. 10.81. Annual cycle of the geographic distribution of regions supporting tropical and baroclinic storm development in the a) NH and b) SH. Light (medium) blue shading indicates regions in which the monthly-mean Eady baroclinic growth rate of the most unstable mode is greater than  $0.25 \text{ day}^{-1}$  ( $0.5 \text{ day}^{-1}$ ); regions of monthly-mean SST  $> 28^\circ\text{C}$  are shaded in red. These diagnostics are calculated from  $2.5^\circ \times 2.5^\circ$  fields (1982–2001 NCEP/NCAR monthly mean reanalyses), so extreme values are likely underestimated. Adapted from Evans and Hart (2003).<sup>32</sup>

## 10.7.2 Definitions of ET Onset and Completion

Tropical cyclones are compact weather systems, with relatively symmetric cloud structures and their most intense winds close to the storm center near the surface. Extratropically transitioning tropical cyclones evolve from this structure to become fast moving ( $>10 \text{ m s}^{-1}$ ) systems, often resulting in a greatly expanded area of gale force winds. In the process of ET, the peak low-level winds are often much reduced (from the peak tropical intensity) and the maximum winds in the storm now occur aloft. Relative to the storm track, the highly asymmetric storm structure results in strong winds equatorward, and a large expanse of heavy precipitation to the poleward side.<sup>227</sup> Thus, to describe the onset and completion of ET comprehensively, measures of both storm symmetry and wind structure must be included – either explicitly or implicitly.

A storm that is commencing the process of ET becomes increasingly asymmetric, due to low-level frontogenesis typically resulting from interaction with a midlatitude trough. This increase in asymmetry is a basic indicator of the onset of transition, but does not guarantee that the system will complete transition<sup>18,23,25</sup> – many tropical cyclones commence extratropical transition, but decay before completing their evolution into a fully cold-core cyclone.

Storms that remain coherent and become increasingly asymmetric may undergo ET. Completion of the ET process signifies that the tropical system has developed midlatitude storm characteristics, in particular the development of a cold-core thermal wind structure (geostrophic wind speed increasing with height).<sup>13,18</sup> Klein et al. (2000)<sup>226</sup> invoke another requirement: that the storm reintensify (in terms of pressure) after completing ET. This last constraint is not applied uniformly. For example, a storm that evolves as described above will be reclassified as “extratropical” by the US National Hurricane Center with no requirement for reintensification. In the context of operational forecasting, it is important to recognize the evolution in the storm structure separately from the evolving intensity because this structure governs the distribution of the significant weather associated with the storm.

A number of new diagnostics have been proposed to characterize ET. Analysis of western North Pacific cases<sup>25,26</sup> provides guidance on characteristic satellite signatures and environments typical of ET cases.<sup>23,24</sup> The Cyclone Phase Space (CPS) was demonstrated to be a useful diagnostic of ET for North Atlantic ET cases.<sup>32</sup> Composite synoptic environments for ET based on the storm’s progression through the CPS<sup>20,22</sup> agree well with those presented here. The combination of these approaches (satellite and CPS) for diagnosing ET is becoming increasingly widely used in operational centers around the globe. Finally, ET is often poorly forecast by numerical forecast models, providing difficult forecast challenges to the responsible forecast centers.<sup>34</sup> The CPS has been proposed as a metric for evaluating storm structure forecasts.<sup>21</sup>



Hurricanes Canadian Style <http://www.meted.ucar.edu/norlat/ett/index.htm>  
Diagnosing and Forecasting ET: Hurricane Michael (2000),  
<http://www.meted.ucar.edu/norlat/ett/michael/>

### 10.7.3 Mechanisms that Lead to Extratropical Transition

The intensity of a tropical cyclone as it begins ET plays a large role in determining whether it will survive transition and ultimately reintensify, or whether it will decay.<sup>229</sup> Another strong indicator of the likelihood that a storm will survive ET is its genesis location (Fig. 10.82). Perhaps surprisingly, tropical storms that form at higher latitudes are less likely to undergo ET than storms that form in the deep tropics. This relationship has been linked<sup>17</sup> to the intensity of the storms at the time of ET onset. Storms forming in the deep tropics are typically much stronger systems when they commence transition.<sup>229</sup>

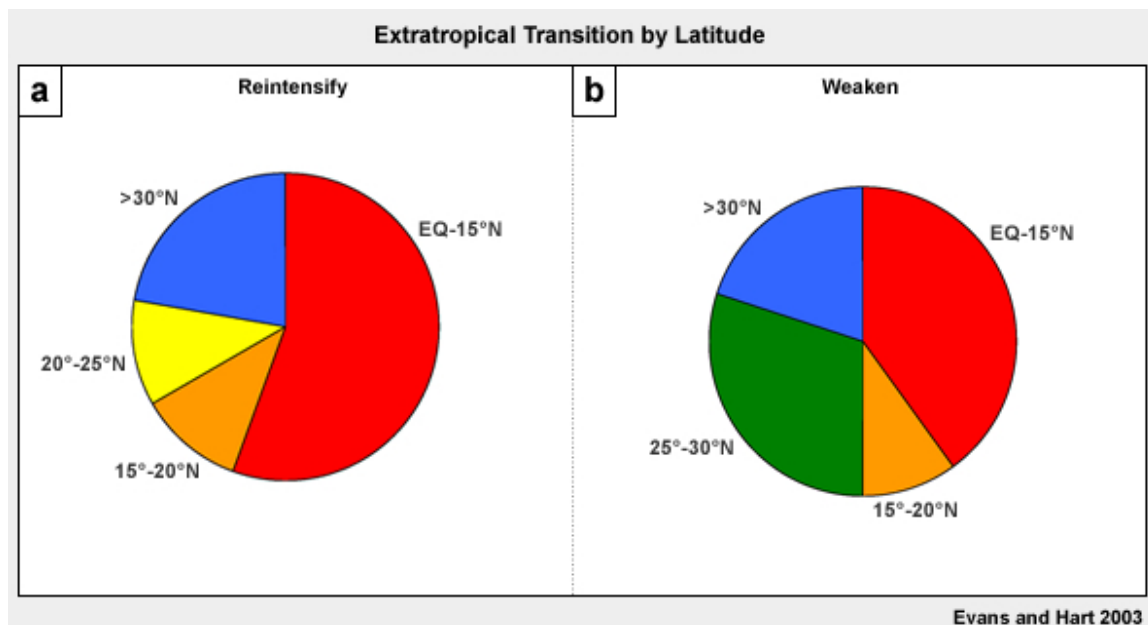


Fig. 10.82. Genesis latitudes for storms that a) reintensify and b) weaken after ET. Colors correspond to these latitude bands: EQ-15°N (red), 15°-20°N (orange), 20°-25°N (yellow), 25°-30°N (green) and >30°N (blue). Adapted from Evans and Hart (2003).

Environmental configurations favorable for ET have been identified from a number of western North Pacific case studies.<sup>227,235,241</sup> These include the “northwest” and “northeast” patterns, where the direction refers to the location of the midlatitude feature that is significant to the ultimate evolution of the transitioning storm. In both cases the recurving tropical cyclone moves poleward ahead of a midlatitude trough, the primary midlatitude circulation is either that trough (northwest) or a quasi-stationary cyclone to the northeast of the transitioning storm. Northwest pattern ET typically results in the development of an intense extratropical cyclone as the tropical cyclone couples with the midlatitude baroclinic zone. Barotropic and baroclinic kinetic energy production through direct solenoidal circulations (which result from the coupling of the tropical cyclone and midlatitude trough), as well as enhanced low-level radial eddy heat fluxes, contribute to the extratropical cyclone development. Tropical cyclones undergoing northeast pattern ET move rapidly eastward in the strong zonal flow between two synoptic features to their east: the quasi-stationary cyclone (northeast) and the subtropical ridge (southeast). These systems do not intensify significantly post-ET, possibly since the strong zonal flow



inhibits direct interaction between the decaying tropical cyclone and the midlatitude baroclinic zone. Eddy heat fluxes do not increase and the storm's motion towards the quasi-stationary extratropical cyclone to its northeast results in barotropic destruction of kinetic energy, further inhibiting reintensification. Composite<sup>237,242,243</sup> and case study analyses<sup>244,245,246,247</sup> of ET in the North Atlantic and western North Pacific exhibit similar synoptic configurations.

These observational studies of ET provide strong evidence of the importance of the phasing between the midlatitude weather systems and the initially tropical cyclone in determining the outcome of transition.

The climatological analysis depicted in Fig. 10.81 provides a global map of the regions most susceptible to ET. The diagnostics chosen here highlight the environments identified in the case studies<sup>227,235,241</sup> and confirmed with synoptic composites.<sup>237,242</sup> Based on this analysis (Fig. 10.81), the most favorable situation for a storm to survive through ET is one in which the storm has either strong “tropical” support for development or strong baroclinic development support<sup>229</sup> — or sometimes both. Promising regions for tropical development are depicted here as being equatorward of the 28°C SST isotherm—and also confirmed using *Potential Intensity* (PI)<sup>18</sup> diagnostics (not shown). The diagnostic used to infer regions favorable for baroclinic development is the monthly-mean Eady baroclinic growth rate of the most unstable mode. The intersection of the monthly tropical cyclone tracks with these diagnostics gives an indication of the likelihood that ET will occur. If the mean storm tracks are almost always in one of the development zones, ET is favored in that month. On the other hand, if the mean storm tracks indicate that the storm will traverse a region not indicated as favorable for development (the white areas in Fig. 10.81) for any substantial time period, ET is less likely. Finally, only intense tropical cyclones typically complete ET<sup>229,242</sup> since they must survive the sheared midlatitude environment until they have completed transition.

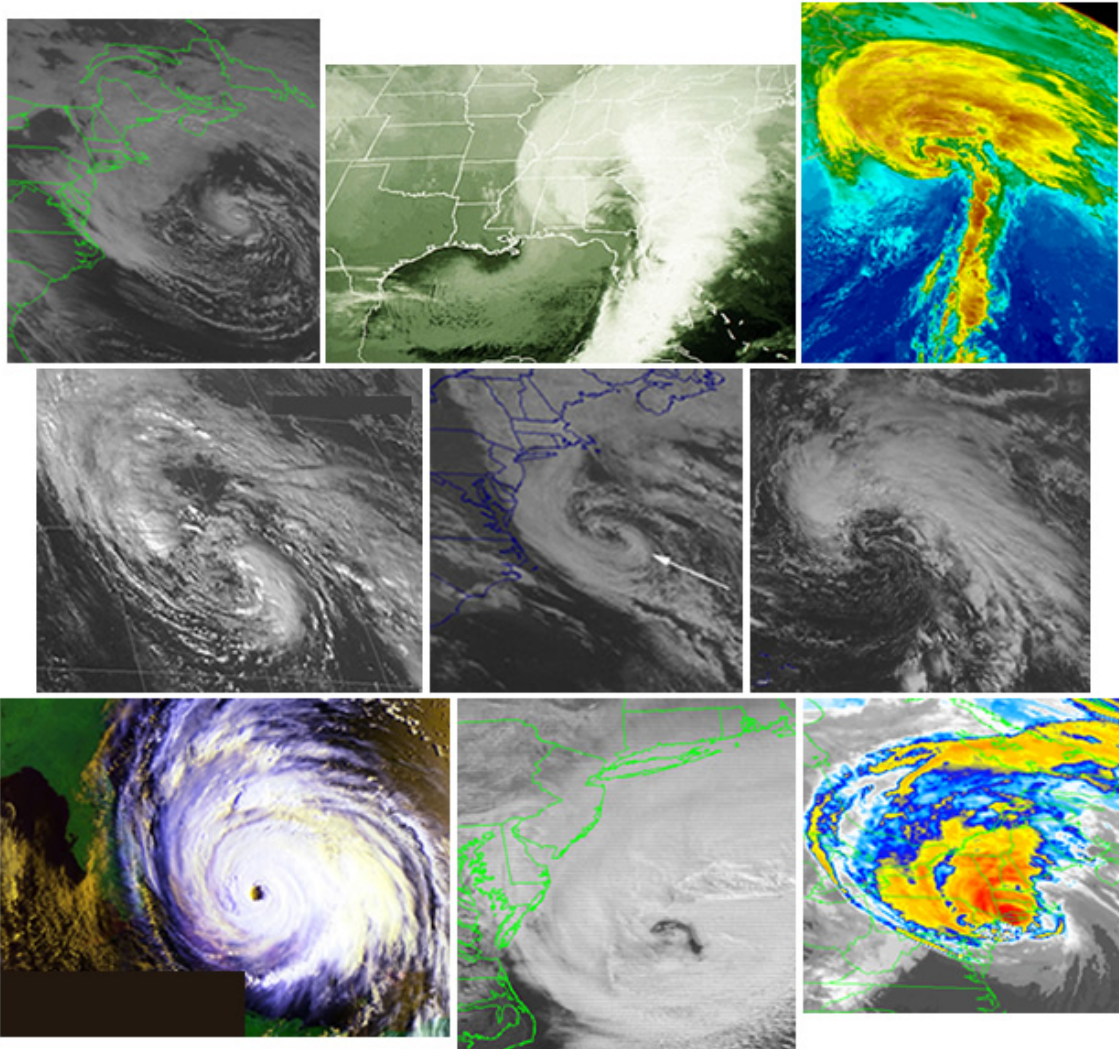
All of these analyses of ET support our earlier statement that the likelihood of ET for an individual storm depends on (i) the structure and intensity of the tropical cyclone, (ii) its thermodynamic environment (represented here by SST), (iii) the structure of the interacting midlatitude trough (represented here by the Eady growth rate), and (iv) the relative location of the tropical cyclone to this trough<sup>234,236,237,242,248</sup> (evident through the seasonality of the ET latitude; Fig. 10.79).<sup>229</sup>




Identify the five ET cases from the sample of storms presented. Beware! These cases are not restricted to storms that began as tropical cyclones.

**Hint:** Remember that the eyewall will be eroded, the rain shield in a storm undergoing ET will expand and shift to the left of track, and a dry slot will wrap cyclonically around the storm from the poleward side.

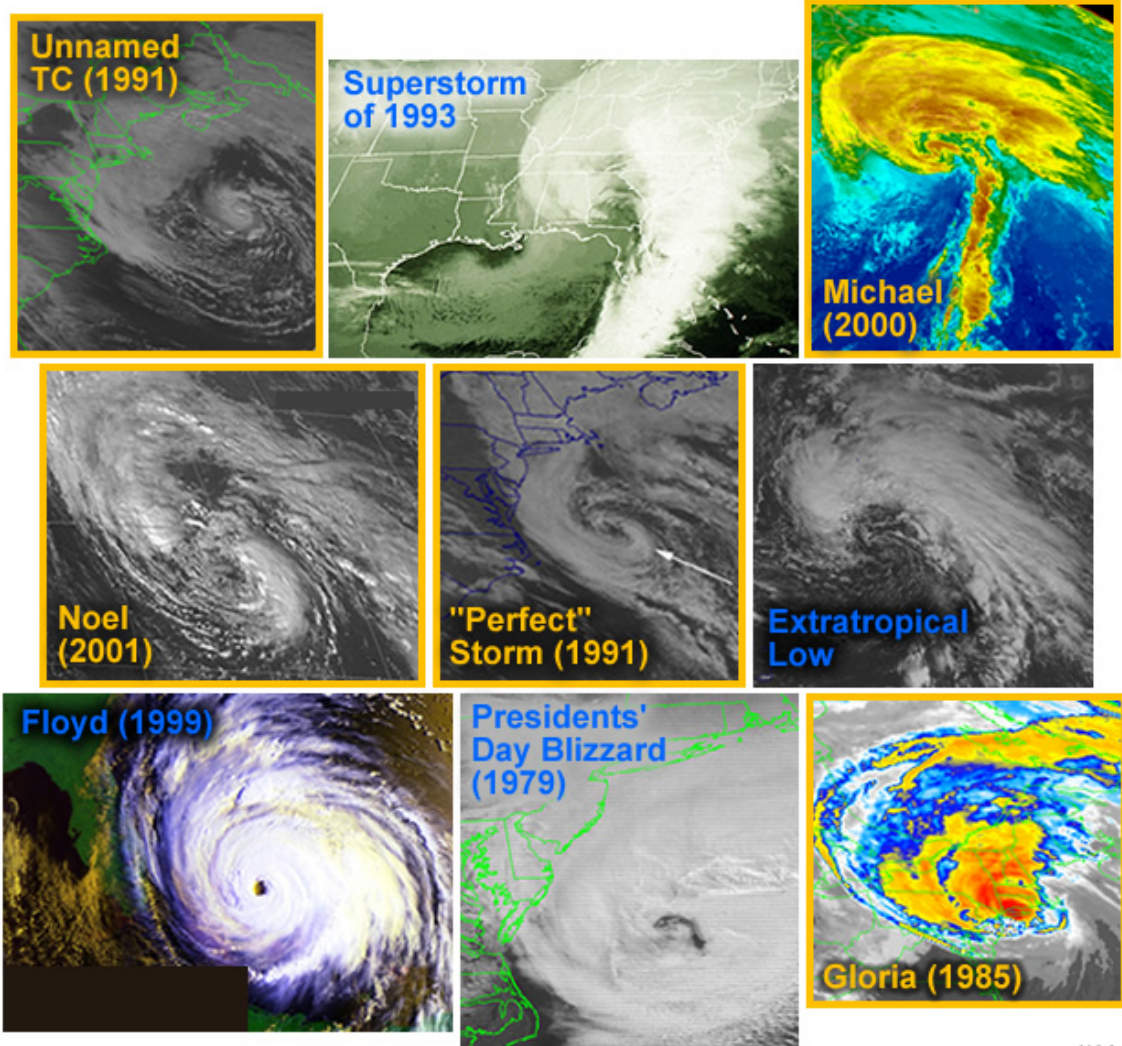
**Identify the five tropical cyclones that have undergone ET**



NOAA

 The ET cases are identified in the following figure: ET cases are named and bordered in orange.

**Tropical cyclones that have undergone Extratropical Transition are outlined in gold**



NOAA

## 10.8 Societal and Environmental Impacts

Tropical cyclones are the most hazardous tropical weather systems. Their hazards include: strong winds, storm surge, wind-driven waves, heavy rainfall and flooding, tornadoes, and lightning.<sup>249,250,251</sup> The impact of tropical cyclones can be categorized as direct and indirect or secondary impact.<sup>252</sup> Direct impacts include coastal erosion by storm surge and loss of infrastructure from wind stress. Examples of indirect impacts are diseases associated with water contamination, oil price increases when drilling platforms and refineries are damaged or closed, and fires started by live, downed power lines. Economic loss from damage to crops and fisheries where livelihoods are dependent on agriculture, post disaster stress<sup>253</sup>, and insurance rate increases are long term indirect effects. TCs remain a serious threat to society, especially as coastal population growth accelerates—a continuing trend in many locations around the world.<sup>248</sup>

### 10.8.1 Storm Surge and Wind-driven Waves

*“The available documentation indicates that whenever there was a large loss of life from tropical cyclones, the predominant cause of death was drowning, not wind or windblown objects or structural failures.” Rappaport and Fernandez-Partagas (1995)*

Globally, storm surge is the most deadly direct TC hazard.<sup>250,254</sup> A storm surge is a large dome of water, 50 to 100 miles wide, that sweeps across the coastline near where a hurricane makes landfall. It can be more than 15 feet deep at its peak (Fig. 10.83). The highest recorded death toll from a tropical cyclone occurred in November 1970; more than 300,000 persons were killed by coastal flooding when a cyclone made landfall in Bangladesh (Box 10-11).

The storm surge is created by wind-driven waves with a very small component due to the low-pressure at the center of the cyclone. The surge is strongest where the winds are enhanced by the motion of the cyclone, therefore, the right forward quadrant of cyclones in the NH are the most dangerous for storm surge; for the SH the left forward quadrant is the most dangerous. While the waves may be relatively low in the open ocean, they gain height as they approach the coast (Fig. 10.83). The surge can move coastal structures and soil several miles inland. Geological studies have revealed layers of sediment, in an Alabama lakebed, that are believed to have been brought inland by storm surges as many as 3000 years ago.<sup>255</sup> Storm surges are aggravated by high tide. Coastal flood models, such as the SLOSH model, are used to predict the storm surge.



Fig. 10.83. Conceptual model of storm surge and photograph of boat carried inland by storm surge.



[Animated damage due to storm surge and wind](#)

### Box 10-11 The Deadliest Storms on Record: The Bangladesh Cyclones of 1970 and 1991

#### Disaster in 1970, The Bhola Cyclone

Imagine waking up to hear that over 300,000 – and possibly as many as 500,000 – of your countrymen had died. This really happened, and it was not hundreds of years ago. **This unfathomable disaster happened on 12 November 1970** when the storm now known as the Bhola Cyclone made landfall in Bangladesh!

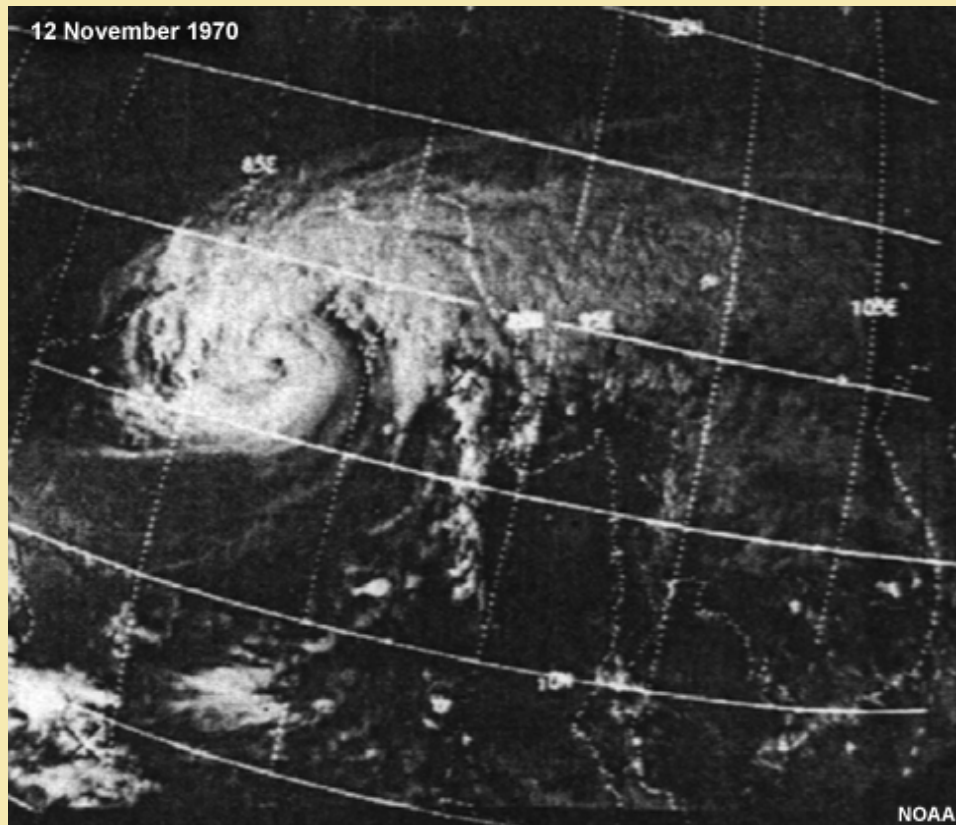


Fig. 10B11.1. The cyclone formed over the central Bay of Bengal on 8 Nov 1970. As it moved north, it intensified, reaching its peak 10-minute sustained wind speed of  $50 \text{ m s}^{-1}$  ( $185 \text{ km h}^{-1}$ ; Category 3 on the Saffir-Simpson scale) with minimum central pressure of 966 hPa on 12 Nov 1970.

That night of 12 November 1970 the storm made landfall on the coast of East Pakistan (now Bangladesh). Many of the offshore islands were devastated by storm surge. The city of Tazumuddin (in the Bhola district of Bangladesh) was the most severely affected, with over 45% of the population of 167,000 killed by the storm. Topographic enhancement of rainfall by the mountains and storm surge make a devastating and deadly combination in the low-lying areas in the northern reaches of the Bay of Bengal.

## Box 10-11 continues

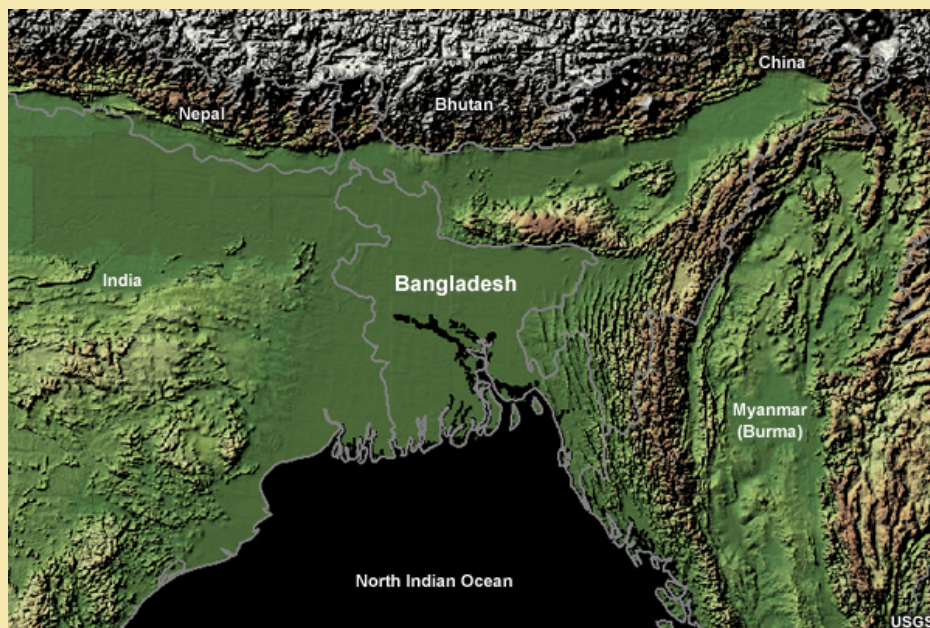


Fig. 10B11.2. Physical geography of the North Indian Ocean (upper-wide view, lower-zoom view) showing the location of Bangladesh in a delta region surrounded by high terrain.

## Box 10-11 continues

Disaster in 1991, the Chittagong Cyclone

Fig. 10B11.3. Tropical Cyclone 02B at ~ 1900 UTC, 29 April 1991.

Tropical Cyclone 02B made landfall in Chittagong, Bangladesh on 29 April 1991 at about 1900 UTC. The official death toll from this storm was 138,000 people. Estimated damage was in excess of US \$1.5 billion (in 1991 dollars). The coastal region was devastated by peak 1-minute averaged surface winds in excess of  $72 \text{ m s}^{-1}$  ( $260 \text{ km h}^{-1}$ ), 898 hPa minimum pressure (Saffir-Simpson Category 5), and a 6.1 meter storm surge. However, as the 1970 Bhola storm demonstrated, the death toll could have been much higher. Evacuations of 2-3 million coastal residents were effective in reducing the fatalities, although the storm was still the largest natural disaster globally in 1991.

The value of evacuation and shelter was demonstrated even more dramatically when powerful Category 4 Cyclone Sidr made landfall on 15 November 2007. The death toll was estimated at just over 3000 persons compared with the hundreds of thousands from the past cyclones. Although the damage was still costly and the destruction affected approximately 8.9 million people, better planning reduced fatalities by two orders of magnitude.<sup>256</sup>

Relative success in Bangladesh stands in contrast to tremendous loss of life in Burma (Myanmar) due to storm surge and flooding from Cyclone Nargis, May 2008. As of 21 July official death toll stood at 84,530; unofficial estimates were considerably higher.



UN Report on TC Nargis, July 2008

<http://www.reliefweb.int/rw/rwb.nsf/db900SID/ONIN-7GRR3J?OpenDocument&rc=3&cc=mmr>

Indian Ocean Tropical Cyclone News,

<http://www.scidev.net/en/agriculture-and-environment/tropical-cyclones-1/>



## 10.8.2 Flooding and Landslides

Tropical cyclones are among the more prolific rainfall producers and the land surface response to heavy rainfall is one of the deadliest aspects of tropical cyclones. TCs rainfall produces flash floods, river floods, urban floods, and landslides. One of the deadliest hurricanes in the past decade was Mitch (1998), which killed more than 10,000 people when a week of rain caused landslides that covered entire villages (Box 10-12).

Major flooding is not limited to hurricanes. Weak tropical storms can cause deaths and catastrophic damage. Recent examples include Tropical Storm Allison (2001) which produced more than 915 mm (36 inches) of rainfall over five days, caused 22 deaths, damage to over 48,000 homes, and exceeded \$5.15 billion dollars in total damage in Texas and neighboring states.



Fig. 10.84. Tracks of Tropical Storms Isidore and Lili (2002) (left), flooding in Maggotty, southwestern Jamaica, 30 Sep 2002 (right).

The amount, extent, and impact of TC flooding depend on the following:

- **Antecedent precipitation:** Saturated soil has greater flood potential than dry soil. An example of this is the case of Jamaica in 2002. The island received heavy rainfall as the eye of Tropical Storm Isidore passed to the south, 17-24 September. Only three days later, Tropical Storm Lili passed to the north and brought more heavy rain from 27-30 September (Fig. 10.84). From the two storms many rainfall records were broken; many places received more than 600% of their September normal rainfall. Another example is Central America, where Mitch (1998) struck near the end of the rainy season when soil was saturated.
- **Speed of movement of the cyclone:** Slower movement leads to greater flooding.
- **Orographic enhancement:** Additional lifting of moist air by high terrain produces more precipitation.
- **Intensification due to synoptic forcing:** Interaction of the cyclone with midlatitude synoptic systems can sometimes enhance the low pressure and increase precipitation. A prime example is Hurricane Agnes (1972), which interacted with a midlatitude trough and produced widespread river flooding in the northeastern US (Fig. 10.85). Property loss from the inland flooding of Agnes

was \$3.5 billion dollars compared with \$10 million of losses from its landfall in Florida.

- **Hydrology:** Narrow river basins are easier to flood than flat, broad river basins. Confluence of multiple rivers can also aggravate flooding. Bangladesh is one of the most vulnerable places for flooding because it is the confluence of major rivers and at the mouth of the Bay of Bengal.
- **Land use:** Urban landscapes are more prone to flash floods because of increased runoff and channeling which causes acceleration of surface water. Denuded hillsides are more prone to landslides; plant roots help to stabilize the soil.
- **Other geographical influences:** Flooding is also influenced by soil type. Soils with slow infiltration lead to greater runoff and flooding.

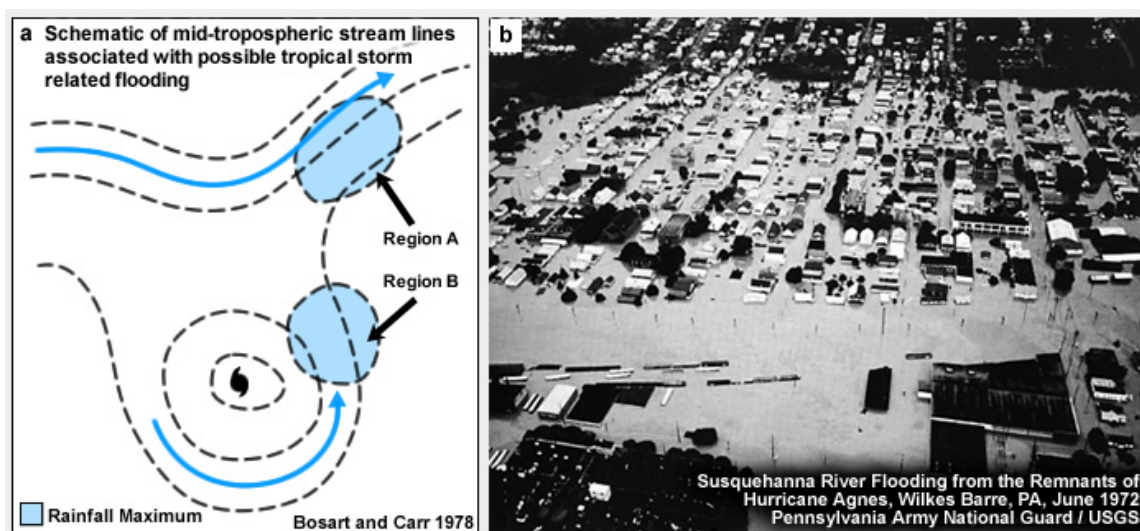


Fig. 10.85. (a) Interactions of Agnes and midlatitude trough. "A" marks the rainfall maximum along the front north of Agnes and "B" marks rainfall maximum in the right forward quadrant of Agnes. (b) Picture of flooded areas in Pennsylvania (more than 1500 km from where Agnes made landfall).

### Box 10-12 Hurricane Mitch (1988): A Devastating Storm in Central America

Over 10,000 fatalities were attributed to Hurricane Mitch, predominantly from flooding in Honduras and Nicaragua due to its slow movement and topographic enhancement of its rainfall. For a week the overall storm motion was less than  $2 \text{ m s}^{-1}$  (4 kts). Heavy rains on unstable hillsides caused large-scale mudslides, which buried or swept away entire villages. Synoptic reports had a maximum of 911mm (35.89in) for 25-31 October but data were missing from many stations. Satellite-based estimates ranged from 900-1500mm. Mitch is the strongest recorded October hurricane in the Atlantic (records began in 1886), with minimum central pressure of 905 hPa (tying Hurricane Camille of 1969) and maximum wind speed estimated at  $80 \text{ m s}^{-1}$  ( $290 \text{ km h}^{-1}$ , 155 kts, 179 mph).

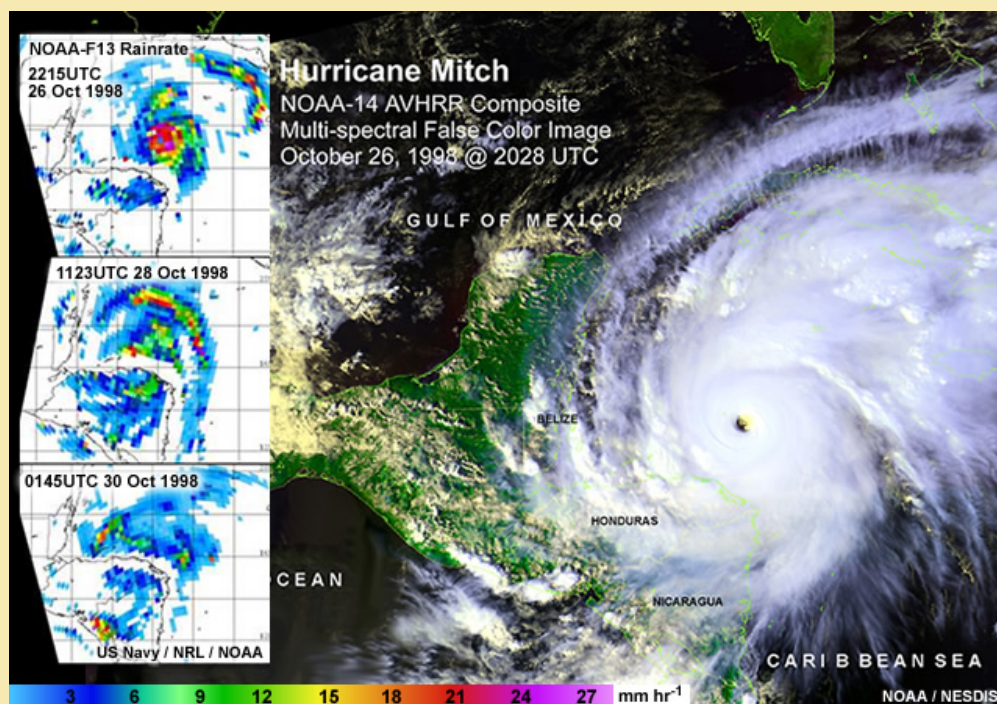


Fig. 10B12.1. Hurricane Mitch at 2028 UTC on 26 Oct 1998 at peak intensity (central pressure, 905 hPa; maximum winds,  $80 \text{ m s}^{-1}$ ) and satellite-derived rainrate, 26-30 Oct.

Very few Atlantic storms have been as devastating as Mitch. Hurricane Fifi (1974, Honduras), a 1930 hurricane (Dominican Republic) and Hurricane Flora (1963, Haiti and Cuba) are all recorded to have caused around 8,000 fatalities, as was the Galveston Hurricane of 1900. However, the largest confirmed loss of life due to a hurricane in the Western Hemisphere was due to The Great Hurricane of October 1780, which is estimated to have caused the deaths of about 22,000 people, with around 9,000 lost in Martinique, 4,000-5,000 in St. Eustatius, and over 4,300 in Barbados.<sup>253</sup> Thousands of deaths also occurred offshore.



The Deadliest Atlantic Tropical Cyclones, 1492-1996, <http://www.nhc.noaa.gov/pastdeadly4.shtml>  
 NHC report on Hurricane Mitch, <http://www.nhc.noaa.gov/1998mitch.html>  
 NCDC, storm review, each country's damage, <http://lwf.ncdc.noaa.gov/oa/reports/mitch/mitch.html>  
 Mitch Rainfall, [http://www.nrlmry.navy.mil/sat\\_training/tropical\\_cyclones/ssmi/rain/index.html](http://www.nrlmry.navy.mil/sat_training/tropical_cyclones/ssmi/rain/index.html)  
 Hurricane Mitch Satellite Time Series, <http://www.osei.noaa.gov/mitch.html>  
 Hurricane of 1780, <http://www.jamaica-gleaner.com/pages/history/story008.html>

### 10.8.3 Strong Winds and Tornadoes

The wind velocity is a defining parameter for TCs because of the deadly and damaging impact of strong winds (Fig. 10.86). The Saffir Scale was created to provide guidance on the effects of strong winds and was later expanded by Robert Simpson to include the effect of storm surge (Box 10-3).

In addition to the strong winds associated with the landfalling tropical cyclone, extremely strong winds are generated in tornadoes that sometimes also accompany a TC. As a tropical cyclone makes landfall, the surface winds decrease faster than winds above, creating vertical wind shear which allows for tornadoes to develop. Most tornadoes develop in the right-forward (left-forward) quadrant of the cyclone in the northern (southern) hemisphere. Most tornadoes are reported in the outer rainbands<sup>257</sup> where vertical wind shear is favorable. Tornadoes in the intense inner core are produced by eyewall mesovortices.<sup>258</sup> In the US, hurricanes recurving to the northeast were more likely to produce tornadoes than those moving westward, possibly due to enhancement of low-level shear from a 500 hPa trough.<sup>259</sup>



Fig. 10.86. Plank driven through a trunk by tropical cyclone winds.



[Animation of damage due to wind](#)

### 10.8.4 Lightning

Lightning in TCs is a small percentage of total global lightning. When lightning does occur in TCs, it most often happens in the convective outer rainbands.<sup>260,261,262</sup> The highest density of flashes is frequently on the eastern side of storms (e.g., Fig. 10.87).

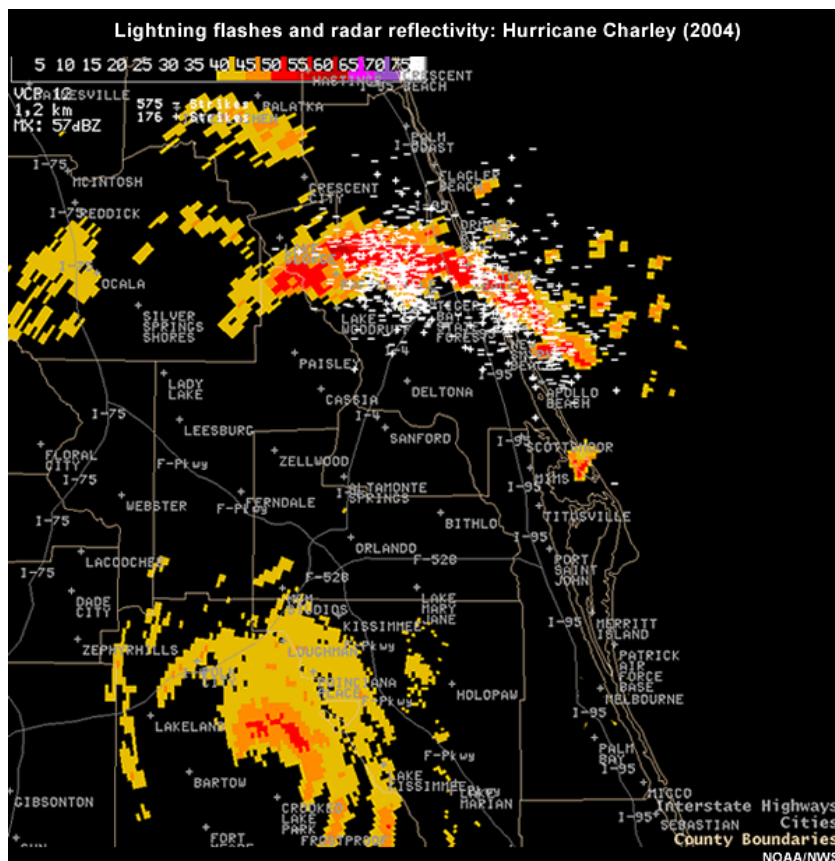


Fig. 10.87. Lightning flashes and radar reflectivity of Hurricane Charley (2004). Maximum flashes are occurring in rainbands to the northeast of the eye, which is over central Florida. (Image courtesy of NOAA/NWS Melbourne, Florida).

### 10.8.5 Impacts of Extratropical Transition

As discussed in Section 10.7, cyclones undergoing ET may initially weaken as they move into the extratropics, but these systems can reintensify into midlatitude storms that are occasionally more intense than their tropical selves (e.g. Hurricane Irene in 1999), often traveling at forward speeds of  $15\text{--}20\text{ m s}^{-1}$ . More commonly, the remnant tropical storm can provide a source of enhanced thermal contrast for the later development of an intense midlatitude storm. The rapid forward speed, the large area of gale force winds, intense asymmetric precipitation zone, and the potentially extreme ocean wave heights associated with ET events provide difficult forecast challenges to the responsible forecast centers around the globe. These intense weather phenomena can exist long after their “tropical storm” status has been discontinued.

In the case of the transitioning Hurricane Luis (1995) peak waves of over 30 meters were generated, causing extensive damage to the Queen Elizabeth II ocean liner. Detailed wave-wind coupling simulation of the transitioning Hurricane Bonnie (1998) reproduced the 14+ meter significant wave heights produced by this ET event and highlighted the challenges in simulating shoaling waves as a storm approaches landfall. These extreme surface waves, often arriving only shortly before the main center of the storm, have been explained by Bowyer and MacAfee<sup>227</sup> in terms of a “trapped fetch” phenomena. In these situations, the rapid forward motion of the storm is similar to that of the wave speed and so the storm moves with the fastest growing waves that it is generating. This results in a longer period of wind forcing of the waves, so creating much larger wind waves than would be possible if the storm were moving at the slower speeds typical of tropical cyclones. The distance over which the waves grow is called the effective or dynamic fetch (Fig. 10.88). Hence, the waves generated by an extratropically-transitioning TC can be much larger than the waves generated by a more intense, but slower moving TC. Enhancement in wave growth occurs only to the right of track in the NH (left in the SH), in the fastest wind region of the ET storm (where the storm’s forward motion is in the same direction as its winds).



Fig. 10.88. Conceptual model of a tropical cyclone with a straight storm path and a fetch in the right of track (outlined with a dotted white line). Waves within the dotted line experience a longer period of wind forcing; the distance over which they grow is called the effective or dynamic fetch (purple outline).



Conceptual animation of wave growth within the dynamic fetch,  
[http://www.meted.ucar.edu/marine/mod2\\_wlc\\_gen/dynamic\\_fetch.htm](http://www.meted.ucar.edu/marine/mod2_wlc_gen/dynamic_fetch.htm)

### 10.8.6 Hazard Mitigation

Catastrophes such as the Bangladesh cyclones, TC Nargis, and Hurricane Katrina highlight the need for mitigation measures that incorporate the physical and social aspects of tropical cyclones. Mitigation against tropical cyclone impacts includes, improvements in TC intensity and track forecasting, understanding the long-term impact of coastal environmental change (e.g., removal of marshes), updating floodplain maps, reviewing and/or revising land use planning and building codes for coastal and flood prone areas, creating warning systems to reach more people, and understanding vulnerability of different populations (e.g., the elderly). Hazard mitigation is multi-faceted, involving long-term and short term planning. Long term aspects include education, public policies on building codes and zoning, and insurance. Short term aspects occur when the system is imminent, such as forecasting, warning, and response as well as short term response in the immediate aftermath of the event.

In response to high numbers of deaths from storm surge and coastal flooding in the late 1960s and early 1970s (Box 10-11), governments began public education on the dangers of storm surge. The result has been very positive as the numbers of deaths from coastal flooding and storm surge has decreased. The success of TC hazard mitigation was demonstrated during the landfall of Cyclone Sidr, a category-4 cyclone, in Bangladesh on 15 November 2007. Deaths numbered a few thousands<sup>263</sup> instead of the hundreds of thousands during past cyclones of similar magnitude. Unfortunately, mitigation against deaths from storm surge remains uneven around the Bay of Bengal, as demonstrated by the tremendous loss of life when Tropical Cyclone Nargis made landfall in Burma (Myanmar) on 2 May 2008. As of 21 July 2008, the official death toll is 84,530; however, unofficial estimates from international organizations are considerably higher. In the US, public education on inland flooding was jumpstarted when it was reported that freshwater flooding from tropical cyclones was the largest single cause of hurricane-related deaths in the United States between 1970 and 1999.<sup>264</sup> Figure 10.89 is an example from the US National Weather Service public education campaign.



Fig. 10.89. US National Weather Service warning against entering flooded areas.

Successful mitigation involves planning and coordinated response at various levels: individual, community, regional, national, and international. On the personal scale, planning must consider not only protection of property but also personal health. Normal routine will be disrupted, health-care facilities will be closed, medical records may be misplaced or destroyed, and adequate medication may be unavailable. The latter is especially critical for those with chronic illnesses.<sup>265</sup> At the community level, it involves public education, land use planning, and implementation of emergency warning systems and evacuation plans. At the local, state, and national levels, long-term mitigation and coordination of relief is critical. Failure of coordination aggravates the cyclone impact—dramatically demonstrated in the aftermath of Hurricane Katrina.



Timely evacuation from storm surge has been successful in reducing loss of life from tropical cyclone. However, evacuation is a complex issue for officials and the general population. Can you think of some issues that need to be considered? For example, think of situations in which evacuation may not be possible or advisable.



NOAA NWS, Turn Around Don't Drown, <http://www.srh.noaa.gov/tadd/>  
 UN Report, TC Sidr, <http://www.reliefweb.int/rw/dbc.nsf/doc108?OpenForm&rc=3&emid=TC-2007-000208-BGD>  
 NASA, TC Nargis, [http://www.nasa.gov/mission\\_pages/hurricanes/archives/2008/h2008\\_nargis.html](http://www.nasa.gov/mission_pages/hurricanes/archives/2008/h2008_nargis.html)  
 UN Report, TC Nargis, <http://www.reliefweb.int/rw/rwb.nsf/db900SID/ONIN-7GRR3J?OpenDocument&rc=3&cc=mmr>





Issues associated with evacuation include, but are not limited to the following:  
On small islands, residents must shelter in place, unlike continental regions where coastal residents can move far inland. Evacuation is costly and the cost will not be replaced if there is no impact. It is not advisable to evacuate when the evacuation time is longer than the forecast lead time or when the evacuation route is impassable. Maps of evacuation boundaries often do not recognize the difference between discomfort (standing, shallow water) and deadly harm (moving water and drowning). Assessment of those differences could reduce the number of unnecessary evacuees. .  
Uncertainty in the forecast makes evacuation decisions more difficult.

Effective warning systems require the integration of monitoring technology, evacuation plans and procedures, and personnel. Sorensen<sup>266</sup> reviewed twenty years of warning systems and found several major factors that affect the warning response. Response was most affected by physical cues (e.g., images of the size and intensity of the storm); proximity to the threat; experience with hazards (e.g., experience with Hurricane Camille led some coastal residents to flee from Hurricane Katrina while others stayed because they had survived Camille), and social cues (e.g., trusted neighbors evacuating). It should be understood that mitigation is a continuous process of adjustment and improvement.



WMO Links to Active National Warnings of Tropical Cyclones,  
<http://www.wmo.int/pages/prog/www/tcp/National%20Warnings.html>  
United Nations Stop Disasters game, <http://www.stopdisastersgame.org/en/>

## **Operational Focus**

Review topics of interest to operational forecasting on the pages listed.

### Why we forecast tropical cyclones

Video of conditions at landfall, Box 10-1, 7-8  
Hazards, 164

### Global Distribution and Monitoring of Tropical Cyclones (TC)

Classification of Tropical Cyclone Intensity around the World, 9-15  
Animation of wind damage (Saffir-Simpson Scale), 14, 172  
Animation of storm surge and wind damage, 14, 165  
Monitoring of Tropical Cyclones, WMO Regional Centers, 16

### Tropical Cyclone Structure

3-D structure of tropical cyclones, 19-23, 100  
Post landfall structure, 33

### Tropical Cyclogenesis

Necessary conditions for tropical cyclone formation, 37-40  
Genesis in the monsoon trough, schematic of TC formation region, 41  
West Pacific flowchart of TC formation pathways, 42  
TC formation and Tropical Upper Tropospheric Troughs (TUTT), 43  
TC formation and Equatorial Waves,  
Twin NH, SH formation from Equatorial Rossby waves, 46  
TC formation from Mixed Rossby Waves, 47  
TC formation and African Easterly Waves, 49  
Mesoscale Influences on TC formation, 54  
TC formation from subtropical storms or “Tropical Transition”, 54  
TC formation and Mesoscale Convective Systems, 57  
Global maps of tropical cyclogenesis sources and modulating influences, 70

### Will the Tropical Cyclone Vortex survive?

The role of shear and convection, 58  
Exercise: Will the TC vortex survive or die? 60  
The impact of shear on TC vortex survival, 58, 63  
Trough interaction and TC vortex survival, 65  
Saharan Air Layer, TC formation and survival, 67-69

### Tropical Cyclone Intensity

Lifecycle of Tropical Cyclones, Section 10.4.1, 72  
Example of Rita (2005), 74-75  
Dvorak Technique, Satellite Estimates of TC Intensity, 98-101  
Why is it that every storm is not a Cat. 5? 92  
SST and intensity in each ocean basin, 93  
Frequency of storms of particular intensity and SST, 94  
Eyewall replacement cycles and TC intensity, 107-109

Inner core features and links to intensity 107-109, 111-113  
TC Intensity and radius of 34-kt wind, 110

### Satellite and Radar Remote Sensing of Tropical Cyclones

Observing 3-D structure from remote sensing, 100  
Dvorak enhanced IR technique for estimating intensity, 98-102  
Satellite microwave analysis of TCs, 103-105  
Parallax error in locating the eye, 106  
Eyewall replacement cycles and TC intensity, 107-108  
Satellite-derived winds, 109-110

### Climatology of Tropical Cyclones

Seasonality of TC formation, 114  
    Average seasonal cycle in all basins, 116  
    Catarina (2004): Rare South Atlantic Tropical Cyclone, 117-119  
Intraseasonal or sub-seasonal influences on TC occurrence  
    MJO influence on tropical cyclogenesis, 121  
    Monitoring the MJO, 123  
    Saharan Air Layer: Impacts and Monitoring, 123  
Seasonal Forecasting of TC Activity, 130  
    Table 10.3, List of organizations doing seasonal forecasts, 130  
    Table 10.4, List of variables predicted, 131  
Interannual Variability  
    ENSO: Impacts and Monitoring, 126

### Tropical Cyclone Motion

The Beta-Effect or why tropical cyclones move westward and poleward even without steering flow, 141-142  
How tropical cyclones move relative to each other, the Fujiwhara Effect, 149-151

### Extratropical Transition

ET onset and completion, 159  
Exercise: Identify ET from satellite images, 162-163  
Impacts of ET: Wind and waves, 173-174

### Impacts of Tropical Cyclones

Video of landfalling TC Ingrid (2005), 8  
Storm surge and wind-driven waves, 164-165  
    Animation of storm surge, 165  
    Bangladesh cyclones and lessons learned, 166-168  
Flooding and landslides, 169  
    Flooding and midlatitude trough interaction, 170  
    Hurricane Mitch, Deadly Atlantic storm, 171  
Post-landfall structural changes, 32-34  
Strong Winds and Tornadoes, 172  
    Animation of wind damage, 172  
Lightning, 173

## Tropical Cyclone Hazard Mitigation

Most deadly tropical cyclones, Bay of Bengal, 166-168

Hurricane Mitch, Deadly Atlantic storm, 171

Summary of mitigation issues, concerns, and lessons learned, 175-177

### **Summary**

Tropical cyclones affect around half of the globe and more than half of the Earth's population. Familiarity with the necessary large-scale environmental conditions for tropical cyclogenesis helps explain the distribution of these storms around the world. Understanding of both extratropical and tropical transitions provides insights into the sources of tropical storm activity in other regions. Theories for potential intensity (PI) give guidance on likely tropical cyclone peak intensity, but the effects of environmental factors ensure that very few tropical cyclones achieve their PI. Their three-dimensional rotational wind distribution results in inertially stable, warm-cored vortices. This inertial stability provides some insulation for the tropical cyclone from environmental forcings; however weak tropical cyclones and the upper tropospheric outflow region of all storms are less protected by inertial stability. The societal impacts of tropical cyclones can be devastating and widespread, inspiring our attention and further studies of the atmosphere.

## Keywords

Tropical cyclone  
 Hurricane  
 Typhoon  
 Tropical Storm  
 Tropical Depression  
 Tropical Wave  
 Tropical cyclogenesis  
 Core  
 Eye  
 Eyewall  
 Intensity  
 Surface winds  
 Maximum winds  
 Minimum central pressure  
 Saffir-Simpson Scale  
 Radius of maximum winds  
 Boundary layer inflow  
 Cirrus shield  
 Upper-tropospheric outflow  
 Strength  
 Size  
 Rainband  
 Intertropical Convergence Zone (ITCZ)  
 Monsoon trough  
 Monsoon region  
 Incipient disturbance/vortex  
 Absolute vorticity  
 Potential vorticity (PV)  
 Moist static energy  
 Equivalent potential temperature  
 Equatorial Rossby wave  
 Mixed Rossby-gravity wave (MRG)  
 Mesoscale Convective System (MCS)  
 Rossby Radius of Deformation  
 Tropical transition  
 Subtropical cyclone  
 Tropical upper-tropospheric trough (TUTT)  
 Potential intensity (PI)  
 Conditional Instability of the Second Kind (CISK)  
 Wind-Induced Surface Heat Exchange (WISHE)  
 Carnot cycle  
 Sea surface temperature (SST)  
 African Easterly Jet (AEJ)  
 African Easterly Wave  
 Saharan Air Layer (SAL)  
 Vertical wind shear  
 Angular momentum  
 Inertial stability  
 Barotropic ITCZ breakdown  
 Eyewall Mesovortices  
 Vortex Rossby Waves  
 Eyewall replacement cycles  
 Dvorak Technique  
 Microwave sensors  
 Satellite-derived winds  
 Radar  
 Fujiwhara Effect  
 Beta-Effect  
 Beta-Gyres  
 Tropical cyclone activity  
 Interannual variability  
 El Niño Southern Oscillation (ENSO)  
 Quasi-Biennial Oscillation (QBO)  
 Intraseasonal variability  
 Madden-Julian Oscillation (MJO)  
 Multidecadal cycles  
 Extratropical transition  
 Landfall  
 Decay  
 Societal impacts  
 Mitigation  
 Warning  
 Evacuation  
 Storm surge  
 Flood and Landslides  
 Tornadoes  
 Wind-driven waves  
 Dynamic Fetch  
 Lightning

## Appendix A: Acronyms

AEJ	African Easterly Jet
AEW	African Easterly Wave
AMO	Atlantic Multidecadal Oscillation
AMS	American Meteorological Society
CDO	Central Dense Overcast
CIMSS	Cooperative Institute for Meteorological Satellite Studies
CPS	Cyclone Phase Space
CISK	Conditional Instability of the Second Kind
CLIPER	CLImatology and PERsistence model
ECMWF	European Center for Medium-range Weather Forecasting
ENSO	El Niño - Southern Oscillation
ERW	Equatorial Rossby Waves
ET	Extratropical Transition
GFS	Global Forecast System
GMS	Geostationary Meteorological Satellite
GPS	Global Positioning System
IRI	International Research Institute for Climate and Society, Columbia University
ITCZ	Inter-Tropical Convergence Zone
IWTC	International Workshop on Tropical Cyclones (of the WMO)
JMA	Japan Meteorological Agency
JTWC	Joint Typhoon Warning Center
MCS	Mesoscale Convective System
MDR	Main Development Region (in the North Atlantic)
MIMIC	Morphed Integrated Microwave Imagery at CIMSS
MJO	Madden-Julian Oscillation
MPI	Maximum Potential Intensity
MRG	Mixed Rossby-gravity (wave)
NCEP	National Centers for Environmental Prediction (NOAA)
NHC	National Hurricane Center (NCEP/NOAA)
NOAA	National Oceanic and Atmospheric Administration
NOGAPS	Navy's Operational Global Atmospheric Prediction System
NRL	Naval Research Laboratory
OLR	Outgoing Longwave Radiation
PDO	Pacific Decadal Oscillation
PI	Potential Intensity
PV	Potential Vorticity
QBO	Quasi-Biennial Oscillation
RSMC	Regional Specialized Meteorological Centre
SAL	Saharan Air Layer
SHIPS	Statistical Hurricane Intensity Prediction Scheme
SLP	Sea Level Pressure
SOI	Southern Oscillation Index
SST	Sea Surface Temperature
TC	Tropical Cyclone
TCWC	Tropical Cyclone Warning Centre
TMI	TRMM Microwave Imager
TRMM	Tropical Rainfall Measurement Mission
TUTT	Tropical Upper-Tropospheric Trough
UTC	Universal Time Coordinated
WISHE	Wind-Induced Surface Heat Exchange
WMO	World Meteorological Organization

**Appendix B: List of Principal Symbols**

$\theta_e$	Equivalent potential temperature (K)
$Ro = \frac{V}{fL}$	Rossby number (non-dimensional)
$V$	scale wind speed ( $\text{m s}^{-1}$ )
$L$	scale length (m)
$f = 2\Omega \sin(\varphi)$	vertical component of the Coriolis parameter ( $\text{s}^{-1}$ )
$\Omega$	Earth rotation rate = $7.292 \times 10^{-5}$ ( $\text{s}^{-1}$ )
$\varphi$	latitude (radians)
$\beta = [2\Omega \cos(\varphi)]/a$	latitudinal gradient of the Coriolis parameter ( $\text{s}^{-1} \text{m}^{-1}$ )
$a$	radius of the Earth = $6.37 \times 10^6$ (m)
$f_o$ ( $^1$ )	reference value of the Coriolis parameter, $f$ , at latitude $\varphi_o$ ( $\text{s}^{-1}$ )
$I^2 = (\zeta + f_o)(f_o + v/r)$	inertial stability
$\zeta$	vertical component of relative vorticity
$v$	rotational wind speed
$r$	radius
$\overrightarrow{V}_T$	thermal wind
	geostrophic wind
$p_A$	pressure above
$p_B$	pressure below
$R$	Universal gas constant = $287 \text{ J kg}^{-1} \text{ K}^{-1}$
$g$	gravity ( $\text{m s}^{-2}$ )
$B$	CPS parameter (thermal asymmetry)
$V_T^L$	CPS parameter (lower tropospheric thermal wind)
$V_T^U$	CPS parameter (upper tropospheric thermal wind)

$L_R = \frac{NH}{f_0}$	Rossby radius of deformation (m)
$(\bar{u}, \bar{v})$	symmetric averages of the cylindrical wind components
$(u', v')$	asymmetric components of the cylindrical wind
$g_e^*$	saturation equivalent potential temperature
$\vec{M} = \vec{r} \times \vec{v}_a = r\mathbf{v} + \frac{f_o r^2}{2}$	specific absolute angular momentum ( $\text{m}^2 \text{s}^{-1}$ )
$\vec{r}$	vector radius from the Earth axis of rotation
$r$	distance from the Earth axis for this application (m)
$\vec{v}_a$	absolute velocity (Earth motion plus wind) ( $\text{m s}^{-1}$ )
$\zeta_a = \zeta + f$	vertical component of the absolute vorticity ( $\text{s}^{-1}$ )
$\frac{d}{dt}$	Lagrangian (total) derivative (“following the flow”)
$\frac{\partial}{\partial t}$	Eulerian derivative (at a fixed location)
$-\vec{v} \cdot \nabla(\zeta + f)$	advection of the vertical component of absolute vorticity
$\vec{v} = \vec{v}_s + \vec{v}_a$	total wind partitioned into symmetric and asymmetric components
$\vec{v} = \vec{v}_s + \vec{v}_e + \vec{v}_g$	total wind partitioned into symmetric, environment, gyres



## Questions for Review

1. Identify five parts of the tropical cyclone and where you would expect to find them with respect to the surface center of the storm.
2. List six necessary, but not sufficient, conditions that must be present in the large-scale environment for tropical cyclogenesis to occur.
3. Summarize the six conditions you have just listed into two physical constraints necessary to achieve genesis.
4. Discuss the tropical cyclone mean spatial and seasonal distribution (global climatology) with reference to these “necessary but not sufficient conditions.”
5. Identify (a) two intraseasonal and (b) two interannual or interdecadal phenomena that modulate tropical cyclone activity. In the context of the “necessary but not sufficient conditions for genesis, discuss how one phenomena from each of (a) and (b) leads to variations from the mean tropical cyclone climatology.
6. Identify four potential incipient disturbances that could lead to tropical cyclogenesis.
7. Can tropical cyclogenesis occur without an incipient disturbance? Discuss.
8. Identify and describe the six possible stages of a tropical cyclone lifecycle. Two of these stages may not occur in an individual tropical cyclone lifecycle – which ones?
9. Using satellite remote sensing techniques, describe how you could detect changes in the intensity and structure of tropical cyclones.
10. Describe the process of evolution from an incipient tropical disturbance to an intense tropical cyclone.
11. How does evolution from a subtropical cyclone (tropical transition) differ from the answer just given?
12. Discuss how inner core dynamics can lead to changes in cyclone structure and intensity.
13. Define potential intensity (PI).
14. The two main theories for potential intensity are CISK and WISHE. What is the key distinction in the fundamental CISK and WISHE assumptions?

15. Why does every tropical cyclone not become a severe tropical cyclone? Discuss with reference to both the PI theories and the climatological atmospheric flow patterns of the global tropics.
16. What are the characteristics of tropical cyclones that undergo extratropical transition?
17. What kind of environmental support is necessary for extratropical transition?
18. Describe various mechanisms that lead to extratropical transition.
19. Describe the mechanisms that influence tropical cyclone motion. Consider the impacts of the storm environment, including the presence of multiple storms.
20. Describe the hazards of tropical cyclones particularly those at landfall (storm surge, heavy rain and floods, strong winds, tornadoes, ocean waves) and discuss the basic mechanisms for each type of hazard.

## References

1. Hatada, T., 1965: *The Mongol invasions*. Chuokoron Sha, 182 pp.
2. Yanai, M., 1975: English translation of the letter by the Khubilai Khan to the Japanese emperor in 1266.
3. Reiss, W. C., 2001: *Angel Gabriel: The elusive English galleon, its history and the search for its remains*. 1797 House, 117 pp.
4. Simpson, R. H., 1974: The hurricane disaster potential scale. *Weatherwise*, **27**, 169-186.
5. NOAA Hurricane Awareness, 2007: Saffir Simpson Hurricane Scale. [Available online at [http://www.nhc.noaa.gov/HAW2/english/basics/saffir\\_simpson.shtml](http://www.nhc.noaa.gov/HAW2/english/basics/saffir_simpson.shtml), accessed 7 Aug 2008].
6. Piddington, H., 1848: *The Sailor's Horn Book for the Law of Storms*. Smith, Elder and Co., 305 pp.
7. Louie, K. -, K. - Liu, 2004: Ancient records of typhoons in Chinese historical documents. *Hurricanes and Typhoons, Past, Present and Future*, Anonymous Columbia University Press, 462.
8. Hung, C. -, R. Fovell, and M. Yanai, 2005: Origins of "Typhoon," "Tai-feng," and "Taifu". *UCLA Trop. Meteor. Clim. Newsletter*, **67A**.
9. Chou, M. -, 1992: *The wind and rain in Taiwan - The meteorological proverb and history of Taiwan*. Liang-Ming publishing Co, 172 pp.
10. Neumann, C. J., 1999: *Tropical cyclones of the north Atlantic ocean, 1871-1998*. National Oceanic and Atmospheric Administration, 193.
11. Holland, G. J., Ed., 1993: *The global guide to tropical cyclone forecasting* Vol. WMO/TD-560, World Meteorological Organization, 342 pp.
12. Frank, W. M., 1977: The structure and energetics of the tropical cyclone I. Storm structure. *Mon. Wea. Rev.*, **105**, 1119-1135.

13. Hart, R. E., 2003: A cyclone phase space derived from thermal wind and thermal asymmetry. *Mon. Wea. Rev.*, **131**, 585-616.
14. Merrill, R. T., C. S. Velden, 1996: A three-dimensional analysis of the outflow layer of Supertyphoon Flo (1990). *Mon. Wea. Rev.*, **124**, 47-63.
15. Cione, J. J., P. G. Black, and S. H. Houston, 2000: Surface observations in the hurricane environment. *Mon. Wea. Rev.*, **128**, 1550-1561.
16. Wroe, D. R., G. M. Barnes, 2003: Inflow layer energetic of Hurricane Bonnie (1998) near landfall. *Mon. Wea. Rev.*, **131**, 1600-1612.
17. Emanuel, K. A., 1986: An air-sea interaction theory for tropical cyclones. Part I: Steady-state maintenance. *J. Atmos. Sci.*, **43**, 585-605.
18. Emanuel, K. A., 1995: Sensitivity of tropical cyclones to surface exchange coefficients and a revised steady-state model incorporating eye dynamics. *J. Atmos. Sci.*, **52**, 3969-3976.
19. Franklin, J. L., M. L. Black, and K. Valde, 2003: GPS dropwindsonde wind profiles in hurricanes and their operational implications. *Weather and Forecasting*, **18**, 32-44.
20. Kepert, J., 2001: The dynamics of boundary layer jets within the tropical cyclone core. Part I: Linear theory. *J. Atmos. Sci.*, **58**, 2469-2484.
21. Kepert, J., Y. Wang, 2001: The dynamics of boundary layer jets within the tropical cyclone core. Part II: Nonlinear enhancement. *J. Atmos. Sci.*, **58**, 2485-2501.
22. Willoughby, H. E., 1990: Gradient balance in tropical cyclones. *J. Atmos. Sci.*, **47**, 265-274.
23. Eliassen, A., 1951: Slow thermally or frictionally controlled meridional circulation in a circular vortex. *Astrophisica Norvegica*, v.5, 19.
24. Sundqvist, H., 1970: Numerical simulation of the development of tropical cyclones with a ten-level model. Part I. *Tellus*, **22**, 359.
25. Sundqvist, H., 1970: Numerical simulation of the development of tropical cyclones with a ten-level model. Part II. *Tellus*, **22**, 504.
26. Carrier, G. F., A. L. Hammond, and O. D. George, 1971: A model of the mature hurricane. *Journal of Fluid Mechanics Digital Archive*, **47**, 145-170.
27. Holland, G. J., R. T. Merrill, 1984: On the dynamics of tropical cyclone structural changes. *Quart. J. Roy. Meteor. Soc.*, **110**, 723-745.
28. Shapiro, L. J., H. E. Willoughby, 1982: The response of balanced hurricanes to local sources of heat and momentum. *J. Atmos. Sci.*, **39**, 378-394.
29. Tuleya, R. E., Y. Kurihara, 1978: A numerical simulation of the landfall of tropical cyclones. *J. Atmos. Sci.*, **35**, 242-257.
30. Corbosiero, K. L., J. Molinari, 2002: The effects of vertical wind shear on the distribution of convection in tropical cyclones. *Mon. Wea. Rev.*, **130**, 2110-2123.
31. Guishard, M. P., E. A. Nelson, J. L. Evans, R. E. Hart, and D. G. O'Connell, 2007: Bermuda subtropical storms. *Meteor. and Atmos. Phys.*, **97**, 239-253.

32. Evans, J. L., and R. E. Hart, 2003: Objective indicators of the life cycle evolution of extratropical transition for Atlantic tropical cyclones. *Mon. Wea. Rev.*, **131**, 909-925.
33. Gray, W. M., 1968: Global view of the origin of tropical disturbances and storms. *Mon. Wea. Rev.*, **96**, 669-700.
34. McBride, J. L., R. Zehr, 1981: Observational analysis of tropical cyclone formation. Part II: Comparison of non-developing versus developing systems. *J. Atmos. Sci.*, **38**, 1132-1151.
35. Ooyama, K. V., 1963: Hurricane development. *Proc. Technical Conference on Hurricanes and Tropical Meteorology*, Mexico, 6-12 June, 1963.
36. Charney, J. G., A. Eliassen, 1964: On the growth of the hurricane depression. *J. Atmos. Sci.*, **21**, 68-75.
37. Fraedrich, K., J. L. McBride, 1989: The physical mechanism of CISK and the free-ride balance. *J. Atmos. Sci.*, **46**, 2642-2648.
38. Simpson, J., E. Ritchie, G. J. Holland, J. Halverson, and S. Stewart, 1997: Mesoscale interactions in tropical cyclone genesis. *Mon. Wea. Rev.*, **125**, 2643-2661.
39. Ooyama, K. V., 1982: Conceptual evolution of the theory and modeling of the tropical cyclone. *Meteorological Society of Japan, Journal*, **60**, 369-380.
40. Briegel, L. M., W. M. Frank, 1997: Large-scale influences on tropical cyclogenesis in the western North Pacific. *Mon. Wea. Rev.*, **125**, 1397-1413.
41. McBride, J. L., T. D. Keenan, 1982: Climatology of tropical cyclone genesis in the Australian region. *Int. J. Climatol.*, **2**, 13-33.
42. Ritchie, E. A., G. J. Holland, 1999: Large-scale patterns associated with tropical cyclogenesis in the western Pacific. *Mon. Wea. Rev.*, **127**, 2027-2043.
43. Ferreira, R. N., W. H. Schubert, 1999: The role of tropical cyclones in the formation of tropical upper-tropospheric troughs. *J. Atmos. Sci.*, **56**, 2891-2907.
44. Dickinson, M., J. Molinari, 2002: Mixed Rossby-gravity waves and western Pacific tropical cyclogenesis. Part I: Synoptic evolution. *J. Atmos. Sci.*, **59**, 2183-2196.
45. Frank, W. M., and P. E. Roundy, 2006: The role of tropical waves in tropical cyclogenesis. *Mon. Wea. Rev.*, **134**, 2397-2417.
46. Zehnder, J. A., 1991: The interaction of planetary-scale tropical easterly waves with topography: A mechanism for the initiation of tropical cyclones. *J. Atmos. Sci.*, **48**, 1217-1230.
47. Zehnder, J. A., R. L. Gall, 1991: On a mechanism for orographic triggering of tropical cyclones in the Eastern North Pacific. *Tellus A*, **43**, 25.
48. Sadler, J. C., 1976: A role of the tropical upper tropospheric trough in early season typhoon development. *Mon. Wea. Rev.*, **104**, 1266-1278.
49. Sadler, J. C., 1978: Mid-season typhoon development and intensity changes and the tropical upper tropospheric trough. *Mon. Wea. Rev.*, **106**, 1137-1152.
50. Schubert, W. H., P. E. Ciesielski, D. E. Stevens, and H. C. Kuo, 1991: Potential vorticity modeling of the ITCZ and the Hadley Circulation. *J. Atmos. Sci.*, **48**, 1493-1509.

51. Lander, M. A., 1994: Description of a monsoon gyre and its effects on the tropical cyclones in the western North Pacific during August 1991. *Wea. Forecasting*, **9**, 640-654.
52. Ferreira, R. N., W. H. Schubert, 1997: Barotropic aspects of ITCZ breakdown. *J. Atmos. Sci.*, **54**, 261-285.
53. Nitta, T., 1989: Development of a twin cyclone and westerly bursts during the initial phase of the 1986-87 El Niño. *J. Meteor. Soc. Japan*, **67**, 677-681.
54. Gill, A. E., 1980: Some simple solutions for heat-induced tropical circulation. *Quart. J. Roy. Meteor. Soc.*, **106**, 447-462.
55. Kiladis, G. N., M. Wheeler, 1995: Horizontal and vertical structure of observed tropospheric equatorial Rossby waves. *J. Geophys. Res.*, **100**, 22981-22998.
56. Ekman, V. W., 1905: On the influence of the Earth's rotation on ocean currents. *Arkiv for Matematik. Astronomi och Fysik*, **2**, 1-53.
57. Tomas, R. A., P. J. Webster, 1997: The role of inertial instability in determining the location and strength of near-equatorial convection. *Quart. J. Roy. Meteor. Soc.*, **123**, 1445-1482.
58. Molinari, J., D. Knight, M. Dickinson, D. Vollaro, and S. Skubis, 1997: Potential vorticity, easterly waves, and eastern Pacific tropical cyclogenesis. *Mon. Wea. Rev.*, **125**, 2699-2708.
59. Charney, J., M. E. Stern, 1962: On the stability of internal baroclinic jets in a rotating atmosphere. *J. Atmos. Sci.*, **19**, 113-126.
60. Dickinson, M., J. Molinari, 2000: Climatology of sign reversals of the meridional potential vorticity gradient over Africa and Australia. *Mon. Wea. Rev.*, **128**, 3890-3900.
61. Reed, R. J., D. C. Norquist, and E. E. Recker, 1977: The structure and properties of African wave disturbances as observed during phase III of GATE. *Mon. Wea. Rev.*, **105**, 317-333.
62. Harr, P. A., R. L. Elsberry, 1996: Structure of a mesoscale convective system embedded in Typhoon Robyn during TCM-93. *Mon. Wea. Rev.*, **124**, 634-652.
63. Hebert, P. H., K. O. Potat, 1975: A satellite classification technique for subtropical cyclones. **NWS SR-83**, 25pp.
64. Simpson, J., J. B. Halverson, B. S. Ferrier, W. A. Petersen, R. H. Simpson, R. Blakeslee, and S. L. Durden, 1998: On the role of "hot towers" in tropical cyclone formation. *Meteor. Atmos. Phys.*, **67**, 15-35.
65. Bister, M., K. A. Emanuel, 1997: The genesis of Hurricane Guillermo: TEXMEX Analyses and a Modeling Study. *Mon. Wea. Rev.*, **125**, 2662-2682.
66. Zehr, R. M., 1992: Tropical cyclogenesis in the western North Pacific. NESDIS **61**, NOAA Tech. Rep., 181 pp.
67. Bosart, L. F., J. A. Bartlo, 1991: Tropical storm formation in a baroclinic environment. *Mon. Wea. Rev.*, **119**, 1979-2013.
68. Davis, C. A., L. F. Bosart, 2001: Numerical simulations of the genesis of Hurricane Diana (1984). Part I: Control Simulation. *Mon. Wea. Rev.*, **129**, 1859-1881.

69. Davis, C., L. F. Bosart, 2002: Numerical simulations of the genesis of Hurricane Diana (1984). Part II: Sensitivity of track and intensity prediction. *Mon. Wea. Rev.*, **130**, 1100-1124.
70. Davis, C. A., L. F. Bosart, 2003: Baroclinically induced tropical cyclogenesis. *Mon. Wea. Rev.*, **131**, 2730-2747.
71. Davis, C. A., L. F. Bosart, 2004: The TT problem. *Bull. Amer. Meteor. Soc.*, **85**, 1657–1662.
72. Thorncroft, C. D., B. J. Hoskins, and M. E. McIntyre, 1993: Two paradigms of baroclinic-wave life-cycle behaviour. *Quart. J. Roy. Meteor. Soc.*, **119**, 17-55.
73. Guishard, M. P., 2006: Atlantic subtropical storms: climatology and characteristics. PhD Thesis, Department of Meteorology, Pennsylvania State University, 158 pp .
74. Möller, J. D., M. T. Montgomery, 1999: Vortex Rossby waves and hurricane intensification in a barotropic model. *J. Atmos. Sci.*, **56**, 1674-1687.
75. Enagonio, J., M. T. Montgomery, 2001: Tropical cyclogenesis via convectively forced vortex Rossby waves in a shallow water primitive equation model. *J. Atmos. Sci.*, **58**, 685-706.
76. Möller, J. D., M. T. Montgomery, 2000: Tropical cyclone evolution via potential vorticity anomalies in a three-dimensional balance model. *J. Atmos. Sci.*, **57**, 3366-3387.
77. Jones, S. C., 1995: The evolution of vortices in vertical shear. I: Initially barotropic vortices. *Quart. J. Roy. Meteor. Soc.*, **121**, 821-851.
78. Schechter, D. A., M. T. Montgomery, and P. D. Reasor, 2002: A theory for the vertical alignment of a quasigeostrophic vortex. *J. Atmos. Sci.*, **59**, 150-168.
79. Jones, S. C., 2004: On the ability of dry tropical-cyclone-like vortices to withstand vertical shear. *J. Atmos. Sci.*, **61**, 114-119.
80. Möller, J. D., S. C. Jones, 1998: Potential vorticity inversion for tropical cyclones using the asymmetric balance theory. *J. Atmos. Sci.*, **55**, 259-282.
81. Elsberry, R. L., R. A. Jeffries, 1996: Vertical wind shear influences on tropical cyclone formation and intensification during TCM-92 and TCM-93. *Mon. Wea. Rev.*, **124**, 1374-1387.
82. Molinari, J., D. Vollaro, and K. L. Corbosiero, 2004: Tropical cyclone formation in a sheared environment: A case study. *J. Atmos. Sci.*, **61**, 2493-2509.
83. Kimball, S. K., J. L. Evans, 2002: Idealized numerical simulations of hurricane–trough interaction. *Mon. Wea. Rev.*, **130**, 2210-2227.
84. Bister, M., 2001: Effect of peripheral convection on tropical cyclone formation. *J. Atmos. Sci.*, **58**, 3463-3476.
85. Willoughby, H. E., J. A. Clos, and M. G. Shoreibah, 1982: Concentric eye walls, secondary wind maxima, and the evolution of the hurricane vortex. *J. Atmos. Sci.*, **39**, 395-411.
86. Jones, S. C., 2000: The evolution of vortices in vertical shear. II: Large-scale asymmetries. *Quart. J. Roy. Meteor. Soc.*, **126**, 3137-3159.
87. Jones, S. C., 2000: The evolution of vortices in vertical shear. III: Baroclinic vortices. *Quart. J. Roy. Meteor. Soc.*, **126**, 3161-3186.

88. Pfeffer, R. L., M. Challa, 1992: The role of environmental asymmetries in Atlantic hurricane formation. *J. Atmos. Sci.*, **49**, 1051-1059.
89. Challa, M., R. L. Pfeffer, Q. Zhao, and S. W. Chang, 1998: Can eddy fluxes serve as a catalyst for hurricane and typhoon formation? *J. Atmos. Sci.*, **55**, 2201-2219.
90. Molinari, J., P. Dodge, D. Vollaro, K. L. Corbosiero, and F. Marks Jr, 2006: Mesoscale aspects of the downshear reformation of a tropical cyclone. *J. Atmos. Sci.*, **63**, 341-354.
91. McBride, J. L., 1981: Observational analysis of tropical cyclone formation. Part III: Budget analysis. *J. Atmos. Sci.*, **38**, 1152-1166.
92. Carlson, T. N., J. M. Prospero, 1972: The large-scale movement of Saharan air outbreaks over the northern equatorial Atlantic. *J. Appl. Meteor.*, **11**, 283-297.
93. Karyampudi, V. M., H. F. Pierce, 2002: Synoptic-scale influence of the Saharan air layer on tropical cyclogenesis over the eastern Atlantic. *Mon. Wea. Rev.*, **130**, 3100-3128.
94. Pratt, A. S., 2005: Tropical cyclogenesis forecasting skill of the Global Forecasting System (GFS) during the 2002 and 2003 Atlantic hurricane seasons., Masters Thesis, Department of Meteorology, Pennsylvania State University, 135 pp.
95. Dunion, J. P., C. S. Velden, 2004: The impact of the Saharan air layer on Atlantic tropical cyclone activity. *Bull. Amer. Meteorol. Soc.*, **85**, 353-365.
96. DeMaria, M., J. A. Knaff, and B. H. Connell, 2001: A tropical cyclone genesis parameter for the tropical Atlantic. *Weather and Forecasting*, **16**, 219-233.
97. Hennon, C. C., J. S. Hobgood, 2003: Forecasting tropical cyclogenesis over the Atlantic basin using large-scale data. *Mon. Wea. Rev.*, **131**, 2927-2940.
98. Frank, N. L., 1969: The "Inverted V" cloud pattern — An easterly wave? *Mon. Wea. Rev.*, **97**, 130-140.
99. Reasor, P. D., M. T. Montgomery, and L. D. Grasso, 2004: A new look at the problem of tropical cyclones in vertical shear flow: Vortex resiliency. *J. Atmos. Sci.*, **61**, 3-22.
100. Dunnavan, G. M., J. W. Diercks, 1980: An analysis of Super Typhoon Tip (October 1979). *Mon. Wea. Rev.*, **108**, 1915-1923.
101. Palmén, E., 1948: On the formation and structure of tropical cyclones. *Geophysica*, **3**, 26-38.
102. Miller, B. I., 1958: On the maximum intensity of hurricanes. *J. Atmos. Sci.*, **15**, 184-195.
103. Merrill, R. T., 1988: Environmental influences on hurricane intensification. *J. Atmos. Sci.*, **45**, 1678-1687.
104. Emanuel, K. A., 1988: The maximum intensity of hurricanes. *J. Atmos. Sci.*, **45**, 1143-1155.
105. Bister, M., K. A. Emanuel, 1998: Dissipative heating and hurricane intensity. *Meteorology and Atmospheric Physics*, **65**, 233-240.
106. Emanuel, K., C. DesAutels, C. Holloway, and R. Korty, 2004: Environmental control of tropical cyclone intensity. *J. Atmos. Sci.*, **61**, 843-858.

107. Willoughby, H. E., 1990: Temporal changes of the primary circulation in tropical cyclones. *J. Atmos. Sci.*, **47**, 242-264.
108. Holland, G. J., 1997: The maximum potential intensity of tropical cyclones. *J. Atmos. Sci.*, **54**, 2519-2541.
109. Andreas, E. L., K. A. Emanuel, 2001: Effects of sea spray on tropical cyclone intensity. *J. Atmos. Sci.*, **58**, 3741-3751.
110. Hart, R. E., R. N. Maue, and Watson, M. I. C., 2008: Estimating local memory of tropical cyclones through MPI anomaly evolution. *Mon. Wea. Rev.*, **135**, 3990-4005.
111. DeMaria, M., J. Kaplan, 1994: A Statistical Hurricane Intensity Prediction Scheme (SHIPS) for the Atlantic basin. *Weather and Forecasting*, **9**, 209-220.
112. DeMaria, M., M. Mainelli, L. K. Shay, J. A. Knaff, and J. Kaplan, 2005: Further improvements to the Statistical Hurricane Intensity Prediction Scheme (SHIPS). *Weather and Forecasting*, **20**, 531-543.
113. Evans, J. L., 1993: Sensitivity of tropical cyclone intensity to sea surface temperature. *J. Clim.*, **6**, 1133-1140.
114. Harr, P. A., M. S. Kalafsky, and R. L. Elsberry, 1996: Environmental conditions prior to formation of a midget tropical cyclone during TCM-93. *Mon. Wea. Rev.*, **124**, 1693-1710.
115. Frank, W. M., E. A. Ritchie, 1999: Effects of environmental flow upon tropical cyclone structure. *Mon. Wea. Rev.*, **127**, 2044-2061.
116. Frank, W. M., E. A. Ritchie, 2001: Effects of vertical wind shear on the intensity and structure of numerically simulated hurricanes. *Mon. Wea. Rev.*, **129**, 2249-2269.
117. Katsaros, K. B., P. W. Vachon, W. T. Liu, and P. G. Black, 2002: Microwave remote sensing of tropical cyclones from space. *J. Oceanogr.*, **58**, 137-151.
118. Evans, J. L., K. McKinley, 1998: Relative timing of tropical storm lifetime maximum intensity and track recurvature. *Meteor. Atmos. Phys.*, **65**, 241-245.
119. Riehl, H., 1972: Intensity of recurved typhoons. *J. Appl. Meteorol.*, **11**, 613-615.
120. Merrill, R. T., 1984: A comparison of large and small tropical cyclones. *Mon. Wea. Rev.*, **112**, 1408-1418.
121. Wang, Y., C. C. Wu, 2004: Current understanding of tropical cyclone structure and intensity changes—a review. *Meteor. Atmos. Phys.*, **87**, 257-278.
122. Zeng, Z., Y. Wang, and C. C. Wu, 2007: Environmental dynamical control of tropical cyclone intensity—An observational study. *Mon. Wea. Rev.*, **135**, 38–59.
123. Dvorak, V. F., 1975: Tropical cyclone intensity analysis and forecasting from satellite imagery. *Mon. Wea. Rev.*, **103**, 420-430.
124. Velden, C. S., J. Daniels, D. Stettner, D. Santek, J. Key, J. Dunion, K. Holmlund, G. Dengel, W. Bresky, and P. Menzel, 2005: Recent innovations in deriving tropospheric winds from meteorological satellites. *Bull. Amer. Meteor. Soc.*, **86**, 205-223.



125. Velden, C., B. Harper, F. Wells, J. L. I. Beven, R. Zehr, T. Olander, M. Mayfield, C. Guard, M. Lander, R. Edson, L. Avila, A. Burton, M. Turk, A. Kikuchi, A. Christian, P. Caroff, and P. McCrone, 2006: The Dvorak tropical cyclone intensity estimation technique: A satellite-based method that has endured for over 30 years. *Bull. Amer. Meteor. Soc.*, **87**, 1195-1210.
126. Olander, T. L., C. S. Velden, 2007: The advanced Dvorak technique: Continued development of an objective scheme to estimate tropical cyclone intensity using geostationary infrared satellite imagery. *Weather and Forecasting*, **22**, 287-298.
127. Knaff, J. A., S. A. Seseske, M. DeMaria, and J. L. Demuth, 2004: On the influences of vertical wind shear on symmetric tropical cyclone structure derived from AMSU. *Mon. Wea. Rev.*, **132**, 2503-2510.
128. Wimmers, A. J., C. S. Velden, 2007: MIMIC: A new approach to visualizing satellite microwave imagery of tropical cyclones. *Bull. Amer. Meteor. Soc.*, **88**, 1187-1196.
129. Hawkins, J. D., M. Helveston, T. F. Lee, F. J. Turk, K. Richardson, C. Sampson, J. Kent, and R. Wade, 2006: Tropical cyclone multiple eyewall characteristics. *Proc. Preprints, 26th Conference on Hurricanes and Tropical Meteorology*, Monterrey, CA, Amer. Meteor. Soc., [Available at <http://ams.confex.com/ams/pdfpapers/108864.pdf>, accessed 7 Aug 2008]
130. Weissman, D. E., M. A. Bourassa, and J. Tongue, 2002: Effects of rain rate and wind magnitude on SeaWinds scatterometer wind speed errors. *J. Atmos. Ocean. Tech.*, **19**, 738-746.
131. Kossin, J. P., J. A. Knaff, H. I. Berger, D. C. Herndon, T. A. Cram, C. S. Velden, R. J. Murnane, and J. D. Hawkins, 2007: Estimating hurricane wind structure in the absence of aircraft reconnaissance. *Weather and Forecasting*, **22**, 89-101.
132. Weatherford, C. L., W. M. Gray, 1988: Typhoon structure as revealed by aircraft reconnaissance. Part I: Data analysis and climatology. *Mon. Wea. Rev.*, **116**, 1032-1043.
133. Kossin, J. P., W. H. Schubert, and M. T. Montgomery, 2000: Unstable interactions between a hurricane's primary eyewall and a secondary ring of enhanced vorticity. *J. Atmos. Sci.*, **57**, 3893-3917.
134. Montgomery, M. T., V. A. Vladimirov, and P. V. Denissenko, 2002: An experimental study on hurricane mesovortices. *J. Fluid. Mech.*, **471**, 1-32.
135. Persing, J., M. T. Montgomery, 2003: Hurricane superintensity. *J. Atmos. Sci.*, **60**, 2349-2371.
136. Montgomery, M. T., M. M. Bell, S. D. Aberson, and M. L. Black, 2006: Hurricane Isabel, 2003: New insights into the physics of intense storms. Part I: Mean vortex structure and maximum intensity estimates. *Bull. Amer. Meteor. Soc.*, **87**, 1335-1347.
137. Kossin, J. P., W. H. Schubert, 2001: Mesovortices, polygonal flow patterns, and rapid pressure falls in hurricane-like vortices. *J. Atmos. Sci.*, **58**, 2196-2209.
138. Schubert, W. H., M. T. Montgomery, R. K. Taft, T. A. Guinn, S. R. Fulton, J. P. Kossin, and J. P. Edwards, 1999: Polygonal eyewalls, asymmetric eye contraction, and potential vorticity mixing in hurricanes. *J. Atmos. Sci.*, **56**, 1197-1223.
139. McTaggart-Cowan, R., L. F. Bosart, C. A. Davis, E. H. Atallah, J. R. Gyakum, and K. A. Emanuel, 2006: Analysis of Hurricane Catarina (2004). *Mon. Wea. Rev.*, **134**, 3029-3053.
140. Simpson, J., C. Kummerow, W. K. Tao, and R. F. Adler, 1996: On the Tropical Rainfall Measuring Mission (TRMM). *Meteor. Atmos. Phys.*, **60**, 19-36.

141. Madden, R. A., P. R. Julian, 1971: Detection of a 40-50 day oscillation in the zonal wind in the tropical Pacific. *J. Atmos. Sci.*, **28**, 702-708.
142. Madden, R. A., P. R. Julian, 1972: Description of global-scale circulation cells in the tropics with a 40-50 day period. *J. Atmos. Sci.*, **29**, 1109-1123.
143. Madden, R. A., P. R. Julian, 1994: Observations of the 40–50-day tropical oscillation—A review. *Mon. Wea. Rev.*, **122**, 814–837.
144. Maloney, E. D., D. L. Hartmann, 1998: Frictional moisture convergence in a composite life cycle of the Madden–Julian Oscillation. *J. Clim.*, **11**, 2387-2403.
145. Evans, J. L., F. A. Jaskiewicz, 2001: Satellite-based monitoring of intraseasonal variations in tropical Pacific and Atlantic convection. *Geophys. Res. Lett.*, **28**, 1511–1514.
146. Maloney, E. D., D. L. Hartmann, 2000: Modulation of eastern North Pacific hurricanes by the Madden–Julian Oscillation. *J. Clim.*, **13**, 1451-1460.
147. Maloney, E. D., D. L. Hartmann, 2000: Modulation of hurricane activity in the Gulf of Mexico by the Madden-Julian Oscillation. *Science*, **287**, 2002-2004.
148. Liebmann, B., H. H. Hendon, and J. D. Glick, 1994: The relationship between tropical cyclones of the western Pacific and Indian Oceans and the Madden–Julian oscillation. *J. Meteor. Soc. Japan*, **72**, 401–411.
149. Molinari, J., D. Vollaro, 2000: Planetary-and synoptic-scale influences on eastern Pacific tropical cyclogenesis. *Mon. Wea. Rev.*, **128**, 3296-3307.
150. Ayyer, A., J. Molinari, 2008: MJO and tropical cyclogenesis in the Gulf of Mexico and eastern north Pacific: Case study and idealized numerical modeling. *J. Atmos. Sci.* (in press).
151. Maloney, E. D., D. L. Hartmann, 2001: The Madden–Julian Oscillation, barotropic dynamics, and North Pacific tropical cyclone formation. Part I: Observations. *J. Atmos. Sci.*, **58**, 2545-2558.
152. Hartmann, D. L., H. H. Hendon, 2007: Atmospheric science: Resolving an atmospheric enigma. *Science*, **318**, 1731-1732.
153. Carlson, T. N., 1969: Some remarks on African disturbances and their progress over the tropical Atlantic. *Mon. Wea. Rev.*, **97**, 716-726.
154. Karyampudi, V. M., T. N. Carlson, 1988: Analysis and numerical simulations of the Saharan air layer and its effect on easterly wave disturbances. *J. Atmos. Sci.*, **45**, 3102-3136.
155. Jones, S. C., P. A. Harr, J. Abraham, L. F. Bosart, P. J. Bowyer, J. L. Evans, D. E. Hanley, B. N. Hanstrum, R. E. Hart, and F. Lalaurette, 2003: The extratropical transition of tropical cyclones: Forecast challenges, current understanding, and future directions. *Weather and Forecasting*, **18**, 1052-1092.
156. Wu, L., 2007: Impact of Saharan air layer on hurricane peak intensity. *Geophys. Res. Lett.*, **34**, L09802, doi:10.1029/2007GL029564.
157. Carlson, T. N., 1969: Synoptic histories of three African disturbances that developed into Atlantic hurricanes. *Mon. Wea. Rev.*, **97**, 256-276.

158. Landsea, C. W., 1993: A climatology of intense (or major) Atlantic hurricanes. *Mon. Wea. Rev.*, **121**, 1703-1713.
159. Klotzbach, P. J., W. M. Gray, 2006: Causes of the unusually destructive 2004 Atlantic basin hurricane season. *Bull. Amer. Meteor. Soc.*, **87**, 1325-1333.
160. Chan, J. C. L., J. Shi, and C. Lam, 1998: Seasonal forecasting of tropical cyclone activity over the western North Pacific and the South China Sea. *Wea. Forecasting*, **13**, 997-1004.
161. Evans, J. L., R. J. Allan, 1992: El Niño/Southern Oscillation modification to the structure of the monsoon and tropical cyclone activity in the Australasian region. *Int. J. Climatol.*, **12**, 611-623.
162. Gray, W. M., 1984: Atlantic seasonal hurricane frequency. Part I: El Niño and the 30mb Quasi-Biennial Oscillation influences *Mon. Wea. Rev.*, **112**, 1649-1668.
163. Shapiro, L. J., 1982: Hurricane climatic fluctuations. Part I: Patterns and cycles. *Mon. Wea. Rev.*, **110**, 1007-1013.
164. Shapiro, L. J., 1982: Hurricane climatic fluctuations. Part II: Relation to large-scale circulation. *Mon. Wea. Rev.*, **110**, 1014-1023.
165. Chan, J. C. L., 1995: Tropical cyclone activity in the western North Pacific in relation to the stratospheric Quasi-Biennial Oscillation. *Mon. Wea. Rev.*, **123**, 2567-2571.
166. Landsea, C. W., W. M. Gray, Mielke Jr, P. W., and K. J. Berry, 1992: Long-term variations of western Sahelian monsoon rainfall and intense US landfalling hurricanes. *J. Clim.*, **5**, 1528-1534.
167. Gray, W. M., 1990: Strong association between West African rainfall and U.S. landfall of intense hurricanes. *Science*, **249**, 1251-1256, doi:10.1126/science.249.4974.1251.
168. Holland, G. J., P. J. Webster, 2007: Heightened tropical cyclone activity in the North Atlantic: natural variability or climate trend? *Philosophical Transactions of the Royal Society A: Mathematical, Physical and Engineering Sciences*, **365**, 2695-2716.
169. Virmani, J. I., R. H. Weisberg, 2006: The 2005 hurricane season: An echo of the past or a harbinger of the future? *Geophys. Res. Lett.*, **33**, L05707, doi:10.1029/2005GL025517.
170. Gray, W. M., 1984: Atlantic seasonal hurricane frequency. Part II: Forecasting its variability. *Mon. Wea. Rev.*, **112**, 1669-1683.
171. Gray, W. M., C. W. Landsea, Mielke Jr, P. W., and K. J. Berry, 1994: Predicting Atlantic basin seasonal tropical cyclone activity by 1 June. *Weather and Forecasting*, **9**, 103-115.
172. Nicholls, N., 1979: A possible method for predicting seasonal tropical cyclone activity in the Australian region. *Mon. Wea. Rev.*, **107**, 1221-1224.
173. Nicholls, N., 1992: Recent performance of a method for forecasting Australian seasonal tropical cyclone activity. *Aust. Meteor. Mag.*, **40**, 105-110.
174. Landsea, C. W., G. D. Bell, W. M. Gray, and S. B. Goldenberg, 1998: The extremely active 1995 Atlantic hurricane season: Environmental conditions and verification of seasonal forecasts. *Mon. Wea. Rev.*, **126**, 1174-1193.
175. Liu, K. -, M. L. Fearn, 2000: Reconstruction of prehistoric landfall frequencies of catastrophic hurricanes in NW Florida from sediment records. *Quat. Res.*, **54**, 238-245.

176. Street-Perrott, F. A., R. A. Perrott, 1990: Abrupt climate fluctuations in the tropics: The influence of the Atlantic circulation. *Nature*, **343**, 607-612.
177. Landsea, C. W., W. M. Gray, 1992: The strong association between western Sahelian monsoon rainfall and intense Atlantic hurricanes. *J. Clim.*, **5**, 435-453.
178. Chan, J. C. L., 2006: Possible causes of interdecadal variations in tropical cyclone activity in the western North Pacific. *27th Conference on Hurricanes and Tropical Meteorology*, .
179. Matsuura, T., M. Yumoto, and S. Iizuka, 2003: A mechanism of interdecadal variability of tropical cyclone activity over the western North Pacific. *Clim. Dyn.*, **21**, 105-117.
180. Bell, G. D., M. Chelliah, 2006: Leading tropical modes associated with interannual and multidecadal fluctuations in North Atlantic hurricane activity. *J. Clim.*, **19**, 590-612.
181. Xu, M., Q. Yang, Y. Duan, and M. Ying, 2006: Temporal variance of typhoon disasters in recent six centuries in Shanghai and preventing, mitigating strategies. *Proc. 27th AMS Conference on Hurricanes and Tropical Meteorology*, Monterey, CA, American Meteorological Society.
182. Konnen, G. P., M. Zaiki, Baede, A. P. M., T. Mikami, P. D. Jones, and T. Tsukahara, 2003: Pre-1872 extension of the Japanese instrumental meteorological observation series back to 1819. *J. Clim.*, **16**, 118-131.
183. Allan, R. J., 2000: ENSO and climatic variability in the past 150 years. *El Niño and the Southern Oscillation: Multiscale Variability and Its Impacts on Natural Ecosystems and Society*, H. F. Diaz and V. Markgraf, Eds., Cambridge University Press, 3-55.
184. Allan, R. J., J. Lindesay, and D. Parker, 1996: El Niño/Southern Oscillation and climatic variability. CSIRO Publishing. Australia, 408 pp.
185. Allan, R., T. Ansell, 2006: A new globally complete monthly Historical Gridded Mean Sea Level Pressure Dataset (HadSLP2): 1850-2004. *J. Climate.*, **19**, 5816-5842.
186. Kleeman, R., S. B. Power, 2000: Modulation of ENSO variability on decadal and longer timescales. *El Niño and the Southern Oscillation: Multiscale variability and its impacts on natural ecosystems and society*. H. F. Diaz and V. Markgraf, Eds., Cambridge University Press, 413-441.
187. McPhaden, M. J., D. Zhang, 2002: Slowdown of the meridional overturning circulation in the upper Pacific Ocean. *Nature*, **415**, 603-608.
188. Broecker, W. S., 1991: The great ocean conveyor. *Oceanography*, **4**, 79-89.
189. Lamb, P. J., 1978: Large-scale tropical Atlantic surface circulation patterns associated with sub-Saharan weather anomalies. *Tellus*, **30**, 240-251.
190. Goldenberg, S. B., L. J. Shapiro, 1996: Physical mechanisms for the association of El Niño and west African rainfall with Atlantic major hurricane activity. *J. Climate.*, **9**, 1169-1187.
191. Avila, L. A., 1991: Atlantic tropical systems of 1990. *Mon. Wea. Rev.*, **119**, 2027-2033.
192. Folland, C. K., T. N. Palmer, and D. E. Parker, 1986: Sahel rainfall and worldwide sea temperatures, 1901-85. *Nature*, **320**, 602-607.

193. Knight, J. R., R. J. Allan, C. K. Folland, M. Vellinga, and M. E. Mann, 2005: A signature of persistent natural thermohaline circulation cycles in observed climate. *Geophys. Res. Lett.*, **32**, L20708, doi:10.1029/2005GL024233.
194. Mann, M. E., K. A. Emanuel, 2006: Atlantic hurricane trends linked to climate change. *Eos Trans. AGU*, **87**, 233,238,241.
195. Kossin, J. P., K. R. Knapp, D. J. Vimont, R. J. Murnane, and B. A. Harper, 2007: A globally consistent reanalysis of hurricane variability and trends. *Geophys. Res. Lett.*, **34**, L04815, doi:10.1029/2006GL028836.
196. Knaff, J. A., 1997: Implications of summertime sea level pressure anomalies in the tropical atlantic region. *J. Climate.*, **10**, 789-804.
197. Ballester, M., C. González, and R. Pérez Suárez, 2004: Modelo estadístico para el pronóstico de la actividad ciclónica en el Océano Atlántico, el Golfo de México y el Mar Caribe. **11**, 9.
198. Klotzbach, P. J., W. M. Gray, 2004: Updated 6–11-month prediction of Atlantic basin seasonal hurricane activity. *Wea. Forecasting*, **19**, 917-934.
199. Vitart, F. D., 2006: Seasonal forecasting of tropical storm frequency using a multi-model ensemble. *Quart. J. Roy. Meteor. Soc.*, **132**, 647-666.
200. Lea, A. S., M. A. Saunders, 2006: How well forecast were the 2004 and 2005 Atlantic and US hurricane seasons? *Weather*, **61**, 245-249.
201. Owens, B. F., C. W. Landsea, 2003: Assessing the skill of operational Atlantic seasonal tropical cyclone forecasts. *Wea. Forecasting*, **18**, 45-54.
202. Camargo, S. J., A. G. Barnston, P. J. Klotzbach, and C. W. Landsea, 2007: Seasonal tropical cyclone forecasts. *WMO Bulletin*, **56**, 1-14.
203. Fujiwhara, S., 1921: The natural tendency towards symmetry of motion and its application as a principle of meteorology. *Quart. J. Roy. Meteor. Soc.*, **47**, 287-293.
204. Helmholtz, H., 1867: On integrals of the hydrodynamical equations which express vortex motion. *Philos. Mag.*, **33**, 485-512.
205. Kasahara, A., 1957: The numerical prediction of hurricane movement with a barotropic model. *J. Meteor.*, **14**, 386-402.
206. Kasahara, A., 1960: The numerical prediction of hurricane movement with a two-level baroclinic model. *J. Meteor.*, **17**, 357-370.
207. Fiorino, M., R. L. Elsberry, 1989: Contributions to tropical cyclone motion by small, medium and large scales in the initial vortex. *Mon. Wea. Rev.*, **117**, 721-727.
208. Velden, C. S., L. M. Leslie, 1991: The basic relationship between tropical cyclone intensity and the depth of the environmental steering layer in the Australian region. *Weather and Forecasting*, **6**, 244-253.
209. Adem, J., 1956: A series solution for the barotropic vorticity equation and its application in the study of atmospheric vortices. *Tellus*, **8**, 364-372.

210. Adem, J., P. Lezama, 1960: On the motion of a cyclone embedded in a uniform flow. *Tellus*, **12**, 255-258.
211. Fiorino, M., R. L. Elsberry, 1989: Some aspects of vortex structure related to tropical cyclone motion. *J. Atmos. Sci.*, **46**, 975-990.
212. Madala, R. V., A. A. Piacsek, 1975: Numerical simulation of asymmetric hurricane on a beta-plane with vertical shear. *Tellus*, **27**, 453-468.
213. Evans, J. L., G. J. Holland, and R. L. Elsberry, 1991: Interactions between a barotropic vortex and an idealized subtropical ridge. Part I: Vortex motion. *J. Atmos. Sci.*, **48**, 301-314.
214. Holland, G. J., J. L. Evans, 1992: Interactions between a barotropic vortex and an idealized subtropical ridge. Part II: Structure changes. *J. Atmos. Sci.*, **49**, 963-975.
215. Chan, J. C. -, Law, A. C. K., 1995: The interaction of binary vortices in a barotropic model. *Meteor. Atmos. Phys.*, **56**, 135-155.
216. Dong, K., C. J. Neumann, 1986: On the relative motion of binary tropical cyclones. *Mon. Wea. Rev.*, **111**, 945-953.
217. Brand, S., 1970: Interaction of binary tropical cyclones of the western North Pacific Ocean. *J. Appl. Meteor.*, **9**, 433-441.
218. Liu, K. S., Chan, J. C. L., 1999: Size of tropical cyclones as inferred from ERS-1 and ERS-2 data. *Mon. Wea. Rev.*, **127**, 2992-3001.
219. Lander, M., G. J. Holland, 1993: On the interaction of tropical-cyclone-scale vortices. I: Observations. *Quart. J. Roy. Meteor. Soc.*, **119**, 1347-1361.
220. DeMaria, M., Chan, J. C. L., 1984: Comments on "A numerical study of the interactions between two tropical cyclones". *Mon. Wea. Rev.*, **112**, 1643-1645.
221. Holland, G. J., G. S. Dietachmayer, 1993: On the interaction of tropical-cyclone-scale vortices. III: Continuous barotropic vortices. *Quart. J. Roy. Meteor. Soc.*, **119**, 1381-1398.
222. Ritchie, E. A., G. J. Holland, 1993: On the interaction of tropical-cyclone-scale vortices. II: Discrete vortex patches. *Quart. J. Roy. Meteor. Soc.*, **119**, 1363-1379.
223. Wang, Y., G. J. Holland, 1996: The beta drift of baroclinic vortices. Part II: Diabatic vortices. *J. Atmos. Sci.*, **53**, 3737-3756.
224. Hart, R. E., J. L. Evans, 1999: Simulations of dual-vortex interaction within environmental shear. *J. Atmos. Sci.*, **56**, 3605-3621.
225. Chan, J. C. L., R. T. Williams, 1987: Analytical and numerical studies of the beta-effect in tropical cyclone motion. Part I: Zero mean flow. *J. Atmos. Sci.*, **44**, 1257-1265.
226. Shapiro, L. J., 1996: The motion of Hurricane Gloria: A potential vorticity diagnosis. *Mon. Wea. Rev.*, **124**, 2497-2508.
227. Klein, P. M., P. A. Harr, and R. L. Elsberry, 2000: Extratropical transition of western North Pacific tropical cyclones: An overview and conceptual model of the transformation stage. *Weather and Forecasting*, **15**, 373-395.

228. Bowyer, P. J., A. W. MacAfee, 2005: The theory of trapped-fetch waves in tropical cyclones – An operational perspective. *Weather and Forecasting*, **20**, 229-244.
229. Hart, R. E., J. L. Evans, 2001: A climatology of the extratropical transition of Atlantic tropical cyclones. *J. Clim.*, **14**, 546-564.
230. Pierce, C., 1939: The meteorological history of the New England hurricane of Sept. 21, 1938. *Mon. Wea. Rev.*, **67**, 237-288.
231. Sekioka, M., 1956: A hypothesis on complex of tropical and extratropical cyclones for typhoon in the middle latitudes. I. Synoptic structure of Typhoon Marie passing over the Japan Sea. *J. Meteor. Soc. Japan*, **34**, 276-287.
232. Sekioka, M., 1956: A hypothesis on complex of tropical and extratropical cyclones for typhoon in the middle latitudes. II. Synoptic structure of Typhoons Louise, Kezia, and Jane passing over the Japan Sea. *J. Meteor. Soc. Japan*, **34**, 336-345.
233. Palmén, E., 1958: Vertical circulation and release of kinetic energy during the development of Hurricane Hazel into an extratropical storm. *Tellus*, **10**, 1-23.
234. Rößke, M., S. C. Jones, and D. Majewski, 2004: The extratropical transition of Hurricane Erin (2001): a potential vorticity perspective. *Meteorologische Zeitschrift*, **13**, 511-525.
235. Harr, P. A., R. L. Elsberry, and T. F. Hogan, 2000: Extratropical transition of tropical cyclones over the western North Pacific. Part II: The impact of midlatitude circulation characteristics. *Mon. Wea. Rev.*, **128**, 2634-2653.
236. Ritchie, E. A., R. L. Elsberry, 2001: Simulations of the transformation stage of the extratropical transition of tropical cyclones. *Mon. Wea. Rev.*, **129**, 1462-1480.
237. Hart, R. E., J. L. Evans, and C. Evans, 2007: Synoptic composites of the extratropical transition life cycle of north Atlantic tropical cyclones: Factors determining posttransition evolution. *Mon. Wea. Rev.*, **134**, 553-578.
238. Foley, G. R., B. N. Hanstrum, 1994: The capture of tropical cyclones by cold fronts off the west coast of Australia. *Weather and Forecasting*, **9**, 577-592.
239. Sinclair, M. R., 2002: Extratropical transition of southwest Pacific tropical cyclones. Part I: Climatology and mean structure changes. *Mon. Wea. Rev.*, **130**, 590-609.
240. Harr, P. A., R. L. Elsberry, 2000: Extratropical transition of tropical cyclones over the western North Pacific. Part I: Evolution of structural characteristics during the transition process. *Mon. Wea. Rev.*, **128**, 2613-2633.
241. Klein, P. M., P. A. Harr, and R. L. Elsberry, 2002: Extratropical transition of western North Pacific tropical cyclones: Midlatitude and tropical cyclone contributions to reintensification. *Mon. Wea. Rev.*, **130**, 2240-2259.
242. Arnott, J. M., J. L. Evans, and F. Chiaromonte, 2004: Characterization of extratropical transition using cluster analysis. *Mon. Wea. Rev.*, **132**, 2916-2937.
243. Hanley, D., J. Molinari, and D. Keyser, 2001: A composite study of the interactions between tropical cyclones and upper-tropospheric troughs. *Mon. Wea. Rev.*, **129**, 2570-2584.

244. DiMego, G. J., L. F. Bosart, 1982: The transformation of Tropical Storm Agnes into an extratropical cyclone. Part I: The observed fields and vertical motion computations. *Mon. Wea. Rev.*, **110**, 385-411.
245. DiMego, G. J., L. F. Bosart, 1982: The transformation of Tropical Storm Agnes into an extratropical cyclone. Part II: Moisture, vorticity and kinetic energy budgets. *Mon. Wea. Rev.*, **110**, 412-433.
246. Kitabatake, N., 2002: Extratropical transformation of Typhoon Vicki (1987): Structural changes and the role of upper-tropospheric disturbances. *J. Meteor. Soc. Japan*, **80**, 229-247.
247. Thorncroft, C., S. C. Jones, 2000: The extratropical transitions of Hurricanes Felix and Iris in 1995. *Mon. Wea. Rev.*, **128**, 947-972.
248. McTaggart-Cowan, R., L. F. Bosart, J. R. Gyakum, and E. H. Atallah, 2006: Hurricane Juan (2003). Part II: Forecasting and numerical simulation. *Mon. Wea. Rev.*, **134**, 1748-1771.
249. Simpson, R. H., H. Riehl, 1981: *The Hurricane and its impact*. 398 pp.
250. Simpson, R., R. A. Anthes, and M. Garstang, Eds., 2002: *Hurricane! Coping with disaster: Progress and challenges since Galveston*. American Geophysical Union (AGU), 360 pp.
251. Pielke, R. A., Jr., R. A. S. Pielke, 1997: *Hurricanes: Their nature and impacts on society*. John Wiley and Sons, England, 279 pp.
252. Pielke Jr, R. A., J. Gratz, C. W. Landsea, D. Collins, M. A. Saunders, and R. Musulin, 2008: Normalized hurricane damages in the United States: 1900-2005. *Nat. Hazards Rev.*, **9**, 29-42.
253. Bland, S. H., E. S. O'Leary, E. Farinaro, F. Jossa, and M. Trevisan, 1996: Long-term psychological effects of natural disasters. *Psychosom. Med.*, **58**, 18-24.
254. Rappaport, E. N., J. Fernández-Partagás, 1995: The deadliest Atlantic tropical cyclones, 1492-1994. NWS NHC-47, 41pp.
255. Liu, K.-., M. L. Fearn, 1993: Lake-sediment record of late Holocene hurricane activities from coastal Alabama. *Geology*, **21**, 793-796.
256. International Federation of Red Cross and Red Crescent Societies, 2008: Bangladesh: Cyclone Sidr Appeal No. MDRBD003 Operations Update No. 8. [Available online at <http://www.reliefweb.int/rw/RWB.NSF/db900SID/EDIS-7BHM45?OpenDocument&rc=3&emid=TC-2007-000208-BGD>, accessed 7 Aug 2008].
257. Spratt, S. M., D. W. Sharp, P. Welsh, A. Sandrik, F. Alsheimer, and C. Paxton, 1997: A WSR-88D assessment of tropical cyclone outer rainband tornadoes. *Wea. Forecasting*, **12**, 479-501.
258. Willoughby, H. E., P. G. Black, 1996: Hurricane Andrew in Florida: Dynamics of a disaster. *Bull. Amer. Meteor. Soc.*, **77**, 543-549.
259. Verbout, S. M., D. M. Schultz, L. M. Leslie, H. E. Brooks, D. Karoly, and K. Elmore, 2007: Tornado outbreaks associated with landfalling hurricanes in the North Atlantic basin: 1954-2004. *Meteor. Atmos. Phys.*, **97**, 255-271.
260. Samsury, C. E., R. E. Orville, 1994: Cloud-to-ground lightning in tropical cyclones: A study of Hurricanes Hugo (1989) and Jerry (1989). *Mon. Wea. Rev.*, **122**, 1887-1896.
261. Molinari, J., P. K. Moore, V. P. Idone, R. W. Henderson, and A. B. Saljoughy, 1994: Cloud-to-ground lightning in Hurricane Andrew. *J. Geophys. Res.*, **99 (D8)**, 16665-16676.



262. Cecil, D. J., E. J. Zipser, and S. W. Nesbitt, 2002: Reflectivity, ice scattering, and lightning characteristics of hurricane eyewalls and rainbands. Part I: quantitative description. *Mon. Wea. Rev.*, **130**, 769-784.
263. United Nations, Office for the Coordination of Humanitarian Affairs (OCHA), 2007: Bangladesh: Cyclone SIDR OCHA Situation Report No. 8. [Available at <http://www.reliefweb.int/rw/RWB.NSF/db900SID/YSAR-799NYQ?OpenDocument>, accessed 7 Aug 2008].
264. Rappaport, E. N., 2000: Loss of life in the United States associated with recent Atlantic tropical cyclones. *Bull. Amer. Meteor. Soc.*, **81**, 2065-2073.
265. Cefalu, W. T., S. R. Smith, L. Blonde, and V. Fonseca, 2006: The Hurricane Katrina aftermath and its impact on diabetes care: observations from "ground zero": lessons in disaster preparedness of people with diabetes. *Diabetes Care*, **29**, 158-160.
266. Sorensen, J., 2000: Hazard warning systems: Review of 20 years of progress. *Natural Hazards Review*, **1**, 120-125.

## Brief Biographies

### Dr. William M. Gray

*“He’s still lanky, like the baseball player he used to be back at Woodrow Wilson High School in Washington in the 1940s. He’s the guy who, every year, predicts the number of hurricanes that will form during the coming tropical storm season. He’s mentored dozens of scientists.” Washington Post (26 May 2006)*

William M. (Bill) Gray is an Emeritus Professor of Atmospheric Science at Colorado State University. While hurricane enthusiasts in the wider community may recognize Dr Gray specifically for his seasonal hurricane forecasting, his scientific career has spanned all aspects of tropical cyclones from their genesis and motion to their climate variability. Through his adept use of the available observations, Professor Gray has shed insight on tropical cyclogenesis and climatology, the evolution of storm structure and intensity, and tropical cyclone motion. He has mentored numerous students and colleagues throughout his career of more than 40 years, further extending his impact on the field. Bill Gray’s achievements have been widely recognized, including the Jule L. Charney and Banner I. Miller Awards of the American Meteorological Society.

Early in his career, Professor Gray served as a weather forecaster for the United States Air Force. He received his Ph.D. from the Department of Geophysical Sciences at the University of Chicago in 1964 and has served since 1961 on the Department of Atmospheric Science faculty at the Colorado State University. Bill Gray is a Fellow of the American Meteorological Society.

### Dr. Kerry A. Emanuel

*“Behold, a whirlwind of the Lord is gone forth in fury, even a grievous whirlwind: it shall fall grievously upon the head of the wicked.” Jeremiah, 23:19.*

And so begins The Divine Wind, Emanuel’s comprehensive review of the history and scientific understanding of hurricanes. Kerry Emanuel is a Professor of Earth, Atmospheric and Planetary Sciences (Program in Atmospheres, Oceans, and Climate) at the Massachusetts Institute of Technology. Kerry received his doctorate from MIT in 1978, then joined the faculty of UCLA. After some years, Kerry returned to MIT, now as a member of its faculty.

Dr Emanuel’s contributions to the understanding of tropical cyclones are broad and include the ongoing development, rigorous review and refinement of a theory for the potential peak intensity for tropical cyclones, mechanisms of scale selection in the tropics, tropical convection and climate change impacts on hurricanes. His theory of tropical cyclone potential intensity has provided a framework for considering the impacts of climate change on tropical cyclones. Kerry has mentored many young scientists; he is the author (or co-author) of more than 100 journal and review articles, as well as three books. Kerry Emanuel’s honors and awards include the American Meteorological Society’s Meisinger Award and Carl Gustaf Rossby Medal.

## Glossary

**Absolute vorticity** — A vector quantity calculated by taking the curl (cross product) of the vector wind. Typically, the vertical component of the absolute vorticity is larger (by orders of magnitude) than the other components. Thus, we most often use scalar absolute vorticity component when discussing tropical cyclones.

**African easterly wave** — A trough or cyclonic curvature maximum in the trade-wind easterlies. The wave may reach maximum amplitude in the lower middle troposphere.

**Atlantic Multidecadal Oscillation (AMO)** — A natural oscillation of the North Atlantic SST between warm and cool phases. The SST difference between these warm and cool phases is about 0.5°C and the period of the oscillation is roughly 20-40 years (the period is variable, but is a few decades long). Evidence suggests that the AMO has been active for at least the last 1,000 years.

**Available potential energy (APE)**—The portion of the total potential energy available for adiabatic conversion to kinetic energy. The total potential energy is a combination of the APE and the potential energy representing the mass distribution needed to balance the mean atmospheric motions.

**Baroclinic** — Dependence on the horizontal temperature contrast between warm and cold air masses. In a baroclinic atmosphere, the geostrophic wind varies with height in direction as well as speed and its shear is a function of the horizontal temperature gradient (the thermal wind equation).

**Barotropic** — The atmosphere has the same horizontal structure at all levels in the vertical. This is equivalent to the absence of horizontal temperature gradients.

**Barotropic-Baroclinic Instability** — Barotropic and baroclinic instability analyses are used to explain the growth of a small perturbation to the flow. A perturbation growing due to baroclinic instability draws its energy from the available potential energy (APE). A perturbation growing due to barotropic instability draws its energy from the kinetic energy of the background flow. A perturbation growing through both APE and mean kinetic energy conversion to kinetic energy of the growing system (intensifying the system) is developing through combined barotropic baroclinic instability.

**Beta ( $\beta$ ) effect** — Denotes how fluid motion is affected by spatial changes of the Coriolis parameter, for example, due to the earth's curvature. The term takes its name from the symbol  $\beta$  representing the meridional gradient of the Coriolis parameter at a fixed latitude. The asymmetric flows resulting from the interaction of the vortex with the changing Coriolis parameter is known as the  $\beta$ -gyres.

**Center** — Location of the vertical axis of a tropical cyclone, usually defined by the location of minimum wind or minimum pressure. The cyclone center position can vary with altitude.

**Conditional Instability of the Second Kind (CISK)** — A theory for tropical cyclone development that relates boundary layer moisture convergence (driven by Ekman pumping) to the potential for tropical cyclone intensification. As the storm intensifies, the moisture convergence

must increase, providing a feedback to the system. As with WISHE, CISK relies on the presence of an incipient disturbance.

**Cyclogenesis** — The formation of a cyclone.

**Cyclone** — A closed low pressure circulation, rotating counter-clockwise in the Northern Hemisphere and clockwise in the Southern Hemisphere.

**Cyclone Phase Space (CPS)** — A concise, three-parameter summary of the structure of a storm. It can be used to describe the structure of any synoptic or meso-synoptic cyclone.

**Dvorak Technique** — a classification scheme for estimating the intensity of TCs from enhanced IR and visible satellite imagery. It is the primary method of estimating intensity everywhere, except the North Atlantic and North Pacific where aircraft reconnaissance is routine.

**Eddy angular momentum flux (EAMF)** — Flux (net transport) of angular momentum into a circle centered on the storm. If EAMF is positive, the flow inside the circle will become more cyclonic; negative EAMF render the system less cyclonic (more anticyclonic). See Box 10-6 for a definition and discussion of angular momentum.

**Ekman pumping** — The force balance determining the vector wind is modified by friction at the Earth's surface. The addition of friction changes the force balance to slow the winds and change their direction: winds now flow into a low and out of a high pressure system. Winds flowing into a low because of friction are forced upwards and out of the boundary layer. This process is known as Ekman pumping.

**El Niño-Southern Oscillation** — An oscillation of the ocean-atmosphere system in the tropical Pacific which affects global weather and climate. El Niño, the warm phase of ENSO, is a quasi-periodic (2-7 years) warming of ocean surface waters in the equatorial and eastern tropical Pacific and an eastward shift in convection from the western Pacific climatological maximum. Changes occur in the trade easterlies, vertical wind shear, and ocean height. Cool ocean temperature anomalies are observed in the tropical western Pacific extending eastward into the subtropics of both hemispheres. “La Niña” refers to the less intense, anomalous cool phase of ENSO. The Southern Oscillation refers to the atmospheric pressure difference between Darwin and Tahiti that is correlated with El Niño.

**Entrainment** — The integration of unsaturated environmental air into the turbulent cloud-scale circulation. The antonym of entrainment is “detrainment”.

**Eye** — The roughly circular area of comparatively light winds that encompasses the center of a tropical cyclone. The eye is either completely or partially surrounded by the eyewall cloud.

**Eyewall / Wall Cloud** — An organized band or ring of cumulonimbus clouds that surround the eye, or light-wind center of a tropical cyclone. Eyewall and wall cloud are used synonymously.

**Explosive Deepening** — A decrease in the minimum sea-level pressure of a tropical cyclone of  $2.5 \text{ hPa hr}^{-1}$  for at least 12 hours or  $5 \text{ hPa hr}^{-1}$  for at least six hours.

**Extratropical** — A term used to indicate that a cyclone has lost its “tropical” characteristics. The term implies both poleward displacement of the cyclone and the conversion of the cyclone’s primary energy source from the release of latent heat of condensation to baroclinic processes. It is important to note that cyclones can become extratropical and still retain winds of hurricane or tropical storm force. Given that these dangerous winds can persist after the cyclone is classified as extratropical, the Canadian Hurricane Centre (for example) follows them as “Former hurricane XXX.”

**Extratropical Transition (ET)** — The evolution of a poleward-moving initially tropical cyclone resulting in an extratropical cyclone. In the process of this evolution the energy source of the storm shifts from latent heat release to baroclinic development.

**Fujiwhara Effect** — The mutual advection of two or more nearby tropical cyclones about each other. This results in cyclonic rotation of the storms about each other.

**Gale Force Wind** — A sustained surface wind in the range  $17 \text{ m s}^{-1}$  (39 mph,  $63 \text{ km hr}^{-1}$  or 34 knot) to  $24 \text{ m s}^{-1}$  (54 mph,  $87 \text{ km hr}^{-1}$  or 47 knot) inclusive, and not directly associated with a tropical cyclone.

**Horizontal Convective Rolls** — Lines of overturning motion with axes parallel to the local surface. These rolls result from a convective instability (high density over low density – often corresponding to cool air over warm) and can mix strong winds from above down towards the surface.

**Hurricane** — A tropical cyclone in which the maximum sustained surface wind (using the local time averaging convention) is at least  $33 \text{ m s}^{-1}$  (74 mph,  $119 \text{ km hr}^{-1}$  or 64 knot). The term “hurricane” is used for in the Northern Atlantic and Northeast Pacific; “tropical cyclone” east of the International Dateline to the Greenwich Meridian; and “typhoon” in the Pacific north of the Equator and west of the International Dateline.

**Inertial period** — The time taken to complete one rotation. In the tropical cyclone this is calculated by dividing the circumference at the radius of interest (commonly, the radius of maximum winds) by the wind speed at that radius.

**Intraseasonal** — Varying on time scales shorter than one season.

**Intensity** — The peak sustained surface wind in the region immediately surrounding the storm center, or the minimum central pressure measured in the eye.

**Inter-tropical Convergence Zone (ITCZ)** — The zone where the northeast and southeast trade winds converge. It is marked by low pressure, rising motion, and thunderstorms, which occur with strong surface heating. Its latitudinal position shifts in response to the solar maximum and heating response of the surface. It is recognized in satellite images as a band of thunderstorms across the tropics. It is also known as the “Equatorial Trough” or “Inter-tropical Front”.

**Landfall** — The intersection of the surface center of a tropical cyclone with a coastline. Because the strongest winds in a tropical cyclone are not located precisely at the center, it is possible for the strongest winds to be experienced over land even if landfall does not occur.

**Madden-Julian Oscillation (MJO)** — Tropical rainfall exhibits strong variability on intraseasonal time scales. These fluctuations in tropical rainfall often undergo a 30-60 day cycle that is referred to as the Madden-Julian Oscillation or intraseasonal oscillation. The MJO is a naturally occurring component of the Earth's coupled ocean-atmosphere system that significantly affects the atmospheric circulation throughout the global tropics and subtropics.

**Mixed Rossby-Gravity (MRG) Wave** — A divergent Rossby wave, resulting from conservation of potential vorticity and buoyancy forcing.

**Monsoon Region** — Refers to the combination of features including a monsoon trough, confluence zone, and the ITCZ.

**Monsoon Gyre** — A closed, symmetric circulation at 850 hPa with horizontal extent of 25° latitude that persists for at least two weeks. The circulation is accompanied by abundant convective precipitation around the south-southeast rim of the gyre.

**Ocean conveyor belt** — The name given to summarize the pattern of global ocean currents. The surface ocean currents generally transport warm salty water polewards, out of the tropics. The water cools as it moves polewards, becoming increasingly dense (remember that salty water is more dense than fresh water). This water sinks in the North Atlantic and also in the Southern Ocean near Antarctica. The deep water currents transport the water around the globe until it rises to the surface again, once more part of the surface ocean currents.

**Pacific Decadal Oscillation (PDO)** — The PDO is a basin-scale pattern of Pacific climate variability; PDO climate anomalies are most visible in the North Pacific and North American regions, with secondary features in the tropics. The phases of the PDO persist for 20-to-30 years. Causes for the PDO have not yet been explained.

**Potential Intensity (PI)** — The largest possible intensity (maximum wind, minimum pressure) expected to be possible for a particular tropical cyclone.

**Potential vorticity** — A scalar measure of the balance between the vorticity and the thermal structure of the atmosphere.

**Quasi-Biennial Oscillation (QBO)** — An oscillation in the lower stratospheric zonal winds averaged around the equator. It is typically diagnosed from the zonal winds between 30-70 hPa (although it is evident as high as 10 hPa). The QBO has a varying period of about 24 to 30 months. The zonal winds change by about 20 m s<sup>-1</sup> between the maximum easterly and maximum westerly phase.

**Radius of Maximum Winds** — The distance from the center of a tropical cyclone to the location of the cyclone's maximum winds. In well-developed systems, the radius of maximum winds is generally found at the inner edge of the eyewall.

**Rapid Deepening** — A decrease in the minimum sea-level pressure of a tropical cyclone of 1.75 hPa hr<sup>-1</sup> or 42 hPa for 24 hours.

**Relative vorticity** — see vorticity.

**Remnant Low** — Used for systems no longer having the sufficient convective organization required of a tropical cyclone (e.g., the swirls of stratocumulus in the eastern North Pacific).

**Recurvature**— The poleward motion of a tropical cyclone taking it from the mean tropical easterlies to the midlatitudes westerlies. This change in the advection of the storm results in curvature in the storm track.

**Rossby Radius of Deformation** — The Rossby radius is the critical scale at which rotation becomes as important as buoyancy, which allows an initial disturbance to be sustained. It is a function of the absolute vorticity, stability, and depth of the disturbance. When a disturbance is wider than  $L_R$ , it will persist; systems that are smaller than  $L_R$  will dissipate.

**Rossby Wave** — A planetary wave, resulting from conservation of potential vorticity. This chapter focuses on Rossby waves centered on the equator — equatorial Rossby waves.

**Saffir-Simpson scale**— A scale that links the observed damage and the effects of wind, pressure and storm surge that could lead to such damage. Initial wind damage scale was defined by Herbert Saffir and later expanded by Robert Simpson to include storm surge.

**Size** — The mean radius of a tropical cyclone enclosed by winds of at least  $17 \text{ m s}^{-1}$ . Size may also be defined as the outer closed isobar of the surface pressure.

**Storm Surge** — An abnormal rise in sea level accompanying a tropical cyclone or other intense storm, and whose height is the difference between the observed level of the sea surface and the level that would have occurred in the absence of the cyclone. Storm surge is usually estimated by subtracting the normal or astronomic high tide from the observed storm tide.

**Storm Tide** — The actual level of sea water resulting from the astronomic tide combined with the storm surge.

**Subtropical Cyclone** — A non-frontal low pressure system that has characteristics of both tropical and extratropical cyclones.

The most common type is an upper-level cold low with circulation extending to the surface layer and maximum sustained winds generally occurring at a radius of about 100 miles or more from the center. In comparison to tropical cyclones, such systems have a relatively broad zone of maximum winds that is located farther from the center, and typically have a less symmetric wind field and distribution of convection.

A second type of subtropical cyclone is a mesoscale low originating in or near a frontolyzing (dying frontal) zone of horizontal wind shear, with radius of maximum sustained winds generally less than about 50 km (30 miles). The entire circulation may initially have a diameter less than 160 km (100 miles). These generally short-lived systems may be either cold core or warm core.

**Subtropical Depression** — A subtropical cyclone in which the maximum sustained surface wind speed does not exceed  $17 \text{ m s}^{-1}$  (39 mph,  $63 \text{ km hr}^{-1}$  or 34 knot).

**Subtropical Storm** — A subtropical cyclone in which the maximum sustained surface wind speed is at least  $17 \text{ m s}^{-1}$  (39 mph,  $63 \text{ km hr}^{-1}$  or 34 knot).

**Thermocline** — The inversion separating the near-surface warm waters from the deeper cool waters for oceans and lakes. In the ocean, it also separates the fresher waters near the surface from the saltier waters below.

**Tropical Cyclone** — A warm-core, non-frontal synoptic-scale cyclone, originating over tropical or subtropical waters, with organized deep convection and a closed surface wind circulation about a well-defined center. Once formed, a tropical cyclone is maintained by the extraction of heat energy from the ocean at high temperature and heat export at the low temperatures of the upper troposphere. In this they differ from extratropical cyclones, which derive their energy from horizontal temperature contrasts in the atmosphere (baroclinic effects). Also see **Hurricane**.

**Tropical Cyclone Season** — The portion of the year having a relatively high incidence of tropical cyclones. Also known as “Hurricane Season” or “Typhoon Season”.

**Tropical Depression** — A tropical cyclone in which the maximum sustained surface wind speed is not more than  $17 \text{ ms}^{-1}$  (39 mph,  $63 \text{ km hr}^{-1}$  or 34 knot).

**Tropical Disturbance** — A discrete tropical weather system of apparently organized convection – generally 185 to 550 km (100-300 n mi) in diameter – originating in the tropics or subtropics, having a non-frontal migratory character, and maintaining its identity for 24 hours or more. It may or may not be associated with a detectable perturbation of the wind field.

**Tropical Storm** — A tropical cyclone in which the maximum sustained surface wind speed ranges from  $17 \text{ ms}^{-1}$  (39 mph,  $63 \text{ km hr}^{-1}$  or 34 knot) to  $33 \text{ ms}^{-1}$  (74 mph,  $119 \text{ km hr}^{-1}$ , 64 knot).

**Typhoon**— See Hurricane.

**Vorticity** — The local rotation of the flow, calculated as the the curl (cross product) of the vector wind. Vorticity has units of inverse seconds ( $\text{s}^{-1}$ ).

“Relative vorticity” is the vorticity calculated for the observed winds. It is called “relative” since the winds are the flow relative to the Earth’s rotation.

The vertical component of the vorticity vector is most often used since it is much larger than the other vorticity components. This is because the horizontal winds in tropical cyclones are much greater than the vertical wind component.

“Absolute vorticity” is the vorticity calculated for the total motion of the atmosphere — the combination of the observed winds and the Earth’s rotation.

**Warning** — A warning that sustained winds exceeding the threshold for either tropical storm or tropical cyclone and associated with such a storm are expected in a specified coastal area in 24 hours or less.

**Watch** — An announcement for specific coastal areas that either tropical storm or tropical cyclone conditions are possible within 36 hours.

**Wind-Induced Surface Heat Exchange (WISHE)** — A tropical cyclone development theory based on a conceptual model of a tropical cyclone as an atmospheric Carnot engine. Consistent with its Carnot engine roots, WISHE relates (i) fluxes of heat and moisture from the ocean surface and (ii) the temperature of the tropical cyclone outflow layer to the potential for continued storm development. The fluxes increase with surface wind speed providing a feedback to the system. As with CISK, WISHE relies on the presence of an incipient disturbance.